

**APPLICATION OF MATRIX-ASSISTED LASER  
DESORPTION/IONISATION (MALDI) IMAGING MASS SPECTROMETRY  
AND HIGH RESOLUTION FOURIER TRANSFORM MASS  
SPECTROMETRY FOR PROFILING PHARMACEUTICALS AND  
BIOMARKERS IN A VARIETY OF BIOLOGICAL SAMPLES.**

A THESIS PRESENTED FOR THE DEGREE OF DOCTOR OF  
PHILOSOPHY IN  
THE FACULTY OF SCIENCE  
THE UNIVERSITY OF STRATHCLYDE  
BY  
LYNSEY MACINTYRE

BSc. (Honours)

Strathclyde Institute of Pharmacy and Biomedical Sciences

University of Strathclyde,

161 Cathedral Street,

Glasgow,

G4 0RE,

United Kingdom.

March, 2011

This thesis is the result of the author's original research. It has been composed by the author and has not been previously submitted for examination which has led to the award of a degree.

The copyright of this thesis belongs to the author under the terms of the United Kingdom Copyright Acts as qualified by University of Strathclyde Regulation 3.50. Due acknowledgement must always be made of the use of any material contained in, or derived from, this thesis.

Signed:

Date:

## ACKNOWLEDGMENTS

I would like to thank my principle supervisor Dr Dave Watson for giving me the opportunity to carry out this project and for offering help and support during my time at Strathclyde. Dave allowed me to undertake exciting projects and cutting edge research providing encouragement, advice and ideas throughout. He also gave me the opportunity to travel to conferences and meetings which allowed me to present my work to others. Dave also arranged many collaborative ventures which enabled us to maximise the output from this project. Secondly, I would like to thank my supervisor from industry, Dr Paul Scullion who also gave me a lot of support and encouragement. Paul provided most of the samples utilised in this project which gave me the opportunity to work on projects relevant to the pharmaceutical industry. Paul also arranged for me to visit another site in Oss, The Netherlands which gave me the opportunity to work abroad within an industrial setting.

I would also like to thank Dr Leon Zheng and Dr Tong Zhang for their advice and support during this project. I would also like to thank collaborators from the University of Glasgow, Dr Richard Goodwin and Dr Andy Pitt. I would also like to thank Ms Pat Keating, from the Chemistry Department who helped me greatly during the method development stages of this project. Thanks also to Azra, Wei and Ruwida and my other colleagues in write up room 309 for support. Thanks also to the BBSRC and MSD at Newhouse (formerly Organon) for providing funding to enable me to carry out this project. Finally, I would like to thank my family, my partner Garry and my friends for their support and encouragement during my PhD studies.

## CONTENTS

Contents Pages.....	iv
Abstract.....	xvi
Abbreviations.....	xviii
Publications.....	xx

### **Chapter 1 – General Introduction**

1. Introduction .....	2
1.1. The Expanding Role of Mass Spectrometry in Metabolite Profiling and Characterisation.....	2
1.2. An Introduction to Mass Spectrometry: Principles .....	3
1.3. Mass Spectrometry Ionisation Sources .....	4
1.3.1. Electrospray Ionisation (ESI).....	5
1.3.2. Atmospheric Pressure Chemical Ionisation (APCI). .....	11
1.3.3. Nano-Electrospray.....	14
1.3.4. Matrix-Assisted Laser Desorption/ionisation (MALDI).....	15
1.3.4.1. MALDI Profiling Experiments .....	17
1.3.5. Desorption Electrospray Ionisation (DESI) Mass Spectrometry .....	20
1.3.6. SIMS Secondary Ion Mass Spectrometry .....	22
1.3.7. Fast Atom Bombardment (FAB).....	23
1.3.8. Electron Impact (EI) and Chemical Ionisation (CI).....	23

1.4.	Ion Separation Methods: Mass Analysers.....	26
1.4.1.	Quadrupole Instruments.....	27
1.4.2.	Ion Traps: Ion Trap, Linear Ion Trap, Quadrupole Ion Traps.....	29
1.4.3.	Time of Flight: TOF-Linear, TOF-Reflectron, Q-TOF.....	31
1.4.4.	FT-ICR-MS- Fourier Transform Ion Cyclotron Resonance.....	33
1.4.5.	LTQ-Orbitrap Mass Analyser.....	34
1.4.5.1.	Development of the LTQ-Orbitrap.....	34
1.4.5.2.	Features and Advantages of the LTQ-Orbitrap.....	35
1.4.5.3.	Ion Separation in the Orbitrap.....	37
1.4.5.4.	LTQ Exactive Mass Analyser.....	40
1.5.	Separation Methods.....	41
1.5.1.	Reversed Phase Chromatography.....	42
1.5.2.	Hydrophilic Interaction Chromatography (HILIC).....	44
1.5.3.	Capillary Gas Chromatography.....	46
1.5.4.	Capillary Electrophoresis.....	48
1.6.	Introduction to the Metabolome and Metabolomics/Metabonomics.....	49
1.7.	Introduction to Imaging Mass Spectrometry for Visualisation of Small Exogenous and Endogenous Molecules <i>in Situ</i> .....	50
1.7.1.	Introduction to Use of MALDI Mass Spectrometry for Tissue Imaging Studies.....	51
1.7.2.	MALDI Mass Spectrometry for Metabolomics Experiments.....	53

1.7.2.1.	Ion Mobility Separation for MALDI Imaging Experiments.....	55
1.7.2.2.	MALDI-LTQ-Orbitrap Technology .....	55
1.7.3.	Desorption Electrospray Ionisation (DESI) Imaging.....	57
1.7.4.	SIMS Imaging and Other Novel Mass Spectrometry Imaging Techniques...	58
1.8.	Aims and Objectives .....	60

## **Chapter 2 - Mapping the Distribution of Endogenous Metabolites in Brain Tissue Using MALDI-MSI**

2.	Introduction .....	63
2.1.	Designing MALDI Imaging Experiments.....	63
2.2.	Sample Preparation Stages of MALDI Imaging .....	63
2.2.1.	Harvesting Tissue from Study Animals .....	64
2.2.2.	Tissue Sectioning and the Thaw-Mounting Process .....	65
2.2.3.	Pre-treatment of Tissue Prior to MALDI-MSI Analysis.....	67
2.3.	MALDI Matrix Selection.....	68
2.3.1.	Variations in Matrix and Solvent Combinations.....	72
2.3.2.	Use of Liquid Ionic Matrices .....	74
2.3.3.	Improving Signal Sensitivity .....	75
2.4.	Matrix Application Methods for MALDI Imaging Experiments.....	75
2.4.1.	Application of Discrete Droplets of Matrix .....	76
2.4.2.	Application of a Homogenous Layer of Matrix.....	78
2.4.3.	Novel Matrix Application Methods .....	80
2.5.	Instrumental Set Up and Experimental Parameters .....	82
2.6.	Data Analysis Software for MALDI Imaging.....	83
2.6.1.	Introduction to BioMap.....	83
2.6.2.	Use of Principle Component Analysis and other Statistical Tools for the Interpretation of MALDI-MSI Data Sets.....	85

2.7.	Imaging Endogenous Molecules Using MALDI-MSI – Examples .....	85
2.7.1.	Analysis of Peptide and Proteins using MALDI-MSI .....	86
2.7.2.	Analysis of Lipids .....	87
2.8.	Introduction to Main Classes of Glycerophospholipids and Sphingolipids...	89
2.8.1.	Analysis of Lipids by MALDI MS Profiling and Imaging .....	97
2.9.	Analysis of Polar Metabolites .....	100
2.10.	Study Aims .....	102
2.11.	Methodology .....	103
2.11.1.	Materials.....	103
2.11.2.	Animals .....	103
2.11.3.	Tissue Sectioning Procedures .....	103
2.11.3.1.	MALDI Profiling Experiments .....	104
2.11.3.1.1.	Testing MALDI Matrices .....	104
2.11.3.1.2.	Analysis of Standards .....	105
2.11.3.1.3.	Profiling Metabolite Extracts and On Tissue.....	106
2.11.4.	MALDI Tissue Imaging Experiments.....	108
2.11.4.1.	Matrix Selection and Application Methods for Imaging Experiments..	108
2.11.5.	MALDI Mass Spectrometry.....	109
2.11.5.1.	Calibration of Axima-CFR TOF MALDI Instrument .....	109
2.11.5.2.	Setting MALDI MS Instrumental Parameters for Profiling Experiments.....	110



2.11.5.3. Optimisation of MALDI MS Instrument Parameters for Tissue Imaging Experiments.....	110
2.11.6. Data Analysis and Interpretation.....	112
2.12. Results.....	113
2.12.1. Analysis of MALDI Matrices and Matrix Selection for Imaging Experiments.....	113
2.12.2. Matrix Interferences.....	121
2.12.3. Investigations of Detection of Lipid Classes in Reflectron Positive and Negative Ionisation Modes.....	126
2.12.3.1. Profiling Lipids in Rat Brain Sections.....	126
2.12.3.2. Imaging Lipids in Rat Brain Sections in Reflectron Positive Ionisation Mode.....	127
2.12.3.2.1. Phosphatidylcholine Localisation in Rat Brain Sections.....	129
2.12.3.2.2. Formation of Phosphatidylcholine Dimers.....	134
2.12.3.2.3. Lysophospholipid Localisation in Rat Brain Sections.....	137
2.12.3.2.4. Mapping the Distribution of Cholesterol in Rat Brain Sections.....	139
2.12.3.2.5. Mapping the Distribution of Sphingomyelins in Rat Brain Sections....	140
2.12.3.2.6. Utilisation of Tools in Biomap for Investigation Lipid Distribution.....	141
2.12.3.3. Imaging Lipids in Rat Brain Sections in Negative Ionisation Mode.....	144
2.12.4. Profiling Energy Metabolites Utilising 9-aminoacridine as Matrix.....	146
2.12.5. Confirmation of Tentative Assignments of Lipids using Fragmentation Experiments, PSD and Analysis of Lipid Standards.....	157

2.13. Discussion .....	160
2.13.1. Advantages and Limitations of MALDI-MSI.....	160
2.13.2. Mapping Endogenous Lipids Using MALDI-MSI .....	161
2.13.3. Mapping Endogenous Polar Metabolites Using MALDI-MSI .....	162
2.14. Conclusions and Future Work.....	163

**Chapter 3 - Development of a Dry Matrix Application Method For Mapping  
Pharmaceuticals *in situ* using Matrix-Assisted Laser Desorption/Ionisation  
Mass Spectrometry Imaging (MALDI-MSI).**

3.	Introduction.....	165
3.1.	Introduction to use of MALDI-MSI for Drug Metabolism and Pharmacokinetic Studies .....	165
3.2.	Imaging Mass Spectrometry Versus Traditional Imaging Methods .....	166
3.3.	Utilisation of MALDI-MSI for Mapping the Distribution of Pharmaceuticals <i>in situ</i> – Documented Studies.....	167
3.4.	Matrix Application Methods for Drug Metabolism and Pharmacokinetic Studies .....	170
3.5.	Background Information and Receptor Pharmacology – Clozapine Study .	171
3.6.	Background Information and Receptor Pharmacology – SSR180718 Study.....	174
3.7.	Use of Laser Capture Microdissection for Quantitation of Drug in Regions of Rat Brain Tissue Sections .....	176
3.8.	Aims of Clozapine and SSR180711 Studies.....	177
3.9.	Methodology .....	178
3.9.1.	Materials.....	178
3.9.2.	Animals .....	178
3.9.3.	Tissue Sectioning Procedures .....	179
3.9.4.	Preparation and Analysis of Drug Standards by MALDI Profiling.....	181
3.9.5.	Preparation of Matrices for MALDI Experiments and Matrix Coating.....	181

3.9.5.1.	Dry Matrix Application .....	181
3.9.5.2.	Wet Matrix Application .....	182
3.9.6.	MALDI-MSI analysis .....	182
3.9.6.1.	Multiple Reaction Monitoring Characterisation using Bruker Ultraflex III TOF/TOF Instrument .....	183
3.9.7.	MALDI-MSI Data Interpretation .....	184
3.9.8.	Quantitation of clozapine in Single Rat Brain Tissue Sections Determined by LC-MS.....	184
3.9.9.	Investigations into Effects of Washing Tissue on Intensity of Clozapine using LC-MS.....	185
3.9.10.	Validation of Relative Quantitation of SSR180711 in Rat Tissue Determined by Laser Micro-Dissection and LC-MS.....	185
3.9.10.1.	Preparation of Samples for Validation.....	187
3.9.11.	Liquid Chromatography Mass Spectrometry Method for both Studies .....	187
3.10.	Results .....	189
3.10.1.	Results of the Clozapine Study .....	189
3.10.1.1.	Analysis of Clozapine Standard.....	189
3.10.1.2.	Clozapine Limit of Detection Study .....	192
3.10.1.3.	Imaging Clozapine in Liver using a Conventional Wet Matrix Coating.....	196
3.10.1.4.	Imaging Clozapine in Liver using a Dry Matrix Coating .....	200
3.10.1.5.	Imaging Clozapine in Kidneys using Wet and Dry Matrix Coatings ....	202

3.10.1.6. Imaging Clozapine in Rat Brain Tissue – Axima CFR TOF Mass Spectrometer .....	208
3.10.1.7. Imaging Clozapine in Rat Brain Tissue – Bruker Ultraflex III Mass Spectrometer .....	211
3.10.1.8. Use of LC-MS Analysis for Quantification of Clozapine in Rat Brain Sections.....	214
3.10.1.9. Profiling the Effects of a Washing Step on the Distribution of Clozapine in Rat Brain Tissue Sections using MALDI-MSI and LC-MS .....	219
3.10.2. SSR180711 Study .....	224
3.10.2.1. MALDI-MSI Results .....	224
3.10.2.2. SSR180711 Study – Results of Relative Quantitation.....	237
3.10.2.3. Biomarker Identification From Analysis of Laser Microdissected Tissue .....	240
3.11. Discussion .....	242
3.11.1. Discussion - Clozapine Study .....	242
3.11.2. Discussion - SSR180711 Study .....	243
3.12. Conclusions and Future Work.....	245

## **Chapter 4 - Metabolomic Profiling of Biomarkers of Liver X Receptor-Induced Toxicity in Mouse Liver Tissue.**

4.	Introduction .....	247
4.1.	Introduction to Metabolomics .....	248
4.1.1.	Key factors Governing the Success of Metabolite Profiling Experiments ..	250
4.1.2.	Sample Preparation for Metabolomics.....	250
4.1.3.	Introduction to Data Analysis for Metabolomics.....	252
4.1.4.	Introduction to Analytical Platforms for Metabolomics .....	255
4.1.5.	Metabolomics for Toxicological Studies .....	257
4.2.	Aims .....	258
4.3.	Materials and Methods .....	260
4.3.1.	Chemicals.....	260
4.3.2.	Animals .....	260
4.3.3.	Sample Preparation for MALDI-MS Imaging Experiments.....	261
4.3.4.	Instrumentation for MALDI MS Imaging Experiments .....	261
4.3.5.	Extraction of Lipids From Liver Tissue Homogenates for LC-MS and GC-MS Analysis .....	262
4.3.6.	Preparation of Fatty Acid Methyl Esters For GC-MS Analysis .....	263
4.3.7.	Instrumentation and method for GC-MS Analysis .....	263
4.3.8.	Extraction of Polar Metabolites from Liver Tissue Homogenates for LC-MS Analysis.....	264

4.3.9. LC-MS Analysis of Polar Metabolites .....	264
4.3.10. LC-MS Analysis of Lipids .....	265
4.4. Results .....	267
4.4.1. MALDI-MS Analysis of Liver Sections .....	267
4.4.2. Analysis of Fatty Acids by GC-MS .....	274
4.4.3. Analysis of Lipids by LC-MS .....	278
4.4.4. Analysis of Polar Metabolites by LC-MS .....	289
4.5. Discussion .....	300
4.6. Conclusions and Future Work.....	304

## **Chapter 5 - General Project Summary**

5. General Project Summary .....	308
6. References .....	310

## ABSTRACT

Matrix-assisted laser desorption ionisation mass spectrometry imaging (MALDI-MSI) enables the spatial distribution of small molecules to be determined *in situ* without the prerequisite for molecular tags such as radiolabels. The mass spectra of compounds in a tissue matrix are usually in the form of pseudo molecular ions and allow imaging of the distribution of potentially hundreds of small molecules according to their relative intensity, with the added possibility of biomarker identification in a single experiment.

Methods based on MALDI-MSI were used to investigate the distribution of drugs and endogenous metabolites *in situ* in a variety of tissue samples including murine brain, liver and kidney sections. Optimisation of experimental parameters was carried out in order to image lipids and other small molecules in naive rat brain sections (Chapter 2). It was then illustrated how MALDI-MSI could be utilised to investigate the distribution pattern of two CNS-targeted drugs, clozapine and 4-bromophenyl 1,4 diazabicyclo(3.2.2) nonane-4-carboxylate monohydrochloride (SSR180711) in intact tissue sections. This involved the development of a dry matrix application method which minimised drug delocalisation associated with the application of a conventional wet matrix coating, enabling the distribution of the drugs to be reliably determined (Chapter 3). The distribution of SSR180711 in brain tissue was confirmed by using laser micro-dissection followed by quantitative LC-MS analysis of the dissected tissues.

Studies of the metabolome of brain and liver tissue utilising high resolution mass spectrometry enabled the global profile of these tissues to be determined and the



methods were then utilised to investigate metabolic changes in response to drug treatment. Metabolite profiling was carried out utilising a linear ion trap-Fourier transform Orbitrap mass spectrometer (LTQ-Orbitrap MS) which offered high mass accuracy and sensitivity for these studies. MALDI-MSI and metabolomic profiling were then used to investigate changes in the small molecule profiles of mouse liver in response to the administration of an LXR agonist as part of a five day dosage study (Chapter 4). These studies illustrate that MALDI-MSI and high resolution Fourier transform mass spectrometry can be utilised successfully to profile pharmaceuticals and biomarkers during drug research and development.

## ABBREVIATIONS

$\alpha$ -CHCA	$\alpha$ -Cyano-4-hydroxycinnamic acid
ADP	Adenosine diphosphate
AGC	Automatic gain control
APCI	Atmospheric pressure chemical ionisation
API	Atmospheric pressure ionisation
ATP	Adenosine triphosphate
CE	Capillary electrophoresis
CI	Chemical ionisation
CNS	Central nervous system
CoA	Coenzyme A
COSHH	Control of substances hazardous to health
DAG	Diacylglycerol
DC	Direct current
DESI	Desorption electrospray ionisation
DHA	2, 6-dihydroxyacetophenone
DHAP	Dihydroxyacetophenone
DHB	2, 5-dihydroxybenzoic acid
DMPK	Drug metabolism and pharmacokinetics
EC-NCI	Electron capture-negative chemical ionisation
EI	Electron ionisation
ESI	Electrospray ionisation
GC-MS	Gas chromatography mass spectrometry.
GDP	Guanosine diphosphate
GTP	Guanosine triphosphate
FAB	Fast atom bombardment
FAMES	Fatty acid methyl esters
FT-ICR	Fourier transform ion cyclotron resonance
FT-MS	Fourier transform mass spectrometry
FWHM	Full width at half maximum
HCD	Higher energy collisional dissociation
HMGC	Hydroxymethylglutaryl carnitine
HMGCoA	3-hydroxy-3-methylglutaryl-coenzyme A
HPLC	High pressure liquid chromatography
IMP	Inosine monophosphate
LC-ESI-MS	Liquid chromatography electrospray ionisation mass spectrometry
LC-FTMS	Liquid chromatography Fourier transform mass spectrometry
LC-MS	Liquid chromatography mass spectrometry
LMD	Laser microdissection
LPC	Lysophosphatidylcholine

LTQ-Orbitrap MS	Linear ion trap-Fourier transform Orbitrap mass spectrometer
LXR	Liver X receptor
MALDI-MS	Matrix-assisted laser desorption/ionisation mass spectrometry
MALDI-MSI	Matrix-assisted laser desorption/ ionisation mass spectrometry imaging
MeOH	Methanol
MGC	Methylglutarylcarnitine
micro-ES	Micro-electrospray
MRI	Magnetic resonance imaging
MS	Mass spectrometry
MUFA	Mono-unsaturated fatty acid
<i>m/z</i>	Mass to charge
nano-ES	Nano-electrospray
Nd:YAG	Neodymium-doped yttrium aluminium garnet
NGA	N-acetylglucosamine
NIMS	Nanostructure initiator mass spectrometry
PA	Phosphatidic acid
PC	Phosphatidylcholines
PE	Phosphatidylethanolamines
PET	Positron emission tomography
PG	Phosphatidylglycerol
PI	Phosphatidylinositols
PS	Phosphatidylserine
PUFA	Poly-unsaturated fatty acid.
Q-TOF	Quadrupole-time of flight
RF	Radio frequency
RP	Reverse phase
RPC	Reverse phase chromatography
SREPB-1C	Sterol regulatory element binding protein-1C
SSR180711	4-bromophenyl 1, 4-diazabicyclo(3.2.2) nonane-4-carboxylate monohydrochloride
TAG	Triacylglycerol
TOF	Time of flight
UDP	Uridine diphosphate
UNGA	Uridine diphosphate N-acetylglucosamine
UPLC	Ultra-high performance liquid chromatography
ZIC-HILIC	Zwitterionic-hydrophilic interaction chromatography
<sup>1</sup> H-NMR	Proton Nuclear Magnetic Resonance

## PUBLICATIONS

Sha, L., MacIntyre, L., Machell, J.A., Kelly, M.P., Porteous, D.J., Brandon, N.J., Muir, W.J., Blackwood, D.H., Watson, D.G., Clapcote, S.J. and Pickard B.S. (2010) **Transcriptional regulation of neurodevelopmental and metabolic pathways by the psychiatric illness candidate gene *NPAS3***. *Article submitted*.

Xiao, X, Dawson, N, MacIntyre, L, Morris, B.J., Pratt, J.A., Watson, D.G and Higham, D.J. (2010) **Exploring metabolic pathway disruption in the subchronic phencyclidine model of schizophrenia with the Generalized Singular Value Decomposition**. *Article submitted*.

MacIntyre, L., Zheng, L., Scullion, P., Keating, P. & Watson, D.G. (2010) **Metabolomic profiling of biomarkers of liver X receptor-induced toxicity in mouse liver tissue**. *Metabolomics* DOI: 10.1007/s11306-010-0235-6

Goodwin, R. J., Scullion, P., MacIntyre, L., Watson, D.G. & Pitt, A.R. (2010) **Use of a solvent-free dry matrix coating for quantitative matrix-assisted laser desorption ionization imaging of 4-bromophenyl-1,4-diazabicyclo(3.2.2)nonane-4-carboxylate in rat brain and quantitative analysis of the drug from laser microdissected tissue regions**. *Anal Chem* **82**(9): 3868-73.

Goodwin, R. J., MacIntyre, L., Watson, D.G. & Pitt, A.R. (2010) **A solvent-free matrix application method for matrix-assisted laser desorption/ionization imaging of small molecules**. *Rapid Commun Mass Spectrom* **24**(11): 1682-6.

## **Chapter 1 – General Introduction**

## **1. Introduction**

### **1.1. The Expanding Role of Mass Spectrometry in Metabolite Profiling and Characterisation.**

Mass spectrometry can be used in combination with prior separation techniques to achieve high sensitivity and specificity for the analysis of a wide variety of pre-prepared biological samples. Recent developments in mass spectrometry instrumentation have enabled comprehensive metabolite profiling and characterisation studies to be carried out. As a result, mass spectrometry is one of the major techniques that is utilised for metabolite profiling studies along with NMR (nuclear magnetic resonance) which provides complementary information for analytical scientists. Additionally, over the past decade there has been a great interest in the use of mass spectrometry imaging techniques such as matrix-assisted laser desorption/ionisation mass spectrometry (MALDI-MS) which allows characterisation of the spatial distribution of endogenous and exogenous compounds *in situ*, in samples such as rat brain or liver tissue sections, preserving the anatomical information without the pre-requisite for tags/radiolabels required for traditional imaging techniques.

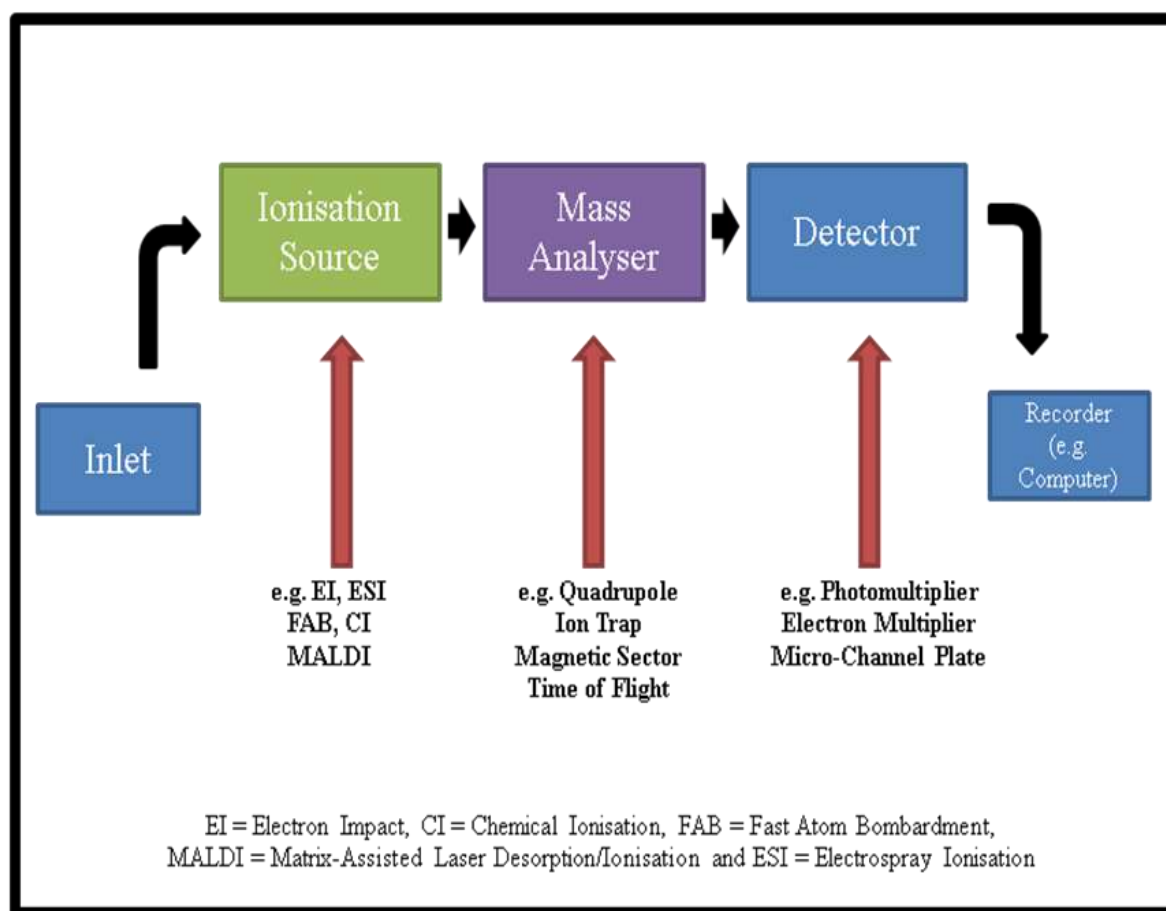
This chapter will provide an introduction to mass spectrometry, before describing in detail ionisation methods, mass analysers and separation methods that have been developed with particular focus on currently utilised techniques for metabolite profiling and characterisation. There will then be an introduction into the field of metabolomics/metabonomics with more detailed information provided in chapter 4.

Finally, there will be an introduction to the development of imaging mass spectrometry techniques, with particular focus on MALDI Imaging.

## **1.2. An Introduction to Mass Spectrometry: Principles**

Mass spectrometers are made up of three main parts; the ion source, the mass analyser and the detector. The schematic diagram shown below gives an overview of this set up and summarises some of the commonly used types of ionisation sources, mass analysers and detectors (Figure 1) which are discussed in greater detail later in this chapter. As a simple overview, samples are injected into the source where they become ionised. Here, the ions are now in the gas-phase and they can be separated according to their mass/charge ( $m/z$ ) ratio in the mass analyser. These signals are then detected by an electron or photomultiplier and the output is recorded by the data system, usually a computer. A mass spectrum is thus generated which plots ion abundance against  $m/z$  ratio. Small molecule experiments usually involve the analysis of complex samples and so prior separation is often required before sample injection and subsequent ion generation in the mass spectrometer. These separation methods include high performance liquid chromatography, capillary gas chromatography and capillary electrophoresis and they will also be discussed later in this chapter in section 1.5.

**Figure 1 - The Basic Components of a Mass Spectrometer**



### **1.3. Mass Spectrometry Ionisation Sources**

Several types of ionisation methods exist. Commonly utilised techniques for small molecule profiling include the atmospheric pressure ionisation (API) techniques such as electrospray ionisation (ESI), atmospheric pressure chemical ionisation (APCI) and desorption electrospray ionisation (DESI). Other ionisation techniques that are also used for specific applications includes matrix-assisted laser desorption/ionisation (MALDI) which has been applied extensively for biomedical imaging applications and will be discussed in detail in sections 1.3.4 and section 1.7.



Further examples include electron ionisation (EI) which is used in gas-chromatography mass spectrometry (GC-MS), chemical ionisation (CI), and fast atom bombardment (FAB).

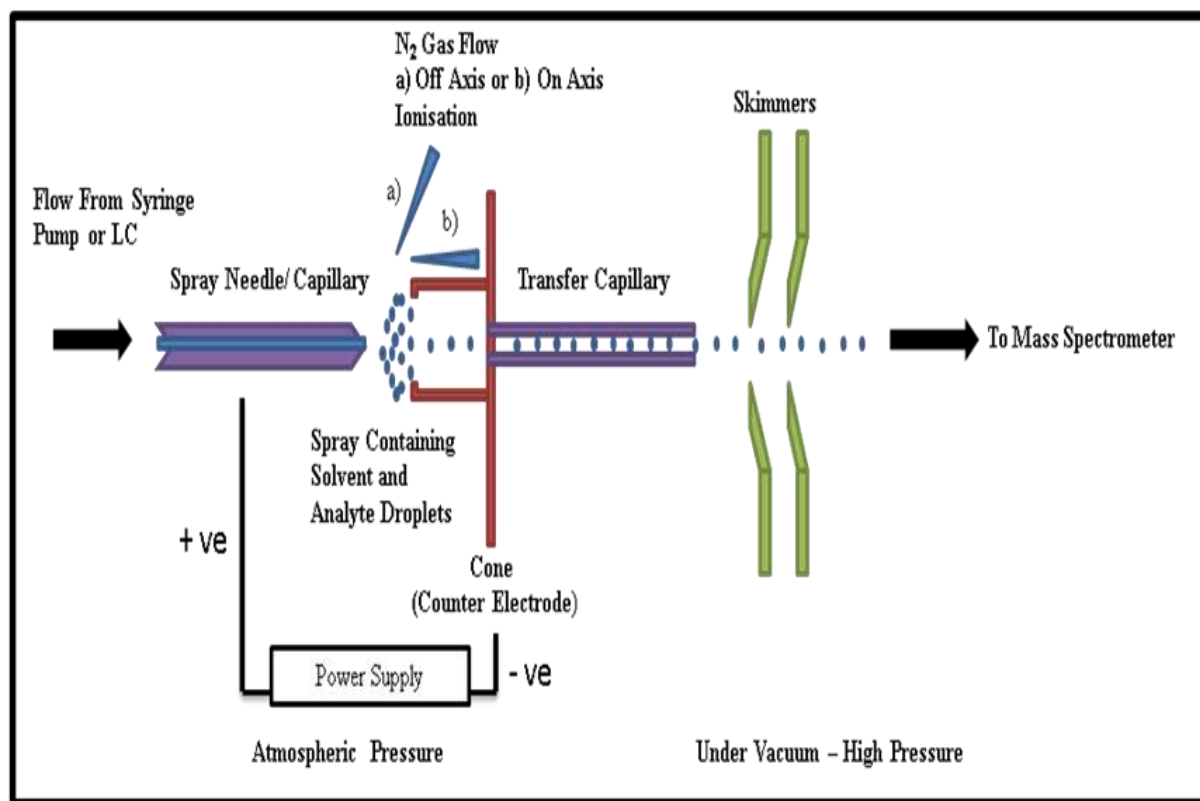
### **1.3.1. Electrospray Ionisation (ESI)**

Electrospray ionisation (ESI) is a soft ionisation technique which transforms ions in solution into the gas phase. The concept of electrospray ionisation was described in the early 20<sup>th</sup> Century [1]. It wasn't until approximately 30 years later that Malcolm Dole and colleagues showcased the use of electrospray to ionise intact chemical species [2,3]. Approximately 20 years later, John Fenn and colleagues demonstrated that ESI could be used to ionise high molecular weight biological compounds and showed they could then be analysed by mass spectrometry [4-6] which resulted in John Fenn being awarded a share of the 2002 Nobel Prize for Chemistry [7]. ESI can be utilised for the ionisation of involatile and thermally labile compounds, multiply charged proteins and intact ionisation of complexes e.g. between DNA and binding agent. Electrospray ionisation mass spectrometry (ESI-MS) is now common place in analytical laboratories all over the world. For ESI, the sample is dissolved in a solvent such as methanol, water or acetonitrile or a mixture of the above which may also contain formic acid to aid ionisation. It is best practise to alter the ionisation mode depending on the polarity and molecular weight of analytes. For example, electrospray is better suited to the analysis of polar compounds that are already in solution whilst a complementary ionisation technique, atmospheric pressure chemical ionisation (APCI) is useful for analysis of non polar compounds such as steroids.

In ESI, the analyte(s) is introduced into the source in solution either via a syringe pump (direct injection) or as the eluent flow from liquid chromatography that is interfaced with the mass spectrometer. Flow rates vary according to sample and injection mode but are usually within range of 1  $\mu\text{l}/\text{min}$  to 500  $\mu\text{l}/\text{min}$ . The analyte solution flowing through the electrospray needle has a high potential difference applied to it (+ 2.5- 4 kV in positive mode or - 2.5- 4kV in negative mode) compared to the counter electrode. In positive mode, positive ions in solution drift towards the tip of the capillary where a Taylor cone is formed which becomes unstable as more liquid is drawn into the capillary [8]. This along with the back pressure applied to the capillary from the syringe pump (direct infusion) or high pressure liquid chromatography (HPLC) pump forces the spraying of charged droplets with the same charge which repel each other from the needle with a surface charge of the same polarity as that of the spray needle. The droplets are repelled from the needle towards the circular orifice on the counter electrode which is at a lower electrical potential creating an electrospray.

As the droplets travel between needle tip and counter electrode, solvent evaporation will occur, desolvating the sample before injection into the mass spectrometer. Whilst the source is under atmospheric pressure, most of the other components are held under high vacuum. This aids transfer of charged droplets towards the circular orifice of the counter electrode. Figure 2 shows a schematic diagram of an ESI source in positive ionisation mode. In negative ionisation mode, negatively charged ions are formed due to the negative polarity of the electrospray needle, with negatively charged analytes now drawn towards the now positively charged counter electrode.

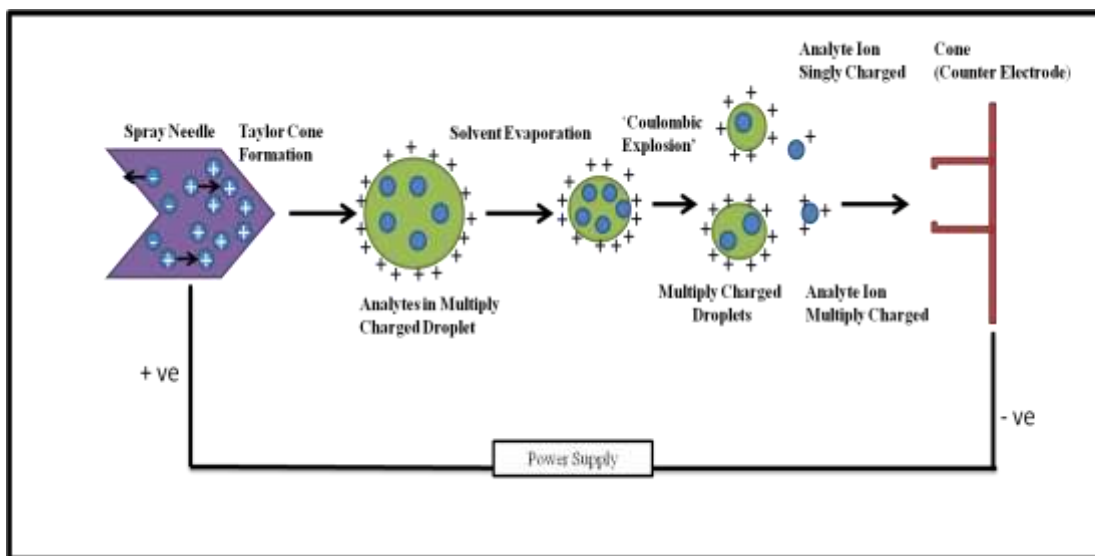
**Figure 2 - Schematic Diagram of an Electrospray Ionisation (ESI) Source in Positive Ionisation Mode**



In positive mode, there will be the continuous removal of positively charged droplets from the capillary, so to maintain charge balance, oxidation can occur within the capillary [9]. To maintain this balance, there may be oxidation of the metal capillary where metal and solution meet or there may be the removal of negative ions from the solution by electrochemical oxidation. In negative ion mode, this will be reversed and there may be reduction of cations and neutrals in the capillary [10].

In the solvent removal stage of electrospray ionisation there are two main theories as to the mechanism by which this occurs. The first model was described by Dole and is known as the 'charged residue model' [2]. Solvent evaporation is aided by the flow of N<sub>2</sub> gas either a) off axis or b) on axis (Figure 2) which also facilitates nebulisation. The 'charged residue model' proposes that each individual droplet will shrink until the surface tension can no longer sustain the electrostatic repulsion of the surface charges (Rayleigh stability limit) (Figure 3). This causes a 'Coulombic explosion', ripping the droplet apart. This will produce either smaller offspring droplets which will repeat the process or freely charged analytes (singly or multiply charged).

**Figure 3 - A Schematic Diagram Illustrating the Mechanism of Ion Formation in Electrospray Ionisation in Positive Ionisation Mode**



The second mechanism was suggested by Iribarne and Thompson and is known as the ion evaporation model [11]. This theory suggests that spray droplets which have radius of less than 10 nm can allow field desorption – the direct emission of a gaseous ion. The charge state of this ion will depend upon the number of charges that are transferred from the droplet surface to the ion during the desorption process. The ‘charged residue model’ is the most widely accepted theory although the ion evaporation model may be involved in the formation of gaseous macromolecules such as ion clusters and adducts.

Ions are pulled into the circular orifice of the counter electrode and then transferred into the vacuum chamber of the mass spectrometer. When charged analytes move from the source to the mass analyser, they must do so without coming into contact with any solid internal parts of the mass spectrometer to prevent neutralisation. This is achieved by the use of ion optics which use direct current (DC) voltage, radio

frequency (RF) voltages and vacuum gradient to draw the ions into the mass spectrometer. The ions travel through differentially pumped regions via skimmers which aids their transmission to the high vacuum region of mass spectrometer for analysis. Little residual energy is retained by the analyte following ionisation, making ESI a soft ionisation technique, thus little fragmentation of the analytes will occur. This makes it necessary to perform tandem mass spectrometry to fragment the analytes to enable structural elucidation.

For small molecule analysis, positive ESI facilitates the ionisation of compounds containing amines and amides and other positively charged groups. Negative ESI is used for the detection of polar acids such as citrate, sugar phosphates, neutral sugars, fatty acids and several lipid classes such as gangliosides, cerebroside and phosphatidylinositols. In positive ionisation mode, protonated molecules are usually observed, however, due to complex nature of biological samples,  $\text{Na}^+$ ,  $\text{K}^+$  adducts are also observed. Ammonium adducts may also be observed. Pseudo molecular ions of isotopes will be observed assuming appropriate spectral resolution. Spectra can be further complicated by the formation of multimers ( $[\text{xM}+\text{H}]^+$ ) and ionisation of environmental contaminants. In negative ionisation mode, predominantly molecular ions will be observed which have lost one proton ( $[\text{M}-\text{H}]^-$ ). Additionally, adduct ions with formate ( $[\text{M}+\text{HCO}_2]^-$ ) and chloride ( $[\text{M}+\text{Cl}]^-$ ) ions may be observed.

ESI also enables mass spectral analysis of proteins and other multiply charged macromolecules. Whilst in the past protein digestion was relied upon, direct measurements of proteins can now be made using ESI. It is common to observe the formation of multiply charged ions by electrospray for masses  $> 1000$  Da, which in

biological samples are often peptides. A series of pseudo molecular ion peaks are observed in electrospray which represents multiple charge states of the same analyte. The charge state of peptides will depend on factors such as the number of acid or basic amino acids in the peptide and the size of the peptide. The charge state of a multiply charged ion can be determined by examining the  $m/z$  separation of isotope peaks; isotopes of singly charged ions are separated by 1 Da, doubly charged ions are separated by 0.5 Da and triply charged ions are separated by 0.33 Da or from the highest peak in adjacent ion clusters in the spectrum according to the equation:

$$n = \frac{M_A - 1.0078}{M_A - M_B}$$

Where  $n$  = the charge on  $M_B$  and  $M_A$  and  $M_B$  are adjacent ions with  $M_A$  the higher in mass.

### 1.3.2. Atmospheric Pressure Chemical Ionisation (APCI).

Atmospheric pressure chemical ionisation (APCI) is a popular ionisation technique that is used for the analysis of neutral molecules such as fatty acids, sterols, steroids and oils. The hardware required for APCI and the arrangement of the needles and cones are similar to those in ESI with the main difference being in terms of the ionisation method employed. In APCI, the sample is passed through a fused sample needle (similar to ESI) but this is then attached to a heated quartz tube. After the sample has been nebulised from the spray needle, it passes into the heated tube and a high charge (approx 5 kV) is applied to a corona pin which is situated at the end of the heated quartz tube. The corona discharge around the pin causes the vaporised

solvent molecules to ionise and form a reagent gas plasma and the vaporised sample molecules are ionised by proton transfer (Figure 4) and (Figure 5).

**Figure 4 - Schematic Diagram Illustrating the Process of Atmospheric Pressure Chemical Ionisation (APCI).**

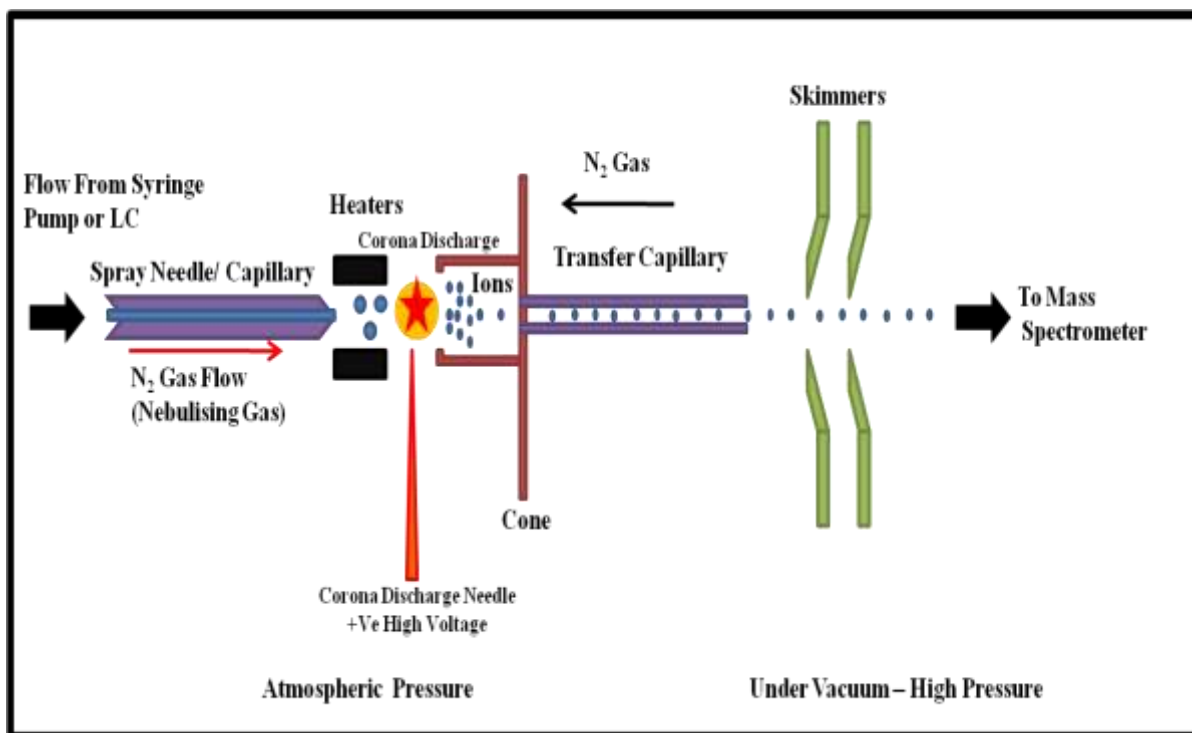
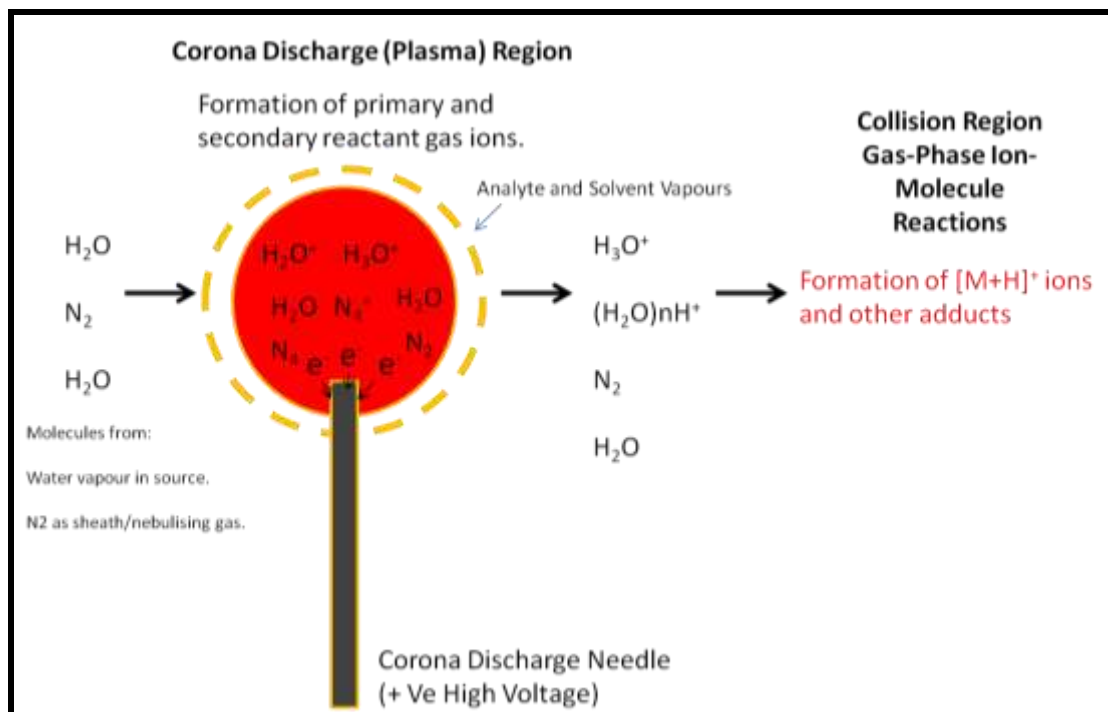


Diagram drawn is based on diagram in [12].



**Figure 5 - Schematic Diagram Illustrating the Process of ion Formation in the Corona Discharge Region and Collision Regions during Atmospheric Pressure Chemical Ionisation (APCI).**



The corona discharge produces both primary and secondary reactant gas ions. Primary ions are  $N_2^+$  and  $N_4^+$  which collide with vaporised solvents to form secondary reactant gas ions such as  $H_3O^+$  and  $(H_2O)nH^+$ . The secondary reactant gas ions collide with the analytes resulting in the formation of analyte ions. Due to a high frequency of collisions between the analytes and reactant gas ions, there is high ionisation efficiency which results in the formation of molecular species and adducts with little fragmentation of the analytes. The protonated analyte ions are formed by gas-phase ion-molecule reactions of these charged cluster ions with the analyte molecules. This results in the formation of mainly  $[M+H]^+$  ions.

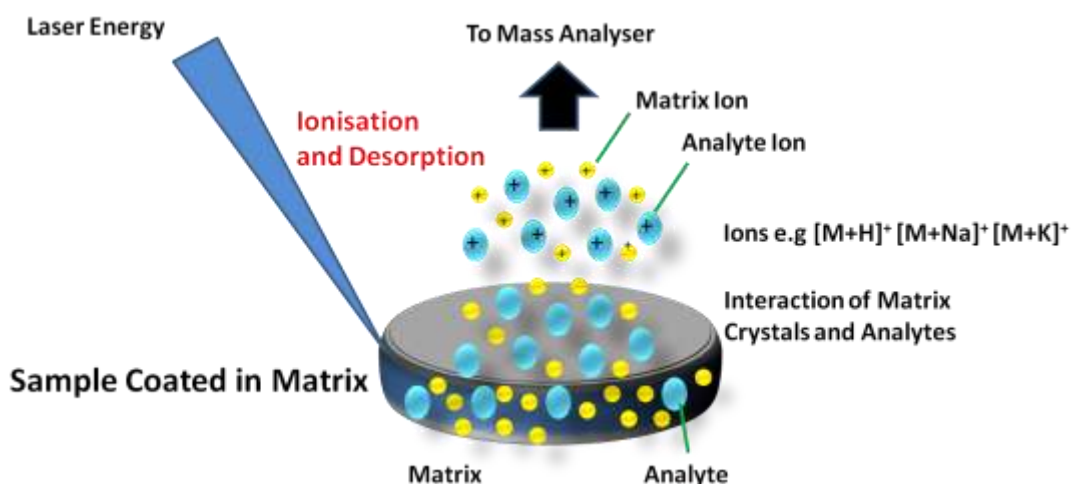
### 1.3.3. Nano-Electrospray

Nano-electrospray (nano-ES) or micro-electrospray (micro-ES) are terms used to describe combining a lower flow rate HPLC (less than 1  $\mu\text{l}/\text{min}$ ) with electrospray ionisation with the aim of improving sensitivity and reducing sample consumption. These were first described by two separate research groups in 1994. Micro-ES was originally described by Emmett and Caprioli and described the development of an ionisation source which was pressure-driven and optimised to accommodate nanolitre flow rates, 300 to 800  $\text{nl}/\text{min}$  [13]. This involved spraying sample from a capillary needle that was packed with C18 liquid chromatography packing for the analysis of peptides to aid in concentrating samples and desalting [13]. Nano-ES does not rely on an HPLC system to generate sample flow, this is initiated by the electrical potential between the capillary tip and the counter electrode. This process was first described by Wilm and Mann [14]. Its unique properties include its low flow rate of approximately 20  $\text{nL}/\text{min}$ , small size of droplets generated, 1-2  $\mu\text{m}$  spraying orifice and the absence of solvent pumps and inlet valves [15]. Today, the terms micro-ES and nano-ES are used interchangeably and both have been utilised extensively for proteomics [16,17]. Other applications include mapping and sequencing of underivatized O-glycans [18] and metabolite identification in drug metabolism studies [19] and [20].

#### **1.3.4. Matrix-Assisted Laser Desorption/ionisation (MALDI)**

Matrix-assisted laser desorption/ionisation (MALDI) is a soft ionisation technique which involves mixing/coating samples with an excess of a UV absorbing matrix. This interacts with analytes to form analyte-doped matrix co-crystals on the surface of a MALDI plate (Figure 6). A laser is then used to ablate the matrix-analyte mixture with either a UV pulsed nitrogen laser with a wavelength of  $\lambda = 337$  nm or frequency tripled Nd:YAG laser  $\lambda = 355$  nm. Nd:YAG lasers are now more popular due to their fast laser repetition rates ( $> 1$  kHz) enabling quicker sampling compared to standard nitrogen lasers (10-20 Hz). They also have a longer life span compared to nitrogen lasers which need to be replaced after approximately  $6 \times 10^7$  shots have been fired. Laser energy is absorbed by the analytes which induces rapid heating and excitation of the matrix causing irradiation of the sample which results in desorption of the matrix and analytes from the surface of the plate generating a small volume of vapour [21,22]. Photo-activated reactions lead to ionisation of both matrix and analytes. Due to the pulsed nature of the laser used in the MALDI process, ions are often analysed using a Time of Flight (TOF) mass spectrometer. Many commercial MALDI TOF/TOF instruments are now available.

**Figure 6 - Schematic Diagram Summarising Processes of Desorption and Ionisation in MALDI Experiment**



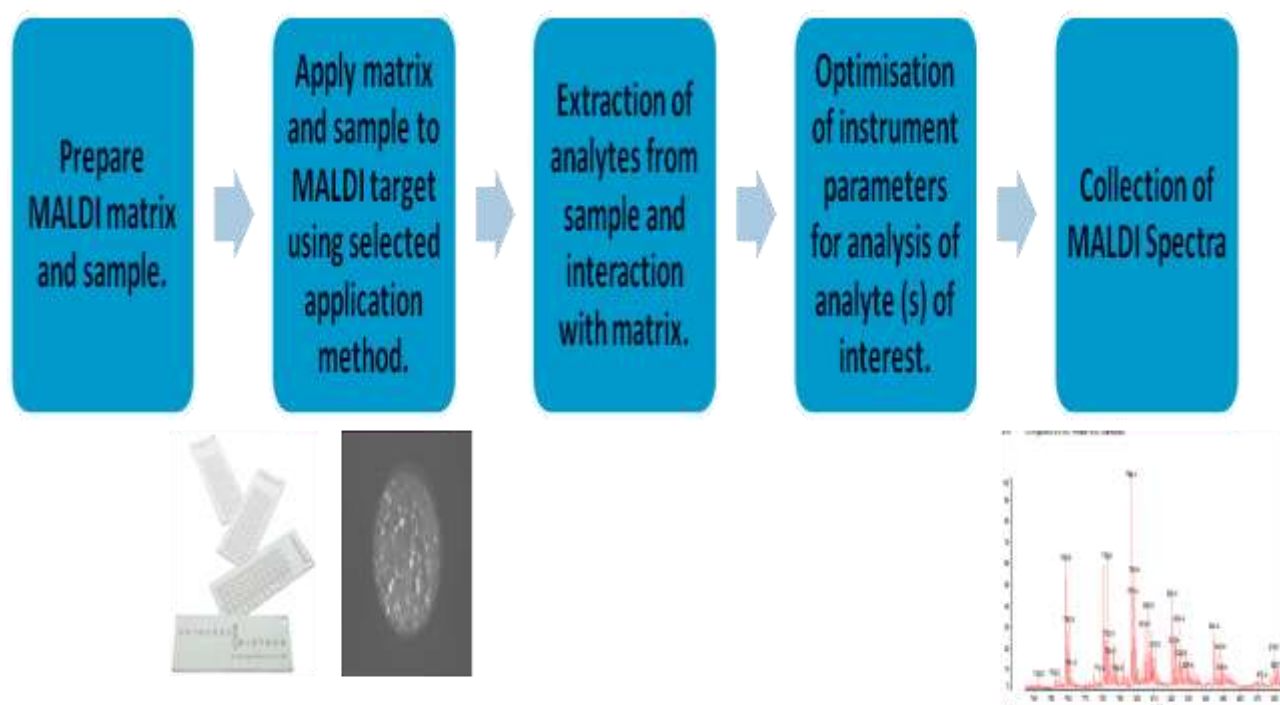
The use of a matrix to enable volatilisation of small molecules was first described by Karas *et al* in 1985 when it was shown that the amino acid tryptophan, employed as a crystalline matrix, could ionise alanine using a 266 nm laser [23]. Following this discovery, MALDI-mass spectrometry was described by Karas *et al* [24] who then illustrated the use of a YAG laser and nicotinic acid to facilitate desorption and ionisation thus demonstrating that molecules with molecular weights of up to 10000 Da could be successfully ionised using this method [25]. However, work published in the same year by a Japanese scientist demonstrated that even larger molecular weight molecules could be ionised [26]. He used glycerol as a solvent combined with a fine metal powder to absorb laser energy and established that proteins and polymers with molecular weights of up to 100 000 Da could be analysed using this technique [26]. Tanaka received a Nobel Prize in 2002 for his work in this area and his contribution to the discovery that MALDI mass spectrometry required the combination of both an appropriate matrix and suitable laser wavelength for the

successful ionisation of molecules. It has been argued that Karas and Hillenkamp were more deserving winners of this prize as they played a substantial role in the development of the technique and described the ‘dried droplet’ method of matrix application which is still used today for MALDI profiling experiments [24,25]. Subsequently, 335 nm radiation was used successfully for MALDI-MS accompanied with derivatives of cinnamic acid such as caffeic, ferulic and sinapinic acid [27,28]. Altogether, this groundwork in the 1980s laid the foundations for the production of the first commercial MALDI mass spectrometers in the early 1990s. Later in this decade, important advances in the technology laid the foundations for the development of proteomics. MALDI matrix selection is discussed in detail in section 2.3.

#### **1.3.4.1. MALDI Profiling Experiments**

Originally, MALDI experimentation centred on the use of profiling for the analysis of small sample spots mixed with matrix and spotted onto a wellled MALDI target (Figure 7). Profiling can be used to analyse homogenised tissue extracts, polymers, oligosaccharides or newly synthesised drug molecules.

**Figure 7 – MALDI Profiling Experiment Work Flow**



There are various sample preparation techniques that have been employed for the application of matrix and analytes for MALDI profiling experiments. The original sample preparation method mentioned above was described by Karas and Hillenkamp and is known as the ‘dried droplet’ method [24,25]. This involves mixing the sample with matrix and spotting this directly onto a MALDI target. Alternative approaches include the crushed crystal method which enables the growth of analyte doped matrix crystals in the presence of a high concentration of a non volatile solvent e.g. glycerol. Others are the fast evaporation method which involves spotting matrix, allowing it to dry and then spotting sample on top, a variation of this is the ‘sandwich’ which involves spotting a further layer of matrix on top of the sample. Another common method involves spotting the sample then spotting the analyte and mixing them using a pipette tip on the MALDI target. All methods have

their own advantages and disadvantages and selection will depend on factors such as speed of preparation, whether or not you want to mix the matrix and sample and whether or not semi-quantitation is required. Alternatively, profiling can be used to analyse spectral profiles in different tissue areas providing information on the molecular profiles in different localities, for example profiling phosphatidylcholines and sphingomyelins in different regions of lens tissue [29]. Profiling is also utilised to generate mass spectra of different compounds of interest that will be analysed using MALDI imaging e.g. drug standards to investigate their ionisation characteristics before an imaging experiment is undertaken.

MALDI mass spectrometric analysis can be carried out in either positive or negative ionisation modes. In positive ionisation mode, the ions formed are predominantly in the form of  $[M+H]^+$  as molecules gain a proton but there can also be the formation of sodium and potassium adducts,  $[M+Na]^+$  and  $[M+K]^+$ . The formation of matrix peaks also occurs,  $[Matrix + H]^+$ , and there may also be the formation of matrix dimers or even larger molecules such as trimers and higher clusters. This adds a higher degree of complexity to the spectra and there is also the possibility that there may be interaction of the analyte of interest with matrix ions  $[M + Matrix + H]^+$ . In negative ionisation mode  $[M-H]^-$  ions are observed but there may also be the formation of adducts such as formate adducts. The method of ionisation that is chosen for MALDI-MS will depend on the functional groups that the analyte of interest contains. Although MALDI instruments often utilise TOF or TOF/TOF analysers, hybrid instruments are also available e.g Q-TOF instruments which have a hybrid ion trap-time of flight analyser such as the MALDI Q-TOF Premier™ from Waters. Hybrid instruments are discussed in more detail in 1.4.3.

The first use of MALDI-MS for tissue imaging experiments was described in 1997 [22] and since then, its role has been expanded to include biomedical applications such as biomarker discovery [30], metabolomics [31], lipidomics [32] and drug metabolism and pharmacokinetics [33,34]. The instrumental set up required for MALDI-MS for imaging applications is discussed in greater detail in section 1.7.1.

### **1.3.5. Desorption Electrospray Ionisation (DESI) Mass Spectrometry**

Another ambient ionisation technique is Desorption Electrospray Ionisation (DESI) which has also been utilised for imaging mass spectrometry applications. Desorption electrospray ionisation mass spectrometry was developed by the group of Cooks and colleagues at Purdue in 2004 [35-39] and combines features of both desorption/ionisation techniques including FAB and MALDI with features of electrospray ionisation. It involves the deposition of a sample onto a solid target such as urine or blood on paper [36] or an intact tissue section on a glass slide or additionally, the sample can itself act as a solid surface (e.g. tablet) [37,38] or the surface of fruit to screen for agrochemicals, thus little or no sample preparation is required. The sample is ionised at an ambient temperature and atmospheric pressure and it involves electrospraying nebulised charged droplets onto the surface of the sample. Molecules on the surface are ionised and vaporised and are collected at the opening of an API source such as LTQ-ion trap (Figure 8).

One of the most interesting features of DESI is that the spray solvent applied can be varied depending on the analytes of interest in a particular experiment. Additionally, the ionisation efficiency can be altered by altering the angle of the incoming beam ( $\alpha$ ), the angle of desorbed ions ( $\beta$ ) and the distance of the mass spectrometer inlet



from the sample and the solvent(s) used. Commonly utilised solvents include methanol and water but for selective ionisation, reactive reagents can be utilised to ionise compounds with functional groups of interest. Flow rates are much lower than those used with conventional ESI, requiring only 0.05 – 5  $\mu\text{l}/\text{min}$  making it much more environmentally friendly. In positive mode,  $[\text{M}+\text{H}]^+$ ,  $[\text{M}+\text{nH}]^{\text{n}+}$  or  $[\text{M}]^{\text{n}+}$  ions can be formed whilst in negative mode,  $[\text{M}-\text{H}]^-$ ,  $[\text{M}+\text{Cl}]^-$  or  $[\text{M}]^-$  ions are observed depending on analytical conditions, solvent selection and other parameters. Ion formation by DESI has been suggested to occur through three different mechanisms a) charge transfer between projectile ions, b) ‘droplet pickup mechanism’ from impact of electrospray droplets on surface and c) volatisation/desorption of neutrals from the surface [35]. The applications of DESI for imaging mass spectrometry will be discussed later in this chapter in section 1.7.3.

**Figure 8 - Schematic Diagram Illustrating Principles of Desorption Electrospray Mass Spectrometry**

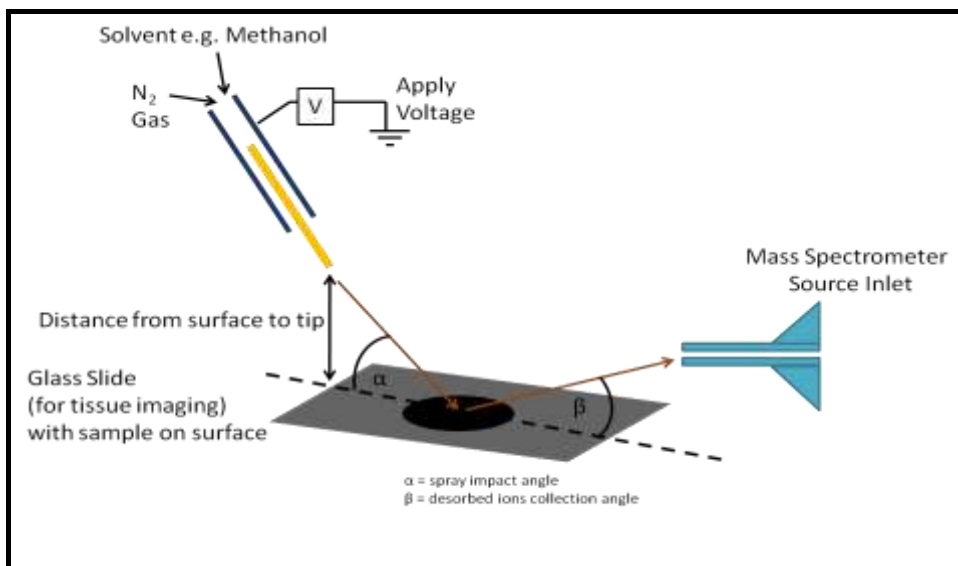


Diagram drawn is based on that in [40].

A related ionisation technique also pioneered by the group of Cooks is Paper Spray, another direct ionisation technique for the analysis of complex mixtures such as blood spots from paper which has had a high voltage applied to it [41,42]. Current applications include therapeutic drug monitoring from analysis of blood spots and monitoring illegal drugs in urine [41].

### **1.3.6. SIMS Secondary Ion Mass Spectrometry**

Secondary Ion Mass Spectrometry (SIMS) is a sensitive ambient ionisation technique which involves bombarding the surface of a sample with high energy ions from a focused primary ion beam. This leads to the ejection of neutral and charged species from the surface which are then collected as secondary ions and analysed by, conventionally, TOF or quadrupole mass analysers. There are three main types of SIMS, Static SIMS, dynamic SIMS and SIMS Imaging.

Static SIMS will provide information on the very top layer of a surface. This is achieved by use of low energy ion fluxes which will impact on the surface of a sample. Static SIMS requires that the ion flux touches a new undamaged surface each time to provide information on the top layer of the sample surface. Dynamic SIMS enables profiling composition of sample below the surface. As it is a destructive technique, SIMS is well suited for this type of application. Depth profiles are obtained by recording SIMS spectra over a point and it will gradually penetrate the surface due to the energy of the ion probe. A plot of intensity of mass signal as a function of time will be directly related to its concentration with depth below the surface. The depth achieved will depend on a variety of factors such as the ion beam and the ion impact on the surface. SIMS imaging [43] involves moving the probe

enabling it to raster across the surface of a sample and is discussed in greater detail in section 1.7.4.

### **1.3.7. Fast Atom Bombardment (FAB)**

Fast atom bombardment was first described in 1981 by Barber and colleagues [44]. It was a pioneering ionisation technique for the analysis of biomolecules such as the neuropeptides enkephalins [45] and was applied for the identification of molecules such as the antibiotics bleomycins [46] in the 1980s and early 1990s which paved the way for the surge in interest in biological mass spectrometry that was to follow. FAB involves the generation of a fast atom beam of neutral atoms (Ar or Xe with kinetic energy of 6-8 keV) in a FAB gun. It involves ionisation, acceleration and neutralisation of this fast atom beam which then penetrates into a viscous sample in a solution dissolved in a matrix, usually glycerol. In positive mode, positive ions are formed whilst in negative ion mode, negative ions are formed,  $[M+H]^+$  and  $[M-H]^-$ , respectively, which are generally stable with little fragmentation occurring. Important applications of these techniques have included analysis of steroids and their metabolites e.g. [47] and bile acid analysis e.g. see [48], for further examples of early work carried out see the review by Mosin [49].

### **1.3.8. Electron Ionisation (EI) and Chemical Ionisation (CI)**

Electron Ionisation (EI) is another important ionisation method which involves bombardment of molecules in the gas phase (M) with high energy electrons ( $e^-$ ), with an energy of 70eV, resulting in the generation of radical cations ( $[M]^+$ ) and thermal energy free electrons ( $e^-$ ) (Figure 9).

## Figure 9 – Process of Ion Formation in Electron Ionisation



*M is a molecule in the gas phase.*

### Equations based on those in [50].

Often the molecular ions formed are unstable and will undergo fragmentation to form stable product ions (Figure 9). Thus, electron ionisation will result in fragmentation which can have both advantages and disadvantages. It will provide structural information. However, as extensive fragmentation can occur, the molecular ion may not always be the most intense ion observed in the spectrum or it may not be observed at all, and thus it may not be possible to determine the molecular weight of the parent. The sample being analysed should be volatile, so it can be converted to the gas-phase before ionisation. This often involves use of a gas-chromatography system as the inlet to the mass spectrometer which will be discussed later in this chapter in section 1.5.3. This has led to the development of derivatisation agents to increase the volatility of non-volatile compounds thus preventing their thermal decomposition, for example see [51] and [52].

Chemical ionisation (CI) is useful if no molecular ion is observed when EI is used. In positive mode the CI ion source contains a reagent gas which is ionised by EI and acts as a proton donor to the analyte and also forms adducts with the analyte. Reagent gases can include methane, ammonia and isobutane. The analyte ions are

formed when reagent gas ions interact with sample molecules (ion-molecule reactions). The resulting product ions are protonated molecules  $[M+H]^+$  which are more stable than the  $[M]^+$  ions formed in EI and thus less fragmentation occurs (Figure 10).

In negative mode, electron-capture negative chemical ionisation (EC-NCI) utilises the electron capturing properties of groups with high electron affinities. Often fluorinated derivatising agents are often used to prepare volatile derivatives with high electron affinities. Ionisation may produce stable  $[M]^-$  ions (Figure 10) or it may result in dissociation into fragments including reagent specific fragments. However, ionisation happens to compounds containing the electron capturing tag, making the technique specific and offering high sensitivity monitoring of a stable  $[M]^-$  ion or a fragment. Often, samples are analysed using both EI and CI to obtain the mass of the parent ion as well as structural information which is useful during chemical synthesis.

**Figure 10 - Process of Ion Formation in a) in Positive Mode Chemical Ionisation using Methane as the Reagent Gas and b) in Electron Capture Negative Chemical Ionisation.**

Positive CI

1.  $\text{CH}_4 (\text{g}) + \text{e}^- \rightarrow \text{CH}_4^{+\bullet} (\text{g}) + 2\text{e}^-$
2.  $\text{CH}_4^{+\bullet} (\text{g}) + \text{CH}_4 (\text{g}) \rightarrow \text{CH}_5^+ (\text{g}) + \text{CH}_3^\bullet (\text{g})$
3.  $\text{CH}_5^+ (\text{g}) + \text{M} (\text{g}) \rightarrow \text{MH}^+ (\text{g}) + \text{CH}_4 (\text{g})$

Electron Capture Negative CI (EC-NCI)

1.  $\text{M} (\text{g}) + \text{e}^- \rightarrow \text{M}^{\bullet-} (\text{g}) + \text{e}^-$
2.  $\text{M}^{\bullet-} (\text{g}) \rightarrow \text{A}^- (\text{g}) + \text{B}^\bullet (\text{g})$
3.  $\text{M}^{\bullet-} (\text{g}) \rightarrow \text{A}^{\bullet-} (\text{g}) + \text{B} (\text{g})$

*Where M is a molecule in the gas-phase and A and B are product ions.*

**Equations based on those in [50].**

#### **1.4. Ion Separation Methods: Mass Analysers**

After ionisation, samples are transferred from the ion source to the mass analyser. Mass analysers separate ions according to their  $m/z$  values using either magnetic or electrical fields. Most of the current mass analysers utilise electrical fields rather than magnetic fields however, ICR (ion-cyclotron resonance) analysers which utilise magnetic fields are popular for small molecule studies. Some of the most common types of mass analysers utilised for biological applications are discussed below.

### 1.4.1. Quadrupole Instruments

The quadrupole mass analyser [53] and quadrupole ion trap instruments were developed by Wolfgang Paul [54]. The linear quadrupole is made up of four parallel rods which have fixed direct current (DC) and alternating radio frequency (RF) potentials applied (Figure 11). Ions from the source are passed along the quadrupole and their motion will depend on the particular electrical fields applied at one particular time. Only ions which have a particular  $m/z$  will have a stable trajectory when a particular electric field is applied, and are able to move through to the detector. Those with unstable trajectories are deflected from the central axis and are not transmitted to the detector. By varying the RF and DC and keeping the ratio between them constant, ions with different  $m/z$  ratios will be brought into focus on the detector, creating a mass spectrum. The mass range that can be detected and the resolution will depend on the length and diameter of the quadrupole rods and this in turn will depend on the range of RF voltages applied to the rods. The applied potentials on the quadrupole rods will alter sinusoidally as  $\cos(\omega t)$  cycles with time (t) (Figure 12).

**Figure 11 - Schematic Diagram of a Quadrupole Mass Analyser**

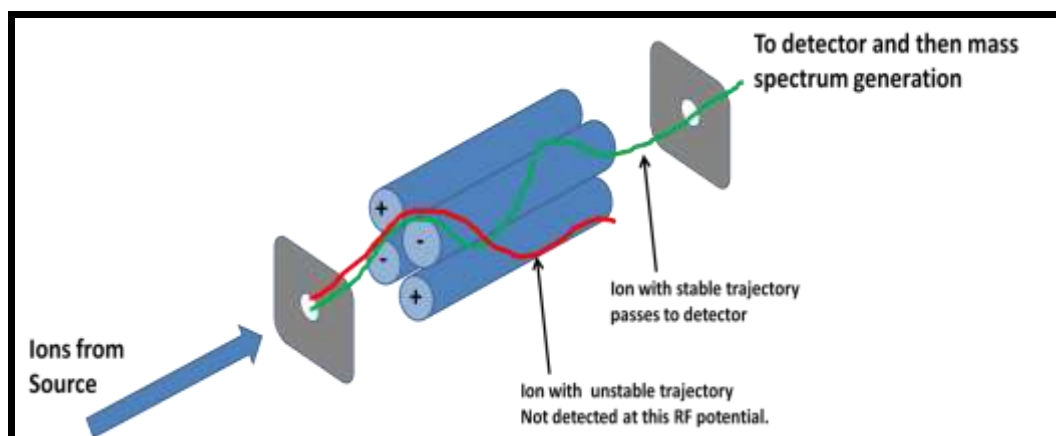


**Figure 12 - Equations at a) Positive and b) Negative Rods in Quadrupole**

a) Positive Rods:  $V(t) = +V_{dc} + V_{rf}\cos\omega t$   
b) Negative Rods:  $V(t) = -V_{dc} - V_{rf}\cos\omega t$

$V(t)$  = voltage at time  
 $V_{dc}$  = direct current voltage (fixed)  
 $V_{rf}\cos\omega t$  = radio frequency (varied)

**Equations based on those in [50].**

Quadrupoles are frequently interfaced with liquid chromatography or gas chromatography systems as they are excellent for high throughput screening studies. They can also be placed in tandem to enable fragmentation studies to be performed such as the triple quadrupole (QQQ) systems [55]. Quadrupoles can also be interfaced with other analysers such as TOF analysers e.g. see [56,57]. Triple quadrupoles are utilised for a variety fragmentation experiments and due to their high specificity and sensitivity they are used for example in drug metabolism and pharmacokinetic studies, [58] and lipidomics [59]. They can be made as bench top



instruments and are relatively inexpensive. However, they are not frequently used for metabolomics studies as the mass accuracy is around 100 ppm and maximum resolution is around 10000 FWHM.

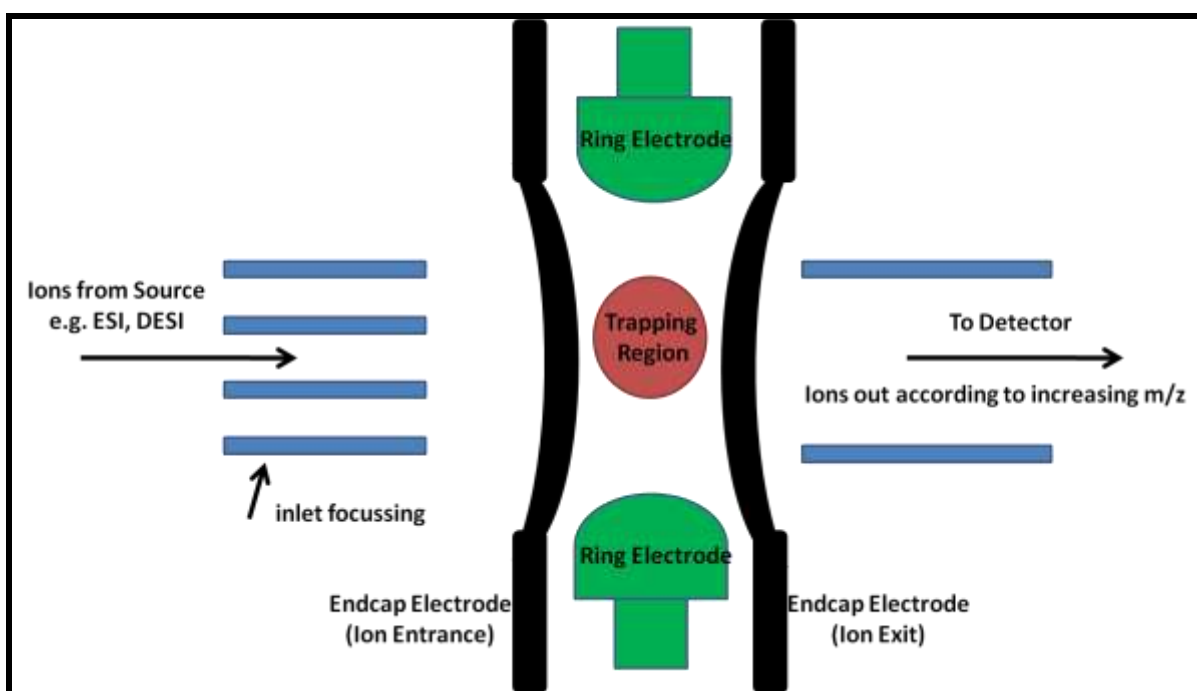
#### **1.4.2. Ion Traps: Ion Trap, Linear Ion Trap, Quadrupole Ion Traps**

As mentioned previously, ion traps were developed alongside quadrupoles by Wolfgang Paul [53,54]. However, it was Stafford and colleagues who developed the quadrupole ion trap allowing it to be developed into a commercial instrument [60,61]. Ions from the source are transported through an endcap electrode to the trapping region. Ions of all  $m/z$  values are kept in the trapping region initially by the action of the ring electrode, entrance endcap electrode and exit endcap electrode which have varying voltages applied that enable ions to be trapped (Figure 13). By ramping linearly the amplitude of the RF applied to the ring electrode (the RF is held at a constant frequency) different ions will be ejected at specific RF amplitudes and the  $m/z$  can be determined since the initial amplitude and the ramping rate are known. A 3D quadrupolar potential will be produced, trapping the ions in a stable oscillating trajectory but by altering the amplitude of the RF applied to the electrode the ion motions will be destabilised resulting in ejection of the ions, which occurs according to increasing  $m/z$ . The stream of ejected ions is then focused onto the detector to generate a mass spectrum. This method to measure the  $m/z$  of confined ions is called the ‘mass-selective axial instability mode’, developed by Stafford *et al* [60,61].

Ion traps have a mass accuracy of approximately 100 ppm, mass resolving power up to 10000 FWHM and like quadrupoles they are compatible with API and vacuum sources. They are a staple in analytical laboratories for compound screening with

low costs,  $MS^n$  capabilities and they are bench top instruments. Linear ion traps can be combined with quadrupoles, (QTrap, Applied Biosystems), Fourier transform (LTQ-FT-Ultra) and LTQ-Orbitrap (Thermo Scientific) as hybrid instruments. As the instrument acts as a trap it is useful for  $MS^n$  studies as ions of interest can be selected in the instrument method and all other ions will be expelled, allowing fragmentation of the isolated precursor ion using collision induced dissociation. The fragmentation can be repeated and assuming the sample is concentrated enough and the trap has good trapping efficiency,  $> MS^5$  can be carried out. A detailed review on the development of quadrupole ion traps has recently been published [62].

**Figure 13 – Schematic Diagram of a Quadrupole Ion Trap.**

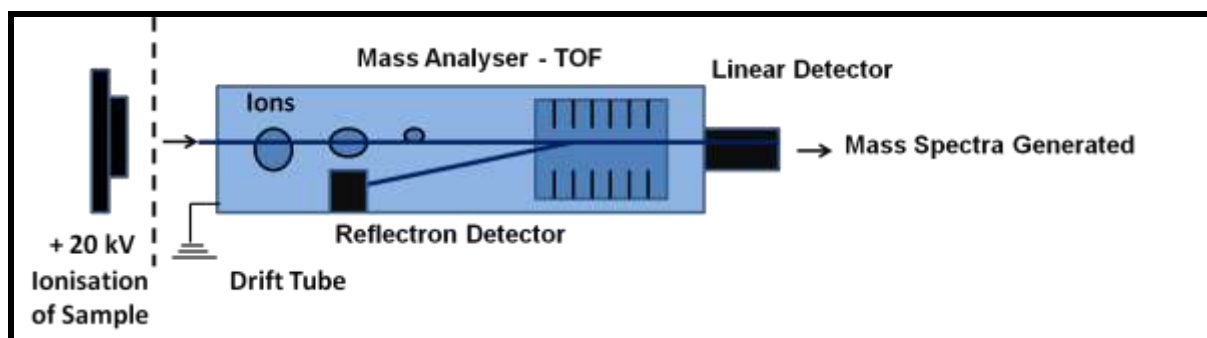


### 1.4.3. Time of Flight: TOF-Linear, TOF-Reflectron, Q-TOF

Time of Flight (TOF) mass analysers provide a useful method for the separation of large ions, allowing the mass determination of peptides and proteins. Time of flight analysers have gained popularity due to the advent of MALDI in the 1980s [24] and early 1990s for MALDI imaging mass spectrometry, discussed in detail in section 1.7.

This type of mass spectrometer separates the ions according to their mass to charge ratios ( $m/z$ ) which are determined by the time it takes for them to travel through the time of flight (TOF) tube. TOF instruments work on the principle that the smallest ions will travel fastest through the flight tube, reaching the detector first. Conversely, larger ions will be collected last at the detector. As the ions reach the detector,  $m/z$  ratio and ion abundance data is collected by a computer thus generating spectra. TOF instruments can be operated in either linear or reflectron mode (Figure 14). In reflectron mode, a series of plates focus the energy of ions from the drift tube and reflects them back along the drift tube to a detector, thus doubling the length of the flight and increasing resolution. Linear mode is utilised for the detection of higher molecular weight ions. In TOF separation, ions are propelled using an electrostatic field into a field free region. The reflectron is used to focus the kinetic energy of a particular ion prior to it entering a second or third field free region.

**Figure 14 - Diagram of TOF Analyser**



Equations used to calculate  $m/z$  values in TOF instruments are shown below (Figure 15). Ions in the source are propelled through a potential ( $V$ ) and there they will gain kinetic energy (Equation 1). Thus  $m/z = 2eV/v^2$  (Equation 2). Then  $t$  is the time taken for the ions to travel down the length of the drift tube to reach the detector (Equation 3). Instrument specifications will mean that different instruments can have different  $d$  (length of drift tube) and  $V$  (potential), (Equation 4).

**Figure 15 - Equations Illustrating the Process of Time of Flight based on those in [50].**

$$1) \quad mv^2/2 = zeV$$

$$2) \quad m/z = 2eV/v^2$$

$$3) \quad (m/z)^{1/2} = (2eV)^{1/2} \cdot t/d$$

$$4) \quad t \propto (m/z)^{1/2}$$

*V = potential  
 $mv^2/2$  = kinetic energy  
 $m$  = mass of ion  
 $z$  = number of charges on ion  
 $e$  = charge of an electron  
 $t$  = time taken for ion to travel down drift tube  
 $d$  = length of drift tube*

TOF instruments are often used with pulsed sources such as MALDI and with API sources. Hybrid mass analysers include the TOF analyser with quadrupoles (Q-TOF), ion traps (QIT-TOF) or arranged in parallel to form (TOF-TOF) instruments enabling tandem mass spectrometry. TOF instruments can also be interfaced with API sources in which the ions are pulsed orthogonally into the TOF analyser [63,64]. Advantages of TOF instruments include that they have an unlimited mass range, enabling detection of intact peptides and proteins e.g. see [22,65-70]. Regarding older TOF instruments, the resolution and mass accuracy is lower than the Orbitrap mass analysers however a mass accuracy of 2-50 ppm can be achieved with a resolution of 20 000 when operating in reflectron mode, offering a cheaper alternative to Orbitraps for metabolomics experiments. However, new generation high performance TOF instruments are now available. They have a resolving power > 30 000 for peptides, mass error of less than 2 ppm and a detection limit of approximately 1 amol. Current goals are to increase the resolving power to > 100 000, mass error to < 1 ppm and to improve the dynamic range.

#### **1.4.4. FT-ICR- Fourier Transform Ion Cyclotron Resonance**

Fourier transform ion cyclotron resonance (FT-ICR) mass spectrometers [71] utilise a magnetic field to trap ions instead of an electrostatic field. Following ionisation, ions are transported into the analyser cell which is in a strong magnetic field held under high vacuum. Ions move within the cell with cyclotron motion which is determined by their cyclotron frequency and this frequency depends on their  $m/z$  value. The cyclotron frequencies are detected as an induced/image current as they pass into a receiver plate and are converted into  $m/z$  values using Fourier

transformation. FT-ICR provides high resolution of  $> 100\,000$  and accurate mass measurement with 1-5 ppm accuracy.  $MS^n$  experiments can be performed and they are compatible with API and vacuum ionisation sources. They can also be interfaced with liquid chromatography e.g. see [72]. However, the scanning speeds are slower because  $m/z$  values are determined by frequencies (which are measured in time (s)). Additionally, these instruments are extremely expensive and require a lot of laboratory space. However, there are many examples of the use of FT-ICR for macromolecule and small molecule studies e.g. see reviews [73,74]. Additionally MALDI sources can also be combined with FT-ICR mass analysers for small molecule imaging experiments [75] and FT-ICR has also been used for metabolomics experiments e.g. see [76].

#### **1.4.5. LTQ-Orbitrap Mass Analyser**

The development of the LTQ-Orbitrap has helped facilitate the explosion in the quantity of metabolite profiling that is being carried out now in many laboratories across the World, offering accurate mass capabilities, high resolution and sensitivity as well as ease of operation. They are also more affordable costs compared to FT-ICR instruments. The development of the LTQ-Orbitrap, its features, the mechanism of ion trapping and the development of second-generation instruments are discussed below.

##### **1.4.5.1. Development of the LTQ-Orbitrap**

Development of the LTQ-Orbitrap has had a huge impact on the field of mass spectrometry. Dr Alexander Makarov is accredited with the discovery and

development of the Orbitrap Mass Analyser. He constructed the first orbitrap with colleagues R Lawther, A Hoffman and S David at HD Technologies in Manchester in 1996/1997, with the first spectra being obtained in 1998 and a resolving power of 160 000 achieved in 1999. The acquisition of HD technologies by Thermo Scientific in 2000 enabled Makarov to further develop the technology, with relocation to Bremen in 2002. The Orbitrap is a type of electrostatic ion trap that forms part of the LTQ-Orbitrap (linear trap quadrupole) hybrid MS/MS (the first commercial orbitrap) that was showcased at the ASMS conference in 2005 by Thermo Scientific and there were several publications released on this groundbreaking instrument in 2005 and 2006 [77-82].

#### **1.4.5.2. Features and Advantages of the LTQ-Orbitrap.**

The LTQ-Orbitrap provides mass accuracy of < 1ppm [82], excellent resolving power up to 100 000 (FWHM), high sensitivity (< 1 ng/ml) and high dynamic range [79]. It is an electrostatic ion trap but utilises Fourier transformation, like an FT-ICR instrument, to determine  $m/z$  values. The  $m/z$  range that can be analysed is 1-4000 making it popular for small molecule profiling experiments. Additionally, the LTQ-Orbitrap is compatible with ESI and APCI sources and recently a MALDI source has been developed to enable accurate mass imaging mass spectrometry to be carried out which is discussed in more detail in section 1.7.2.2. Additionally the instrument is floor standing, less expensive and has lower maintenance costs not requiring liquid helium cooling, giving it advantages over the conventional FT-ICR-MS instruments. The instrument has a linear ion trap, C-trap and Orbitrap parts (Figure 16).

Fragmentation is performed in the linear ion trap but ions formed are then drawn into the Orbitrap for analysis. Thus, sensitivity is provided by the linear ion trap which is combined with the resolving power of the Orbitrap. Ions formed in the source are drawn into the mass spectrometer, first to the linear ion trap where they can be analysed in either full scan or MS<sup>n</sup> modes. Ions can be detected at the linear ion trap or they can be axially injected into the intermediate C-Trap before being drawn into the Orbitrap by increasing the voltage on the central electrode.

**Figure 16 - Diagram of the LTQ-Orbitrap Instrument.**

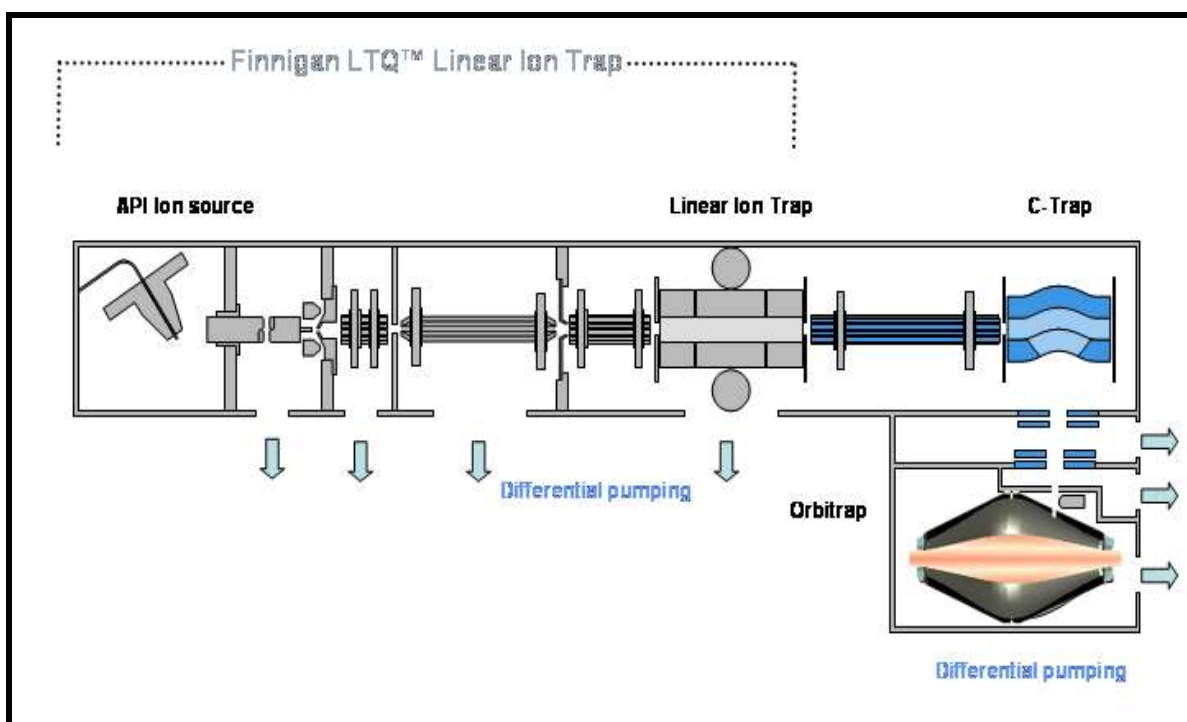


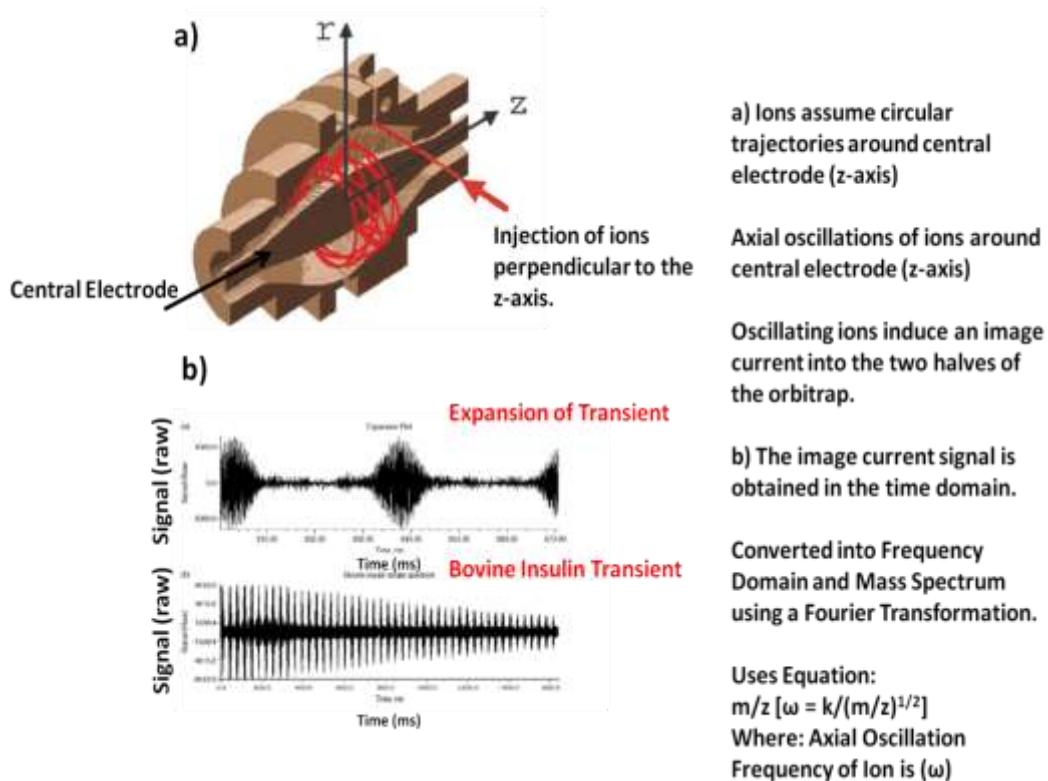
Diagram taken from [83].



### 1.4.5.3. Ion Separation in the Orbitrap

The development of the Orbitrap stems from the principle of Orbital trapping, the ability to trap charged particles in electrostatic fields [84]. The Orbitrap is a purely electrostatic trap with no magnetic or radio frequency (RF) electric fields. Ions are injected into the orbitrap perpendicular to the z-axis (central electrode). When ions are trapped in the Orbitrap, they assume circular trajectories and form axial oscillations around the central electrode z-axis. The ions have energy to do this due to being injected with a velocity perpendicular to the z-axis (displaced from  $z = 0$ ) as this gives the ions energy in the z-direction, causing oscillations. The oscillating ions then induce an image current signal in the time domain. This is then converted into a frequency domain and mass spectrum using a Fourier transformation (Figure 17) [78,80]. The frequencies of rotation of the oscillating ions are related to their  $m/z$  value.

**Figure 17 - Schematic diagram of the orbitrap mass analyser (cut-away view). Ions are injected (red arrow). They are injected with a velocity perpendicular to the long axis of the Orbitrap (z-axis).**



**Original diagrams taken from [81] and adapted.**

The first generation Orbitrap instruments were so successful that the technology is constantly evolving with next generation Orbitraps including the LTQ-Orbitrap Discovery, LTQ Orbitrap XL, LTQ Orbitrap Velos, and the Exactive, (a bench top Orbitrap which is discussed in section 1.4.5.4.) The LTQ Orbitrap Discovery is a highly sensitive system providing accurate mass and high resolution for general metabolomics and proteomics applications [85], The Orbitrap XL has LTQ-XL linear ion trap instead of conventional LTQ which has a built on HCD (higher energy

collisional dissociation) cell for flexibility in fragmentation experiments, enabling high and low energy fragmentation to be carried out [86].

The Orbitrap Velos launched in 2009 is the most advanced Orbitrap instrument to date. It has the same Orbitrap technology but has an API source with new s-lens optical technology and a dual pressure linear ion trap replacing the standard LTQ [87]. The dual pressure linear trap can alternate between high and low pressures to improve isolation, fragmentation efficiency during high pressure and improve scan speed, resolving power and mass accuracy during low pressure. There are also multiple methods for performing fragmentation, CID (collision induced dissociation), HCD (high energy collisional induced dissociation) and ETC (electron transfer dissociation) (Figure 18).

**Figure 18 - Diagram of the LTQ-Orbitrap Velos**

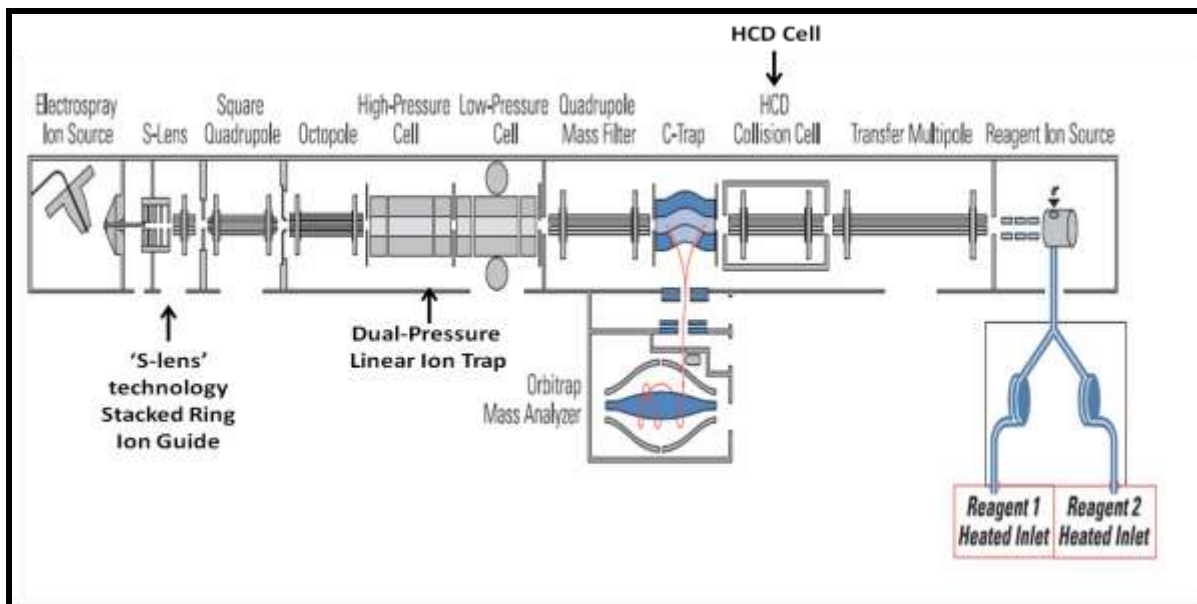


**Figure taken from [88] and adapted.**

#### 1.4.5.4. LTQ Exactive Mass Analyser

The Exactive is a bench-top Orbitrap instrument which is ideal for high throughput screening and compound identification [89]. It has high resolution of up to 100 000, accurate mass from Orbitrap technology, wide dynamic range covering four orders of magnitude and fast scanning capabilities (up to 10 Hz) making it ideal for a variety of experiments [89]. Additionally, fast polarity switching can be used allowing acquisition of positive and negative ion data in a single experiment without compromising mass accuracy. One scan is obtained in positive and one in negative ion modes per second. Samples are introduced through the atmospheric pressure ionisation source by direct infusion or through HPLC. Thus the instrument has a variety of applications including high throughput screening, biomarker discovery, metabolomics, quantitative analysis and for exact mass measurements during organic synthesis. Figure 19 shows a diagram of the Exactive instrument parts.

**Figure 19 - Diagram of the Exactive Instrument.**

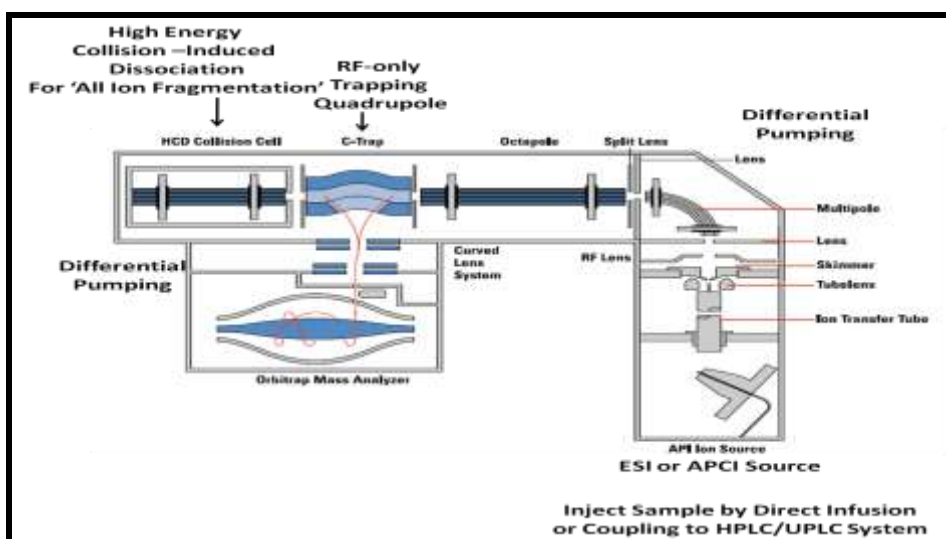


**Figure taken from [89] and adapted.**

Ions are injected into the mass spectrometer via the source which can be ESI or APCI. Ions pass through four stages of differential pumping through RF only multipoles into a curved RF only quadrupole, the C-trap. Ions in the C-trap accumulate and their energy is dampened using nitrogen. They are then injected via a curved lens system which provides a further three areas of differential pumping before being passed into the Orbitrap. Here, mass spectra are acquired via image current detection. The Exactive can be fitted with an HCD cell into which ions are passed from the C-trap to be fragmented. The voltages in the HCD cell are then ramped to allow the ions to be passed back into the C-trap before injection into the Orbitrap.

### **1.5. Separation Methods**

Metabolomics in its simplest form aims to quantitatively measure all metabolites in a biological sample [90] such as plasma, cell or tissue extracts which are complex biological matrices. This means that in any given sample there are a wide variety of small molecules which will have different physiochemical properties with varying size, polarities and charges. Additionally, as some metabolites are very abundant in, for example, membrane components such as phosphatidylcholine lipids, there is a risk of ion suppression associated with direct infusion. There are also structural isomers which cannot be distinguished by using direct infusion. Thus, to combat these issues metabolite analysis using mass spectrometry is often coupled to a prior chromatographic separation stage. Commonly utilised separation methods for metabolomics experiments are discussed below.

### 1.5.1. Reversed Phase Chromatography

Reversed phase chromatography (RPC) is often used for metabolomics analyses. This involves using columns with 2.1-4.6 mm i.d and 5-25 cm length that are packed with 3-5  $\mu\text{m}$  particles. Silica-based particles are used for liquid chromatography column packing and different phase chemistries (e.g. presence of bulky side chains) are developed and optimised for different applications. Improvements in silica manufacturing have meant that smaller particles have been developed which have high efficiencies. These are utilised with a gradient elution with varying run times (minutes to hours). RPC is useful for the analysis of medium to low polarity compounds and is commonly employed for the analysis of lipophilic drug compounds in biological matrices. These columns have some disadvantages. Highly polar compounds are not well retained on reversed phase columns and others may elute in the void volume of the column. Additionally, lipophilic compounds such as phospholipids may accumulate during runs, eluting in subsequent runs, disrupting analysis and causing ion suppression.

Reverse phase chromatography with amine ion pairing agents such as tributylamine [91] or hexylamine [92] is useful for the separation of negatively charged molecules, where they act as volatile cations forming ion pairs with negatively charged molecules to improve resolution and separation on reverse phase C18 columns. It has also been demonstrated that this offers improved sensitivity and separation compared to hydrophilic interaction chromatography for specific analytes (HILIC) [91]. However more work is needed to explore the use of ion pairing reagents in positive mode. Heptafluorobutyric acid and nonafluoropentanoic acid were used as

ion pairing reagents in positive mode for the analysis of cytarabine, an anticancer drug, in mouse plasma using an APCI source [93]. However, reagents such as hexylamine cause ion suppression in positive ESI mode and should not be introduced into an ESI source unless it can be dedicated to one mode of analysis.

Ultra-high performance liquid chromatography (UPLC) has been another development driving the use of liquid chromatography mass spectrometry (LC-MS) for metabolomics which combines smaller particle sizes with systems that can operate with higher than normal pressures [94-96]. When silica based columns with small particle sizes were combined with conventional HPLC systems, flow rate had to be kept low to avoid high back pressures. The UPLC systems combat this with a maximum system back pressure of 15000 psi permitting the use of sub 2  $\mu\text{m}$  particles in columns of 1.0 mm or 2.1 i.d columns and length of 30 or 50 mm at flow rates up to 2 ml/min. Utilising UPLC results in higher chromatographic efficiency, improved resolution and higher peak count.

There are many examples of the use of UPLC for metabolomics studies in the literature including analysis of urine and plasma from normal and diseased animal models [63,64,94,97,98] where it has been shown to offer improved resolution, speed and sensitivity over conventional RP columns [63].

By combining a UPLC method using reverse phase ion pairing liquid chromatography with the Exactive mass spectrometer it has recently been shown that it was possible to detect 137 metabolites from *Saccharomyces cerevisiae* (Baker's yeast) and to conduct fluxomics (measurement of metabolite fluxes by interpreting stable isotopes patterns) on these [99]. By implementing 2 dimensional-LC-MS

chromatographic methods it is possible to detect even more metabolites. Strong anion exchange is used to fractionate samples (for retention of polar compounds) prior to injection onto a reverse phase column for further separation. This method was used in combination with capillary RPLC to increase the number of metabolites detected in *Escherichia* lysates and islets of Langerhans samples [100].

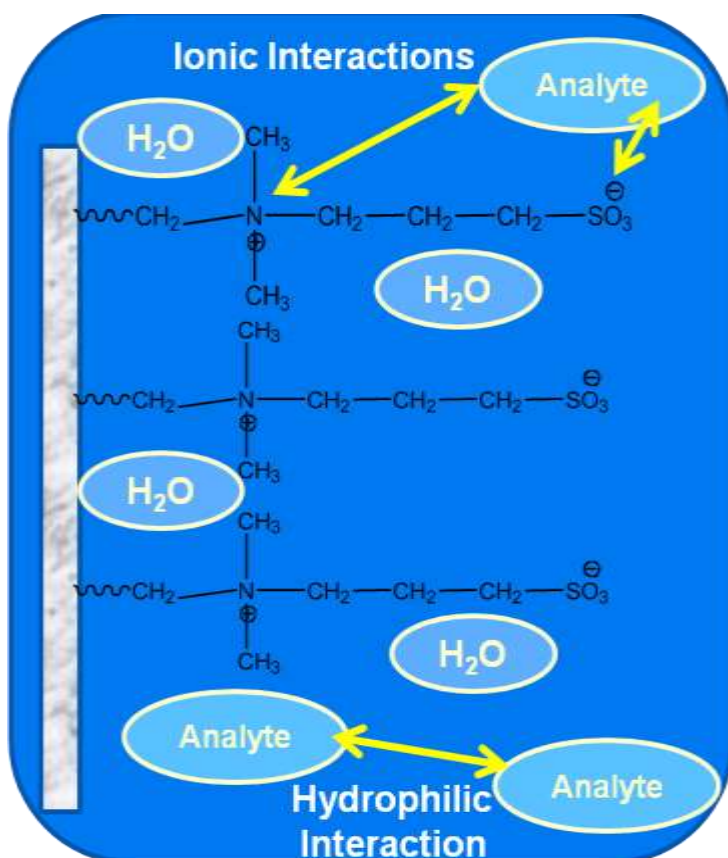
### **1.5.2. Hydrophilic Interaction Chromatography (HILIC)**

Hydrophilic interaction chromatography (HILIC) chromatography is useful for the analysis of highly polar metabolites which are poorly retained on RP columns due to the hydrophobic nature of the stationary phase [101]. In RP chromatography, the more lipophilic a compound is, the more strongly it will be retained (more van der Waals interactions). Modern HILIC columns are silica-based with hydrophilic stationary phase coating, for example in the case of the ZIC-HILIC phase, containing sulfobetaine zwitterionic functional groups. Water binds to these zwitterions, and the low net surface charge associated with this stationary phase enables partitioning of the polar analytes in biological samples into the hydrophilic environment of the HILIC stationary phase [102] without there being strong ion exchange interactions. HILIC chromatography is similar to normal phase liquid chromatography except that the non-aqueous mobile phase is replaced with a water miscible organic solvent, such as acetonitrile, promoting hydrophilic interactions between the analyte and the water-rich stationary phase (Figure 20). Gradients used for HILIC use organic solvents (for example starting at 95% Acetonitrile) in either water or buffer. Suitable buffers that are soluble in a high percentage of organic solvents used in HILIC mode include



ammonium acetate and formate (5-20 mM). The ZIC-HILIC phase is stable over the pH range of 3-8 [103].

**Figure 20 – Mechanism of Hydrophilic Interaction Chromatography**



Consequently, HILIC has been used for the detection of polar metabolites found in aqueous biofluids such as urine, serum and plasma [104-110]. Additionally, it has also been used for the detection of the neurotransmitters acetylcholine, serotonin, dopamine, gamma-aminobutyric acid (GABA), glutamate and aspartate in primate cerebral cortex [111]. Detailed reviews of the principles of HILIC chromatography and its applications for metabolomic studies have recently been published [112,113]. Several groups have also optimised HILIC-ESI-MS conditions for the analysis of various metabolites in different cell populations, such as the bacterium *Escherichia*

*coli*, [114-116] yeast *Saccharomyces cerevisiae*, [116-118] and parasite *Trypanosoma brucei* [119].

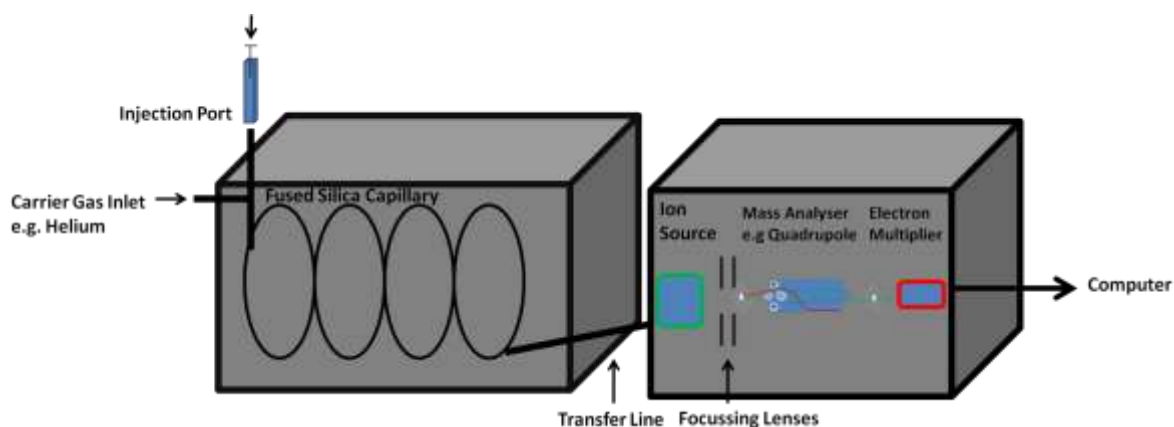
### 1.5.3. Capillary Gas Chromatography

Gas chromatography mass spectrometry (GC-MS) is useful for the identification of volatile and semi-volatile organics in complex mixtures. GC is also highly sensitive, and can detect components at picogram levels. For GC analysis, samples should be thermally stable and volatile. Samples should be in solution in organic volatile solvents prior to injection. Compounds with vapour pressures of  $> 10^{-10}$  Torr can be analysed by GC. For polar compounds with vapour pressures lower than this, samples can be derivatised prior to injection to make them more amenable to sample vaporisation. Gas chromatography is ideally combined with EI and CI sources as both rely on samples being in the gas-phase for analysis. Derivatives should be thermally stable, provide structurally informative mass spectra and be easy to prepare.

GC was developed in the 1950s and shortly after this it was combined with mass spectrometry however pressure incompatibility problems (approximately 8 or 9 orders of magnitude higher in GC than MS) had to be solved, and the first approach was to only put a fraction of the GC sample into the mass spectrometer, venting the remainder to the atmosphere [120] but as this lost a lot of sample better GC-MS interfaces were developed [121]. These reduced the pressure of the GC sample and separated the carrier gas from the analytes. The most important GC carrier gas separator now is the jet separator which interfaces packed GC column with the mass spectrometer [122] but today this is only used for limited number of applications for

example where a thick stationary phase GC column is needed. Today capillary GC columns are utilised and interfacing GC with MS involves injecting all the carrier gas flow into the ion source [123] (Figure 21). This can work because the GC gas flow is kept small and the pumping speed of the mass spectrometer vacuum can handle the high gas flow. Fused silica capillaries are now common place and these are inserted directly into the ion source. The sample is injected into the GC inlet and it is vaporised and swept into the column by the carrier gas which is usually helium, with the compounds separating depending on their interactions with the stationary phase (as in liquid chromatography) and the carrier gas. The column passes into a heated transfer line to the ion source and here ions are generated using EI or CI.

**Figure 21 – Schematic of Gas-Chromatography Mass Spectrometry System**



Commonly utilised derivatisation agents in small molecule profiling experiments include N,O-bis(trimethylsilyl)trifluoroacetamide (BSTFA) to make TMS (trimethylsilyl derivatives) [124] of hydroxyl groups, which are easy to prepare. For example this can be used to derivatise hydroxyl groups from steroids, and for many more examples see Griffiths *et al* in the Encyclopaedia of Mass Spectrometry [125]. Other derivatisations include formation of methyl esters which involves the

esterification of analyte carboxylic acid functional groups for example in the analysis of fatty acids. Additionally alkyl oxime derivatives may also be formed for reacting carbonyl functional groups. For additional information on methods for derivatisation of specific metabolite functional groups see the following as example references: silylation [126], acylation [127] and derivatisation of monofunctional compounds [128].

#### **1.5.4. Capillary Electrophoresis**

Capillary electrophoresis is another separation technique that can be utilised for metabolite profiling experiments. Separation by capillary electrophoresis is based on the principles of electrophoresis, which separates ions depending on their electrophoretic mobility. This will depend on the charge of molecules, their size and the viscosity of the buffer they are run in. The rate ions will move is proportional to the field strength of the applied electric field and their electrophoretic mobility [129]. Capillary electro separation methods include capillary zone electrophoresis (CZE) and capillary gel electrophoresis (CGE). Capillary zone electrophoresis is the most commonly used separation method and it can separate components in a solution with high efficiency.

CE was first presented in 1987 [130] and since then it has been frequently interfaced with electrospray ionisation [131]. Examples of mass analysers utilised included quadrupole ion trap [132], TOF [133,134], and FTICR e.g. see [135]. There are many examples where CE-MS has been used in clinical diagnosis and biomarker identification to investigate charged peptide profiles in samples such as urine and serum, for example see [136-141]. Specific recent examples include profiling saliva

to obtain disease specific profiles in samples from oral, breast and pancreatic cancer patients utilising CE-TOF-MS illustrating the potential of salivary metabolomics as a diagnostic tool for diagnosing cancer [142] and analysis of polypeptides in urine samples to obtain diagnostic markers of kidney cancer [143]. Other examples include using CE offline in combination with MALDI, which involves depositing sample eluting from CE onto a matrix for subsequent MALDI analysis e.g. [144,145].

### **1.6. Introduction to the Metabolome and Metabolomics/Metabonomics.**

It was in 1971 that Horning and Mamer conducted the first ‘metabolomics’ experiments using mass spectrometry [146,147]. In the same year there was also the first publication in this field when Pauling and Robinson illustrated that concentration of >200 substances could be quantitatively determined in human breath and urine vapours [148]. However it was not until nearly 30 years later that the terms metabolomics and metabonomics were coined. Metabolomics was originally described as the measurement of a metabolite pool that exists within a cell under a particular set of conditions [149] whilst the term metabonomics was described as the ‘..quantitative measurement of the dynamic multiparametric metabolic response of living systems to pathophysiological stimuli or genetic modification’[150,151] with ‘meta’ and ‘nomos’ meaning changes and rules/laws respectively [152]. Metabolomics uses mass spectrometry and NMR for the study of the metabolome which is described as all the metabolites found within a sample, which can include cells, tissues, body fluids or organisms [153].

Since the early 1990s there has been some debate over the use of the terms ‘metabolomics’ and ‘metabonomics.’ Today the terms metabolomics and metabonomics are widely used interchangeably in the literature. In this thesis, the term metabolomics shall be used with the realisation that both terms are widely used and are perfectly acceptable to use. Important factors for governing the success of metabolomics experiments such as sample preparation and data processing softwares are discussed in detail in chapter 4 where metabolomics is applied for identification of toxicity biomarkers in the liver in response to treatment with a Liver X receptor agonist.

### **1.7. Introduction to Imaging Mass Spectrometry for Visualisation of Small Exogenous and Endogenous Molecules *in Situ***

Mass spectrometry imaging techniques have gained popularity over the last ten to fifteen years and currently utilised techniques include MALDI, DESI and SIMS. Applications of these techniques include peptide and protein analysis, lipid analysis and detection of drug compounds. The main advantages of imaging mass spectrometry include the ability to map the spatial distribution of compounds *in situ*, preserving the anatomical structure. Sample preparation is relatively quick and easy whilst there is no requirement for radiolabelled compounds/ fluorescent tags. Additionally, sample preparation and instrumental parameters can be tuned to optimise the detection of particular classes of molecules of interest. There is also the possibility of measuring drug metabolites and correlation of levels of metabolites/endogenous metabolites with drug.

There are also limitations of these techniques such as speed of analysis, matrix interferences and effective extraction/co-crystallisation of matrix with analytes in case of MALDI as well as adduct formation and concerns over quantitation. Below, there is an introduction to the use of MALDI, DESI and other ionisation techniques for imaging mass spectrometry applications.

### **1.7.1. Introduction to Use of MALDI Mass Spectrometry for Tissue Imaging Studies**

MALDI imaging experiments involve coating thin cryo-sectioned tissue samples (12  $\mu\text{m}$ ) with an energy absorbing matrix such as  $\alpha$ -cyano-hydroxycinnamic acid ( $\alpha$ -CHCA) which interacts with the sample. Application of laser energy results in interaction of the matrix crystals and analytes and subsequent ionisation of analytes and desorption forming an ion plume (described previously). The sample preparation and matrix application steps are critical for the success of a MALDI imaging experiment. These are discussed in detail in chapter 2. Tissue imaging experimentation involves the generation of a raster across the tissue area whose coordinates are then programmed into the computer. A specific spacing is set up and each (x,y) coordinate scanned will contain a unique spectrum representing the molecular composition of the tissue at that point. A two dimensional molecular map can then be created containing all the data points in the form of pixels which represent particular masses. From this, the image can be analysed to detect the localisation of a specific molecule with a known  $m/z$  within the tissue sample and reveal its relative intensity which is displayed as a heat map [22] (Figure 22). A picture showing the internal components of a MALDI TOF mass spectrometer is

shown in Figure 23 to illustrate where the sample plate is inserted, the position of the camera, laser and the TOF tube.

**Figure 22 - Schematic Diagram of Steps involved in MALDI-MS Tissue Imaging Experiment**

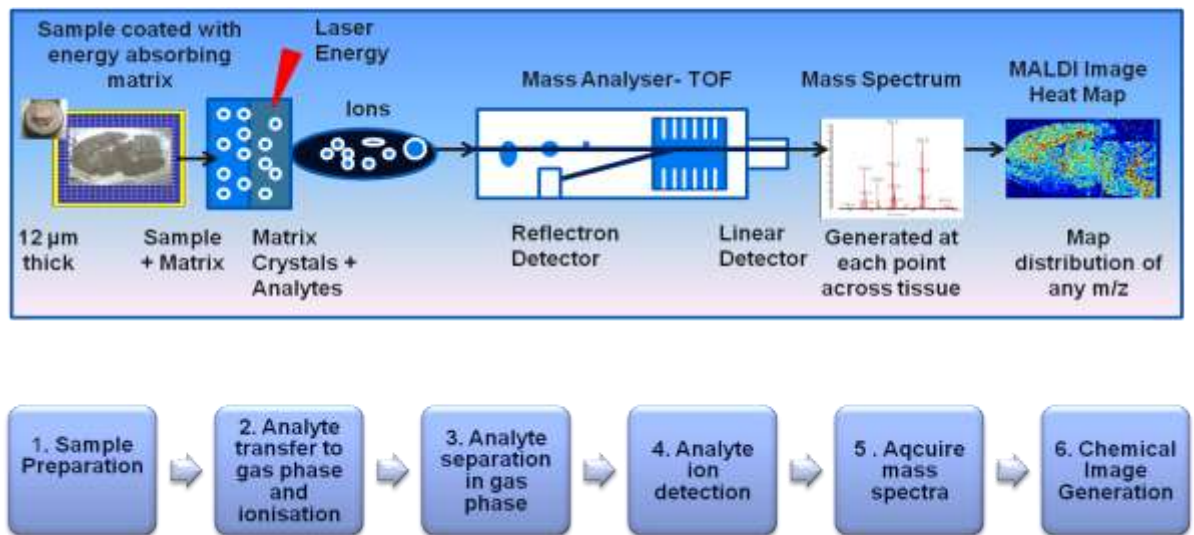
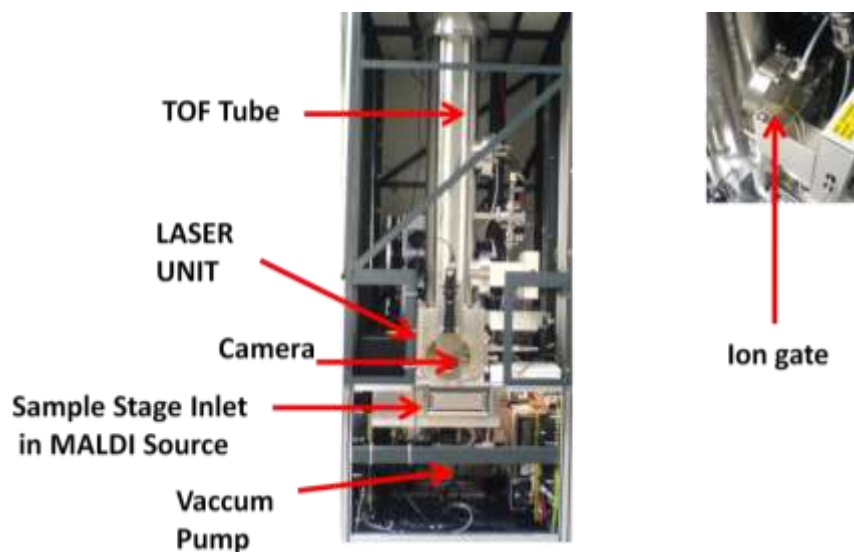


**Figure 23 - Picture of Internal Components of a MALDI TOF Mass Spectrometer**





Files acquired by different manufacturer's instruments can be converted to files compatible with the tissue imaging software BioMap, provided by Novartis Institute of Biomedical Research [154]. Alternatively commercial imaging software packages are available. Particular features of imaging software packages are discussed in more detail in chapter 2. The main goals of imaging software are to enable the conversion of raw data files into imaging files, enabling the distribution of various analytes to be mapped within a selected mass range. From tissue imaging files, specific regions of interest can be selected and the mass spectral data accompanying this displayed. From one tissue raster it is possible to create a set of images corresponding to selected masses of interest, allowing the localisation of potential biomarkers. Analysis of spectra can enable the detection of drug molecules in tissue from animals that have been dosed with a drug. In addition, peaks of interest from the spectrum can also be mapped using this technique to reveal potential biomarkers associated with the drug distribution. Interestingly, 3D reconstruction of images has also been carried out to enable the visualisation of the distribution of proteins and peptides in smaller brain structures such as the substantia nigra in an entire rat brain using virtual z-stacks and three-dimensional (3D) volume renderings [155]. Many more specific examples on application of MALDI mass spectrometry in imaging are discussed in more detail in subsequent chapters.

### **1.7.2. MALDI Mass Spectrometry for Metabolomics Experiments**

MALDI profiling can be utilised successfully to investigate the metabolic profiles of biological extracts and single cells. The major limitation when analysing small molecules using MALDI is the matrix interferences encountered, particularly  $< m/z$

500 and the intensities of endogenous small molecules. Matrix interferences are particularly encountered in positive ionisation mode. However, in negative mode this can be overcome through the use of 9-aminoacridine as an alternative MALDI matrix which shows limited matrix interferences  $< m/z$  500 in negative ionisation mode which is useful for mapping metabolites such as sugar phosphates and energy metabolites [156]. There are many examples where MALDI-MSI using MALDI TOF and TOF-TOF have been utilised successfully for the analysis of small metabolites in combination with the use of 9-aminoacridine as the matrix of choice. The use of 9-aminoacridine for the detection of endogenous molecules is discussed in more detail in chapter 2.

Imaging mass spectrometry has the potential to provide a metabolite profile at the single cell level allowing the spatial distribution of metabolites in cells (e.g. the abundance of metabolites in specific cellular organelles) to be determined and the regulation of metabolism to be investigated. At the moment, there is no published work showing sub-cellular MALDI images that reveal the distribution of metabolites in single animal cells, due to limitations in the laser spot size and concentration of analytes in single cells. For example, even if the laser spot size was decreased to enable the detection of metabolites in single animal cells, the concentration of analytes in these cells may be too low to be detected. The resolution that is routinely achievable using imaging mass spectrometry that maintains sensitivity is  $50 \times 50 \mu\text{m}^2$  [157]. To achieve higher resolution it is necessary to decrease the laser beam diameter which will allow smaller surfaces to be scanned. However, by decreasing the spot laser beam diameter to less than 30 to 40  $\mu\text{m}$ , there is a decrease in sensitivity and ion production [157]. Thus it will be necessary to optimise MALDI

ionisation parameters and to decrease the laser spot size whilst preserving sensitivity before this can be achieved. At present, levels of sensitivity allow the detection of a small group of animal cells but are not sufficient to detect discrete modification at a single cell level. However this is a highly active research area and in the future this will undoubtedly be achieved.

#### **1.7.2.1. Ion Mobility Separation for MALDI Imaging Experiments**

Ion mobility spectroscopy can also be used in conjunction with mass spectrometry to provide an additional dimension of separation, which is particularly useful in imaging experiments to differentiate between isobaric compounds. The separation is based on the conformation of the ion rather than mass alone. This means two ions with the same mass can be determined using ion mobility separation. Ion mobility instruments are now available commercially and include the Waters Synapt High Definition MS system which uses the travelling waveform ion mobility separation. MALDI Ion Mobility mass spectrometry has been utilised for imaging experiments to map the distribution of vinblastine in rat whole body sections where it was possible to differentiate vinblastine and several fragments from isobaric lipids [158].

#### **1.7.2.2. MALDI-LTQ-Orbitrap Technology**

Another interesting development has been the introduction of the MALDI source for the LTQ-Orbitrap which has a direct beam and nitrogen laser and is compatible with the LTQ Orbitrap Discovery and the LTQ Orbitrap XL instruments. This combines the imaging capabilities of a MALDI source for small molecule and peptide/protein analyses with the high mass accuracy and resolving power of the LTQ-Orbitrap

[159]. It enables low concentration metabolites to be detected due to its high sensitivity. Complementary fragmentation techniques of CID and HCD can be used for MS/MS experiments whilst high resolution precursor ion isolation enables MS<sup>n</sup> fragmentation experiments to be carried out. Other applications include high throughput analysis of in-gel digests of 2D gel spots for protein identification and LC-MALDI analysis can be utilised for protein identification using MS/MS. The MALDI source has a collisional cooling interface, Q00, which collects MALDI ions according to a given automatic gain control (AGC) (pre scan) enabling a high dynamic range to be used which is also preserved even when laser power is increased. The ion packages meeting the requested number of ions are then sent to the LTQ or Orbitrap for analysis. Collection of up to ten pulsed laser shots will meet the required  $1e^6$  charges which are acquired per Orbitrap FT-MS full scan using automatic gain control. Higher laser energies can be used than is possible with the conventional TOF instruments where there is no collisional cooling interface. The matrix clusters are also reduced compared to TOF.

There are now several examples of studies that have been carried out utilising a MALDI-Orbitrap for tissue imaging applications. For example, lipid profiles in nerve tissue have been obtained allowing generation of accurate mass images, and it was observed that the background noise was much lower than from conventional MALDI-TOF experiments [160]. An investigation was also carried out to investigate use of MALDI LTQ-Orbitrap XL for imaging and identification and sequencing of secretory neuropeptides in the American cockroach directly from tissue [161] and metabolite profiling in *Arabidopsis thaliana* using colloidal silver to map epicuticular lipids and lipids in roots has also been carried out [162]. Other

examples of applications of MALDI-LTQ-Orbitrap technology to date include peptide mass fingerprinting utilizing a sensitive matrix 4-chloro-alpha-cyanocinnamic to investigate complex peptide mixtures generated by less specific enzymes, chymotrypsin and elastase [163]. Further examples include sequencing single and double stranded oligonucleotides by acid hydrolysis (strong acids with pH 1-2) and then MALDI LTQ-orbitrap mass spectrometry analysis of the degradation products [164]. There has also been an interchangeable MALDI source developed by Mass Tech which can be coupled to the high resolution instruments such as the LTQ-Orbitrap and Exactive and easily changed for ESI, marketed as the AP MALDI PDF+ ion source [165].

### **1.7.3. Desorption Electrospray Ionisation (DESI) Imaging**

Desorption electrospray ionisation (DESI) has also been utilised for imaging applications. One of the main advantages that DESI offers over MALDI is that there is no requirement for the sample to be coated in matrix before analysis. This means the technique can be used to image small molecules such as drugs without the worry of there being extensive matrix interferences. Limited sample preparation is also required before analysis. Cooks *et al* released the first paper showing its application for tissue imaging in 2006 where it was utilised to image lipid distributions in the rat brain with a spacing of  $< 500 \mu\text{m}$  [166]. To carry out DESI imaging, there is an automated surface stage which can move in the x,y direction so that the DESI can be performed over a tissue area. After further development, it was shown that DESI could be used to image chemicals in fingerprint patterns and rat brain sections [167]. It has also been shown that by altering the solvent characteristics, spray

characteristics and the surface that DESI can be used for compound identification even when higher than physiological levels of salts are present due to the high salt tolerance of this technique [168]. It has also been utilised for glycerophospholipid profiling in the rat brain [169]. By altering the composition of the spray solvent, molecules can be derivatised *in situ*. This was used to image cholesterol in arterial plaques using betaine aldehyde which added a charge to cholesterol enabling its ionisation [170]. It has also been utilised to image lipids in tissue taken from the adrenal gland with spacing of approximately 200  $\mu\text{m}$  [171]. DESI was found to be quantitative when used for the analysis of the pharmaceutical propranolol [172] and it has also been utilised to map clozapine in rat brain sections [173]. One of the main draw backs of the technology at present is the spatial resolution that can be achieved is only approximately 200  $\mu\text{m}$  [174]. For further examples of imaging lipids using DESI in normal and diseased tissue see the review from the same group [175] and for a detailed review on DESI and current applications to date see [176].

#### **1.7.4. SIMS Imaging and Other Novel Mass Spectrometry Imaging Techniques**

Secondary ion mass spectrometry (SIMS) is an alternative ionisation technique which has been utilised for biomedical imaging applications [43]. As it is a destructive technique, it is well suited to imaging as the ion probe can penetrate into the deeper layers of the tissue. However, fragmentation will complicate the spectra obtained. It is often combined with a TOF mass analyser and one of the main advantages of SIMS imaging is that high resolution images can be obtained [177]. Additionally, most SIMS instruments have no tandem mass capabilities, making identification of pharmaceuticals challenging. One of the disadvantages of

conventional SIMS imaging is the limit of detection compared with MALDI. However, this can be overcome for example by utilising matrix or metal [178] to enhance the desorption/ionisation processes [179]. This technique has been utilised for imaging single neuroblastoma cells, revealing subcellular information [179]. As metal TOF-SIMS imaging can provide subcellular information, it may become an important technique for *in situ* metabolomics experiments [180]. Other interesting examples include mapping lipids in colon from CFTR knockout (model of cystic fibrosis) and control mice to identify alterations in lipid profiles using TOF-SIMS [181]. A detailed review contrasting the advantages and disadvantages of MALDI and SIMS for imaging experiments has been published [182]. Additionally, they have been utilised as complementary techniques for profiling phospholipids, neuropeptides and proteins in rat spinal cord sections [183]. The raster spacing for MALDI-MSI images was 125  $\mu\text{m}$  whilst the raster spacing for SIMS images was 2-3  $\mu\text{m}$  [183].

Another novel imaging technique is nanostructure initiator mass spectrometry (NIMS) which was developed by Siudzak and colleagues [184,185]. NIMS is a matrix free approach whereby 'initiator' molecules trapped in nano-structured surfaces or 'clathrates' are utilised to release and ionise intact molecules adsorbed from the surface of a sample e.g. lipids/drugs/peptides in rat brain section. Following ionisation, ions are released from the surface for detection. NIMS is utilised with conventional nitrogen or Nd:YAG frequency tripled lasers, is a soft ionisation technique and it can be coupled with other MS/MS platforms e.g. TOF/TOF. A disadvantage of NIMS is that the clathrates must be synthesised as they are not yet available commercially and thus the user must be comfortable with

use of hazardous materials such as hydrofluoric acid [184,185]. NIMS has been utilised for the direct analysis of biofluids [186] and to map the distribution of clozapine and n-desmethylozapine in rat brain sections [187]. Recently, NIMS has been utilised for the detection of cholesterol metabolites in mouse brain in Smith-Lemli-Opitz Syndrome [188].

### **1.8. Aims and Objectives**

The pharmaceuticals and technologies utilised in this project were of interest to the collaborating pharmaceutical company. Four separate studies are reported which involved the development of methods based on matrix-assisted laser desorption/ionisation mass spectrometry imaging (MALDI-MSI) and linear ion trap-Fourier transform Orbitrap mass spectrometry (LTQ-Orbitrap MS).

The main aims and objectives of this project can be summarised as follows:

- (i) Optimisation of sample preparation, matrix selection, matrix application and instrument parameters in order to profile the distribution of lipids and small molecules in murine brain, liver and kidney sections using imaging mass spectrometry.
- (ii) Optimisation of sample preparation, matrix selection, matrix application and instrument parameters in order to profile the distribution of experimental drugs *in situ* in murine brain, liver and kidney sections using imaging mass spectrometry.



- (iii) To use high resolution mass spectrometry in order to obtain information on any metabolomic changes produced in brain tissue by drug treatment.
- (iv) To use MALDI MS to analyse lipid biomarkers in rat liver from animals treated with an experimental LXR agonist.
- (v) To carry out metabolomic profiling of rat liver from animals treated with an experimental LXR agonist.

**Chapter 2 - Mapping the Distribution of Endogenous Metabolites in Brain  
Tissue Using MALDI-MSI**

## **2. Introduction**

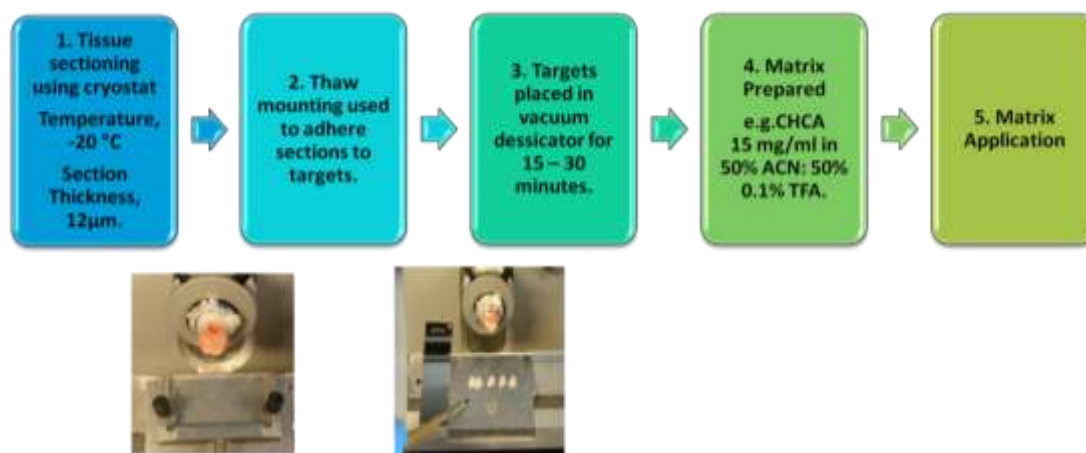
### **2.1. Designing MALDI Imaging Experiments**

The tissue imaging studies in this project will centre on the use of matrix-assisted laser desorption/ionisation mass spectrometry imaging (MALDI-MSI) for imaging endogenous and exogenous molecules *in situ* in animal tissue sections such as rat brain, liver and kidney. Thus, at the beginning of the project, the main aim was to develop methodology to allow the successful detection of common classes of small endogenous molecules found in animal tissues such as lipids, peptides and polar metabolites such as sugar phosphates. The most important factors governing the success of a MALDI imaging experiment are the sample preparation and matrix application steps. These factors are discussed below before details of the methodology utilised are given and the preliminary results are presented and discussed.

### **2.2. Sample Preparation Stages of MALDI Imaging**

In summary, the key sample preparation stages involved in a MALDI imaging experiment are tissue extraction from the study animal, freezing of the samples, sectioning of the samples in a cryostatic chamber, mounting of the samples onto MALDI targets and matrix preparation and application (Figure 24). Each of these key stages is discussed in detail below.

**Figure 24 - Schematic Diagram of Sample Preparation Stages for MALDI MS Imaging Experiment (Parameters Shown are for Brain Samples.)**



### 2.2.1. Harvesting Tissue from Study Animals

Tissue should be removed from the study animal and in order to ensure that the tissue is not degraded or that delocalisation of metabolites occurs, the tissue should be immediately snap frozen in liquid nitrogen cooled isopentane and wrapped in aluminium foil. This will prevent enzyme proteolysis that can lead to tissue degradation [189]. It has been suggested that tissue should be immersed into isopentane very gently as rapidly plunging tissue into it may cause the tissue to shatter [190]. Prior to tissue sectioning, tissues should then be stored at  $-80^{\circ}\text{C}$ . Tissue can be kept at  $-80^{\circ}\text{C}$  until required but it has been suggested that freshly dissected rat brain tissue enables the detection of more peptide and protein signals than tissue sections that have been stored at  $-80^{\circ}\text{C}$  for longer periods of time such as six months [191].

### **2.2.2. Tissue Sectioning and the Thaw-Mounting Process**

Tissue should be sectioned using a cryostat at a temperature of around -20 °C [65]. However, this temperature will vary depending on the sample and lipid content. Generally, tissues which have a high lipid content will require a lower cutting temperature in order to obtain good quality sections with minimum degradation [192]. An important factor to consider when carrying out a tissue imaging study using MALDI MS is that no fixative or embedding agents surround the tissue area that will be sectioned. This is because these agents prevent ionisation of biomolecules and they have been shown to interfere with the MALDI-TOF signals [190,192]. Thus, before tissue sectioning takes place, tissue must be carefully positioned in the cryostat using an embedding agent such as Optimal Cutting Temperature Polymer (OCT) whilst ensuring that the embedding agent does not surround the entire tissue. Depending on the areas of tissue in which localisation of potential biomarkers or drug molecules is required, the tissue can be positioned so that the cryostat will produce tissue sections of the desired orientation. It is also of paramount importance that the slices that are being cut have an even surface, they are taken from the correct depth of tissue and the correct tissue thickness is used. From the current literature, it is clear that the thickness of tissue is dependent on the specific experiment but it has been suggested that the appropriate thickness will range from 5 µm-20 µm [190]. It has also been suggested that thicker slices are easier to handle, although this may compromise spectral quality, but also that thinner slices may become severed more easily [190].

Once the tissue is cut into sections it must be removed from the cryostat and thaw mounted onto a MALDI plate. Sections can be removed using a small brush that should be kept cold in the cryostat, otherwise sections would simply thaw mount onto the brush [190]. Care must be taken to ensure that the sections do not become ripped or curled as this will distort the true nature of the profile within the tissue. The cryostat blade should be kept free from any nicks as these can distort the even surface of the tissue which will be seen on MALDI-MSI analysis. A common method of thaw mounting sections onto the MALDI plate involves positioning a warm hand underneath the plate inside the cryostat once the section has been placed onto the MALDI target plate [65]. Using this method, the tissue section will be quickly thaw mounted onto the MALDI plate [190]. A second, less popular method involves keeping the plate at room temperature and then adhering the frozen tissue to the warmer surface of the plate. However, formation of ice crystals may occur using this method and as soon as the section touches the plate it will thaw mount onto it immediately, making it impossible to change the orientation of the tissue once it has touched the surface of the plate [190]. Another method that has been documented involves sticking tissue sections to double-sided transparent tape which can then be stuck onto the sample plate, eliminating problems such as the difficulty in orientating sections on the target plate or the tissue becoming torn or folded [193]. Additionally, if the analyte of interest is photodegradable care must also be taken to ensure that the tissue and then the prepared slide are kept in the dark in order to prevent degradation [190].

### **2.2.3. Pre-treatment of Tissue Prior to MALDI-MSI Analysis**

After sectioning and thaw mounting the sections can be placed in a vacuum dessicator in order to remove any moisture prior to matrix application. There does not appear to be a clear time scale for maintaining tissue in the vacuum dessicator, it seems to be dependent on tissue type, for example in experiments using rat brain tissue, 1 hour has been suggested [21,194]. A further point for consideration is the pre-treatment of tissue sections with solvents prior to matrix application. From the current literature, it seems that this is dependent on the type of matrix used and the analyte(s) of interest. For example, MALDI plates containing tissue samples can be rinsed twice in 70% ethanol for 30 seconds prior to matrix application for peptide and protein mapping [190]. It has been demonstrated that rinsing mouse liver tissue in 70% ethanol for 30 seconds and then repeating this step will enhance signal quality when using CHCA or Sinapinic acid matrices again for peptide and protein localisation [190]. Variations of this protocol have also been suggested such as rinsing tissue in 70% ethanol for 30 seconds followed by a second rinse for 30 seconds in a solvent mixture containing 90% ethanol, 9% acetic acid and 1% deionised water [65]. In contrast, it has been suggested that rinsing the tissue in ethanol should not be carried out when the analyte of interest is a small molecule such as a drug molecule as its spatial distribution may be altered [193]. Moreover, if the tissue has been pre-treated with ethanol, a longer drying time will be needed before matrix application in order to stop migration of the analytes from the tissue surface when the matrix is applied.

Additionally, two similar tissue sections may be treated using different protocols to allow the comparison of ion images with histological features. One section is prepared using a MALDI matrix in order to obtain a molecular image using MALDI whilst the other is stained with dyes such as haematoxylin and eosin to allow optical evaluation [195] or is photographed using a high resolution digital scanner with medical adapter. This is useful for correlating the distribution of analytes with pathological features in tissue taken from animal models of disease e.g. see [154]. A new protocol has been developed which allows a section to be prepared for both MALDI mass spectrometry and optical microscopy [189]. This method utilises indium-tin oxide (ITO) coated conductive glass slides and staining protocols which are MALDI friendly such as cresyl violet and methylene blue [189].

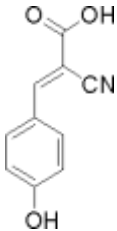
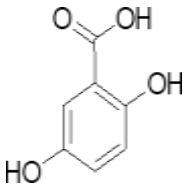
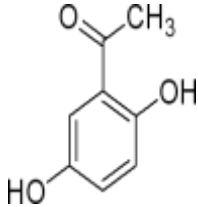
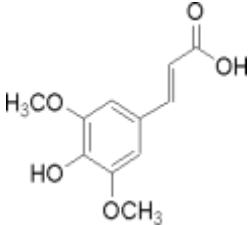
### **2.3. MALDI Matrix Selection**

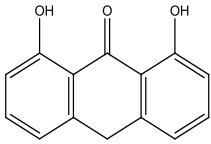
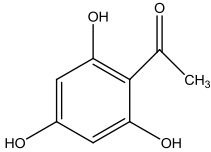
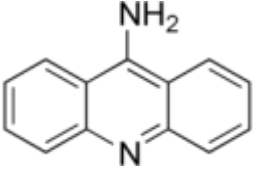
One of the most important factors to consider when carrying out a tissue imaging experiment using MALDI MS is that the most appropriate matrix is selected. This will depend on both the type of tissue that is being utilised and also on the molecular weight of the analyte. Selecting the correct type of matrix for the experiment will ensure that high quality spectra are obtained [190]. MALDI matrices are usually small acidic aromatic molecules which absorb energy at the wavelength of the irradiating laser and there are both solid and liquid types. There are however basic matrices such as 9-aminoacridine. UV absorbing MALDI matrices are benzoic acid based compounds which have chromophores that strongly absorb the laser wavelength and usually have molecular weights of less than 500 Da [193]. Most MALDI matrices are solid substances which are easily protonated and these are



dissolved in a molar excess of solvent that must be compatible with analytes of interest, typically with a ratio of 1:5000 [195]. Other wavelengths include the mid-infrared range where a mixture of matrices are required which are energised by vibrational excitation. Commonly utilised MALDI matrices for tissue imaging studies include  $\alpha$ -Cyano-4-hydroxycinnamic acid (CHCA), 2,5-dihydroxybenzoic acid (DHB), 2,6-dihydroxyacetophenone (DHA) and Sinapinic Acid (3,5-dimethoxycinnamic acid) (Table 1). CHCA and DHB are commonly used for visualising small peptides and small molecules whilst sinapinic acid is commonly used for the identification of larger peptides and proteins. DHA has been shown to have a high sensitivity and it can be used for the detection of lipids, peptides, glycolipids and proteins in the range of 8-100 kDa [196]. It must be noted that because the molecular weights of matrices are usually less than 500 Da, the analysis of small molecules, such as drugs and peptides, can be very challenging when using solely MALDI-MS and often tandem MS is required [193]. Matrix selection for peptides, lipids and polar small molecules are discussed in more detail during this chapter.

**Table 1 - Commonly Utilised MALDI Matrices, Showing Structures and Example uses.**

MALDI Matrix	Structure	Uses
$\alpha$ -Cyano-4-hydroxycinnamic acid (CHCA/ $\alpha$ -Cyano)		Identification of lower mass proteins and peptides (<3 kDa), lipids and exogenous drugs.
2,5-Dihydroxybenzoic acid (DHB)		Identification of small molecules, particularly lipids.
2,5-Dihydroxyacetophenone (DHA)		Identification of molecules such as peptides, proteins and glycolipids with molecular weight of 8 kDa to 100kDa.
3,5-Dimethoxy-cinnamic acid (Sinapinic Acid)		Identification of larger molecular weight proteins.

<p>1,8,9-Anthracerietriol (Dithranol)</p>		<p>Negative mode analysis.</p>
<p>2,4,6-Trihydroxyacetophenone (THAP)</p>		<p>Acidic glycans &amp; glycopeptides in negative mode.</p>
<p>9-Aminoacridine</p>		<p>Basic Matrix Polar metabolites positive and negative mode. Limited interference below <math>m/z</math> 500</p>

The goal of matrix application is to get the matrix to crystallise evenly across the surface of the plate allowing high quality spectra to be obtained [190]. The concentration of matrix that is used is important as it will affect crystal formation and thus the mass spectral data obtained and it has been shown that in general, high matrix concentrations will result in the generation of high quality mass spectral data [190]. The size of crystals that are formed will also depend on the combination of solvents that are used. Crystal formation on the surface of a tissue does not happen as readily as it would on a blank plate due to the presence of lipids, salts, proteins and other biomolecules in tissues so it is of paramount importance that the tissue must have an even surface to maximise crystal formation and create an even coverage of crystals [34]. Additionally, slow crystallisation has been said to reduce the amount of signal suppression that can be produced as a result of salt contamination [22]. Furthermore, light microscopy can be used to assess the formation of a homogenous layer of matrix-analyte co-crystals on the surface of the tissue prior to MALDI-MS analysis [189].

### **2.3.1. Variations in Matrix and Solvent Combinations**

In previous studies, many solvent combinations have been employed to effectively dissolve the matrix of choice and it has been shown that different solvent combinations will also affect the quality of spectral data [190]. Unfortunately, there is not a universal solvent combination that can be used for every tissue imaging experiment. It appears to depend on the analyte of interest and the type of tissue that is being investigated. In some cases, it has been suggested that trifluoroacetic acid (TFA) should be used as a solvent as this will assist with the protonation of proteins

and it has been suggested that TFA at a concentration of 0.3-1% will serve to maximise the number of proteins analysed [190].

Examples of variations in matrix and solvent combination are evident in the literature. For example it has been suggested that solvent combinations consisting of 50% of the organic solvents ethanol or acetonitrile with 50% 0.1% TFA will generate good spectral data when analysing proteins within mouse liver sections [190]. This study also claimed that solvent combinations with 75% or 25% of organic solvents resulted in poorer quality spectra, but it has been suggested that if protein delocalisation occurs to a great extent in a sample, then the 75% solvent combination may minimise this [190]. This study also suggested that sinapinic acid at a concentration of 25mg/ml serves as a good general matrix for tissue applications when analysing proteins when dissolved in 50% acetonitrile and 50% of 0.1% TFA [190]. In contrast, another study utilised CHCA or sinapinic acid dissolved in acetonitrile: water in a ratio of 4:1 [197]. The study demonstrated that these matrices and the above mentioned solvent combinations were best for analysing neuropeptides in the supraoptic nuclei and caudate putamen regions of the rat brain [197]. Moreover, a study investigating lipid distribution in the cerebellum of the rat brain utilised DHA and DHB as the matrices [198]. The study used DHA at a concentration of 10 mg/ml and DHB at a concentration of 20 mg/ml, dissolving both in 50% ethanol [198]. Another study looking at the distribution of the atypical antipsychotic drug clozapine in the rat brain utilised the MALDI matrices CHCA, 3-hydroxypicolinic acid (3-HPA) and sinapinic acid [193]. These matrices were dissolved in either 4:1 acetonitrile: water or methanol:water combinations at concentrations of 25 mg/ml [193]. Interestingly, the addition of TFA or formic acid

did not have any noticeable effects on the quality of mass spectral data that was obtained [193].

### **2.3.2. Use of Liquid Ionic Matrices**

Liquid ionic matrices have also been used for tissue imaging experiments as it is thought that their high polarity allows the matrix to interact strongly with tissue samples [191,199]. They have been used successfully to localise 16 neuropeptides in rat brain tissue with a higher signal intensity than those obtained when CHCA was used alone [199]. Experiments involved using the salts formed from evaporation reactions of CHCA in methanol mixed with an equimolar amount of base such as aniline (CHCA/ANI) or 2,5-dihydroxybenzoic acid (CHCA/DANI) [199]. The salt was then used to prepare a MALDI matrix solution by dissolving it in 2:1 acetonitrile/HPLC water containing 0.1% TFA. Results from these experiments showed that the matrix solutions were better for tissue imaging than the traditional CHCA matrix on its own and factors that were improved included homogenous crystal coverage, resolution and the number of peaks isolated [199]. The use of the liquid meso-tetrakis (pentafluorophenyl) porphyrin as a matrix substance has also been documented [200]. The use of this compound in combination with sodium acetate produced  $[M + Na]^+$  ions and allowed the analysis of some alkylphenol ethoxylates whilst producing less interference from matrix ions compared to CHCA due to its higher molecular weight [200]. However, despite these developments the solid matrices have proven to be a more popular choice and are still used extensively.

### **2.3.3. Improving Signal Sensitivity**

It has also been shown that the addition of other organic solvents can be used to improve signal sensitivity and the localisation of proteins [191]. This group established a tissue washing method to remove lipids from the surface of the tissue, allowing peptide and proteins signals to be detected more easily [191]. The solvents utilised included chloroform, hexane, toluene, acetone and xylene and this study found that far less lipid signals were detected following this rinsing procedure [191].

Another approach that has been utilised to try and improve signal intensity when using MALDI-MS is the use of gold nanoparticles that can be applied to the surface of matrix coated tissue [201]. In one study, rat brain tissue was coated with 10 mg/ml CHCA matrix in 50% ethanol:50% 0.1% TFA using a spraying device and then 5 nm of gold was applied on top of the matrix [201]. The application of gold particles was said to reduce surface charging and charging bias thus improving image quality [201]. This study managed to identify the antidiuretic peptide, vasopressin (ADH) ( $m/z$  1085), in the hypothalamus, which is consistent with the localisation of this peptide using other more established methods and could only be done when the gold particles were present.

### **2.4. Matrix Application Methods for MALDI Imaging Experiments**

A wide range of matrix application methods have been proposed for depositing MALDI matrices onto tissue for imaging experiments and again this really depends on the application. There are both manual and automated application methods. Some of the most commonly utilised and well documented methods include application of

discrete spots of matrix, application of a homogenous layer of matrix, as well as novel methods such as sublimation and these are discussed below in sections 2.4.1, 2.4.2 and 2.4.3 and summarised in Figure 25.

**Figure 25 – Overview of matrix application methods. Images corresponding to several application methods are shown.**



### 2.4.1. Application of Discrete Droplets of Matrix

Methods include applying small droplets of matrix onto specific tissue areas appropriate for the localisation of specific biomolecules. Of these methods, there are both contact deposition methods and non-contact deposition methods and these are described in great detail by Rose [202]. Originally, the most commonly used method of matrix application was the dried-droplet method discussed previously [25].



However, as the technology has advanced, so have the methods for applying small droplets of matrix.

Contact deposition methods may now use pins or capillaries with a diameter of 50-100  $\mu\text{m}$  which make direct contact with the tissue surface [194]. However, the disadvantages of these methods are that cross contamination may occur as well as clogging of the capillary tubules resulting in the need to carry out several washing cycles [194]. There are also non-contact microdispensers which disperse microdroplets of liquid onto the tissue surface by applying pressure pulses [194]. These devices eject droplets with a low velocity onto the surface of the tissue, forming droplets as the matrix solution is expelled [194]. Examples of these non-contact methods include piezo-electric thermal inkjet or syringe solenoid pulsed field ejectors [202]. As these are non-contact methods, cross contamination is not an issue but clogging of the capillaries may still occur, and thus these microdispensers may also require significant cleaning stages.

An automated acoustic method of matrix deposition has also been developed which involves the use of a modified acoustic drop ejector that will deposit MALDI matrices [194]. This is a novel technique adapted from acoustic technology which allows the ejection of discrete droplets with a controlled velocity from a free liquid surface [203]. The technology is also a non-contact method but it is free from capillaries and the possibility of clogging that has been associated with other microdispensers. Moreover, it has been shown to produce a homogenous layer of matrix on the tissue surface [194]. Similarly, with this method the crystal size is important in order to obtain good quality spectra [194]. Many of these automated

methods of matrix deposition have similar advantages in that they avoid the human variation associated with the use of hand held pipettes or nebulisers. However, there are always problems associated with automated methods, particularly with large pieces of machinery which may break down and cost a lot to repair.

#### **2.4.2. Application of a Homogenous Layer of Matrix**

One of the most commonly used methods involves applying a homogenous layer of matrix over the entire surface of the tissue [190]. The matrix interacts with analytes to form analyte-doped matrix co-crystals on the surface of a MALDI plate. One of the main advantages of applying a homogenous layer of matrix is that very small crystals are formed which is advantageous for imaging the distribution of pharmaceuticals, offering higher spatial resolution of <50  $\mu\text{m}$  compared to when spotting devices are used which offer a limited spatial resolution of 100-200  $\mu\text{m}$ . There are several types of sprayer that have been utilised to coat tissue sections including hand held spraying devices. These sprayers contain a pressurised gas that acts as a nebuliser to propel the matrix through a tube and onto the tissue surface in the form of droplets. It has been suggested that the sprayer should be held around 30 cm away from the surface of the plate to ensure the formation of an even coat of matrix [190]. Moreover, it has been suggested that the plate be kept within a box to minimise the loss of matrix to the surrounding atmosphere and thus hopefully allow the application of a more even coat of matrix. Each layer should be applied very lightly, just wetting the tissue surface and it should also be ensured that the matrix does not accumulate on certain areas of the plate [190]. For example, this can occur at the corners, particularly if too much pressure is applied whilst spraying causing the

matrix to move outwards towards the edges of the plate. Another factor to consider when using this method is the amount of time to wait between application and this appears to vary greatly between experiments as it may depend on the type of solvent(s) used and the solvent to water ratio. Another important parameter is the number of passes of matrix applied. Roughly ten to twenty passes are used with each pass covering the tissue twice from left to right and then vice versa. However, again this will depend on the type of tissue being used in the experiment and the concentration of matrix being utilised. Dry powder matrix can be applied to the surface of tissue and that the excess be blown off to allow a homogenous layer of matrix crystals to form before spraying the tissue using a hand held sprayer [194]. There may be considerable variability between the results obtained using a hand held sprayer since it is very difficult to apply the same amount of matrix during each cycle and also to apply the same amount of pressure when spraying. In addition, the sprayer may clog, particularly when using a saturated matrix solution. Whilst application of a homogenous layer of matrix dissolved in an appropriate solvent in combination with using hand held spraying devices is common for experiments analysing lipids, peptides and proteins, other methods may be required for other applications such as DMPK studies where drug delocalisation becomes an issue.

There are also numerous commercially available robotic sprayers for applying MALDI matrices in order to carry out a tissue imaging experiment. The most advanced versions are non-contact and nozzle free and some utilise acoustic technology, described previously, to allow precision, high sensitivity and reproducibility. Examples of spraying devices include the Bruker ImagePrep system which is a vibrational sprayer that propels a spray of droplets onto the surface of

tissue samples. Parameters including velocity, number of application cycles and speed of cycling can be controlled by the operator. There are also commercially available chemical inkjet printers for example the ChIP printer manufactured by Shimadzu Biotech. This non-contact robotic spotter utilises piezoelectric technology and can deposit <100 pL droplets of matrices onto a tissue surface. Disadvantages of spotting devices include limited spatial resolution and time taken to apply the matrix (several hours).

### **2.4.3. Novel Matrix Application Methods**

Several other novel approaches have also been developed that all have the common aim of making matrix deposition quicker and easier. Immersion methods have been used to bathe tissue directly in a solution of matrix. It has been demonstrated that direct deposition of a matrix solution onto the surface of a tissue allows high quality spectra to be obtained [154]. For example, 50 µl of 10 mg/ml sinapinic acid in 70/30/1 acetonitrile/HPLC grade water/TFA was pipetted onto a mouse brain tissue held on a MALDI plate with a surface temperature of 4°C. Crystals with a diameter of around 50µm were formed as the solvent evaporated slowly at 4°C resulting in formation of a homogenous layer of matrix [154]. Advantages include ease of preparation but immersion may result in the delocalisation of proteins, resulting in the generation of inaccurate images [194].

An ordinary inkjet printer capable of printing directly onto CDs and DVDs has been utilised as an automated method of depositing matrix [204]. This involved the modification of an Epson Photo Inkjet printer to allow the CD holder to hold MALDI plates [204]. Empty inkjet cartridges were filled with ordinary matrix solutions and

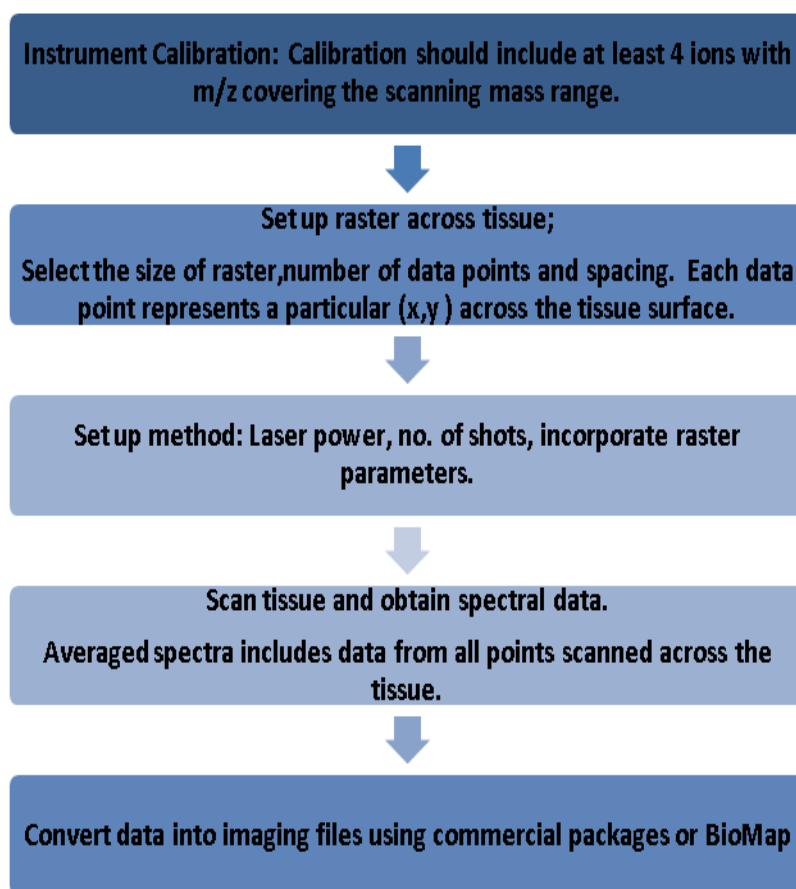
the normal printer software was utilised in the usual manner to control ‘printing,’ in other words, deposition of the MALDI matrix [204]. This method is fairly cheap and the authors claim that it allows high quality spectra and reproducible images to be produced when they compared their results to those obtained using airbrushing or electrospray methods which were also tested [204]. From the data presented in the article, it was clear to see that the printer offered a high level of precision for droplet application compared to that of the airbrush or electrospray methods [204]. Interestingly, Epson use piezo-electric spray heads unlike other manufacturers who use thermal inkjets, which could explain why this was successful. However, this was trialled in our laboratory using a different Epson printer model and it was found that a very small amount of matrix was applied to the surface and clogging was a big problem. This could be attributed to the smaller size of piezo-electric spray heads in the model utilised by our group.

Another approach that has been utilised in order to apply matrices to tissue samples is sublimation which was used to apply CHCA, DHB and sinapinic acid [205]. Again, this method was less expensive and it involved the use of a glass sublimator [205]. Interestingly, this method of matrix deposition does not require the use of any organic solvents such as acetonitrile or methanol which should serve to minimise the spread of analytes on the tissue surface. Although the authors obtained good image quality using this method it is clear that the quality of the results depends on a number of factors such as the evenness of deposition. Thus, the quality of the data obtained using this method also depends on many of the same factors that are problematic with other methods of deposition.

## **2.5. Instrumental Set Up and Experimental Parameters**

Before an imaging experiment can be carried out it is important that instrument parameters are optimised for the detection of analyte(s) of interest. This includes calibrating the instrument and selecting the appropriate laser power, optimising laser firing pattern, laser frequency and number of shots to fire (per data point). These steps are summarised in Figure 26. For this project, there were two main types of MALDI instrument that were utilised, Axima CFR TOF from Shimadzu Biotech (single TOF) for most of the endogenous metabolite profiling and Bruker Ultraflex III from Bruker (TOF-TOF) for DMPK studies (Chapter 3). Further details on setting instrumental parameters are provided in the methods section 2.11.5.3.

**Figure 26 - MALDI Imaging Experiment: Setting Instrument Parameters**



## **2.6. Data Analysis Software for MALDI Imaging**

### **2.6.1. Introduction to BioMap**

Whilst it is relatively easy to probe differences in, for example, control samples and drug rat brain treated samples by examination of heat maps, it is more complex to identify unknown differences. This can be overcome through use of commercial data analysis software packages such as those provided with instruments from Shimadzu and Bruker that were utilised in this project. Additionally, files acquired with instruments provided by different manufacturers can also be converted to files

compatible with the tissue imaging software BioMap, provided by the Novartis Institute of Biomedical Research [154].

BioMap is freely available software that can be downloaded from the internet ([www.maldi-msi.org](http://www.maldi-msi.org)). Raw data files are converted to BioMap files which image the distribution of analytes using a selected mass range. Moreover, BioMap has the added feature of baseline correction [206]. It is also possible to normalise images of compounds of interest against matrix ion e.g. CHCA  $[M+H]^+$ ,  $m/z$  190. Normalisation will also remove any background interferences, for example, matrix related peaks that give strong signals around the edge of the raster, just off tissue. BioMap has several other tools that make it useful for tissue imaging applications. For example, if there is a particular region of a tissue that has a higher concentration of drug than another, regions of interest can be selected and statistical tools used to investigate the difference in intensity of the drug's  $m/z$  in the regions of interest. Other interesting tools include correlating the distribution of a drug's  $m/z$  with that of an isotope, for example if the drug has a unique isotopic distribution pattern due to chlorine or bromine. A specialised tool called 'multi image evolution' can be selected which allows the user to visualise all the images created within a certain mass range. This tool is useful for identifying unusual patterns in treated/blank samples. Optical images can also be imported and overlaid with tissue images. The use of BioMap is well documented in recent work as it is utilised extensively by the Group of Markus Stoeckli at Novartis who carries out extensive work utilising MALDI-MSI as a research tool during DMPK studies e.g. see [207].



### **2.6.2. Use of Principle Component Analysis and other Statistical Tools for the Interpretation of MALDI-MSI Data Sets.**

Principle component analysis (PCA) has also been utilised to aid the interpretation of MALDI-MSI datasets and is useful for determining latent variants in untargeted studies. In one study, clustering methods were used to classify pixels according to similarity to define distinct spatial regions. Principle component and discriminant analyses were combined to identify changes in the mass spectra between regions. Images were created by projecting the spectra of each pixel on the discriminant spectra. PCA coefficients were plotted as images in order to identify regions of the tissue that were different [208]. Supervised and unsupervised PCA has also been utilised to aid the interpretation of MALDI-MSI data using as a model system lipid variations within brain tissue. This was utilised to distinguish between grey and white matter of cerebellum and more specifically, the grey cerebellar cortex and hippocampal formation based on supervised PCA scores [209]. PCA has also been utilised to identify data issues resulting from uneven matrix coverage and salt concentrations for the identification of regions of drug treated skin where the ion abundance of hydrocortisone was low [210]. As technology advances, no doubt more comprehensive statistical software packages shall be built into MALDI-MSI software packages.

### **2.7. Imaging Endogenous Molecules Using MALDI-MSI – Examples**

MALDI-MSI has been used widely for imaging peptide, proteins and lipids. Below, some examples of tissue imaging applications are presented in the areas of peptide,

protein lipid and small polar metabolite analysis with further examples of application to drug metabolism and pharmacokinetic studies given in chapter 3.

### **2.7.1. Analysis of Peptide and Proteins using MALDI-MSI**

As mentioned previously, the first use of MALDI-MS to localise peptides and proteins in biological tissue was in 1997 [22]. These initial experiments were carried out on the rat pancreas to map insulin in the B-cell, the rat pituitary to map neuropeptides and the human mucosal cell membranes to map proteins [22]. Since then, many tissue-imaging experiments have been carried out which have identified peptide and proteins of interest in tissues such as rat brain and liver.

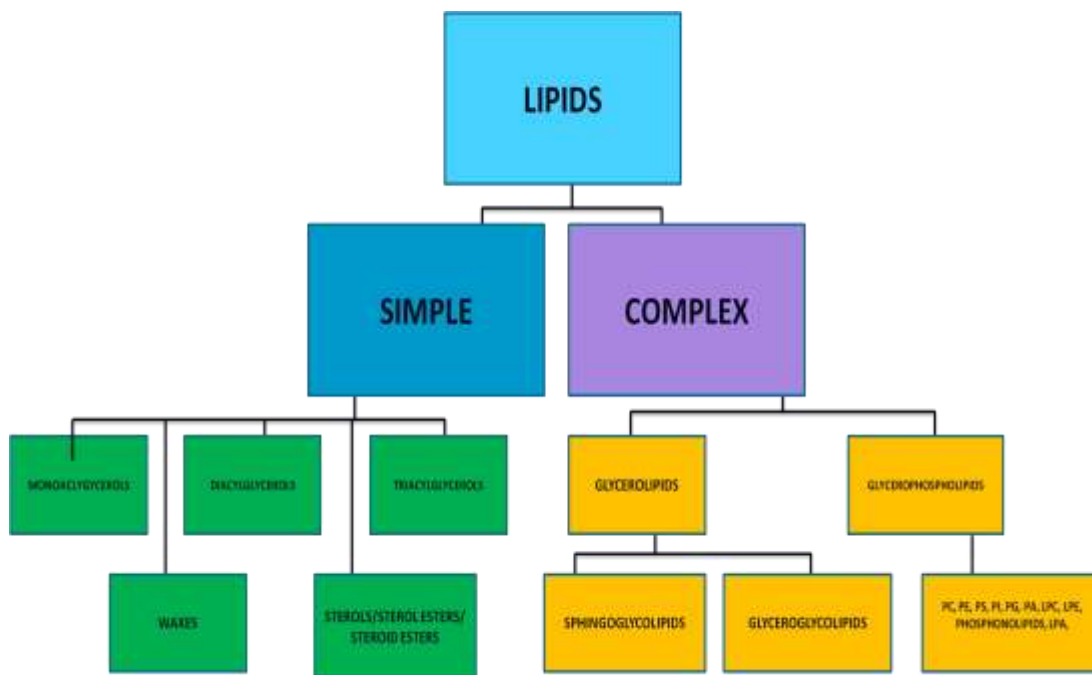
MALDI-MS imaging can also be used to localise the distribution of biomarkers that are known to be important in disease states, aiding the understanding of some of the most important mechanisms of disease. MALDI-MS has been employed as a method to detect one of the common pathological features of Alzheimer's Disease, AB plaques, in coronal mouse brain sections from APP23 transgenic mice which over express the amyloid precursor protein (APP) [206]. MALDI imaging has also been utilised to identify phenotypic characteristics associated with Parkinson's Disease [211]. MALDI-MS was used to analyse the expression patterns of peptides and proteins in an experimental model of Parkinson's disease, unilaterally 6-hydroxydopamine treated rats. Differences in several protein expression profiles were found in the dopamine depleted side of the brain when compared to the corresponding intact side, for example there were differences in calmodulin, cytochrome c, and cytochrome c oxidase. An increased ratio of post-translational modifications such as acetylations were also found in the striatum of proteins in the

dopamine depleted side of the brain [211]. MALDI MS has also been used to identify peptides and proteins that are expressed in human glioblastoma D54 cells that were implanted into the hind limb of a mouse and allowed to proliferate [212]. Thus, this demonstrates again that using this technique in conjunction with animal models of disease can lead to further advances in determining the underlying biochemical nature of disease states

### **2.7.2. Analysis of Lipids**

Lipids have been described as ‘fatty acids and their derivatives, and substances related biosynthetically or functionally to these compounds’ [213]. They are important building blocks of membranes, have roles in signal transduction and are important energy stores. They can be subdivided into ‘simple’ and ‘complex’ lipids for ease of understanding. Within these divisions there are many more subdivisions which are summarised below (Figure 27). Alternatively, they have also been divided into 8 main classes: fatty acyls, glycerolipids, glycerophospholipids, sphingolipids, sterol lipids, prenol lipids, saccharolipids and polyketides by the authors of the lipid map database ([www.lipidmaps.org](http://www.lipidmaps.org)).

**Figure 27 - Schematic Diagram Summarising Lipid Classification**



Glycerophospholipids are the subclass of lipids most commonly analysed utilising MALDI-MSI [214]. Glycerophospholipids are a complex group of lipids which are divided into many different subclasses. They all have a glycerol base which is esterified to one or two fatty acids. The subclasses have head groups which all contain a phosphate moiety that is also esterified to the glycerol molecule. This adds to the complexity of this group of lipids as they can have both variations in fatty acid chains as well as the polar head group. In the last ten years, MALDI TOF mass spectrometry has increasingly been applied to lipid research as interest in the roles of lipids in biological systems has grown [214]. MALDI MS offers several advantages for investigation of the composition and distribution of lipids in biological systems. Sample preparation is quick and easy, no complex derivatisation steps are required prior to analysis and many lipid classes can be detected easily using this technique in both positive and negative mode [29,215-218].

## 2.8. Introduction to Main Classes of Glycerophospholipids and Sphingolipids

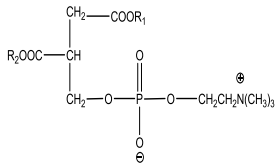
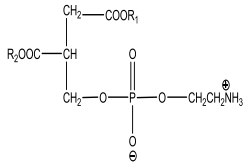
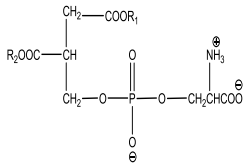
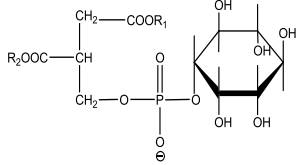
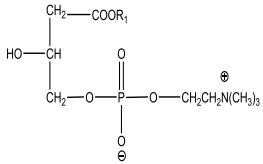
Glycerophospholipids and sphingolipids are the most common subclass of lipid that are found when tissues are analysed directly using MALDI-MSI [214]. Below, an overview of the commonly observed classes of glycerophospholipids is given. Phosphatidylcholines (PC) are very abundant zwitterionic glycerophospholipids found in both plant and animal tissues. They have a glycerol backbone with fatty acid chains attached at sn1 and sn2 positions and a choline head group which contains a quaternary ammonium ion, making the molecules highly detectable by MS in positive ion mode (Table 2) [219]. Phosphatidylcholine fragmentation in positive mode will generate an abundant ion at 184 Da corresponding to the phosphocholine moiety cation but little other fragmentation information from MS2 experiments (Table 3). To overcome this, lithium can be utilised to generate adducts which, following MS/MS fragmentation, enables structural information to be deduced during MALDI MS experiments [198]. Alternatively, during analysis using ESI, MS3 fragmentation is often carried out enabling tentative assignment of the fatty acid chains (Table 3).

Phosphatidylserines (PS), phosphatidylethanolamines (PE) and phosphatidylinositols (PI) are three other subclasses of glycerophospholipid which have different functional groups attached to the phosphate moiety in their head group (Table 2). Commonly observed fragmentation ions for these classes of glycerophospholipid are also shown Table 3. Phosphatidylserines have a head group which has three ionisable functional groups; phosphate, amino and carboxyl groups (Table 2). Phosphatidylserines may be detected in positive and negative modes due to their

amphoterics nature. Phosphatidylethanolamines lipids have a head group containing phosphate and amine functional groups (Table 2). PE species are also zwitterionic phospholipid species, like phosphatidylcholines, making them highly ionisable. However, they may not be as easily observed in positive mode due to the high abundance of phosphatidylcholines which may reduce signals from other species [220]. PI species are acidic and are readily ionisable in negative mode. Phosphatidylinositols have a head group containing phosphate and myo-inositol functional groups (Table 2). Commonly observed fragments of PE, PI and PS observed during ESI or MALDI MS analysis are also shown in Table 3.

Lysophospholipids contain just one fatty acid chain per molecule of glycerol. Lysophosphatidylcholines (LPCs) are a subset of the lysophospholipids which also includes lysophosphatidylserines and lysophosphatidylethanolamine species. LPCs have the same head group that is found in phosphatidylcholines (Table 3).

**Table 2 - Sub-Classes of Abundant Glycerophospholipids showing Structure of Head Group, PC = phosphatidylcholine, PE = phosphatidylethanolamine, PS = phosphatidylserine, PI = phosphatidylinositols, LysoPC =lysophosphatidylcholine.**

Sub-Class of Lipid	Structure of Head Group
PC	 <p>The diagram shows the head group of phosphatidylcholine. It consists of a phosphate group bonded to a glycerol backbone. The glycerol backbone has two fatty acid chains (R<sub>1</sub>COO- and R<sub>2</sub>COO-) and a third carbon bonded to a phosphate group. The phosphate group is further bonded to a choline group (-CH<sub>2</sub>CH<sub>2</sub>N(CH<sub>3</sub>)<sub>3</sub><sup>⊕</sup>).</p>
PE	 <p>The diagram shows the head group of phosphatidylethanolamine. It consists of a phosphate group bonded to a glycerol backbone. The glycerol backbone has two fatty acid chains (R<sub>1</sub>COO- and R<sub>2</sub>COO-) and a third carbon bonded to a phosphate group. The phosphate group is further bonded to an ethanolamine group (-CH<sub>2</sub>CH<sub>2</sub>NH<sub>2</sub><sup>⊕</sup>).</p>
PS	 <p>The diagram shows the head group of phosphatidylserine. It consists of a phosphate group bonded to a glycerol backbone. The glycerol backbone has two fatty acid chains (R<sub>1</sub>COO- and R<sub>2</sub>COO-) and a third carbon bonded to a phosphate group. The phosphate group is further bonded to a serine group (-CH<sub>2</sub>CH(NH<sub>2</sub><sup>⊕</sup>)COO<sup>⊖</sup>).</p>
PI	 <p>The diagram shows the head group of phosphatidylinositol. It consists of a phosphate group bonded to a glycerol backbone. The glycerol backbone has two fatty acid chains (R<sub>1</sub>COO- and R<sub>2</sub>COO-) and a third carbon bonded to a phosphate group. The phosphate group is further bonded to an inositol ring, which is a six-membered ring with four hydroxyl groups (-OH) and one oxygen atom.</p>
LysoPC	 <p>The diagram shows the head group of lysophosphatidylcholine. It consists of a phosphate group bonded to a glycerol backbone. The glycerol backbone has one fatty acid chain (R<sub>1</sub>COO-), one hydroxyl group (-OH), and a third carbon bonded to a phosphate group. The phosphate group is further bonded to a choline group (-CH<sub>2</sub>CH<sub>2</sub>N(CH<sub>3</sub>)<sub>3</sub><sup>⊕</sup>).</p>

**Table 3 - Sub-Classes of Abundant Glycerophospholipids showing Product Ions Commonly Observed using ESI and/or MALDI.**

**PC = phosphatidylcholine, PE = phosphatidylethanolamine, PS = phosphatidylserine, PI = phosphatidylinositols, (table continued on P93 and P94).**

<b>Sub-Class of Lipid</b>	<b>Mode</b>	<b>Head Group</b>	<b>Product Ions Related to Loss of Head Group</b>	<b>Loss of Fatty Acids as Ketene</b>	<b>Loss of Fatty Acid as Carboxylic Acid</b>	<b>Loss of Fatty Acids as Acyl</b>	<b>Other</b>
<b>PC</b>	<b>+</b>	Phosphocholine $C_2H_5O_4P$ <i>m/z</i> 184	$[M+H-183]^+$	MS <sup>3</sup> Reaction $[M+H-R'CH=C=O]^+$ MS <sup>3</sup> Reaction $[M+H-R''CH=C=O]^+$	MS <sup>3</sup> Reaction $[M+H-R'COOH]^+$ MS <sup>3</sup> Reaction $[M+H-R''COOH]^+$	When Lithium Used: $[M+Li-R'CO_2H]^+ [M+Li-R''CO_2H]^+$ $[M-R'CO_2H]^+ [M-R''CO_2H]^+$ $[M+Li-N(CH_3)_3-R'CO_2H]^+$ $[M+Li-N(CH_3)_3-R''CO_2H]^+$	When Lithium Used: Neutral loss of trimethylamine $N(CH_3)_3$ $[M+Li - N(CH_3)_3 - C_2H_5O_4P]^+$ $[M-N(CH_3)_3 - C_2H_5O_4P]^+$



Sub-Class of Lipid Contin	Mode	Head Group	Product Ions Related to Loss of Head Group	Loss of Fatty Acids as Ketene	Loss of Fatty Acid as Carboxylic Acid	Loss of Fatty Acids as Acyl	Other
PC	-		Loss of methyl group from choline head group, [M-15] <sup>-</sup>  Loss of fatty acid chains from [M-15] <sup>-</sup> ion.				Carboxylate anions produced from MS <sup>3</sup> reactions as a result of loss of fatty acid chains.
PE	+	Phosphoethanolamine  <i>m/z</i> 141					
	-			[M-H-R'CH=C=O] <sup>-</sup> [M-H-R''CH=C=O] <sup>-</sup>		[M-H-R'CO <sub>2</sub> H] <sup>-</sup> [M-H-R''CO <sub>2</sub> H] <sup>-</sup>	Carboxylate anions.

Sub-Class of Lipid	Mode	Head Group	Product Ions Related to Loss of Head Group	Loss of Fatty Acids as Ketene	Loss of Fatty Acid as Carboxylic Acid	Loss of Fatty Acids as Acyl	Other
PS	+		Phosphoserine [M+H-185] <sup>+</sup>				
	-		Loss of serine [M-H-87] <sup>-</sup>	Have also lost serine. [M-H-87-R'CH=C=O] <sup>-</sup> [M-H-87-R''CH=C=O] <sup>-</sup>	Have also lost serine. [M-H-87-R'COOH] <sup>-</sup> [M-H-87-R''COOH] <sup>-</sup>	Loss of an acyl group and serine head group. [M-H-C <sub>3</sub> H <sub>5</sub> NO <sub>2</sub> -R'CO <sub>2</sub> H] <sup>-</sup> [M-H-C <sub>3</sub> H <sub>5</sub> NO <sub>2</sub> -R''CO <sub>2</sub> H] <sup>-</sup>	Carboxylate Ions.
PI	-	Phosphoinositol <i>m/z</i> 259	[Inositol phosphate-H <sub>2</sub> O] <i>m/z</i> 241 [Inositol phosphate-2H <sub>2</sub> O] <i>m/z</i> 223 & Loss of inositol			[M-H-R'CO <sub>2</sub> H] <sup>-</sup> [M-H-R''CO <sub>2</sub> H] <sup>-</sup>	Carboxylate Ions.

Sphingolipids contain long chain bases with various substituents on the amino group (Figure 28). The long chain bases have between 12 and 22 carbons and are aliphatic amines with a hydroxyl group and often a trans double bond in position 4. The most common long chain base is known as sphingosine and it has two hydroxyl groups as well as one trans double bond. Other long chain bases have varied structures, for example they may have saturated or unsaturated aliphatic chains, cis or trans double bonds and they can have additional functional groups such as methyl groups. Additionally, they may be trihydroxy bases instead of dihydroxybases again with varying degrees of saturation and in some cases branching. The long chain bases readily ionise in positive ionisation mode. They are observed within the mass range  $m/z$  250 – 450 using ESI. Ceramides contain a fatty acid chain linked to the amide group of a long chain base by an amide bond (Figure 28). Ceramides are important components of the complex sphingolipids such as sphingomyelin. Sphingomyelin has a ceramide component that is linked at position-1 to a phosphorylcholine moiety (Figure 28). Like phosphatidylcholine, it is an abundant component of membranes and also has roles in signal transduction. Sphingomyelin often has sphingosine as its long chain base component of the ceramide unit. Analysis of sphingomyelins produces an abundant  $[M]^+$  ion due to the presence of a quaternary nitrogen. Tandem MS experiments will yield an abundant product ion at  $m/z$  184 corresponding to the phosphocholine moiety. There may also be a product ion corresponding to the neutral loss of  $H_2O$  from the parent molecule. Sphingomyelins are observed within mass range  $m/z$  650-900 and are readily observed using MALDI-MSI. Cerebrosides (galactosylceramides) are the most common sphingoglycolipids and they are composed of a ceramide unit linked to a sugar moiety via a glycosidic

bond. These lipids were originally isolated from brain lipids but they are in fact widespread. Sulfatides are sulfated galactosylceramides. MS/MS analysis should reveal the presence of sulphate group at  $m/z$  97 and a less abundant product ion at  $m/z$  241 from cleavage that corresponds to the sulphated sugar head group. Elevation of sulfatides has been implicated in ovarian cancer and other types of cancer and a recent publication has correlated elevated levels of sulfatides with regions of ovarian epithelial carcinoma [221]. Gangliosides are oligoglycosylceramides which were originally found in the ganglia. They are composed of a ceramide, glucose, galactose and galactosamine sugars as well as sialic groups from derivatives of neuraminic acid (NANA). Gangliosides will be observed within mass range  $m/z$  1200-3000 in negative ionization mode [213].

**Figure 28 – Sphingolipid Classification**

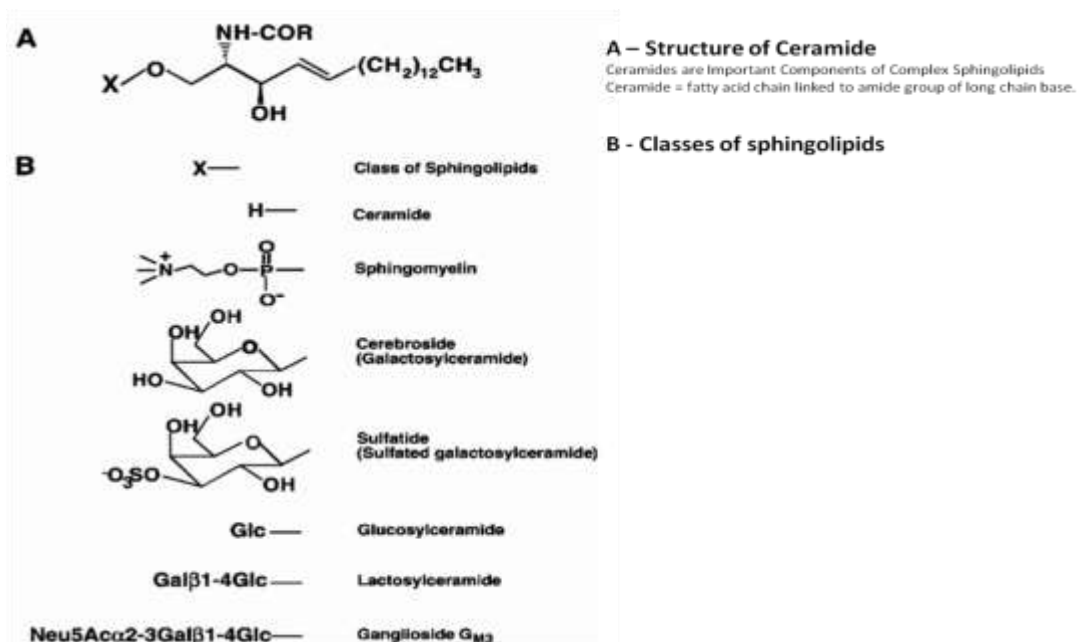


Figure taken from [222].

### 2.8.1. Analysis of Lipids by MALDI MS Profiling and Imaging

Initially, MALDI MS profiling was used in a number of studies to investigate glycerophospholipids and sphingolipids classes in a variety of tissue samples [29,215-218]. It has been demonstrated that positive mode should be used for analysis of phosphatidylcholines and sphingomyelins whilst negative mode should be used for detection of phosphatidylethanolamines, phosphatidylinositols, phosphatidylserines, cardiolipin, gangliosides and sulfatides [215,217,223,224]. Due to ion suppression caused by abundance of phosphatidylcholines it is more useful to analyse phosphatidylethanolamines in negative mode [220,225]. DHB and DHA are most commonly utilised in the literature for MALDI-MSI profiling [215,216,219,223] and imaging of lipids [214,226]. p-nitroaniline has also been

utilised as an alternative matrix offering higher sensitivity for the detection of phospholipids in eye lens tissue [29].

Triacylglycerols have also been analysed using MALDI MS. Triacylglycerols are simple lipids that contain three fatty acid chains esterified to a glycerol backbone. Successful matrix/solvent combinations reported for the analysis of triacylglycerols have included spotting  $K_4Fe(CN)_6$ / glycerol in methanol and then spotting sample in chloroform directly on top [227] or DHB in acetone being applied to target and, again, sample in chloroform applied directly on top [228]. It was found that DHB at a concentration of 40 mg/ml in acetone was the best matrix for quantification of triacylglycerol lipids in edible oils with detection levels in mid fmol region [228]. There are also compatibility issues for the analysis of non-polar triacylglycerols. When triacylglycerols were dissolved in chloroform and then mixed with the matrix in 1:1 water:acetonitrile with 0.25% TFA solvent there was poor shot to shot reproducibility due to solvent incompatibility [228]. However a 10 mg/ml solution of DHB dissolved in chloroform has been utilised for analysis of the lipid component of human serum lipoproteins including cholesterol, lysophosphatidylcholines, phosphatidylcholines and triacylglycerols.

It has also been demonstrated previously that the use of DHB matrix dissolved in solvent combinations which utilised water, resulted in poor crystallisation due to longer evaporation times. The crystals formed were large and angular and did not form a homogenous layer. It has been suggested that drying samples coated with DHB in methanol in 0.1% TFA during MALDI profiling experiments with a warm

stream of air will speed up the drying process resulting in the formation of smaller crystals due to shorter evaporation times [229].

Tandem MS has also been used to provide additional structural information such as fatty acid composition in both positive and negative modes [198,217,223]. For example it has been shown that the addition of lithium chloride to samples and analysis of  $\text{Li}^+$  adducts of phosphatidylcholine lipids and their fragmentation patterns allows more structural information to be deduced [198]. MALDI Imaging experiments have also been carried out to provide additional information on the spatial distribution of lipid molecules that would be otherwise be lost from analysis of tissue homogenate [205,215,216,223,226,230-233]. The use of MALDI MS to map the distribution of lipids in the rat brain has also been widely documented [198,226,234]. MALDI-ion mobility-TOF MS has also been utilised to map the distribution of phosphatidylcholine and cerebroside species in rat brain tissue [226]. A study has identified around 100 lipid species in the plasma membrane of rat brain tissue using infrared laser desorption/ionisation orthogonal-time-of-flight mass spectrometry in both positive and negative modes [234]. Potassium acetate was sprayed onto the rat brain tissue to minimise the formation of different salt adducts and thus minimise their ion intensities allowing data interpretation to be made easier in positive ionisation mode [234].

Lipid profiles have also been investigated in disease tissues, for example colon cancer tissue [235] and leg muscle of mouse model of Duchene muscular dystrophy [218]. Imaging mass spectrometry has been used to analyse lipids in mouse brain in a mouse model of Tay-Sachs/Sandhoff disease to identify lipids of interest in the

mutant [232]. For additional information on analysis of lipids by MALDI MS a review has recently been published [214].

## **2.9. Analysis of Polar Metabolites**

Whilst there are many examples of studies that have mapped the distribution of lipids and peptide and proteins *in situ*, the identification of small polar metabolites is more challenging and therefore less well documented. Examples of studies that have utilised MALDI-MSI to map the distribution of small polar endogenous metabolites such as sugar phosphates and energy metabolites are, at present, very limited. Although this is an active area of research, it is more difficult to obtain results due to the low concentrations of many of these compounds, matrix interferences  $< m/z$  500 and ionisation efficiencies. Currently, work on this type of small molecules has centred on the use of 9-aminoacridine as an alternative matrix for MALDI profiling experiments. 9-aminoacridine was introduced as a MALDI matrix in 2002 for the analysis of acidic compounds including phenols, carboxylic acids, sulfonates, amines and alcohols. In 2005, it was utilised for metabolomic profiling in Islets of Langerhans and *Escherichia coli* strain DH5-alpha and there are now many more metabolomic studies documented [156]. It was reported that by producing a binary matrix of CHCA and 9-aminoacridine which have different proton affinities that there were less background interfering matrix peaks and the presence of CHCA meant that the laser power could be reduced in positive and negative mode analyses of plant extracts [236]. It was also shown that this matrix could be utilised to quantify metabolites by spotting serial dilutions of a metabolite mixture [237] and it



has been shown to be successful for the analysis of groups including aliphatic acids, aromatic acids, phytohormones and amino acids [238].

It has also been utilised for the analysis of negatively charged water-soluble cellular metabolites from powdered mouse heart tissue extracts [239] and analysis of cellular glycerophospholipids [240]. Recently, novel applications have included analysis of archaeobacterial lipids in membrane of *Halobacterium salinarum* [241], the analysis of lipids in the porcine olfactory epithelial membranes [242] and cilia and analysis of lipids from hen egg yolk [243] and analysis of sulfatides in lipid extracts of biological samples [244] amongst others. It has also been utilised to analyse lymphoblastic leukaemia (Jurkat) cells and to investigate changes in metabolite profiles when these cells were treated with three different anticancer drugs [245]. It has also been utilised in combination with FT-ICR to investigate the intracellular metabolism of *Escherichia coli* under different conditions [246].

However, with the increased popularity of metabolomics, *in situ* metabolomics will, undoubtedly, be the next big thing in the 'omics' revolution as it is not only important to identify changes in the metabolome but also to find out exactly where they are occurring within tissues/cells. Recent examples of metabolomic profiling utilising MALDI-MSI include from Malcolm Clench's group at Sheffield Hallam University who illustrated several years ago the usefulness of 9-aminoacridine as a matrix for imaging small metabolites *in situ* where it was utilised to map amino acids, sugars, and phosphorylated metabolites in wheat seeds [247]. It has also been shown that MALDI-MSI can be used to localise metabolites *in situ* in rat brain in sections when applied using an automated spraying device, which ensured rapid

crystal formation on the surface of rat brain utilising 50  $\mu\text{m}$  spacing to detect 13 primary metabolites including ATP, ADP and GDP [31]. Recent publications have also utilised MALDI profiling to investigate metabolite composition in single cells. Sweedler and colleagues have utilised MALDI to study biomolecules in single neurons e.g. cell signalling peptides in pituitary cells [248] and neuropeptide distributions in nervous tissue from *Aplysia californica* using their stretched sample method [249]. Amantano and colleagues have investigated the metabolites in *Colsterium acerosum* (a single cell alga) [250] and *Saccharomyces cerevisiae* [251] using MALDI profiling and a review on the use of analytical techniques for single-cell metabolomics has recently been published [252]. One of the next goals of imaging mass spectrometry will undoubtedly be to map the spatial distribution of metabolites inside single animal cells.

## **2.10. Study Aims**

The main aims of the current study were to optimise experimental parameters including sample preparation, matrix preparation and matrix application steps to maximise the detection of endogenous molecules including lipids and polar metabolites. Reference to the methods utilised in the studies described above was used as a starting point for the design of initial experiments. The methodology utilised and some examples of results obtained are presented and discussed.

## **2.11. Methodology**

### **2.11.1. Materials**

Acetonitrile, methanol and acetone were purchased from Fisher Scientific (Leicestershire, UK). Trifluoroacetic acid (TFA) was purchased from Sigma Aldrich (Dorset, UK). All chemicals used were of analytical reagent grade. A Millipore Direct Q-3 water purification system was used to produce HPLC water which was used in all analyses. MALDI-MS grade alpha-cyano-4-hydroxycinnamic acid (CHCA), dihydroxy-benzoic acid (DHB), sinapinic acid, dihydroxyacetophenone (DHA) and 9-aminoacridine matrices were purchased from Sigma Aldrich (Dorset, UK).

### **2.11.2. Animals**

Frozen tissues were obtained from MSD (formerly Organon Laboratories; Newhouse, Motherwell, Scotland). The animals were sacrificed and the organs were obtained and immediately frozen by slowly immersing them into liquid nitrogen cooled isopentane. Samples were then wrapped in aluminium foil and stored at -80 °C before sectioning, following procedures described in previous studies [69,190].

### **2.11.3. Tissue Sectioning Procedures**

Sectioning was carried out using a Leica CM1850 Cryostat (Leica Microsystems, Milton Keynes, UK). The tissues were removed from a -80 °C freezer and mounted onto a cryostat chuck using Shandon M-1 embedding matrix (Thermo-Scientific,

Cheshire.) Care was taken to ensure that the matrix only touched the base of the tissue and did not cover the area that was going to be sliced. The tissue sectioning procedure was optimised according to the tissues being sectioned and for brain and liver tissues, the cryostat was set at a temperature of -20 °C and 12 µm thick sections were taken as these parameters were optimal to obtain good slices. In all experiments, sections were positioned onto MALDI target plates (Shimadzu Biotech, Milton Keynes, UK) using a small artists brush. Thaw mounting was then used to fuse the sections onto MALDI target plates. MALDI target plates were then utilised immediately or stored at -80 °C prior to matrix application. Sections were kept frozen for a maximum of three weeks before preparing them for MALDI mass spectral analysis.

#### **2.11.3.1. MALDI Profiling Experiments**

Firstly, profiling was utilised to analyse the background ions that came from the analysis of MALDI matrices. Profiling was then used to optimise the detection of some classes of metabolites by analysis of standards and finally it was used to profile metabolites in tissue homogenates and for analysis of profiles directly off tissue for region-specific analysis.

##### **2.11.3.1.1. Testing MALDI Matrices**

To consider the best matrix for small molecule experiments, matrices were tested by spotting them on MALDI targets to obtain spectra of background ions associated with ionisation of the matrix itself. Welled plates were obtained for profiling experiments (Shimadzu Biotech). Small volumes of the matrices (0.5 µl) were then

pipetted into wells and allowed to dry. In positive ionisation mode, four matrices were considered for initial imaging experiments, CHCA, DHA, DHB and Sinapinic Acid. It has been suggested that solvent combinations of 1:1 acetonitrile: water plus 0.1% TFA are the best for obtaining peptide and protein profiles off tissue [190] and so this solvent combination was chosen as a starting point to compare the background spectra observed from analysis of these four different matrices with all solutions being prepared at a concentration of 15 mg/ml. Following initial imaging experiments described in section 2.11.4, to investigate if 15 mg/ml solution of CHCA in 1:1 acetonitrile: water plus 0.1% TFA was best for endogenous small molecule analysis, two other solvent combinations were also tried at two different laser powers; 70% methanol, 50% methanol.

In negative ionisation mode, three matrices were utilised. 9-aminoacridine was prepared at a concentration of 10 mg/ml in 100% methanol for analyses in negative mode. (WARNING: Care should be taken when utilising 9-aminoacridine, hazards are causing skin irritation, severe eye irritation and may cause respiratory irritation. Thus, appropriate COSHH assessment is required prior to use). Again, following matrix optimisation, 40 mg/ml DHB in 100% acetone and 15 mg/ml CHCA in 1:1 acetonitrile: water plus 0.1% TFA were also prepared for negative mode analyses.

#### **2.11.3.1.2. Analysis of Standards**

Profiling experiments were carried out to analyse non-polar triacylglycerols and polar molecule standards as their analysis by MALDI-MSI has not been widely documented. To investigate matrices for analysis of non-polar triacylglycerol lipids, a solution of 15 mg/ml CHCA matrix was prepared using 1:1 acetonitrile: water plus

0.1% TFA or 80:20 methanol: 0.1% TFA or a solution of 40 mg/ml DHB in acetone was prepared. For analysis of polar compounds, matrices were mixed with an equal volume of standard and spotted into wells using the 'dried droplet' method [25]. Alternatively for the analysis of non polar triacylglycerol lipids, 0.5 µl of the standard was pipetted into a well and then 0.5 µl of the matrix solution was pipetted directly on to the surface to prevent any solvent incompatibility issues. Lipid standards utilised were C16:0/C18:1/C18:1 (1-hexadecanoyl-2,3-di-(9Z-octadecenoyl)-sn-glycerol) and b) C18:1/C18:1/C18:1 ,2,3-tri-(9Z-octadecenoyl)-glycerol which were prepared in 1:1 methanol:chloroform at a concentration of 1 mg/ml. The suitability of 9-aminoacridine for metabolite detection in negative ionisation mode was tested using the following standards which were prepared in 1:1 acetonitrile: water at a concentration of 1 mg/ml, Glucose, Ribose 5-phosphate, ATP, Coenzyme A (CoA) mix, to investigate if 9-aminoacridine could be utilised for detection of sugars, sugar phosphates, and CoA's. The dried droplet method was used; 0.5 µl of standards were mixed with 0.5 µl of 9-aminoacridine matrix prepared at a concentration of 10 mg/ml in 100% methanol which was then spotted into target wells.

#### **2.11.3.1.3. Profiling Metabolite Extracts and On Tissue**

Profiling was also utilised to investigate the small molecule profiles in different tissue regions. To profile lipids in grey and white matter of the cerebellum, a Gilson pipette was used to apply 'spots' containing 0.5 µl-1 µl of CHCA matrix in 1:1 acetonitrile: water 0.1% TFA and for each spot this was repeated 4 times until there was a dense layer of matrix crystals on the chosen area of the tissue.

9-aminoacridine was utilised to profile polar metabolites in tissue extracts. But firstly, it was investigated as an alternative matrix for the detection of lipids in negative ionisation mode. Here, 0.5 µl of a 10 mg/ml solution of 9-aminoacridine prepared in methanol was applied to various regions of rat brain tissues using a Gilson pipette and this was repeated 4 times until there was a dense layer of matrix crystals on the regions. Additionally, to investigate 9-aminoacridine as a matrix for the detection of polar metabolites, metabolite extracts containing polar metabolites were prepared by extracting metabolites from ½ mouse brains (weight approximately 10g) utilising the optimised metabolite extraction method using Methanol: Chloroform: Water described by Wu *et al* [253]. For initial profiling experiments, a 10 mg/ml solution of 9-aminoacridine was prepared in 100% methanol, as this solvent combination has been described previously for profiling metabolites in rat brain sections [31].

To optimise polar metabolite profiling directly from tissue sections, different acetone: water solvent combinations were also investigated using profiling on tissue. Acetone and 0.1% TFA has previously been utilised for the detection of metabolites in seeds but it was thought that the addition of water might be required to optimise detection of other metabolites groups such as sugar phosphates [247]. This involved spotting different matrix combinations onto tissue to see which gave best signal to noise. The following were tried: 0.1% TFA in 100% acetone, 0.1% TFA in 90 % acetone: 10 % water, 0.1% TFA in 80% acetone: 20 % water, 0.1% TFA in 95% acetone: 5% water and 0.1% TFA in 85% acetone: 15% water. Based on the results of profiling experiments, the solvent combination utilised for further profiling experiments was 0.1 % TFA in 80 % acetone: 20% water.

## **2.11.4. MALDI Tissue Imaging Experiments**

### **2.11.4.1. Matrix Selection and Application Methods for Imaging Experiments**

Sections were removed from the freezer and placed in a vacuum dessicator for a period of approximately 30 minutes prior to matrix application to aid the removal of moisture from the samples. As the experiments were predominantly looking at small molecules, no washing cycles were carried out prior to this. The matrix and solvent combination that was used in the tissue imaging experiments to optimise spectral and image quality was CHCA at a concentration of 15 mg/ml in 50% acetonitrile: 50% 0.1% TFA in HPLC grade water or DHB at concentration of 40 mg/ml in acetone. Additionally, DHB was prepared in acetonitrile: water 80:20 0.1% TFA to investigate the crystallisation and suitability of DHB for imaging when water was used in the solvent combination. For analysis of polar metabolites directly from tissue samples in initial imaging experiments in negative mode, initially 10 mg/ml 9-aminoacridine was prepared in 100 % methanol. Following experimentation utilising MALDI MS profiling, 80:20 acetone: water plus 0.1% TFA was also utilised for further imaging experiments.

In all cases, matrix preparation involved dissolving the solid matrix into the solvents using a Decon F5200B ultrasonic bath. A hand-held Preval spraying device (Sigma Aldrich, Dorset, UK) was employed to propel small droplets of matrix onto the MALDI target plate as a homogenous layer. Samples were placed in the fume hood during matrix application which also aided the drying of targets in between application of matrix. Between 10 and 20 coats were applied until the surface was



almost wet with next coat applied once the previous coating had dried, allowing time for the matrix to interact with the tissue to form a homogenous layer of crystals on the surface of the plate. Sample plates were then analysed directly or alternatively sample plates were stored at -80 °C for up to a month.

## **2.11.5. MALDI Mass Spectrometry**

### **2.11.5.1. Calibration of Axima-CFR TOF MALDI Instrument**

An Axima-CFR TOF MALDI Mass spectrometer was used to carry out the initial tissue imaging experiments (Kratos Analytical Ltd, A Shimadzu Group Company, Manchester, UK). The machine was operated in reflectron positive ionisation and negative ionisation modes and the power was then adjusted to a level suitable for the matrix that was being used. This was also dependent on other experimental parameters such as the sample type and thickness of the matrix. Before each experiment, the machine was calibrated to within 100 mDa. As small molecule analysis was being carried out, a calibration mix of small molecules was utilised for these experiments which enabled calibration of the instrument in positive and negative ionisation modes (Sigma Aldrich). The mixture contained papaverine (1 mg/ml in methanol), reserpine (1 mg/ml in acetonitrile) and cesium iodide (10 mg/ml in HPLC water) and the papaverine and reserpine solutions were mixed 1:1 to give final concentrations of papaverine and reserpine of 0.5mg/ml. This solution was then mixed 1:1 with cesium iodide solution to give final concentration of papaverine and reserpine of 0.25 mg/ml and cesium iodide 5 mg/ml. The reference peaks in positive mode for this mixture were  $\text{Cs}^+$   $m/z$  132.90, papaverine ( $\text{C}_{20}\text{H}_{21}\text{NO}_4$ ),

$[M+H]^+$   $m/z$  340.15,  $Cs_2I^+$   $m/z$  392.71 and the reduced form of reserpine ( $C_{33}H_{39}N_2O_9$ ),  $[M+H]^+ = 607.26$ . The reference peaks in negative mode for this mixture were  $I^-$ ,  $m/z$  126.905,  $CsI_2^-$ ,  $m/z$  386.714,  $Cs_2I_3^-$ ,  $m/z$  646.524, and  $Cs_3I_4^-$ ,  $m/z$  906.334. For the tissue imaging experiments, 0.5  $\mu$ l of the solution was spotted directly onto the surface of a plate that had already been sprayed with the matrix. Around 4-5 spots were applied to different areas of each plate. For profiling experiments, for example to look at standards, equal volumes of the calibration mix and matrix being utilised in that particular experiment e.g. 15 mg/ml CHCA matrix in 1:1 acetonitrile: water 0.1% TFA were mixed and spotted into adjacent sample wells.

#### **2.11.5.2. Setting MALDI MS Instrumental Parameters for Profiling Experiments**

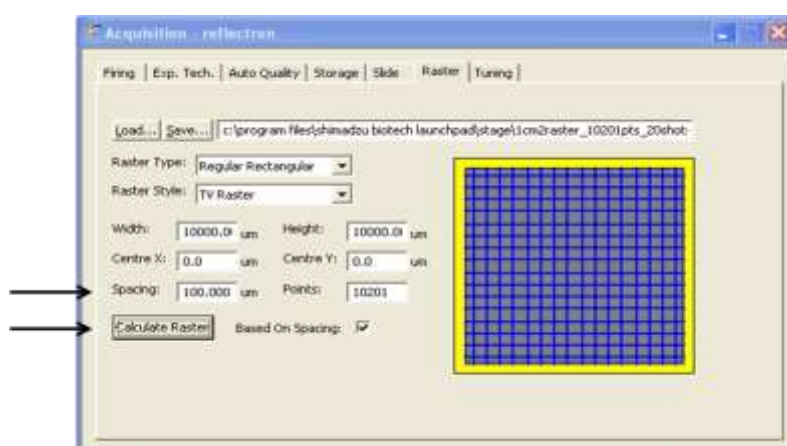
For analysis of standards, spectra were obtained at an appropriate power and enough shots were taken until spectral quality was adequate. A 1 mm raster was scanned across the sample spot or tissue region where the profiling was being carried out, taking 121 data points. This maintained continuity when scanning many sample spots.

#### **2.11.5.3. Optimisation of MALDI MS Instrument Parameters for Tissue Imaging Experiments**

Suitable methods were devised for individual imaging experiments. For each tissue sample, a raster was set up which was approximately the same width and height as the tissue sample being analysed (Figure 29). It was helpful to mark the outline of

the tissue using a blunt point before inserting the plates into the MALDI plate holder. This was because it was very difficult to see the tissue edges via the MALDI-MS camera viewer due to the extensive coverage of matrix on sprayed MALDI target plates.

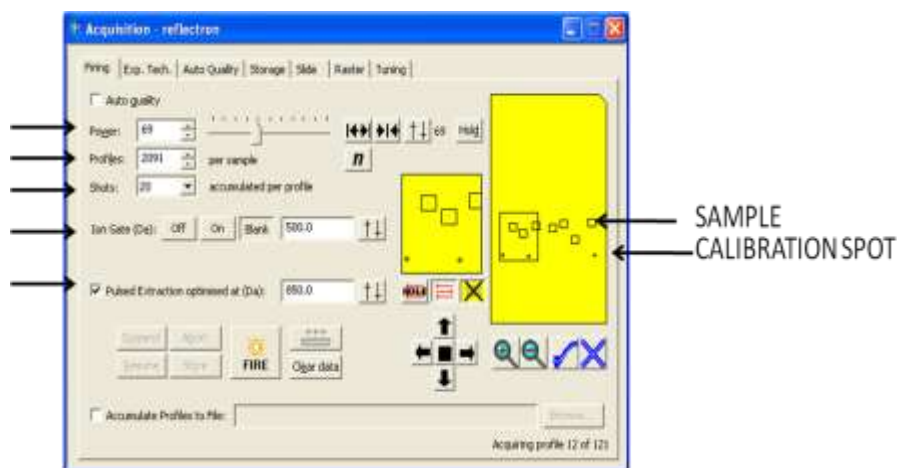
**Figure 29 - Setting up Raster for Tissue Imaging Experiment – Arrows indicate spacing and calculating raster parameters.**



A mass range of 300-2000 Da was chosen in the tissue imaging experiments which included masses of small molecules such as lipids. Pulsed ion extraction was then optimised for a particular mass(es) of interest. Other important MALDI experimental parameters were then adjusted for each experiment to optimise spectral quality. The largest raster size available on this instrument was 1 cm<sup>2</sup> which was utilised for most imaging experiments and 10201 points with either 20 or 50 shots were taken (Figure 30). An auto experiment was then set up meaning that several tissue sections were scanned in a sequence automatically with the correct method file(s) in place. Additionally, before each tissue section was scanned, automated calibrations were carried out. Small calibration spots were placed next to each tissue that was to be analysed and these were analysed before each section was scanned

(Figure 30). This allowed spectra to be comparable even after a long run time. Experiments were carried out in both reflectron positive and negative modes using untargeted approach to obtain a global overview.

**Figure 30 - Setting up experimental parameters – arrows indicate important parameters and show the sample and calibration rasters.**



### 2.11.6. Data Analysis and Interpretation

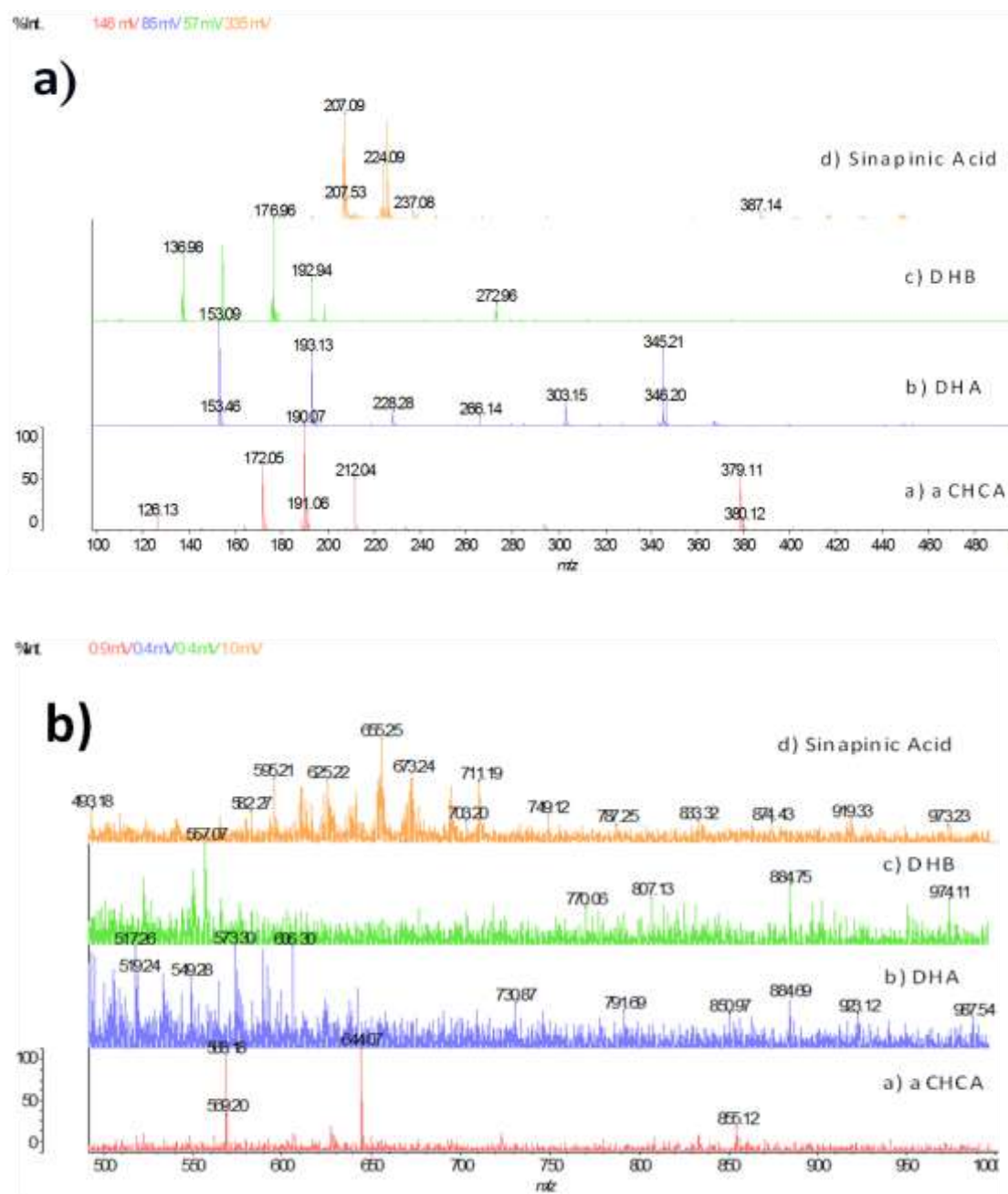
Spectra from the Axima CFR TOF mass spectrometer were analysed using the Shimadzu Biotech Launchpad software package (version 2.7.2). These files were also converted to BioMap files using a conversion tool available in the Launchpad software. The converter allows the user to select a target mass range from a MALDI data file which can then be converted and it also allows the user to either scale intensities to largest or crop saturated intensities. The crop saturated intensities option was selected and after successfully converting the files into a format that was compatible with BioMap, they were then imported into the programme, allowing image analysis to be carried out. All images were normalised in BioMap against the matrix adduct e.g. for CHCA, ion at  $m/z$  190.

## 2.12. Results

### 2.12.1. Analysis of MALDI Matrices and Matrix Selection for Imaging Experiments

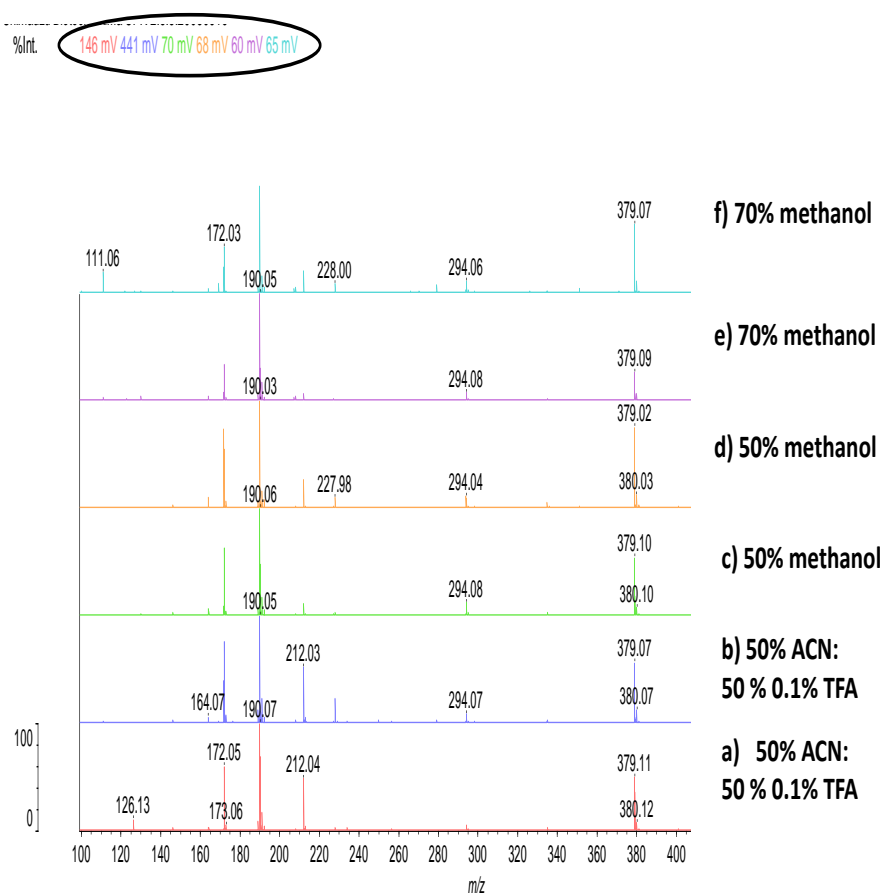
In positive ionisation mode, four matrices were initially considered for imaging experiments, CHCA, DHA, DHB and Sinapinic Acid. For the initial solvent combination of 1:1 acetonitrile: water 0.1% TFA utilised, it was found that both CHCA and DHB were the most appropriate matrices for the analysis of small molecules within mass range  $m/z$  100-1000 as they gave the least interfering signals (Figure 31). Sinapinic Acid and DHA gave many interfering signals within the mass range of  $m/z$  300-700 (Figure 31) and were not considered to be used for any further experiments as this fell within the mass range of interest for this project.

Figure 31 - Background ions observed in mass range a)  $m/z$  100-500 and b)  $m/z$  500-1000 from analysis of different matrices prepared at a concentration of 15 mg/ml in 1:1 acetonitrile: water 0.1% TFA a) CHCA, b) DHA, c) DHB, d) sinapinic acid.



Following this, to investigate if CHCA in a solvent combination of 1:1 acetonitrile: water plus 0.1% TFA was suitable for small molecule analysis, other solvent combinations (suggested in previous studies) were also tried at two different laser powers which varied according to the matrix being used. The initial laser powers utilised gave reproducible MALDI signals and were optimised for each matrix utilised. The second laser powers were then calculated by increasing the initial laser powers by 5%. As the signal intensities were highest when 1:1 acetonitrile: water 0.1% TFA was used, this was selected for further experiments (Figure 32). This was also chosen as it was the standard solvent combination that has been utilised previously in many studies. It can also be observed that increasing the laser power did not really change signal intensities when methanol and water were utilised as solvents.

**Figure 32 – Spectra obtained from the analysis of the CHCA matrix in different solvent combinations that were suggested from previous studies, a) 1:1 acetonitrile: water 0.1% TFA, c) 50% methanol, e) 70% methanol. b), d) and f) show the spectra obtained when laser powers were increased by 5%.**



As polar and non-polar lipids were also of interest during this study, DHB was also chosen as a matrix. From the analysis of sample spots mixed with DHB dissolved in solvent combination of acetonitrile: water 80:20 0.1% TFA which included water, it was observed that there was poor crystallisation during both profiling experiments and imaging experiments due to the length of evaporation time. The crystals formed were large and angular and did not form a homogenous layer and thus were unsuitable for imaging experiments. Thus, it was necessary to consider other solvent



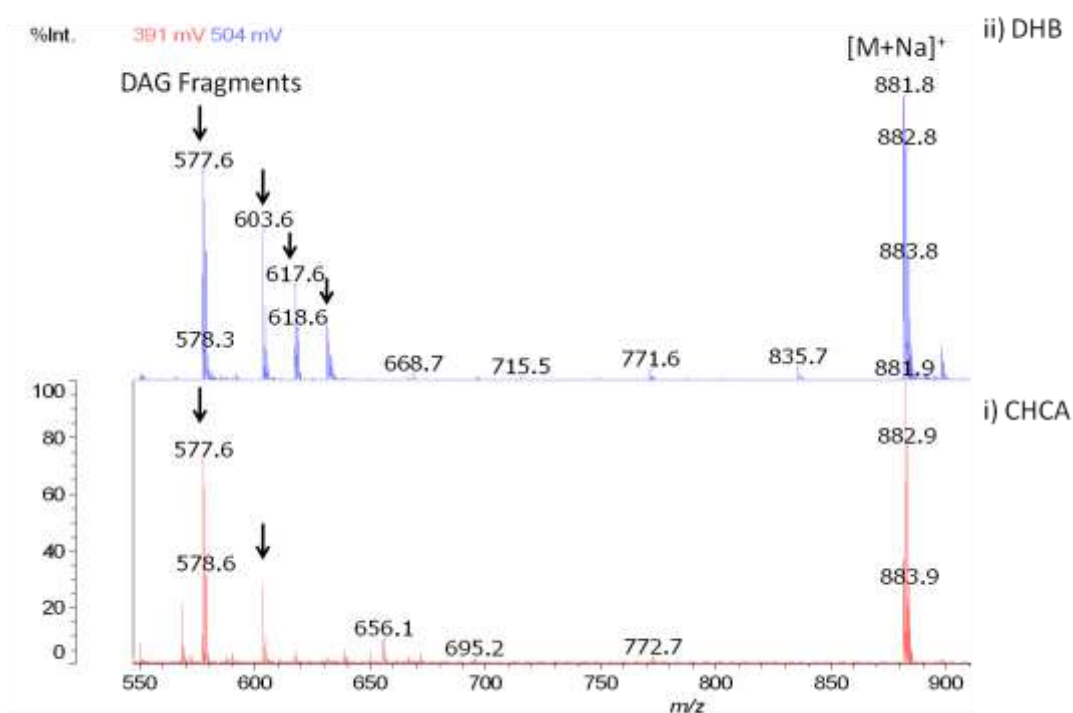
combinations to use with DHB to ensure even matrix coverage and formation of small matrix crystals. To avoid the formation of large crystals, it was proposed that a higher percentage of organic solvent could be used. As described in section 2.8.1, DHB in 100% acetone was the best matrix for quantification of lipids with detection levels in mid fmol region [228]. This matrix and solvent combination was then utilised for profiling lipid standards and imaging experiments and it was found that its rapid drying time ensured the formation of a homogenous layer of matrix crystals in profiling and on tissue sections. Examples below illustrate the suitability of DHB for analysis of non-polar triacylglycerol standards compared to CHCA (Figure 33). DHB gives better signal to noise ratios for the analysis of triacylglycerol standards, and analysis of triacylglycerols in biological samples from profiling and imaging.

Analysis of the triacylglycerol lipid standards using DHB matrix illustrates that they are predominantly found in their sodiated forms which is in agreement with the results of previous studies (Figure 33) [228]. They were also found to exist as potassium adducts but the peak intensity was lower. The potassium adducts had higher intensities when DHB was utilised compared to CHCA. It is also clear that there is formation of DAG- like fragments during MALDI-MS analysis. For triolein (1,2,3-tri-(9Z-octadecenoyl)-glycerol) there was a prominent peak found at  $m/z$  603.6 Da which corresponds to the  $[\text{DAG}]^+$  fragment created through the removal of one oleic fatty acid chain from the parent triolein as a sodium salt  $[\text{RCOONa}]$  (Figure 33). As this TG has three identical fatty acid chains, fragmentation could be happening at sn-1, sn-2 or sn-3 positions. It was also possible to observe the potassium adduct of the  $[\text{DAG}]^+$  fragment at  $m/z$  622.6 Da. For 1-hexadecanoyl-2,3-di-(9Z-octadecenoyl)-sn-glycerol, it was possible to detect the parent as a sodium

adduct and two DAG fragments at  $m/z$  577 and  $m/z$  603 which correspond to  $[\text{DAG}]^+$  fragments created through the removal of either one oleic acid or palmitic fatty acid chain from the TAG molecule as sodium salts  $[\text{RCOONa}]$ . Again, it was also possible to see the potassium adducts of the parent ions as well (Figure 33).

**Figure 33 – Spectra showing suitability of DHB for analysis of triacylglycerol lipid standards, a) C16:0/C18:1/C18:1 (1-hexadecanoyl-2,3-di-(9Z-octadecenoyl)-sn-glycerol) and b) C18:1/C18:1/C18:1 1,2,3-tri-(9Z-octadecenoyl)-glycerol. It can be seen that higher peak intensities are observed from the analysis of triacylglycerol standards when DHB is used as a matrix (ii) compared to CHCA (i). DHB was prepared in 100% Acetone whilst CHCA was prepared in 1:1 acetonitrile: water 0.1% TFA.**

a) C16:0/18:1/18:1



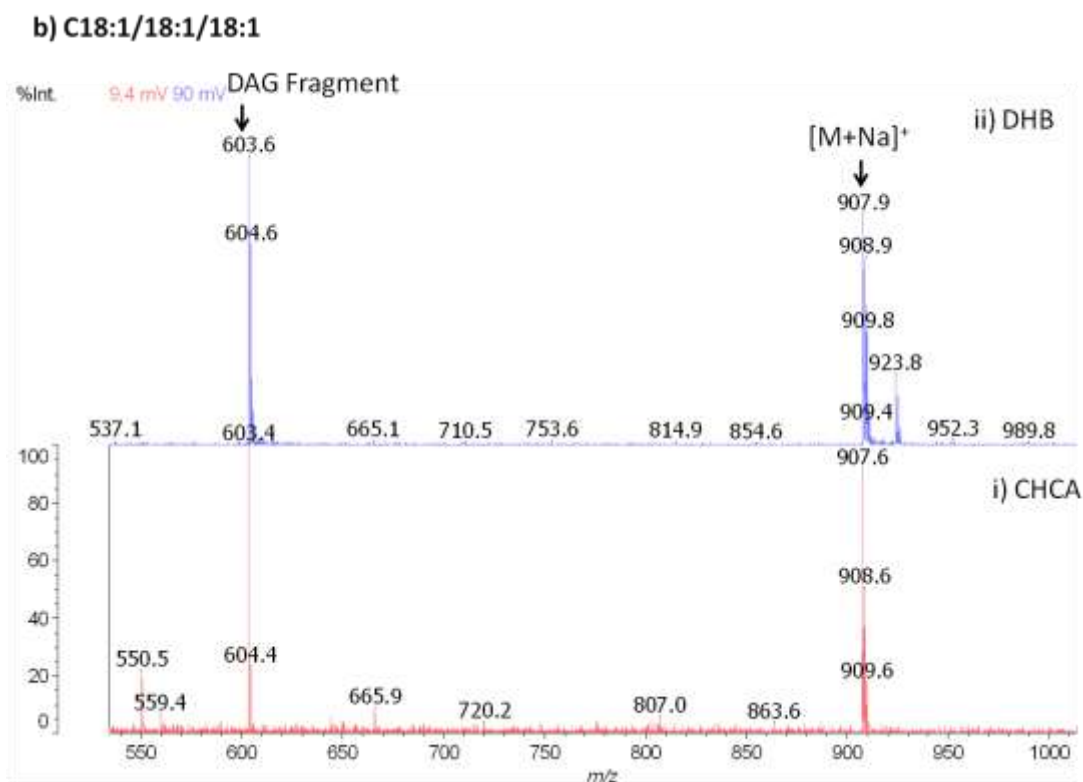
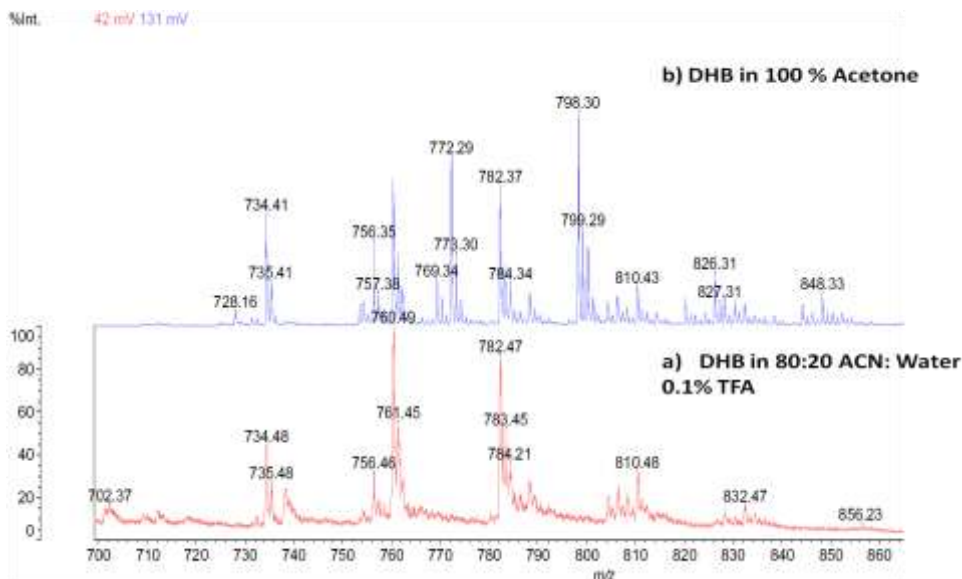
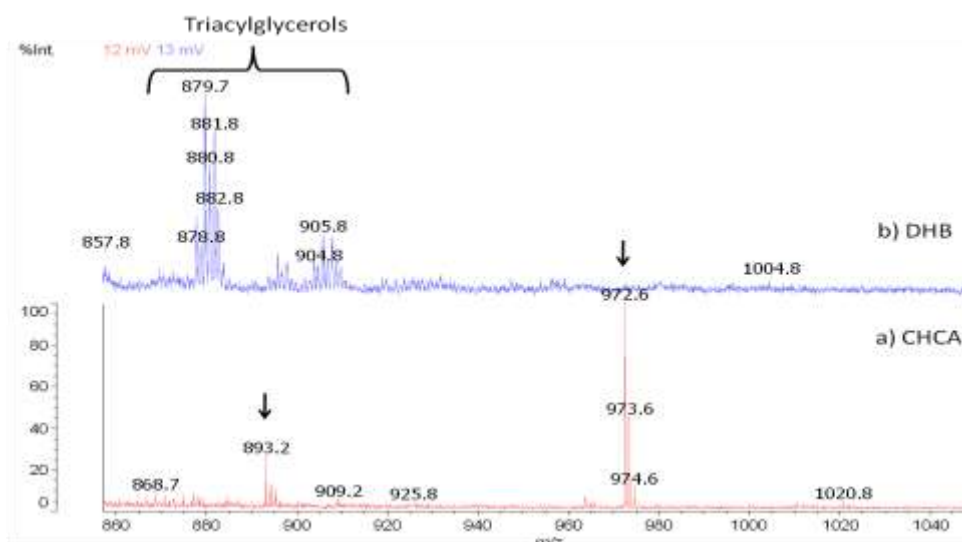


Figure 34 shows example spectra obtained from the analysis of phosphatidylcholines in rat brain when DHB in 100 % acetone was utilised as a solvent compared to DHB in acetonitrile: water 80:20 0.1% TFA. The inclusion of water resulted in the formation of large, angular crystals around the edge of the sample spot only. This resulted in poor ionisation and the spectra reflect this, there are less peaks observed and the resolution is much poorer (Figure 34). Thus, this illustrates that DHB in 100% acetone can also be used successfully for imaging experiments to visualise phosphatidylcholine lipids. DHB was also found to be the most suitable matrix for the analysis of triacylglycerols in biological samples compared to CHCA (Figure 35). The selection of DHB as a matrix for mapping triacylglycerols is discussed in more detail in chapter 4.

**Figure 34 - Comparison of spectra obtained when DHB is utilised in a) acetonitrile: water 80:20 0.1% TFA or b) in 100% acetone to profile lipids in rat brain tissue sections from a MALDI imaging experiment.**

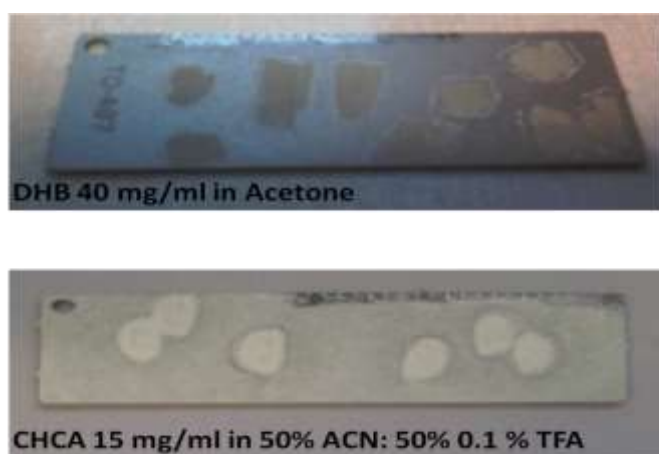


**Figure 35 – Spectra obtained from the analysis of two liver tissue sections with a) CHCA 15 mg/ml in 1:1 acetonitrile: water plus 0.1% TFA and b) DHB 40 mg/ml in 100% acetone from a MALDI imaging experiment.**



Another factor taken into consideration during matrix selection for imaging experiments was homogeneity of matrix following application. CHCA in 1:1 acetonitrile: water plus 0.1% TFA produced homogenous crystallisation and good coverage when utilised for both profiling and imaging experiments. Additionally, DHB in 100% acetone also produced a homogenous layer of crystals when utilised for imaging experiments (Figure 36).

**Figure 36 – Pictures of MALDI Plates Coated with Different Matrices**



### 2.12.2. Matrix Interferences

Even when the best matrices and solvent combinations have been selected for MALDI experiments, one of the main problems that are associated with carrying out small molecule analyses is spectral interference which makes it difficult to identify molecules below  $m/z$  500. This is particularly evident when utilising the CHCA matrix as it forms a lot of singly positively charged matrix clusters (Table 4). The table below illustrates some of the main interfering matrix peaks found when using CHCA with mass to charge ratios between  $m/z$  150-600 which includes  $\text{Na}^+$  and  $\text{K}^+$

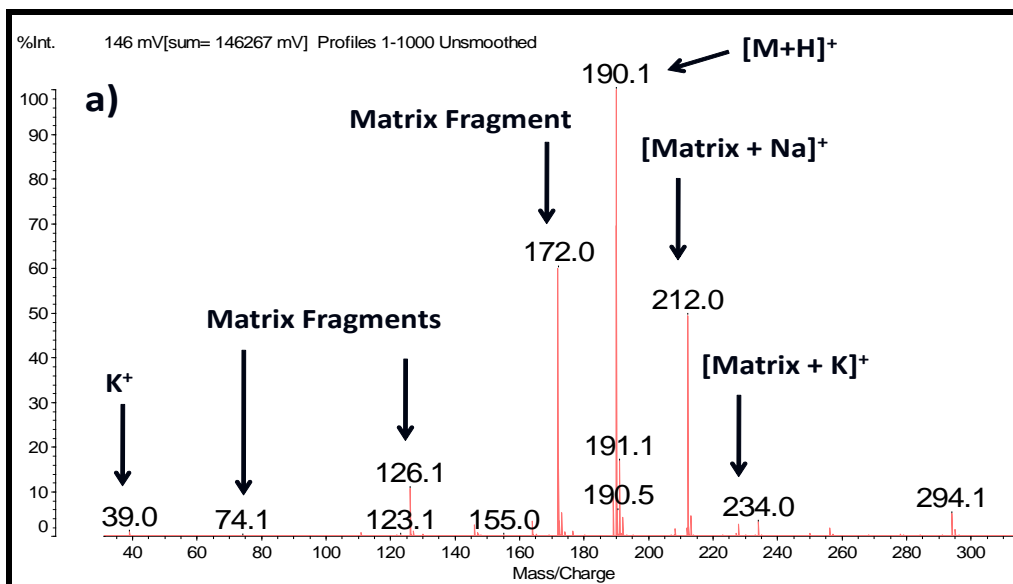
adducts. There are also matrix related peaks, with a lower intensity, found up to  $m/z$  2000. Matrix ions are also observed when DHB is utilised as a matrix but the range of matrix adducts is not as large as when CHCA is utilised. For a full list of commonly encountered interfering ions in MALDI MS the reader is directed to the comprehensive review by Keller [254].

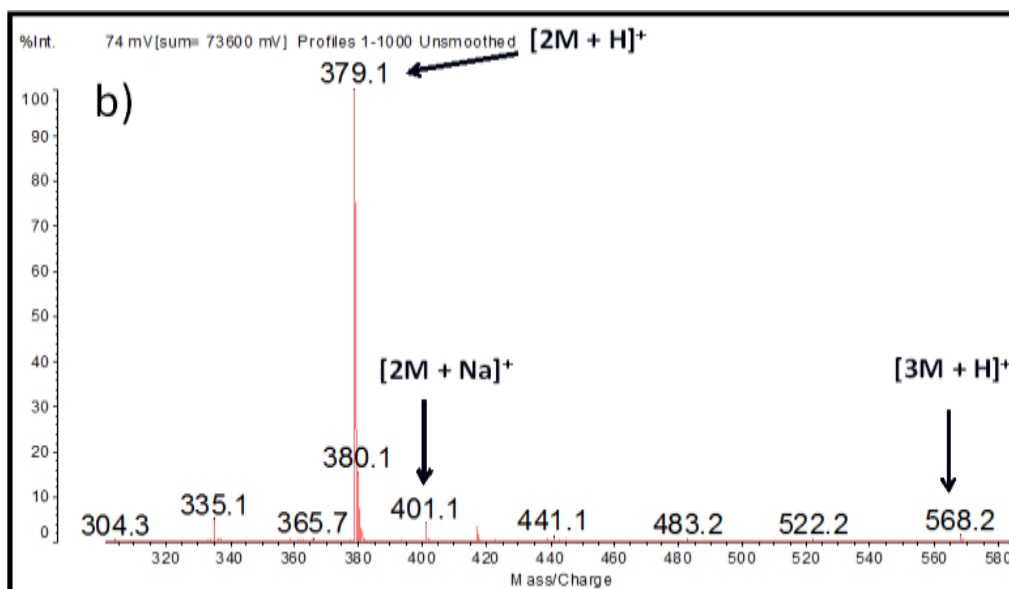
**Table 4- Commonly Encountered Matrix Peaks When Using CHCA <  $m/z$  600.**

<b>Matrix Cluster</b>	<b>Mass/Charge (<math>m/z</math>)</b>
$[M+H]^+$	<b>190.05</b>
$[M+Na]^+$	<b>212.03</b>
$[M+K]^+$	<b>228.01</b>
$[2M+H]^+$	<b>379.09</b>
$[2M+Na]^+$	<b>401.07</b>
$[2M+K]^+$	<b>417.05</b>
$[2M+2Na-H]^+$	<b>423.06</b>
$[2M+Na+K-H]^+$	<b>439.03</b>
$[2M+2K-H]^+$	<b>455.00</b>
$[3M+H]^+$	<b>568.14</b>
$[3M+Na]^+$	<b>590.12</b>

Figure 37 shows some of the most prominent matrix-related peaks that are found when utilising CHCA as a matrix. The spectra are taken from sample spots of CHCA prepared at a concentration of 15 mg/ml in 1:1 acetonitrile: water 0.1% TFA. It can be seen from the spectra that both the protonated matrix monomer and dimer peaks have very high intensities. Signal suppression may occur due to this. As imaging mass spectrometry requires the use of a high laser power to facilitate desorption/ionisation from the tissue surface, fragmentation of the CHCA parent ion also occurs. Some of these ions can also be identified from the spectra shown below for example at  $m/z$  172, 155 and 126 (Figure 37).

**Figure 37 - Two example spectra showing the abundance of peaks generated from MALDI MS profiling of CHCA matrix prepared at concentration of 15 mg/ml in 1:1 acetonitrile: water plus 0.1% TFA that was spotted onto a MALDI Target a) shows mass range  $m/z$  40-300 and b) shows mass range  $m/z$  300-580.**

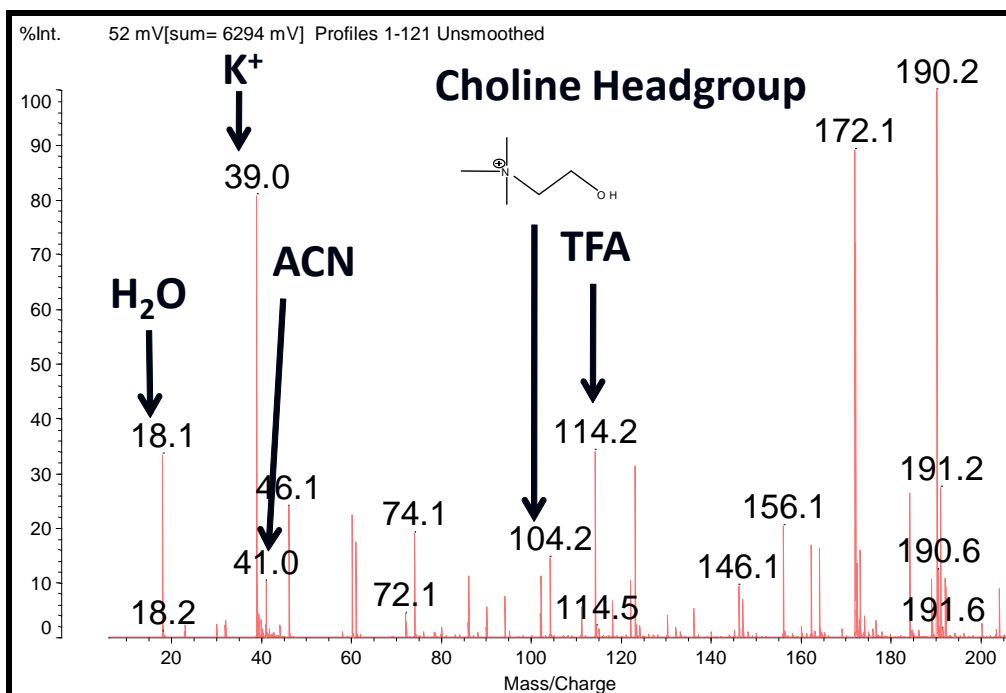




Other peaks that can be found below  $m/z$  500 include solvent peaks and lipid fragments which complicate the spectra further when carrying out tissue imaging experiments. For example, TFA, H<sub>2</sub>O and acetonitrile can be seen in the spectrum shown below that was taken from a tissue imaging experiment (Figure 38) where the matrix utilised was CHCA in 1:1 acetonitrile: water plus 0.1% TFA. Additionally, lipid fragments were found in the spectra such as the choline head group from phosphatidylcholine fragmentation. Additionally, serine, ethanolamine and other lipid moieties may also be found. The number of background ions with low molecular weights indicates why small molecule analyses using MALDI-MS are so complex.



**Figure 38 - Sample spectrum illustrating solvent-related peaks and lipid fragments that may be found during tissue imaging experiments.**



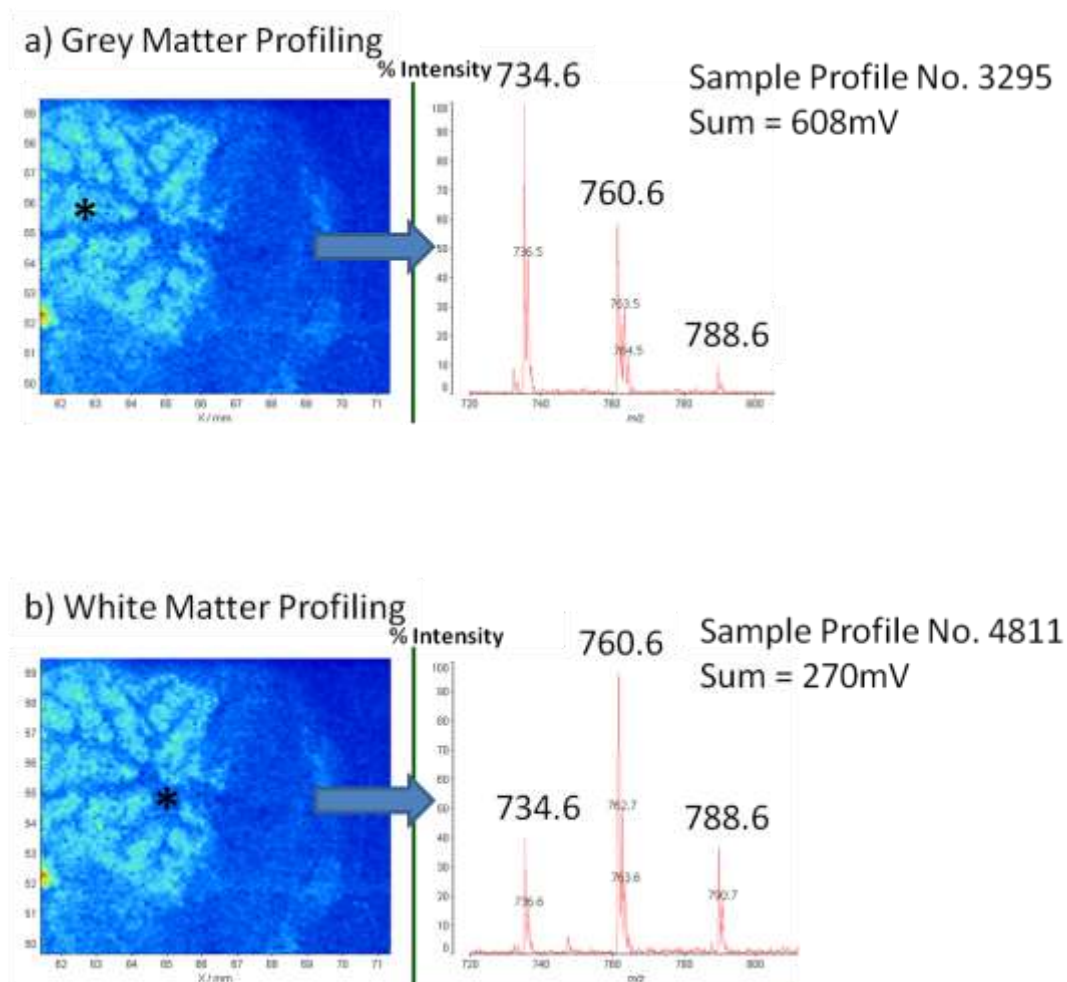
Regardless of these problems, CHCA was found to give good results for the analysis of phosphatidylcholine and sphingomyelin lipids and drug molecules. The use of CHCA for DMPK studies is discussed in chapter 3. However, it was found that DHB matrix in 100% acetone was good for the analysis of lipids as well, and was better for the analysis of triacylglycerol lipids than CHCA. Further examples of results obtained from use of these matrices and solvent combinations are given later in this chapter as well as in chapters 3 and 4.

### **2.12.3. Investigations of Detection of Lipid Classes in Reflectron Positive and Negative Ionisation Modes**

#### **2.12.3.1. Profiling Lipids in Rat Brain Sections**

MALDI profiling can be utilised to investigate lipid profiles in different tissue areas of interest for comparative studies. An example is shown below illustrating the differences in ion intensities of phosphatidylcholine lipids in spectra collected from the white and grey matter of cerebellum (Figure 39). This simple example illustrated that MALDI MS can be utilised to compare relative intensities of ions in different tissue regions. For example, the ion at  $m/z$  734 had a higher relative intensity in grey matter than the ion at  $m/z$  760 whilst in the white matter these differences in intensities were reversed with  $m/z$  760 having a higher relative intensity than  $m/z$  734.

**Figure 39 - Profiling in a) grey matter and b) white matter of the cerebellum showing examples of individual spectra observed in the respective regions. An intensity map plotting the distribution pattern of the ion observed at  $m/z$  734 is used to show the outline of the white and grey matter regions.**

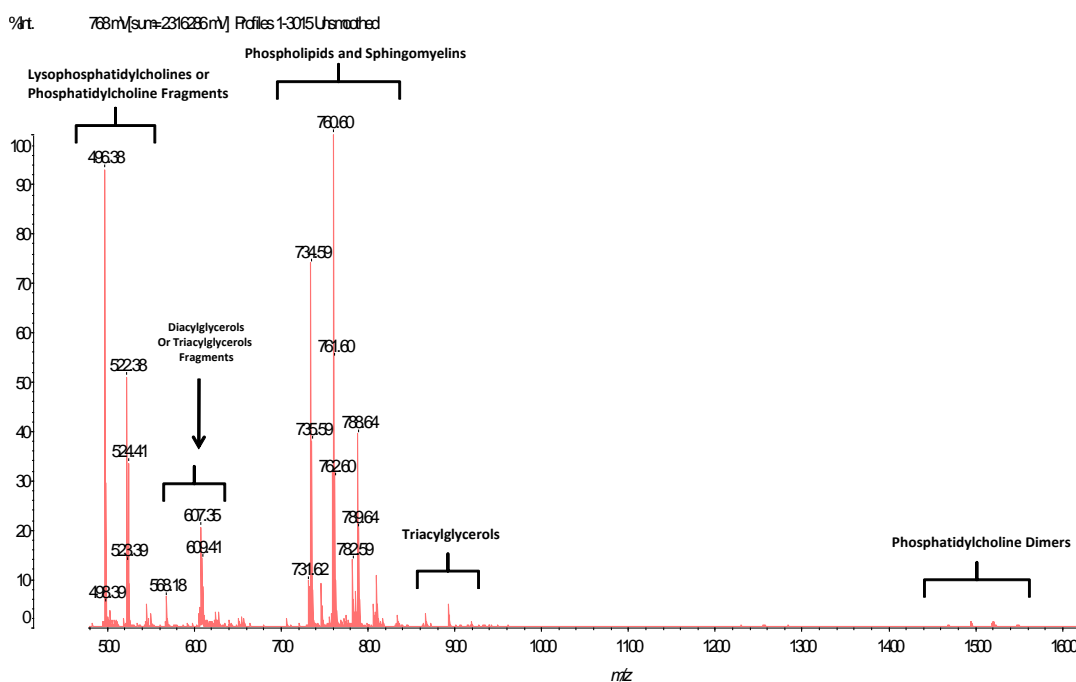


### **2.12.3.2. Imaging Lipids in Rat Brain Sections in Reflectron Positive Ionisation Mode**

To investigate the distribution of lipids in intact rat brain sections, tissue sections were analysed utilising MALDI-MSI. CHCA was utilised as a matrix as it was found to give good signal to noise for the analysis of lipids in reflectron positive mode.

Figure 40 shows an average spectrum obtained from the analysis of a rat brain section in reflectron positive mode. It can be seen that there are clusters of signals observed which correspond to lysophosphatidylcholines, phosphatidylcholines, triacylglycerols and phosphatidylcholine dimers (Figure 40). It can also be seen that there are clusters observed around  $m/z$  550-650 which may correspond to fragments of phosphatidylcholines or triacylglycerols where one fatty acid chain is lost from the parent molecule.

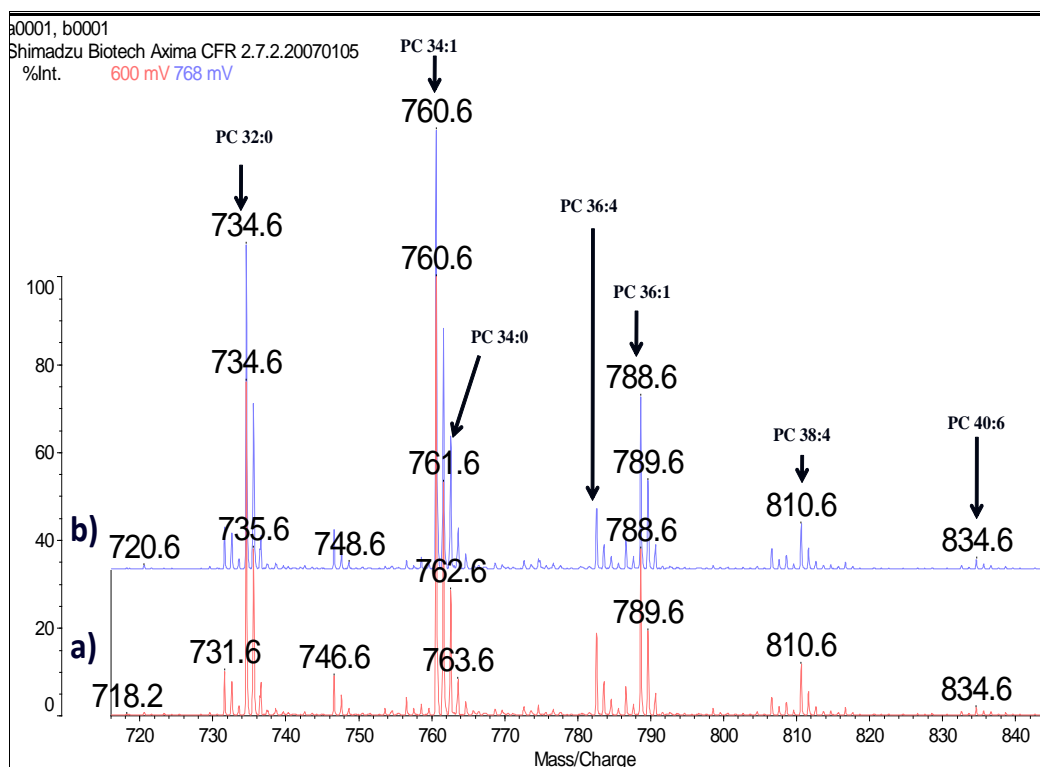
**Figure 40 – Spectrum obtained from analysis of rat brain section using MALDI-MSI illustrating lipid detection within mass range  $m/z$  100-1600. CHCA in 1:1 acetonitrile: water plus 0.1 % TFA was used as a MALDI matrix.**



#### **2.12.3.2.1. Phosphatidylcholine Localisation in Rat Brain Sections**

Imaging experiments revealed that there were many high intensity ions in the region of  $m/z$  700-900. Previous studies utilising MALDI-MS have already identified many of these as phosphatidylcholines in a number of studies [198,219,226,255,256]. Peak intensities were found to vary considerably for different phosphatidylcholines (Figure 41). For example, phosphatidylcholine PC34:1 at  $m/z$  760 had the highest intensity within the mass range of 700-800 Da. This lipid has been characterised as PC16:0/18:1 previously [198,216]. Several other species of phosphatidylcholine were also identified such as PC 32:0, PC 34:0 PC 36:4, PC 36:1, PC 38:4 and PC 40:6. These lipids have been characterised in previous studies as PC 16:0/16:0, PC 16:0/18:0, PC 18:2/18:2, PC 18:0/18:1, PC 18:0/20:4 and PC 18:0/22:6, respectively [198,216].

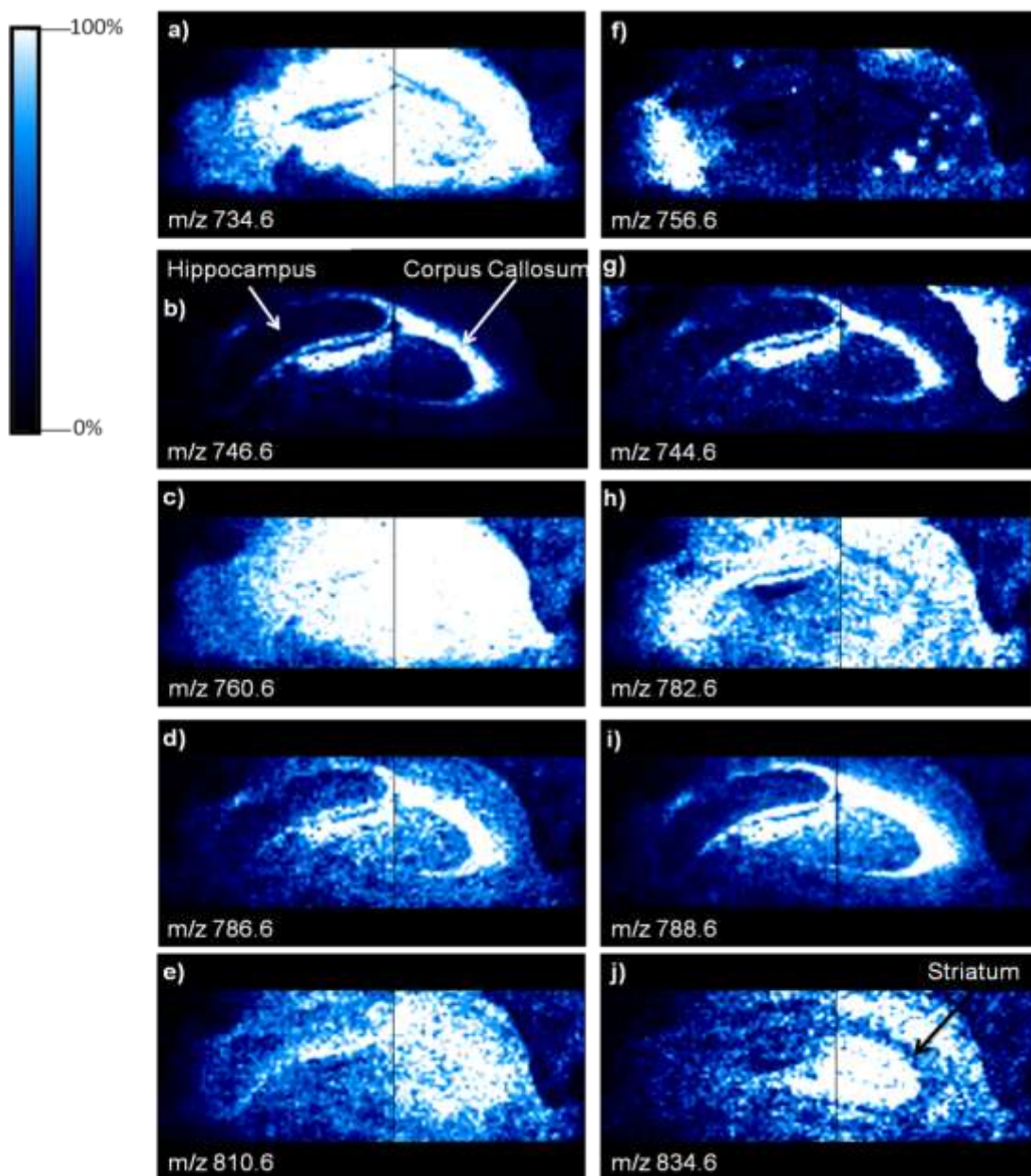
**Figure 41 – Average spectra from analysis of rat brain tissue revealing the presence of several phosphatidylcholines in two 1cm<sup>2</sup> tissue sections (a) and (b). CHCA in 1:1 acetonitrile: water plus 0.1 % TFA was used as a MALDI Matrix.**



By creating corresponding images of these samples and creating heat maps of the various phosphatidylcholines, it was possible to illustrate that they have distinct expression patterns in the rat brain (Figure 42). The ion density map of  $m/z$  760 corresponds to PC 16:0/18:1 and reveals that this lipid was distributed throughout the rat brain with a high intensity (Figure 42). However, the ion density map of  $m/z$  734 corresponds to PC 16:0/16:0 which had the higher intensity in the grey matter regions whilst the ion density map of  $m/z$  788.6 corresponds to PC 18:0/18:1 which had the higher intensity in the white matter regions (Figure 42). Other

phosphatidylcholine species that were profiled included PC 18:1/20:3 and PC 16:0/18:0 and these also had unique distribution patterns. Thus, this example illustrates how MALDI-MS can be used to look at the distribution patterns of endogenous lipid molecules in tissues.

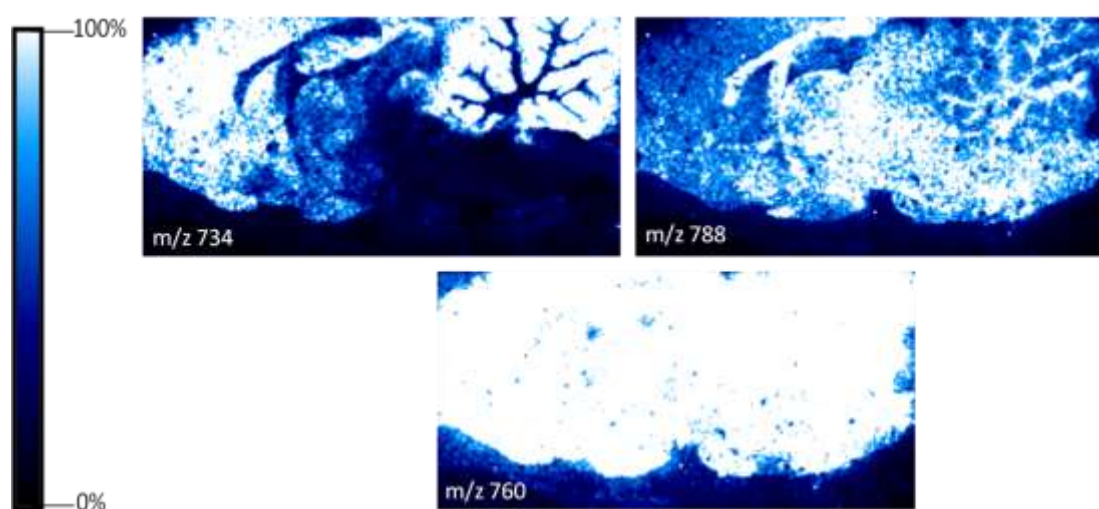
Figure 42 – Images shown in a) to j) correspond to spectra in Figure 41 and illustrate the distribution patterns of selected phosphatidylcholines in naive rat brain tissue sections. CHCA in 1:1 acetonitrile: water plus 0.1 % TFA was used as a MALDI matrix.





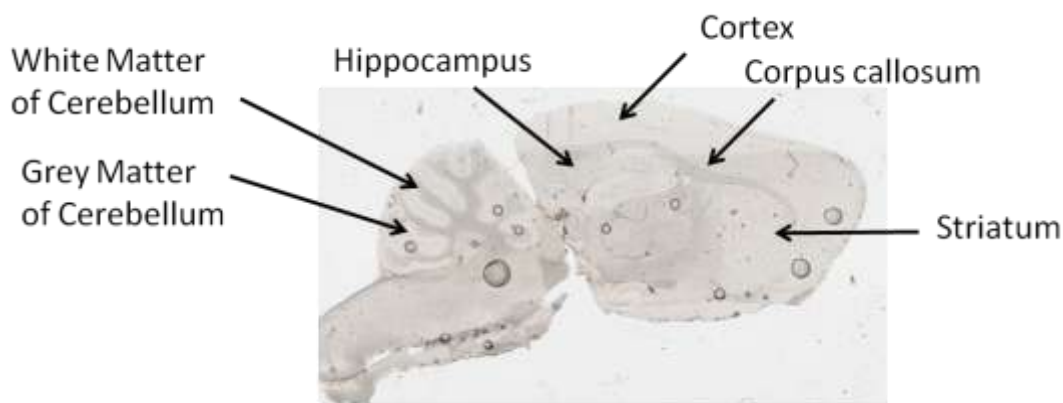
The same sample preparation method was then used but samples were analysed using a higher number of shots (50) to produce more detailed images showing the distribution of lipids, again in the rat brain. Here, the cerebellum can be clearly seen (Figure 43).

**Figure 43 – Additional heat maps illustrating the distribution of phosphatidylcholine lipids in complete rat brain sections, with cerebellum completely visible.**



To aid recognition of the regions observed in the MALDI images in Figure 42 and Figure 43 were compared to a photo of a sagittal rat brain section taken with a Nikon Cool iV scanner, such as that shown below (Figure 44). Gross anatomical regions that were observed in many of the MALDI images of sagittal rat brain sections found in this chapter and chapter 3 are labelled (Figure 44).

**Figure 44 – A photo of a sagittal rat brain section taken with a Nikon Cool Scan iV scanner labelled to illustrate the location of gross anatomical regions including the cortex, white matter of cerebellum, grey matter of cerebellum, hippocampus and striatum.**



#### **2.12.3.2.2. Formation of Phosphatidylcholine Dimers**

Two interesting clusters were also observed within the mass range of  $m/z$  1150-1700 in reflectron positive ionisation mode (Figure 45). The cluster observed within the mass range  $m/z$  1450-1600 corresponds to dimers of common phosphatidylcholine lipids. These are observed due to the use of high laser power for imaging experiments to enable the laser energy to burn through the matrix and tissue during ionisation. The cluster observed within mass range  $m/z$  1200-1300 corresponds to phosphatidylcholine dimers that have lost one fatty acid chain from one of the phosphatidylcholines (Figure 45). This illustrates that complex spectra can be obtained following MALDI-MSI analysis due to abundant compounds forming dimers.

**Figure 45 – Spectra showing mass range  $m/z$  1150 – 1700 reveals lipid clusters from analysis of rat brain samples (a) and (b).**

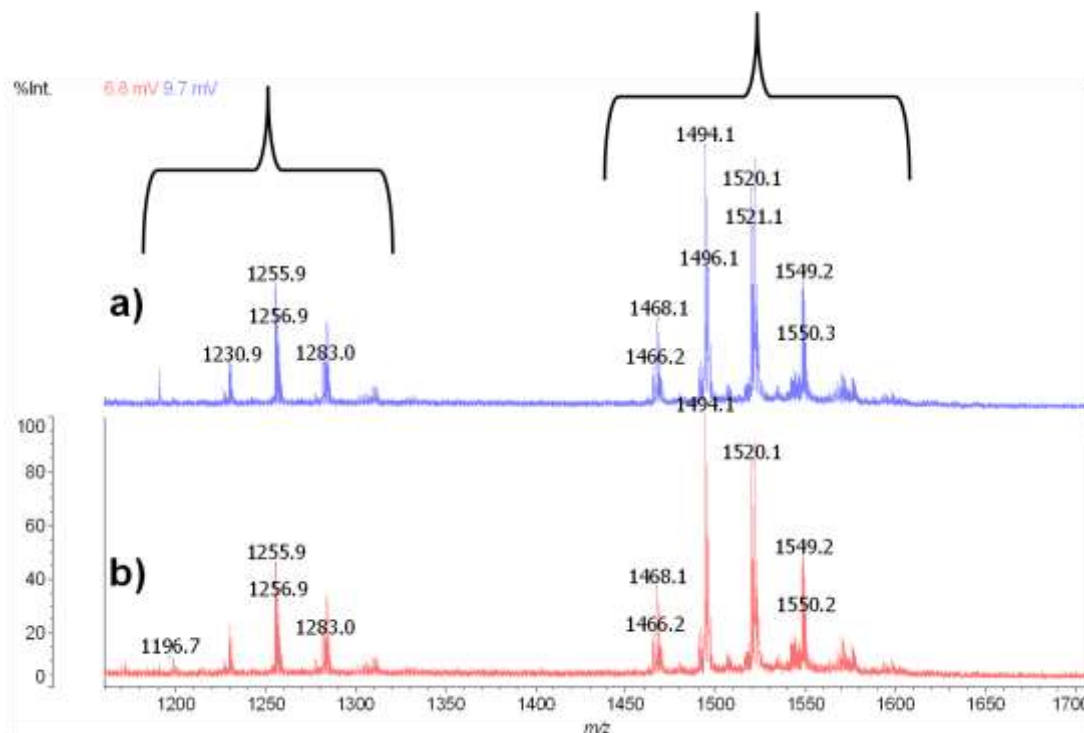
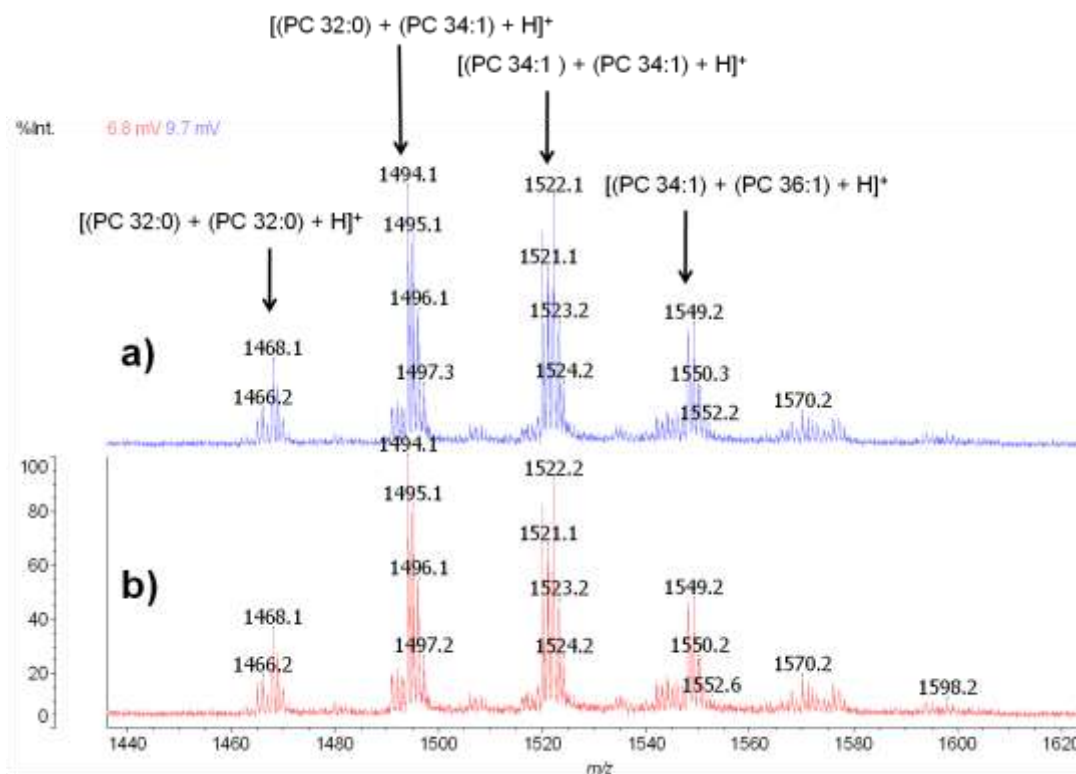


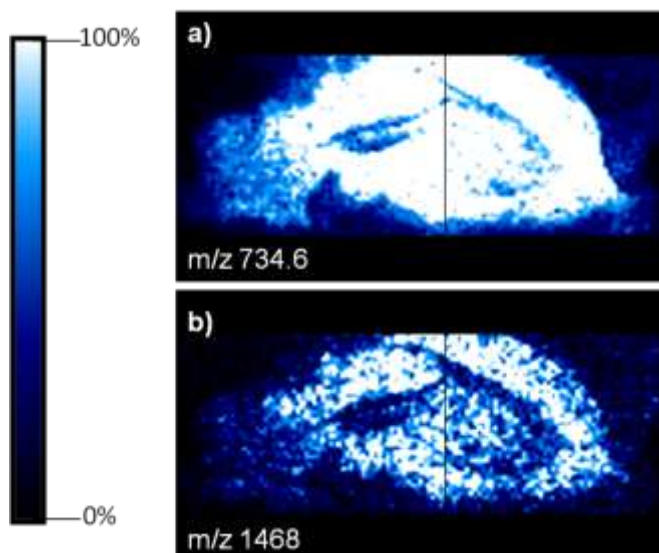
Figure 46 shows the cluster between  $m/z$  1440-1620 more closely and reveals dimers observed include  $[(PC\ 32:0) + (PC\ 32:0) + H]^+$ ,  $[(PC\ 32:0) + (PC\ 34:1) + H]^+$  and  $[(PC\ 34:1) + (PC\ 36:1) + H]^+$ .

**Figure 46 – Spectra zoomed in to reveal cluster within mass range  $m/z$  1440-1620 whose masses corresponds to dimers of phosphatidylcholine lipids in rat brain samples (a) and (b).**



To confirm that these were in fact dimers of phosphatidylcholines, heat maps were generated which illustrate that the ion observed at  $m/z$  1468 has the same distribution pattern as  $m/z$  734.6. However, the signal intensities are not as high as these are products of ionisation and are the mass ion peaks for the respective real lipids (Figure 47).

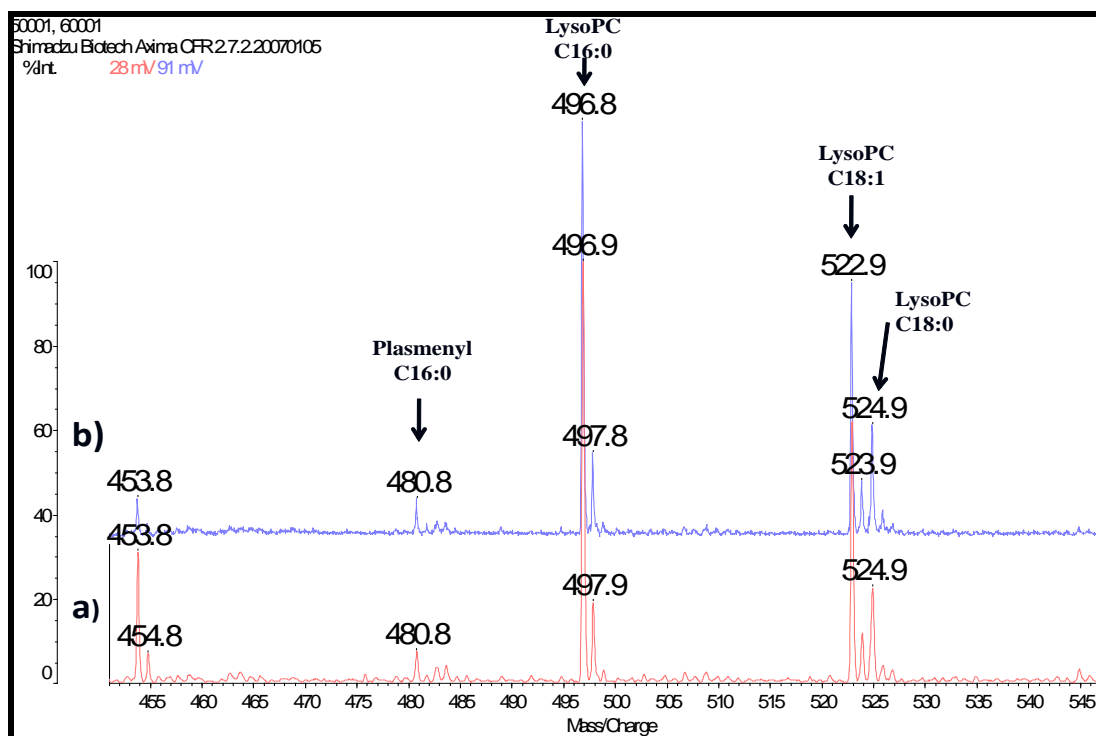
**Figure 47 – Heat maps of phosphatidylcholine C32:0 at  $m/z$  734.6 and its dimer at  $m/z$  1468 in rat brain tissue samples illustrating that the same distribution pattern was observed, whilst a lower signal intensity was exhibited by the dimer. CHCA in 1:1 acetonitrile: water plus 0.1 % TFA was used as a MALDI matrix**



#### **2.12.3.2.3. Lysophospholipid Localisation in Rat Brain Sections**

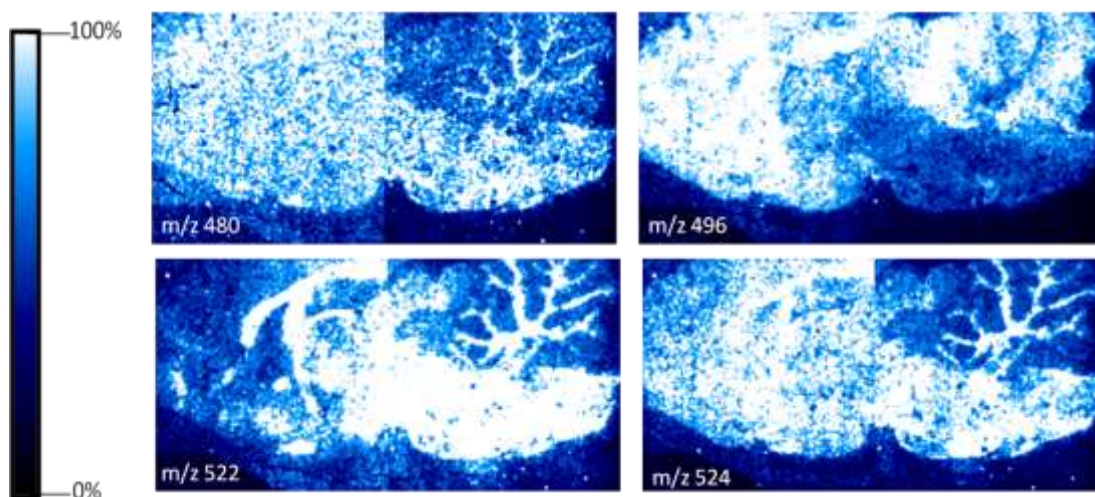
Peaks within the mass range 450-550 were also observed from analysis of rat brain sections. These are thought to correspond to  $H^+$  adducts of lysophosphatidylcholines (LPCs) (Figure 48). The most intense peaks may correspond to lysophosphatidylcholine C16:0 and lysophosphatidylcholine C18:1 which correlated with the result observed for the phosphatidylcholine lipids as the most intense peak corresponded to C16:0/C18:1. However, it is not possible to rule out that these are actually fragments of phosphatidylcholines generated via the loss of an acyl chain.

**Figure 48 - Average spectra in mass range  $m/z$  450-550 from analysis of rat brain tissue revealing the presence of several lysophosphatidylcholines in two  $1\text{cm}^2$  tissue sections (a) and (b). CHCA in 1:1 acetonitrile: water plus 0.1 % TFA was used as a MALDI matrix.**



Tissue images were generated and it was found that the identified species had unique distribution patterns in the tissues (Figure 49). Whilst LPC 16:0 was found in higher intensity in the grey matter, LPC 18:1 and LPC 18:0 had higher intensities in the white matter regions (Figure 49). This corresponded to the distribution patterns observed for phosphatidylcholines, for example PC 16:0/16:0 at  $m/z$  734 was found to be highly distributed in the grey matter regions whilst PC18:0/18:1 at  $m/z$  788.6 was found mainly in the white matter regions. These lipids had similar distribution patterns to phosphatidylcholines, so again it is not possible to rule out that they are in fact fragments of the parent phosphatidylcholine species.

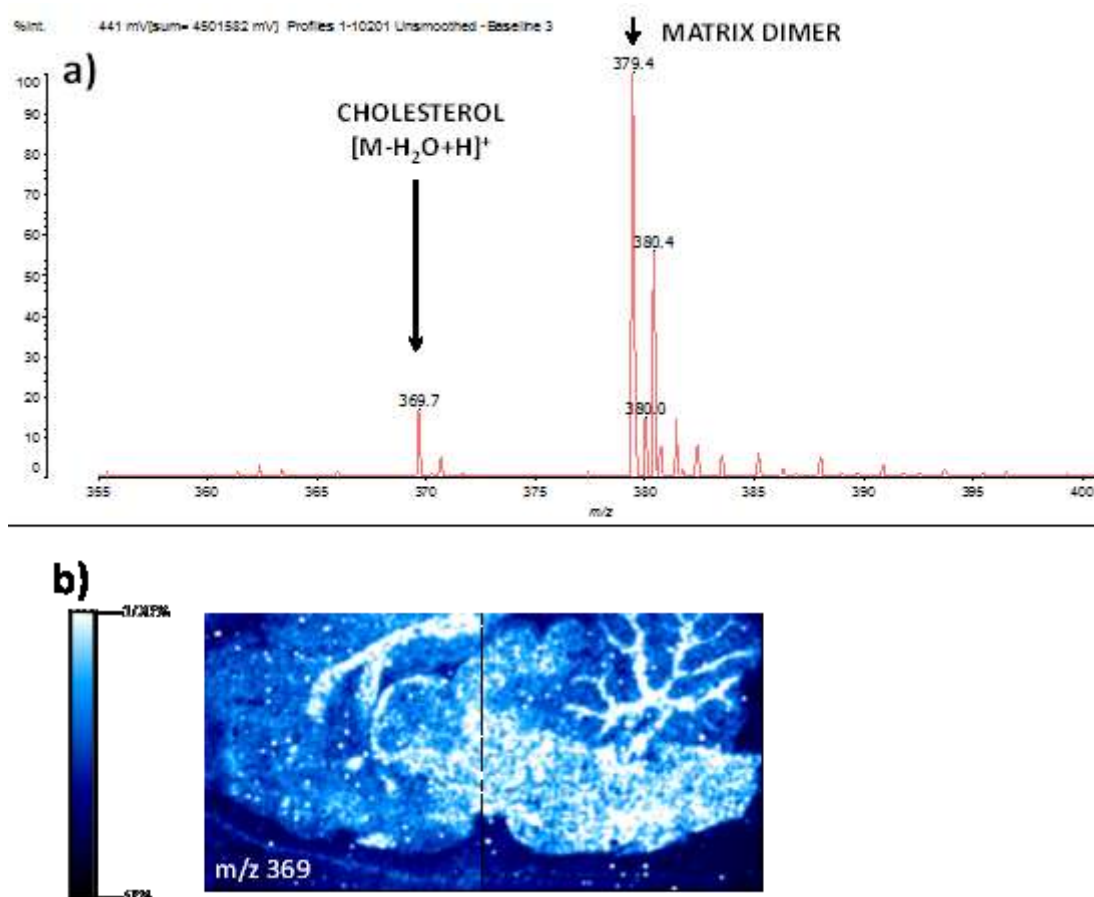
**Figure 49 - Images of lysophospholipid species showing their distribution patterns in naive rat brain tissue sections. Images normalised against matrix ion. CHCA in 1:1 acetonitrile: water plus 0.1 % TFA was used as a MALDI matrix.**



#### **2.12.3.2.4. Mapping the Distribution of Cholesterol in Rat Brain Sections**

Cholesterol is an abundant steroid that has a tetracyclic ring system in its structure. It can be found in two forms, either as free cholesterol or as cholesteryl esters of long chain fatty acids. Cholesterol is the most abundant sterol found in animal tissues. Cholesterol has an  $-OH$  functional group making the molecule slightly polar. In MALDI, free cholesterol is often observed in the form of  $[M-H_2O+H]^+$ . In the rat brain sections it was possible to map the distribution pattern of cholesterol which was observed as  $[M-H_2O+H]^+$ . The generation of a heat map illustrated that cholesterol was highly concentrated in the white matter regions.

**Figure 50 – a) Spectrum showing cholesterol ion at  $[M-H_2O+H]^+$  and b) heat map illustrating the distribution of cholesterol in rat brain sections. CHCA in 1:1 acetonitrile: water plus 0.1 % TFA was used as a MALDI matrix.**



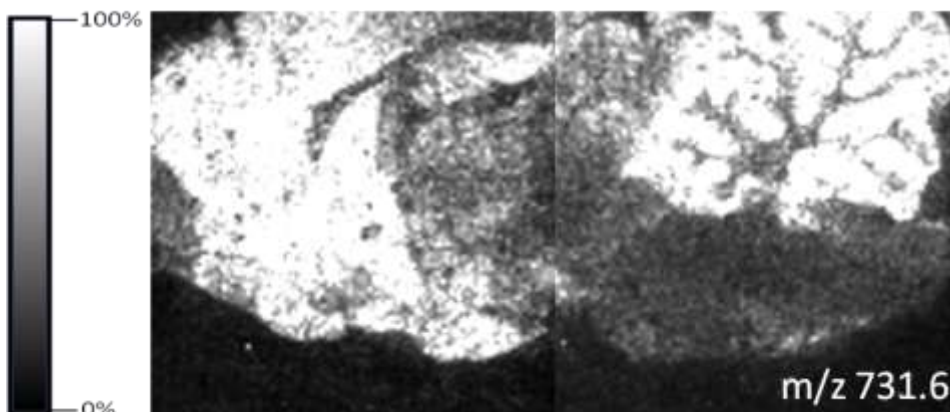
#### 2.12.3.2.5. Mapping the Distribution of Sphingomyelins in Rat Brain Sections

It was also possible to map the distribution of sphingomyelins in the brain sections in reflectron positive mode. Sphingomyelins are found within the same mass range as phosphatidylcholines but since they have an even number of nitrogen atoms the protonated adducts are odd numbers such as  $m/z$  703 and  $m/z$  731 due to the nitrogen



rule. The example below shows the distribution of a sphingomyelin at  $m/z$  731 and it can be seen that it is found in higher intensity in the grey matter (Figure 51).

**Figure 51 - Image of sphingomyelin at  $m/z$  731 showing the distribution patterns in naive rat brain tissue sections. CHCA in 1:1 acetonitrile: water plus 0.1 % TFA was used as a MALDI matrix.**



#### **2.12.3.2.6. Utilisation of Tools in BioMap for Investigation Lipid Distribution**

Tools in BioMap were also utilised to investigate differences in the lipid profiles in different regions of rat brain.. The heat map from a region of rat brain that is generated when  $m/z$  788.6 is plotted in BioMap is shown (Figure 52). It can be seen that  $m/z$  788 has a relative peak intensity approximately 2X greater in the white matter compared to grey matter (Figure 53). A corresponding grey scale image is also shown which shows four regions of interest that were then chosen covering an area of 140 mm<sup>2</sup> each, two in white matter regions (R1 and R3) and two in grey matter regions (R2 and R4). By using this image with clear outline of white and grey matter to pinpoint regions of interest, differences in the intensities of other ions in these grey and white matter were also investigated (Figure 54). Average spectra were

then generated in BioMap to investigate the signal intensities of the phosphatidylcholine lipid at  $m/z$  734 in these four white and grey matter regions (Figure 54). It can be seen that  $m/z$  734 has a relative peak intensity approximately 1.5X higher in the grey matter than white. Thus, this tool allowed further differences to be determined and subsequent image generation of those masses of interest that may otherwise be missed. It also illustrates how tools in BioMap can be utilised to investigate regions of interest which is particularly interesting for DMPK studies (chapter 3).

**Figure 52 - Tissue images generated in BioMap a) shows the heat map of phosphatidylcholine lipid observed at  $m/z$  788 whilst b) shows the four regions of interest that were selected for analysis R1 and R3 were from white matter and R2 and R4 were from grey matter regions. Images were normalised against CHCA matrix ion at  $m/z$  190.**

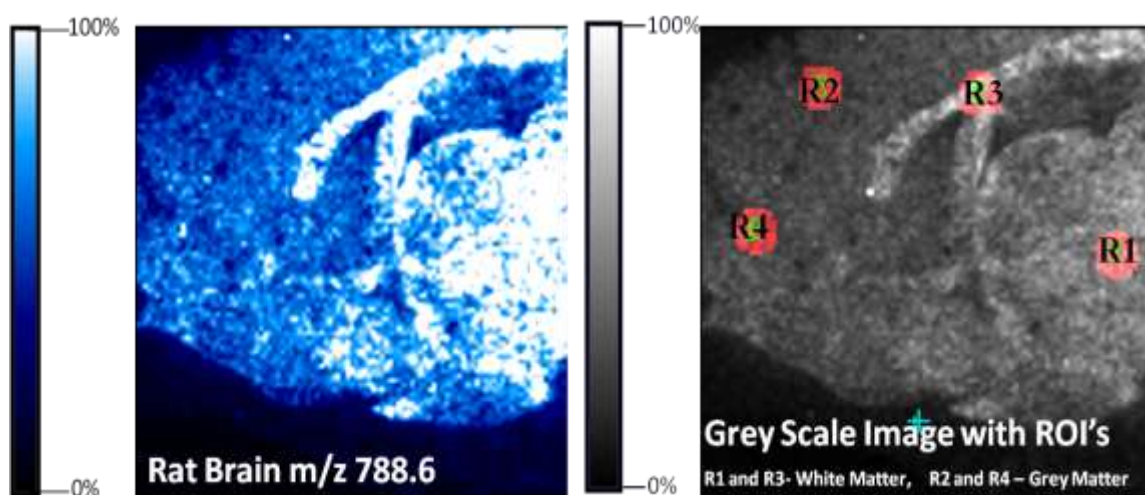


Figure 53 – Average spectra showing intensity of ions at  $m/z$  788.6 in white (R1 and R3) and grey (R2 and R4) matter of rat brain sections.

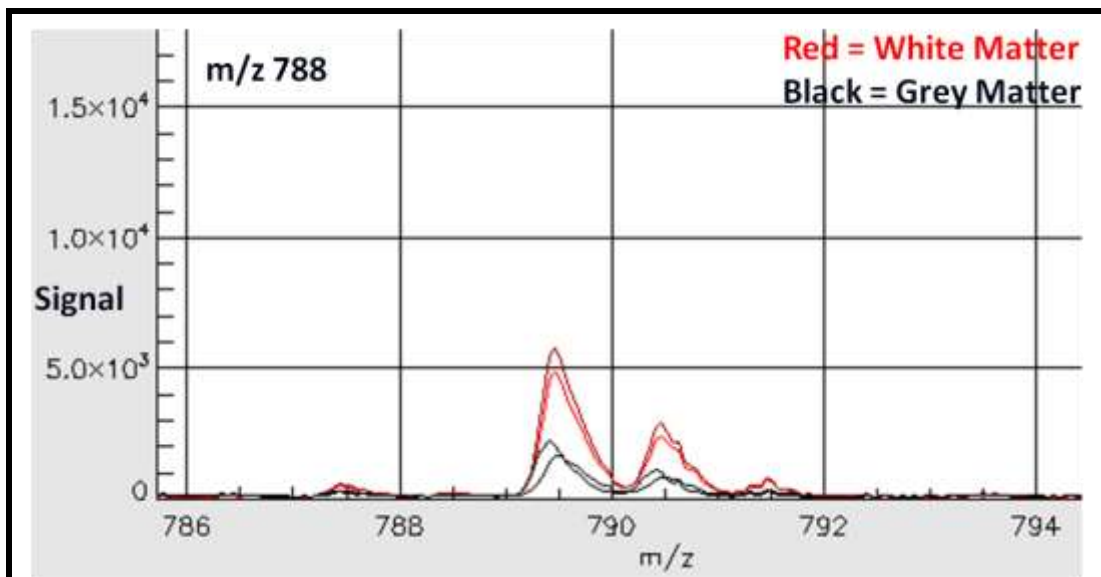
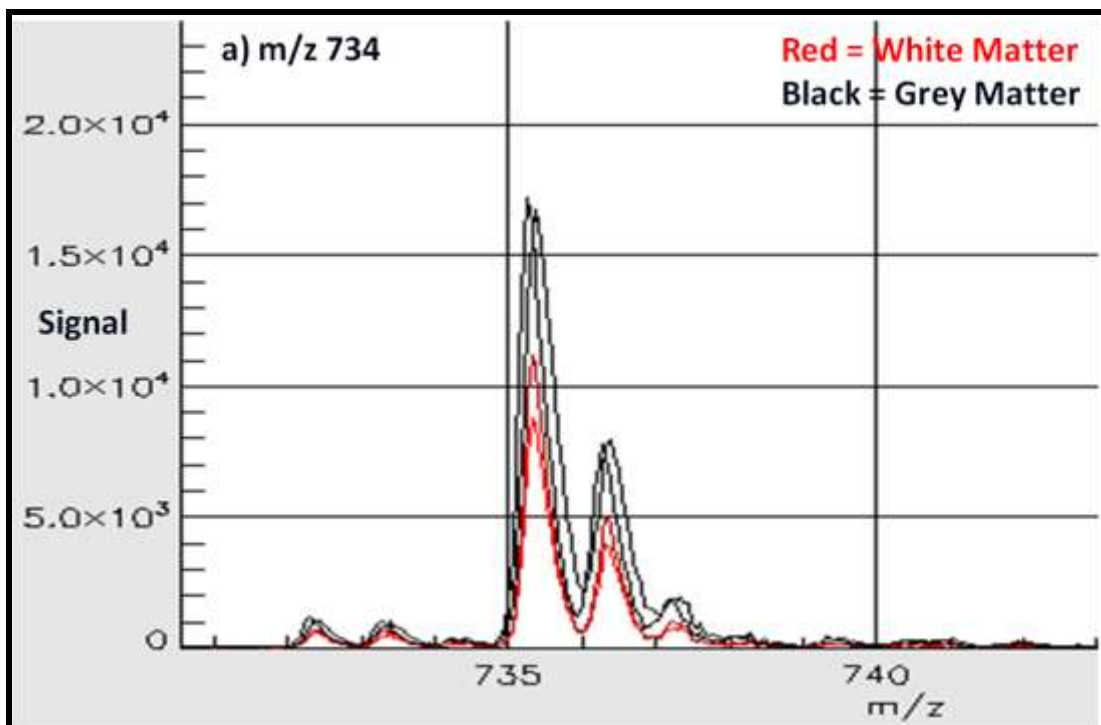


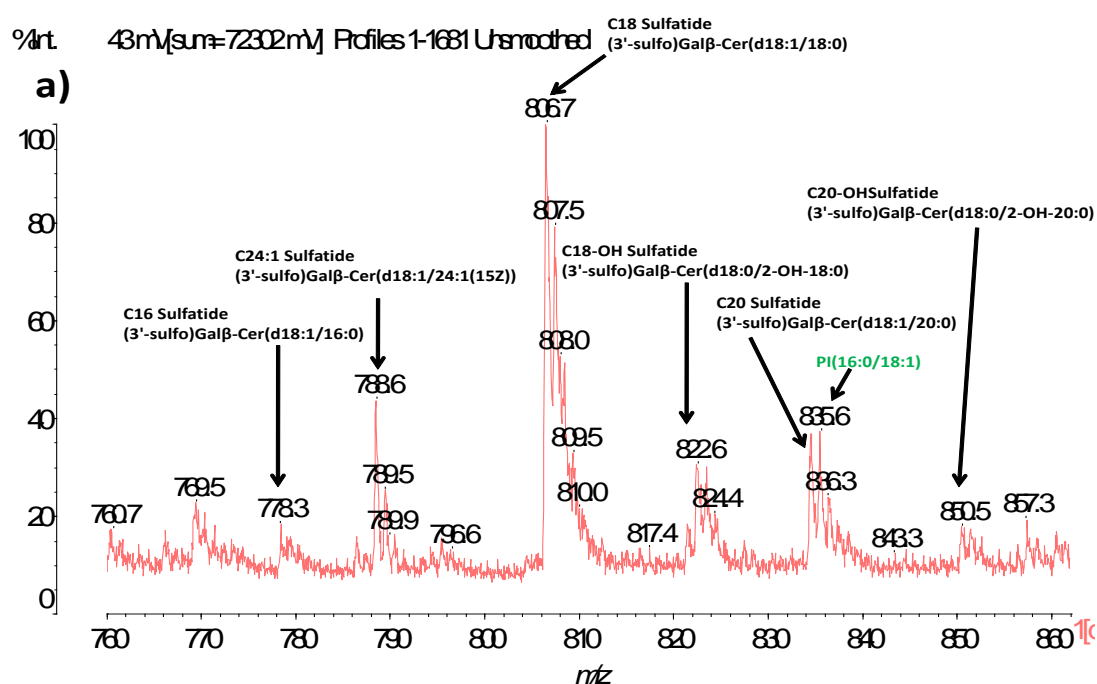
Figure 54 - Average spectra showing intensity of ion at  $m/z$  734 in white (R1 and R3) and grey (R2 and R4) matter of rat brain sections.

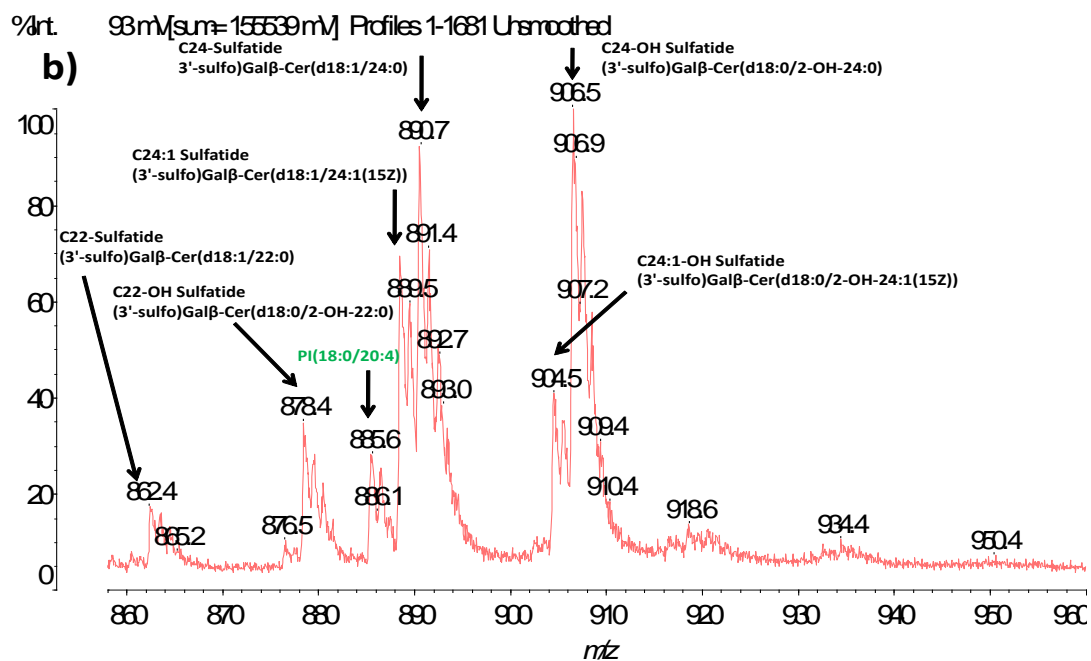


### 2.12.3.3. Imaging Lipids in Rat Brain Sections in Negative Ionisation Mode

Imaging metabolites in the rat brain in negative mode utilising CHCA matrix in 1:1 acetonitrile: water plus 0.1% TFA revealed the presence of sulfatides and phosphatidylinositols within the mass range of  $m/z$  700-980 (Figure 55). Several of these lipids are tentatively assigned in Figure 55 and include hydroxylated sulfatides and phosphatidylinositols.

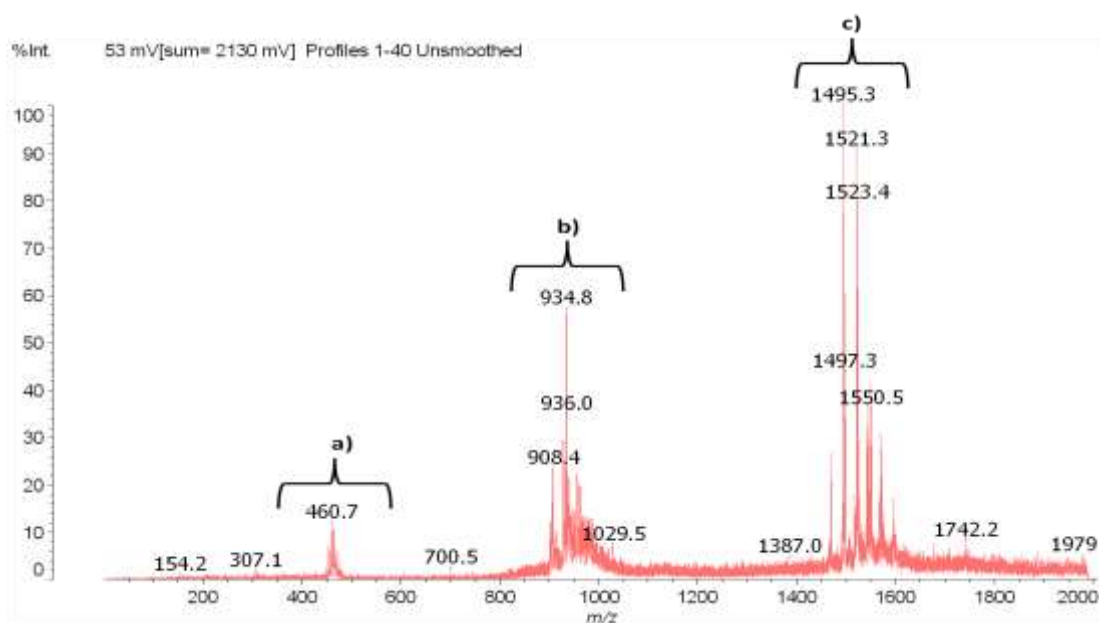
**Figure 55 - Lipid profiling in negative mode reveals the presence of sulfatides and phosphatidylinositols within mass range (a)  $m/z$  760-860 and (b)  $m/z$  860-960 when CHCA in 1:1 acetonitrile: water plus 0.1% TFA was used as a MALDI matrix.**





It was also found that 9-aminoacridine could be used successfully for the detection of lipids in tissue in negative ionisation mode when profiling was done (Figure 56). Detection of lipids was indicated by ion peaks around  $m/z$  460,  $m/z$  850-1050 and  $m/z$  1400-1600 (Figure 56). The identity of these lipids is not clear but it would be interesting to carry out MS/MS experiments to investigate this further. However, 9-aminoacridine was less successful when imaging experiments were carried out (discussed later in 2.12.4).

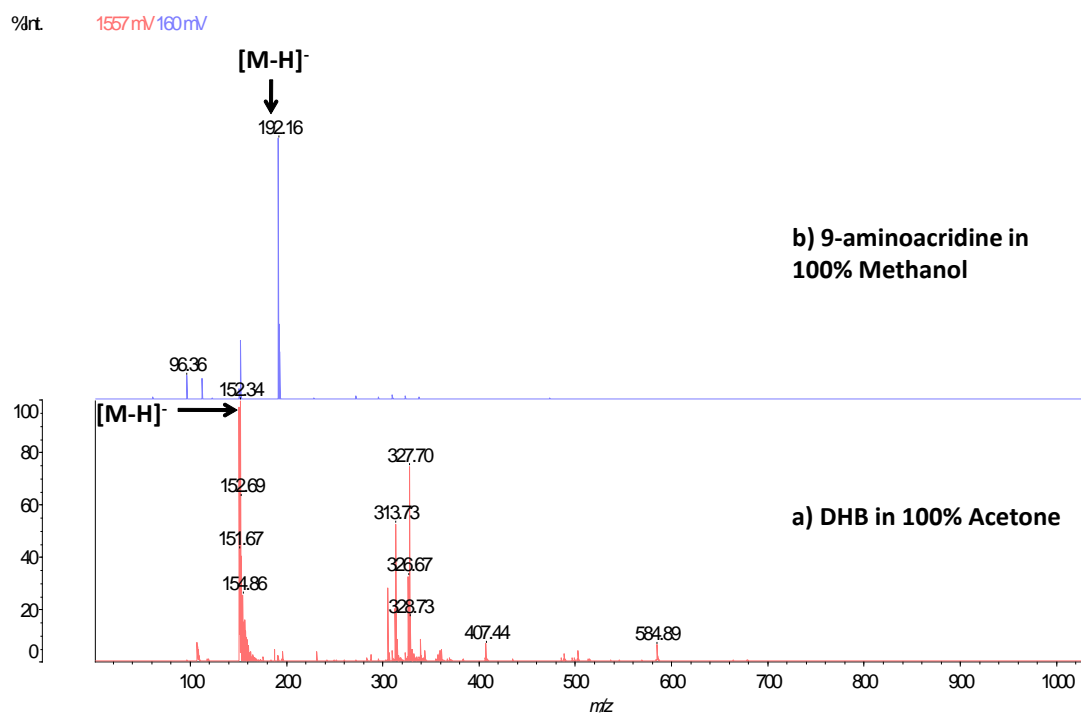
**Figure 56 – Spectra showing lipid clusters observed when 9-aminoacridine was spotted onto rat brain sections in reflectron negative ionisation mode. 9-aminoacridine was prepared at a concentration of 10 mg/ml in 80:20 acetone: water plus 0.1% TFA.**



#### **2.12.4. Profiling Energy Metabolites Utilising 9-aminoacridine as Matrix.**

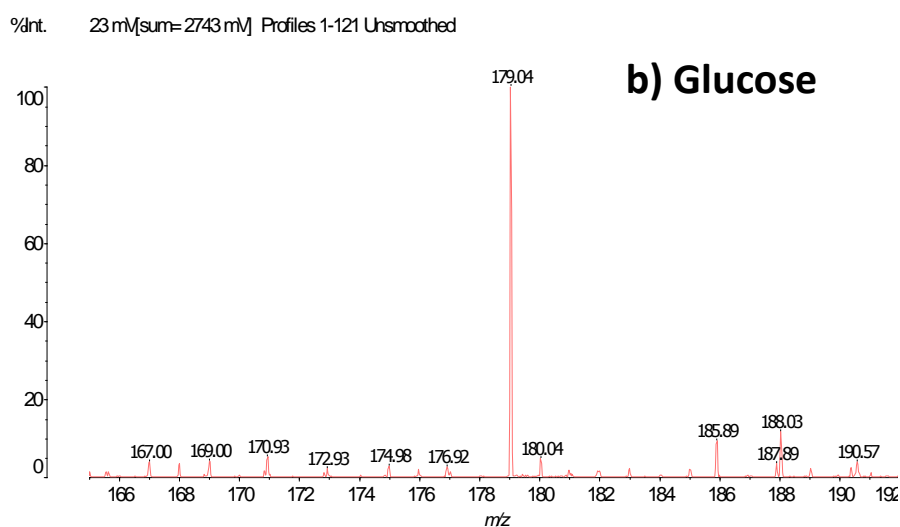
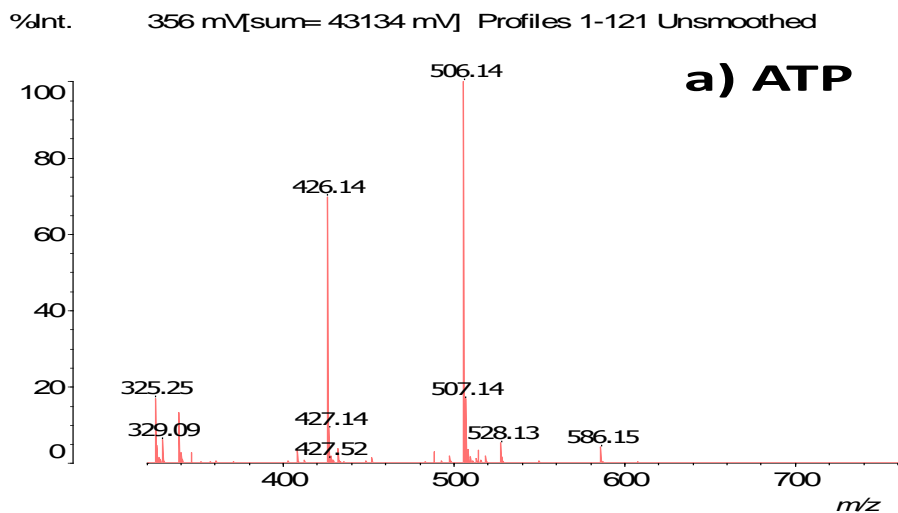
9-aminoacridine has been used as an alternative matrix for the analysis of metabolites in negative mode due to lack of formation of cluster ions from analysis of the matrix in negative mode. Figure 57 illustrates that there is less background noise observed when 9-aminoacridine is analysed in negative mode compared to DHB.

**Figure 57 – Matrix ions observed in negative ion mode from analysis of two matrices commonly utilised for MALDI imaging in optimised solvent combinations a) DHB in 100% acetone and b) 9-aminoacridine in 100% methanol.**

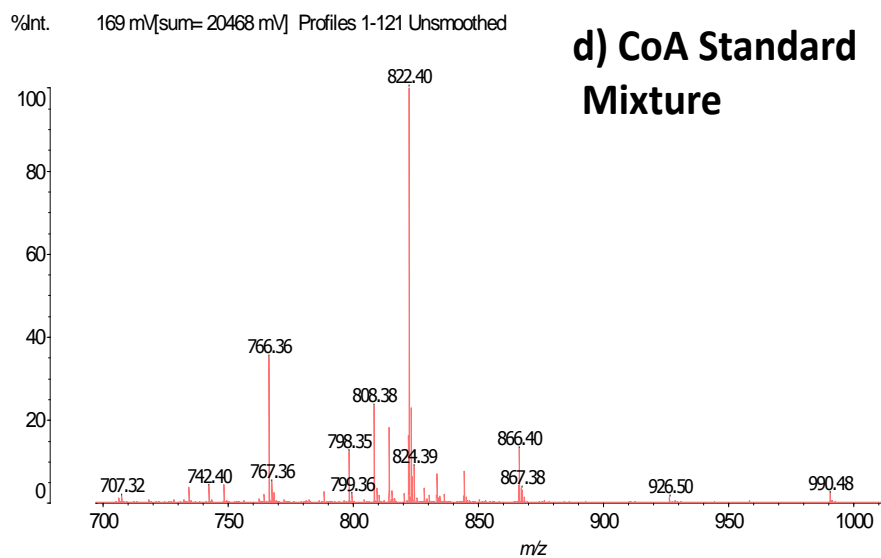
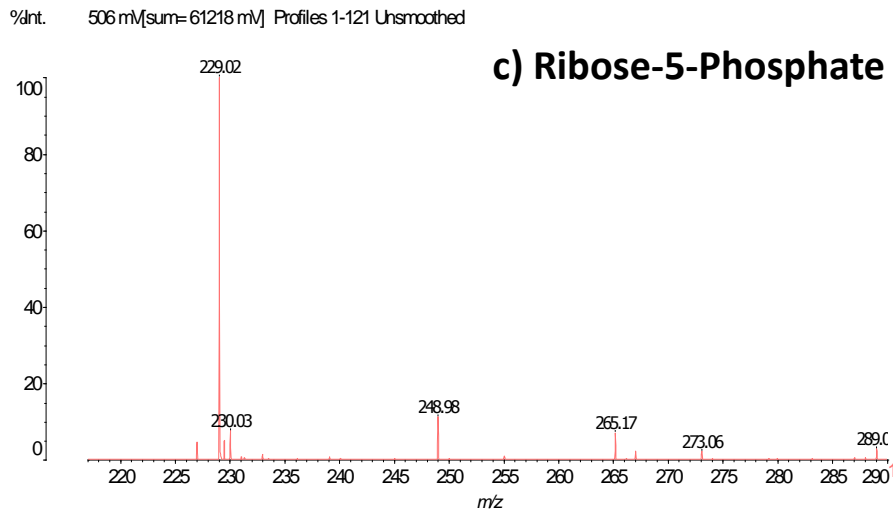


9-aminoacridine was then investigated as an alternative matrix for the analysis of metabolites in negative mode and it was found that it could be used to analyse standards such as ATP, glucose, ribose-5-phosphate and a CoA standard mix illustrating that is a suitable matrix for the analysis of a wide class of metabolites (Figure 58).

**Figure 58 – Spectra from analysis of metabolite standards utilising 9-aminoacridine as a matrix in reflectron negative ionisation mode a) ATP, b) glucose, c) ribose 5-phosphate and d) CoA standard mixture.**

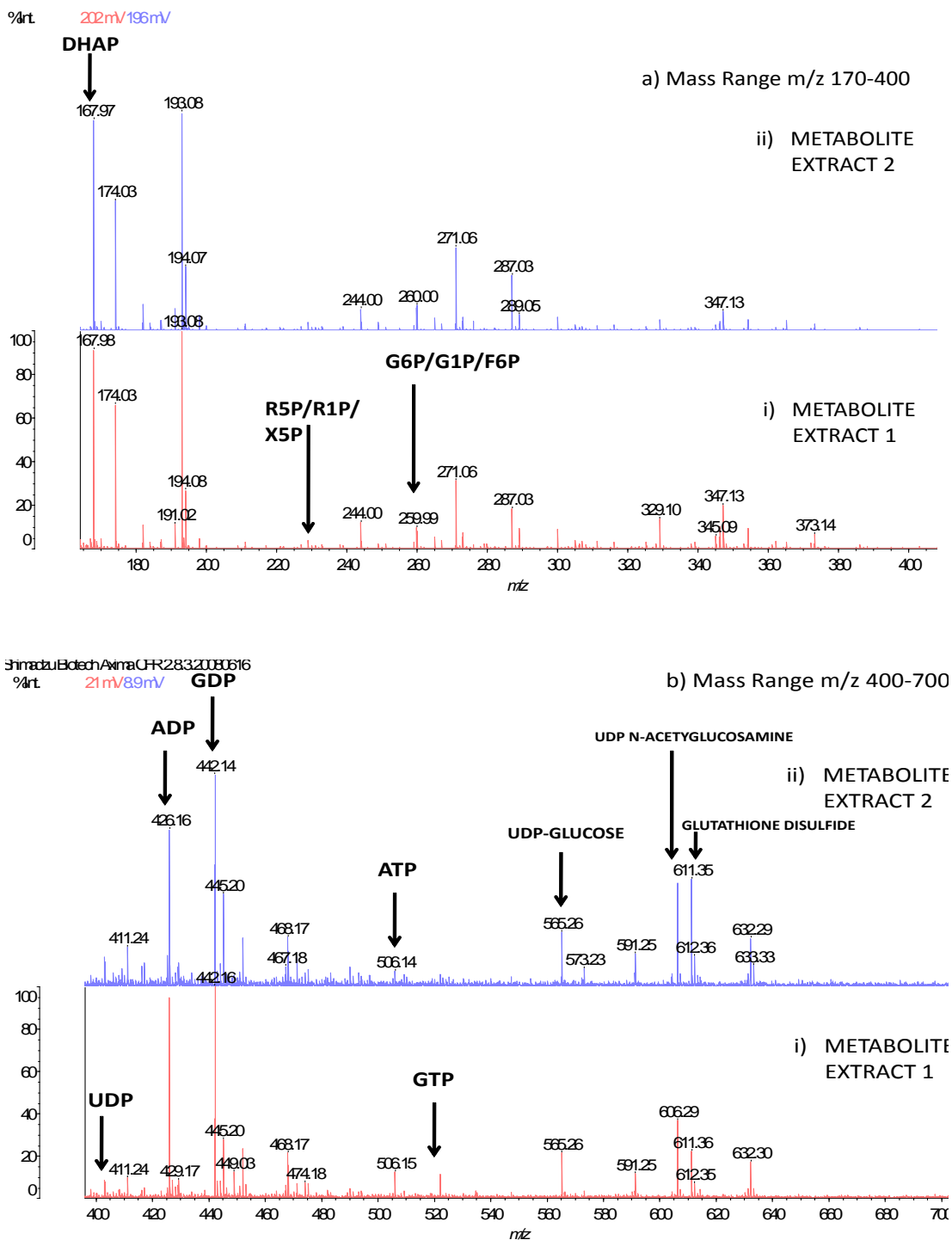






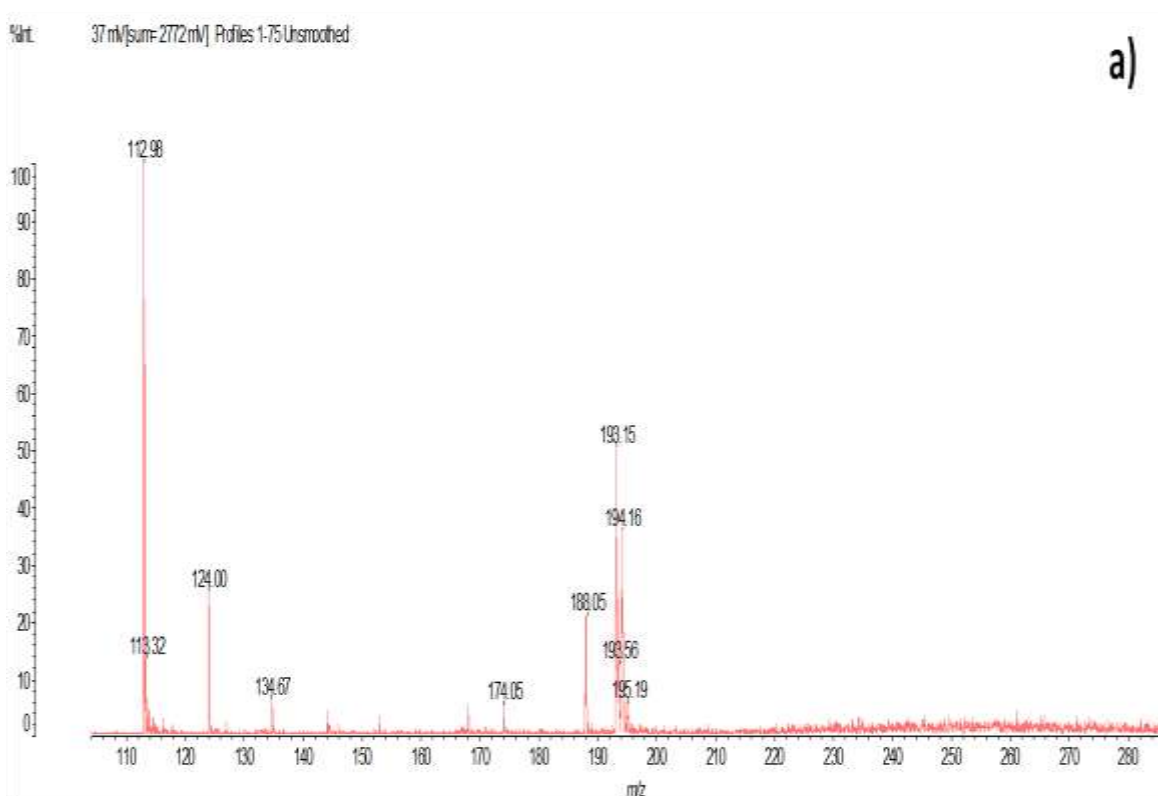
To investigate the suitability of this matrix for the analysis of polar metabolites, rat brain extracts were spotted onto well plates. It was found that it could be used to identify a wide variety of energy metabolites such as adenosine diphosphate (ADP), guanosine diphosphate (GDP), guanosine triphosphate (GTP), uridine diphosphate (UDP), dihydroxyacetophenone (DHAP), UDP-glucose, UDP N-acetylglucosamine and glutathione disulfide from rat brain extracts (Figure 59).

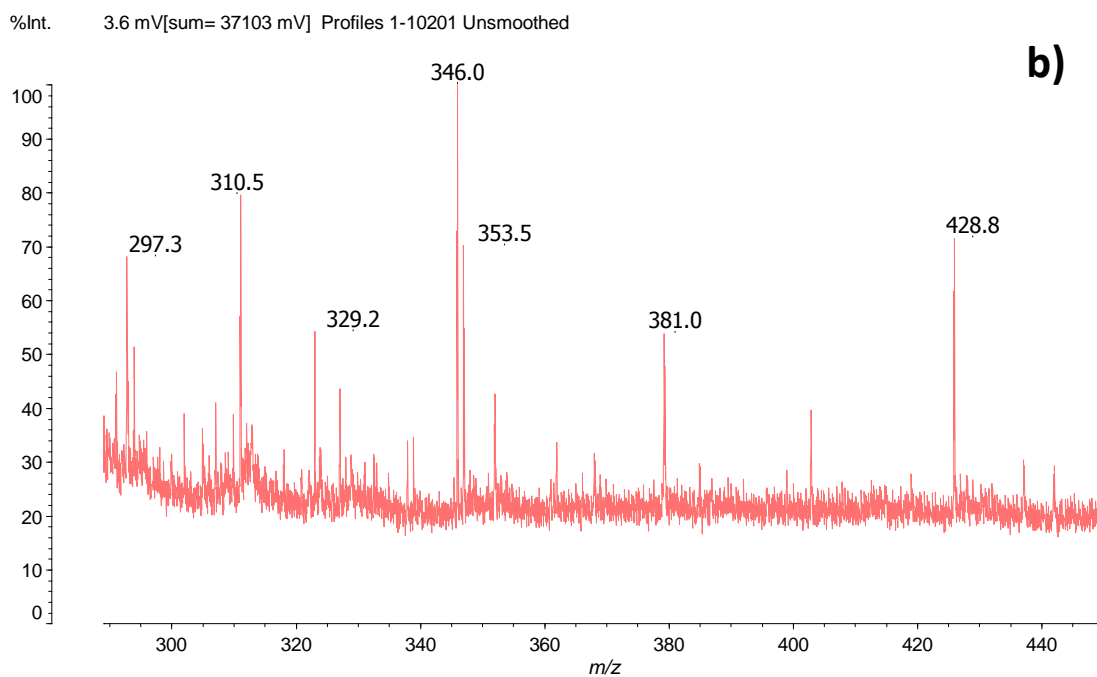
**Figure 59 - Spectra generated from analysis of two polar metabolite extracts from 1/2 mouse brains when utilising 9-aminoacridine in methanol as a matrix in reflectron negative ionisation mode a) mass range  $m/z$  170-400 b)  $m/z$  400-700.**



It was found that whilst 9-aminoacridine in 100% methanol was good for the detection of metabolites in negative mode, it was difficult to obtain signals directly off tissue using this solvent combination (Figure 60). There were few peaks identified above  $m/z$  300 compared to when this matrix was used to analyse rat brain extracts. This could be due to a number of factors such as the concentration of these metabolites in 12  $\mu\text{m}$  tissue sections, the sensitivity of the instrument in negative mode as well as the matrix and solvent combinations.

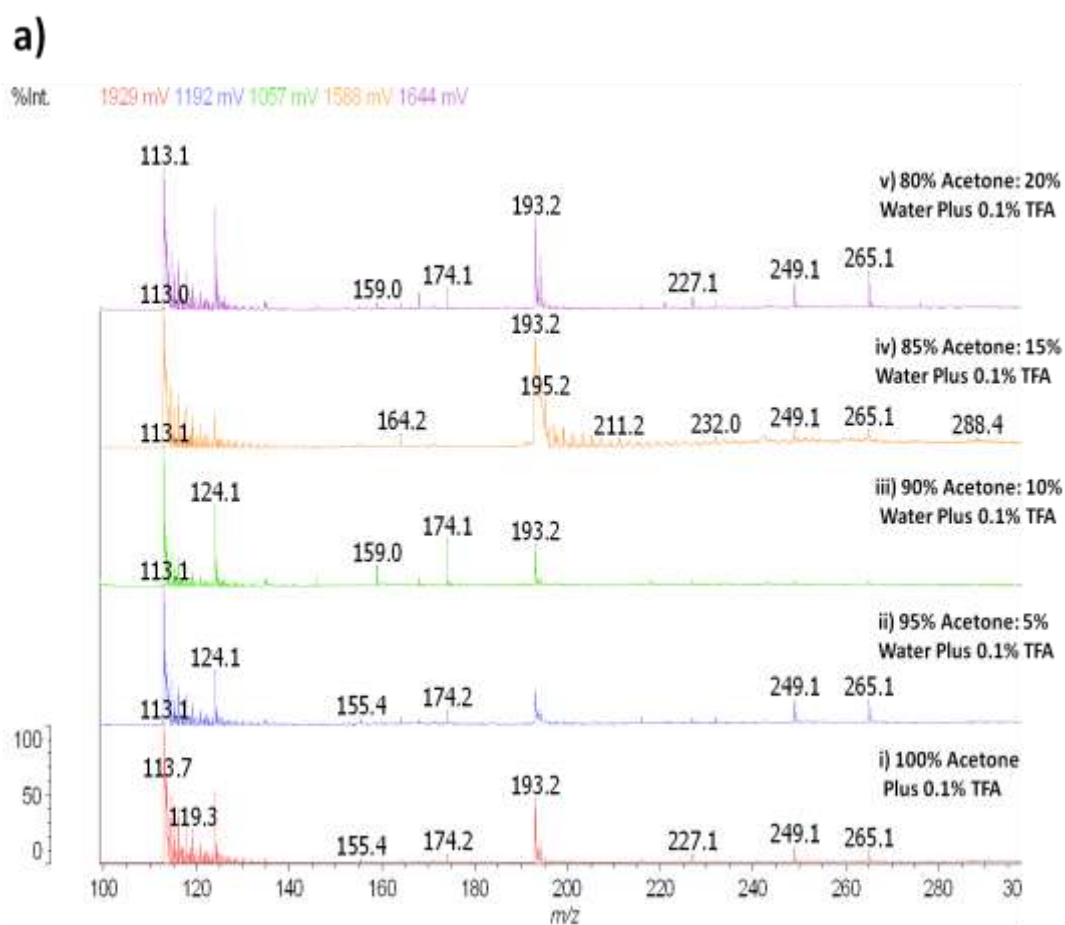
**Figure 60 - Spectra from analysis of metabolites in a rat brain section in reflectron negative mode coated with 9-aminoacridine prepared at a concentration of 10 mg/ml in 100% methanol showing metabolites in mass ranges a)  $m/z$  100-290 and b)  $m/z$  290-450.**

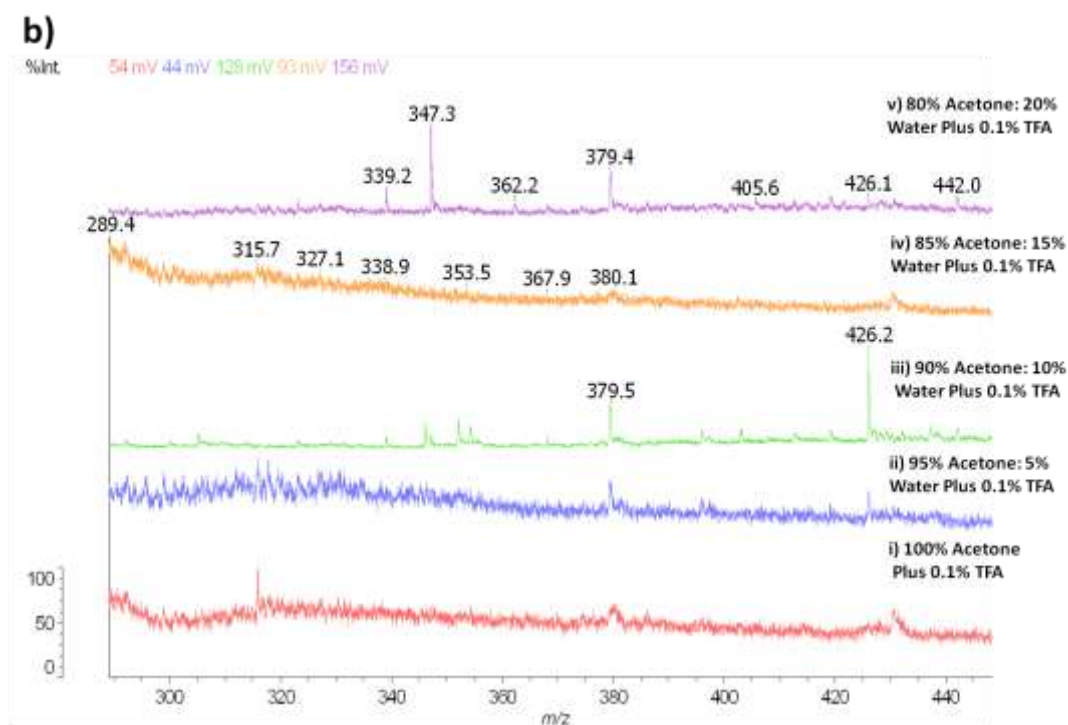




It was proposed that the solvent combination or matrix crystallisation could be having an effect on the ionisation of the metabolites. The use of 0.1% TFA in acetone has also been described for the detection of primary metabolites in seeds [247]. It has also been suggested that adding some water may enhance detection of some endogenous metabolites by enhancing crystallisation. Thus, different solvent combinations based on varying amounts of water and acetone were also utilised (Figure 61).

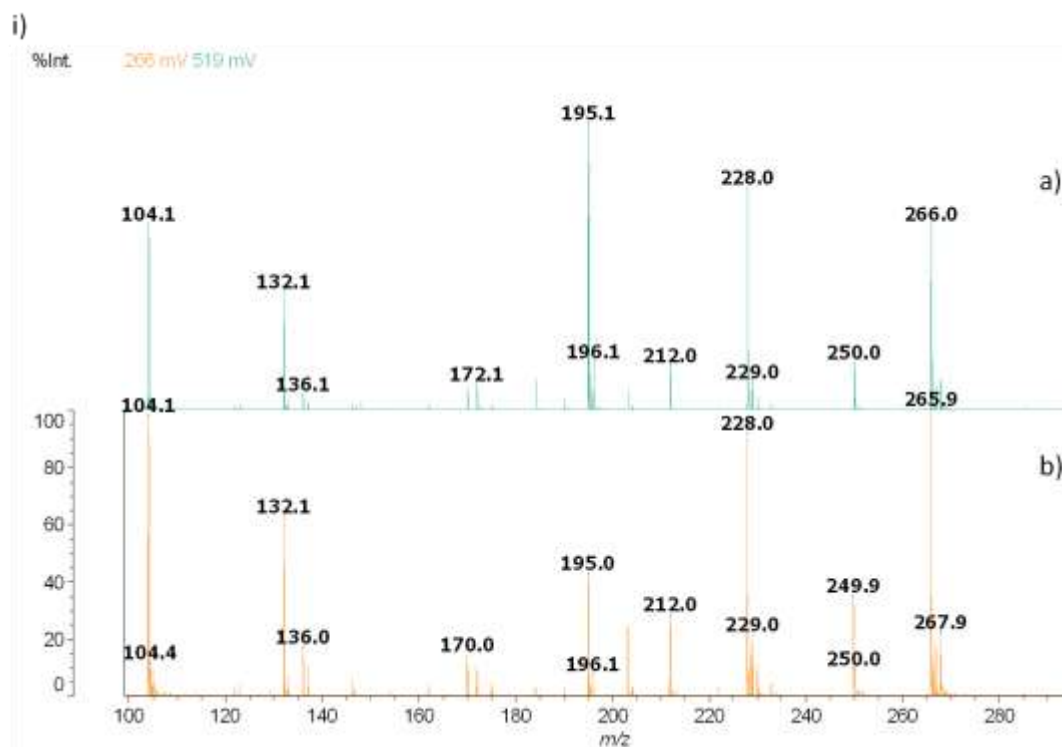
**Figure 61 - Spectra from analysis of metabolites in rat brain section in reflectron negative mode spotted with 9-aminoacridine prepared at concentration of 10 mg/ml in i)100% acetone 0.1% TFA ii)95% acetone: 5% water plus 0.1% TFA iii) 90% acetone: 10% water plus 0.1% TFA, iv) 85% acetone: 15% water plus 0.1% TFA and v) 80% acetone: 20% water plus 0.1% TFA in mass range a)  $m/z$  100-300 and b)  $m/z$  290-450.**



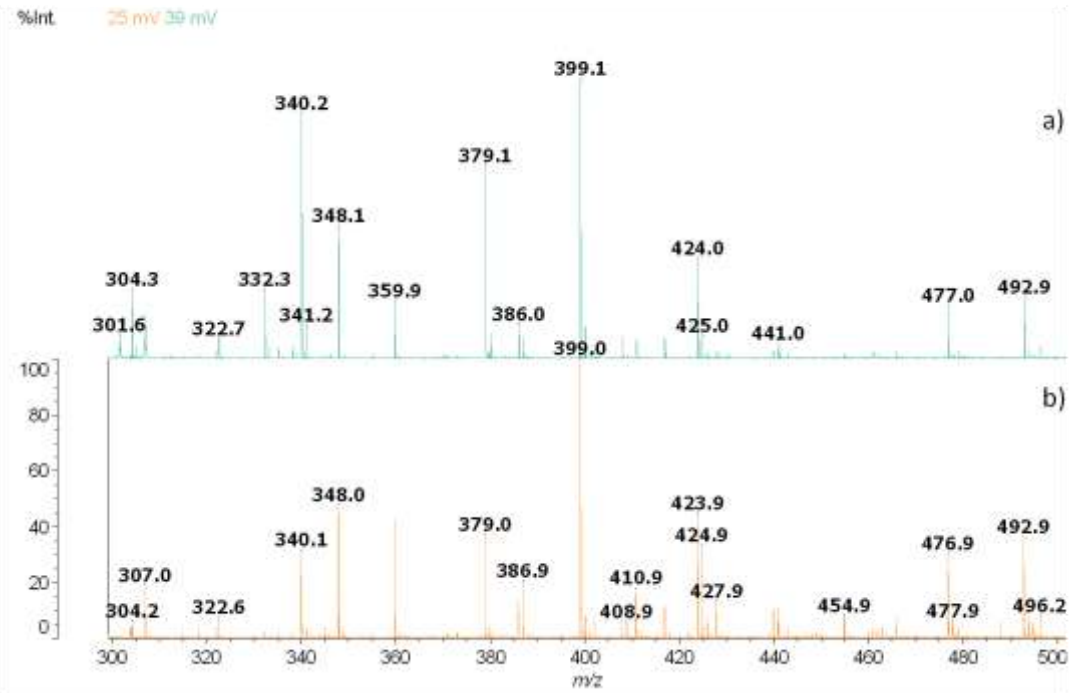


From these results it was decided to try to carry out further profiling experiments on rat brain tissue using 80% acetone: 20% water plus 0.1% TFA for optimised detection of metabolites on tissue. It was found that this solvent combination enabled superior signals to be obtained off tissue than when 9-aminoacridine in 100% methanol was used. For future work, an MS/MS instrument will be used to confirm the identity of these metabolites. Following optimisation of instrument parameters and application of several layers of matrix to individual spots it was possible to obtain many signals off tissue (Figure 62).

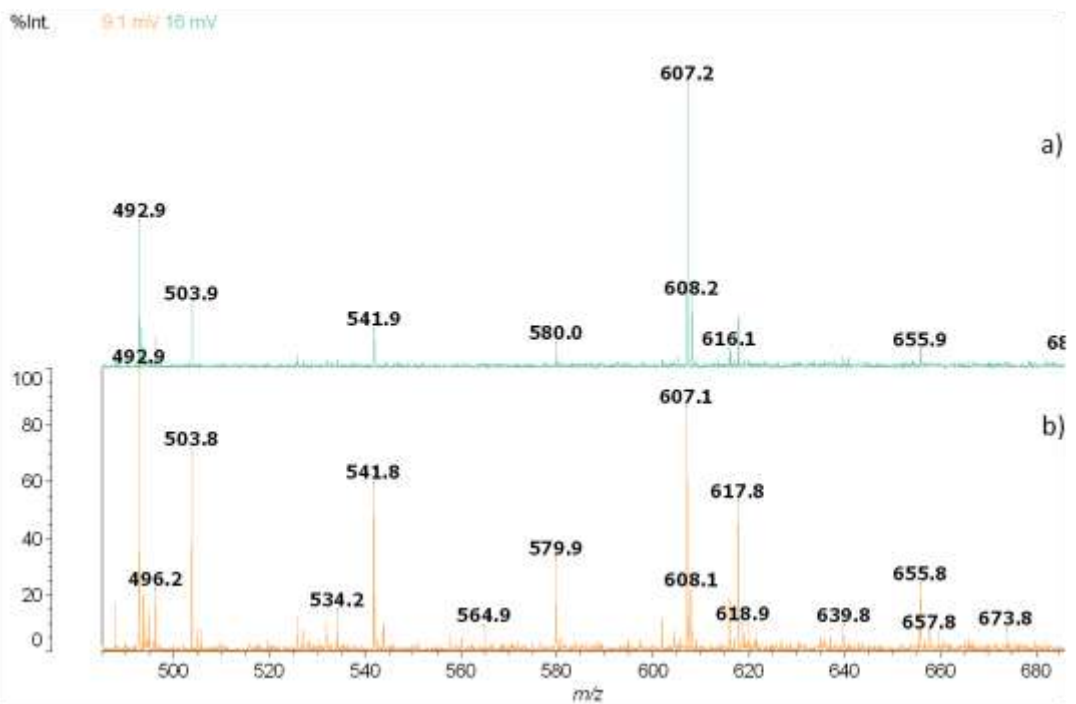
Figure 62 – Spectra obtained from the analysis of two rat brain sections (a) and (b) when 9-aminoacridine in 80 % acetone: 20 % Water plus 0.1% TFA was utilised, i) shows mass range  $m/z$  100-300, ii) shows mass range  $m/z$  300-500 and iii) shows mass range  $m/z$  480-690.



ii)



iii)



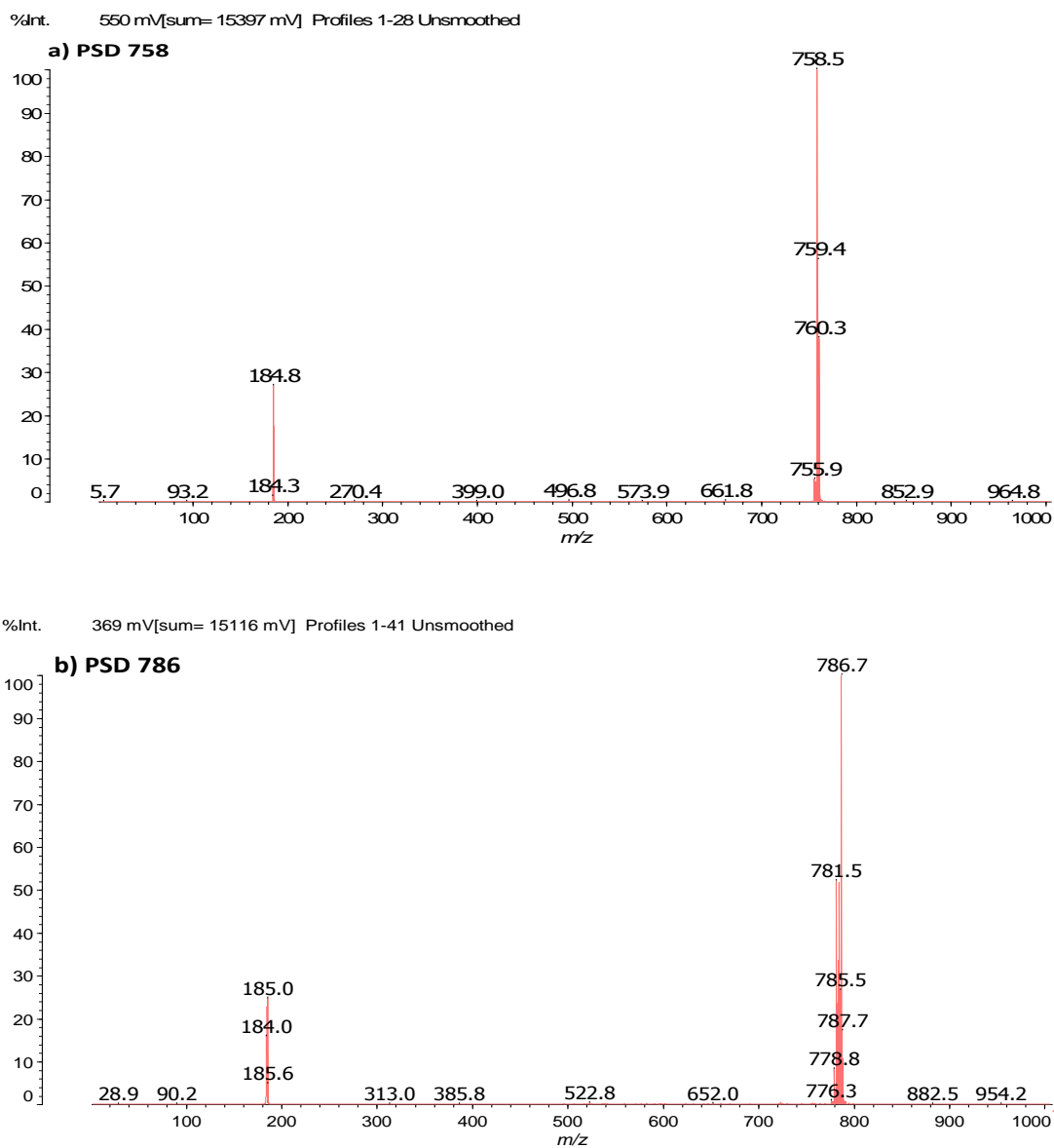


However, when this matrix combination was sprayed onto tissue samples and samples analysed, fewer signals were obtained off tissue. This suggests that something in the matrix preparation or application method is not optimal for imaging experiments. Perhaps the number of matrix coatings utilised was not sufficiently thick to enable ionisation. Future work will involve further investigations into suitable matrix application methods for imaging endogenous polar metabolites in rat brain *in situ*.

#### **2.12.5. Confirmation of Tentative Assignments of Lipids using Fragmentation Experiments, PSD and Analysis of Lipid Standards.**

To confirm the presence of the lipid classes identified in the rat brain tissue using MALDI-MSI, post source decay (PSD) experiments were carried out. PSD analysis of phosphatidylcholine lipids revealed the phosphatidylcholine head group at  $m/z$  184 (Figure 63). However, this does not allow the composition of the fatty acids to be deduced.

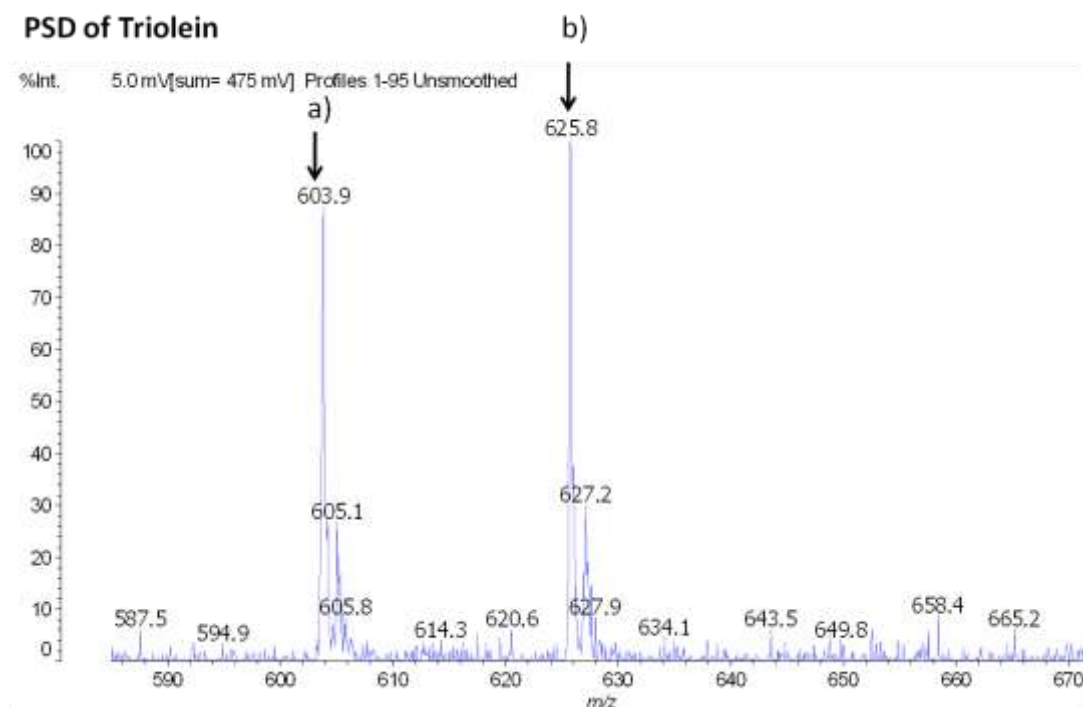
**Figure 63 – Spectra obtained from analysis of post-source decay analysis of phosphatidylcholines on tissue (a)  $m/z$  758 and (b) 786.**



PSD analysis and investigation of lipid standards was carried out to confirm the composition of triacylglycerols. For example Figure 64 shows the products ions observed from the PSD analysis of triolein where it can be seen that there are peaks observed at  $m/z$  603 and 625 which correspond to the loss of one fatty acid chain, which in this case is oleic acid, from a triacylglycerol moiety as a) a sodium

[RCOONa] or b) potassium salt [RCOOK]. However it was also shown in full scan mode that the triacylglycerols fragment easily under MALDI-MS conditions (Figure 33).

**Figure 64 – Spectra obtained from PSD analysis of triolein standard.**



Whilst it is possible to carry out PSD analysis of abundant lipids, this is more difficult with less abundant lipids found in tissues. Thus for application studies on investigating lipid composition in rat brain and liver, additional analysis was carried out utilising the LTQ-Orbitrap (Chapter 4.)

## **2.13. Discussion**

### **2.13.1. Advantages and Limitations of MALDI-MSI**

This preliminary work illustrates that there are both advantages and limitations of the use of MALDI-MSI. For example, it illustrates how it can be utilised to profile and map the distribution of hundreds of molecules within a mass range of interest from a single experiment. It allows direct analysis to be carried out and the spatial distribution of markers can be established in a single experiment, without the need for any molecular probes as required in other imaging techniques such as radiography. Additionally, BioMap image analysis software can be utilised for data interpretation, and comparisons can be made between the distributions of different metabolites from the analysis of a single sample. Additionally it also offers high sensitivity in the pmol range, but this will depend on the instrument being utilised, the analyte of interest and whether full scan or multiple reaction monitoring experiments are being carried out.

Limitations of tissue imaging include quantitation, as several homogenous layers of matrix are being applied. It is important to apply a homogenous layer of matrix using whatever matrix application method you have chosen and if this is being done by hand there will be issues with reproducibility. The main approach to combat this is to normalise all peak intensities against a matrix ion in the spectrum. However, it will be illustrated that MALDI-MSI can be used quantitatively in chapter 3. It has also been shown that there are a lot of matrix interferences observed during tissue imaging experiments and it is important to collect a spectrum from analysis of the matrix itself. Additionally, MALDI also requires time; it may take several hours to

scan a complete tissue section so there may be issues with tissue degradation. It also illustrates that there are a lot of factors to consider when designing a MALDI imaging experiment that can affect your results. It is also important to tentatively assign metabolites carefully and to utilise PSD or MALDI TOF-TOF instruments when possible to produce fragments in order to deduce molecular structure, for example of lipids.

### **2.13.2. Mapping Endogenous Lipids Using MALDI-MSI**

These experiments show how MALDI-MS can be a useful tool for the analysis of lipids, offering several advantages over more traditionally used imaging techniques enabling many lipids to be mapped in a single experiment. MALDI imaging mass spectrometry allows the spatial distribution of lipids to be determined within intact tissue sections. If profiling experiments are to be carried out, MALDI-MS can be used to carry out lipid analysis using homogenised samples without the need for complex sample preparation stages (such as filtering, drying down etc that are required prior to other types of mass spectral analysis for lipid analysis such as LC-MS and GC-MS.)

The initial imaging experiments carried out on naive rat brain sections demonstrate how the technique can be used to map endogenous lipid molecules such as phosphatidylcholines. Tissue images revealed that phosphatidylcholines have unique distribution patterns in rat brain tissue. The high peak intensities found for this species of glycerophospholipid may be due not only to their high abundance in animal tissue but also because they have a choline head group that contains a quaternary ammonium moiety, making them readily ionisable in positive mode. It

was also possible to detect what are thought to be several lysophosphatidylcholine species in the naive rat brain tissues which had unique distribution patterns similar to that of the parent phosphatidylcholine species containing one or more of the fatty acid chain components. The high peak intensity values indicate that these molecules are also readily ionisable by MALDI-MS and it has been suggested that this is because low molecular weight compounds can be detected with a higher sensitivity using MALDI-MS [257]. However, the possibility that these lipids are in fact fragments of phosphatidylcholines cannot be ruled out.

It has been shown that there are differences in the distribution of lipids in the cerebellar peduncle (white matter) and cerebellar cortex (grey matter) in a previous study [198]. Although this study provided excellent tabular description and mass spectral data regarding the most abundant lipid species, it did not display any images to confirm the differential distribution of these lipids [198]. For example, a phosphatidylcholine species with a  $[M+H]^+$  of  $m/z$  734 showed a signal intensity of over 90% in the cortex but had an intensity of less than 5% in the cerebellar peduncle region [198]. Here, we demonstrate the differential distribution pattern of cerebral and cerebellar lipids through profiling and these are then confirmed through use of heat maps. Additionally, it has been illustrated how MALDI MS can be utilised for analysis of lipids in negative ionisation mode and that it is also possible to detect other abundant lipid classes such as sulfatides and PIs in the rat brain.

### **2.13.3. Mapping Endogenous Polar Metabolites Using MALDI-MSI**

It has also been shown how MALDI MS profiling can be used in combination with 9-aminoacridine to allow the successful detection of polar metabolites in negative

ionisation mode. Although it was possible to obtain spectra from the analysis of rat brain tissue sections coated with 9-aminoacridine matrix it was not possible to obtain good images. This could be due to the interaction of energy metabolites with the matrix and solvents. For example, in the paper by Benabdellah et al they utilised a sprayer from Leap technologies which had a nozzle heated to 80 °C for rapid crystallisation [31]. More work will need to be done to optimise the detection of endogenous metabolites *in situ* but this preliminary work illustrates that by using 9-aminoacridine as a matrix, it is possible to detect many metabolites in negative mode when MALDI profiling is used although more work is required to get this method to work for tissue imaging of these metabolites in our hands.

#### **2.14. Conclusions and Future Work**

In conclusion, this chapter illustrates the potential that MALDI-MSI offers as an alternative technique for mapping the distribution of molecules of interest *in situ* such as lipids and small polar metabolites. This preliminary work was necessary for method development. Important parameters explored included sample preparation steps, optimisation of matrix selection and application and tuning of instrument parameters before MALDI-MSI could be used successfully for the application studies presented in chapters 3 and 4. Future work includes continuing with the development and optimisation of MALDI-MSI parameters for the detection of small molecules that are commonly detected using LC-MS. This will allow any differences identified in metabolomics experiments to be mapped *in situ* using MALDI-MSI.

**Chapter 3 - Development of a Dry Matrix Application Method For Mapping  
Pharmaceuticals *in situ* using Matrix-Assisted Laser Desorption/Ionisation  
Mass Spectrometry Imaging (MALDI-MSI).**



### **3. Introduction**

Utilisation of imaging mass spectrometry for the visualisation of pharmaceuticals *in situ* presents several challenges. A major challenge is the solubility of drugs in the matrix solvents which can cause analyte delocalisation during application of the matrix. The advantages and limitations of the use of MALDI-MSI for imaging pharmaceuticals *in situ* are discussed below. Examples of the methods used for application of the matrix are also described. There will then be a description of the pharmaceuticals utilised for this study with background information, receptor pharmacology and aims presented.

#### **3.1. Introduction to use of MALDI-MSI for Drug Metabolism and Pharmacokinetic Studies**

As the field of MALDI mass spectrometry grew in the late 1990s, so did interest in the use of this technique in the pharmaceutical industry. MALDI-MSI has obvious appeal for the pharmaceutical industry. Mass spectrometry is a common method for the identification and quantification of drug compounds and metabolites during research on new chemical entities as is imaging to profile their distribution. The prospect of utilising mass spectrometry to map the distribution of drugs *in situ* without the requirement for radioactive labelling, with the added possibility of metabolite and endogenous biomarker identification from the same experiment, was a novel and exciting prospect. The potential use of MALDI-MSI for the identification of toxicological markers during DMPK studies was also interesting.

Any technique that could be utilised to detect toxicity at an earlier stage would be of significant advantage to the pharmaceutical industry.

### **3.2. Imaging Mass Spectrometry Versus Traditional Imaging Methods**

Examples of established methods employed by the pharmaceutical industry to conduct imaging experiments are magnetic resonance imaging (MRI), positron emission tomography (PET), autoradiography and immunocytochemistry coupled with confocal microscopy. These all share a common disadvantage in that they require the use of molecular probes which selectively bind to the drug or tagging of the drug molecule. These tags may be expensive and in many instances, there are only a select number of tags available that can be used to locate the molecule of interest. Autoradiography is traditionally used by the pharmaceutical industry to map the spatial distribution of a drug molecule within tissue [258]. It enables the production of quantifiable data and it is often used to aid selection of lead compounds. However, autoradiography has the strong disadvantage of requiring radio-labelling of compounds. This requires the synthesis of customised radioactive drugs which are expensive and the use of radioactive materials requires careful handling and recorded disposal. Moreover, techniques such as autoradiography may have both limited sensitivity and spatial resolution. Additionally, autoradiography will only map the distribution of a labelled compound as it measures radioactivity, providing no information on the distribution of drug metabolites and biomarkers which may also have clinical relevance. PET has limited spatial resolution (mm) and again requires synthesis of labelled tracers. Thus, MALDI-MS offers several advantages over other traditional imaging techniques such as autoradiography and

PET imaging as it has the potential to detect hundreds of different molecules in a single experiment which could include parent drugs, metabolites and biomarkers.

### **3.3. Utilisation of MALDI-MSI for Mapping the Distribution of Pharmaceuticals *in situ* – Documented Studies.**

Early studies employed the technique to map the distribution of parent drugs in tissues [21,193,259,260]. However, detection of exogenous parent drug molecules and small endogenous molecules below  $m/z$  500 in intact biological tissue sections using MALDI-MSI is complicated by a number of factors described previously in chapter 2 such as matrix interferences. Drug molecules typically fall within same mass range as many matrix related peaks ( $< m/z$  500) and thus it is not uncommon for a parent drug and matrix related peak to be isobaric. Thus, it was demonstrated early on that tandem mass spectrometry was often required to detect and map pharmaceutical compounds in intact tissue sections to enable differentiation between analytes of interest and background ions [259,261]. Tandem mass spectrometers such as quadrupole TOFs or quadrupole ion traps enable fragmentation of a selected precursor ion to its related product ions by collision activated dissociation. An analyte of interest can then be distinguished from background ions by using the  $m/z$  ratio of a unique product ion related to the dissociation of the analyte of interest in order to map the spatial distribution of the drug.

The application of MALDI-MSI and related ionisation techniques in DMPK studies has since been demonstrated in numerous other articles in order to investigate a wide variety of pharmaceuticals including anti-cancer and anti-psychotic agents. For example, the distribution of pharmaceutical compounds and their metabolites has

been mapped in porcine skin (anti-fungal compound ketoconazole) [262], rat brain tissue (antipsychotic clozapine) [193], rat liver, spleen and muscle (anti-cancer drug erlotinib) [263] and human tumour xenographs (anti-cancer drug banoxantrone) [264]. Additionally, MALDI MS profiling experiments have also been used to identify drugs in rat brain tissue sections (sympathomimetic cocaine and nicotinic antagonist chlorisondamine) using a TOF/TOF instrument thus confirming the localization observed by autoradiography [260].

Other notable developments to date include the use of whole body imaging mass spectrometry to provide detailed information on the distribution and relative concentrations of drugs and metabolites in longitudinal rat brain sections over a given time period within an *ex vivo* setting, for example to map the distribution of the antipsychotic olanzapine [21]. This method offers an alternative to whole body autoradiography which requires the use of radio labelled compounds. This technology was used firstly to successfully localise the distribution of olanzapine and its metabolites in rat organs and the results were shown to be similar to results previously recorded using autoradiography [21]. The work utilised MALDI TOF/TOF MS allowing the detection of not only parent ions but also the fragment ions [21]. Moreover, the IMS technique was further used to look at the distribution of specific proteins throughout the rat organs [21]. The technique enabled the pharmacokinetics of the parent drug and metabolites to be mapped over time which is not possible with a radio-label. If the animal was dosed with a drug for example olanzapine and then sacrificed 2 hours later, the IMS data could be compared to data taken from a rat dosed with the same concentration of drug and sacrificed 6 hours later [21]. This study quantified the percentage of each metabolite that was formed

as a percentage of the MS/MS signal and they also used intensity mapping to demonstrate which organs these metabolites were accumulated in [21]. Whole Body Imaging Mass Spectrometry has also been utilised to map the distribution of a  $^{14}\text{C}$  labelled research compound [207] and the anti cancer drug vinblastine in rat sections using ion-mobility separation [158].

Matrix-assisted laser desorption/ionisation-Fourier transform ion cyclotron resonance (MALDI-FTICR) has also been utilised to map the distribution of the anti psychotic drug olanzapine and metabolites in rat kidney and liver and the anti-cancer drug imatinib in mouse brain/glioma tissue [75]. MALDI-FTICR can separate isobaric compounds due to its high mass resolving power, allowing accurate mass data to be obtained and corresponding accurate mass images to be generated. Currently this technique has a lower throughput compared to standard TOF imaging mass spectrometers. Additionally, MALDI-Orbitrap has been used to map the distribution of tiotropium in mouse lung [265] which is excellent for drug imaging studies due to the high mass accuracy [161].

Alternative imaging mass spectrometry techniques that have been used for imaging pharmaceuticals include DESI MS (Desorption electrospray ionisation mass spectrometry) [35,266] to map clozapine in rat brain, lung, kidney, testis and the N-desmethyl metabolite in lung sections [173] and NIMS (Nanostructure Initiator mass Spectrometry) [184,185] to map the same compounds in mouse brain sections [187]. DESI offers the ability to overcome problems associated with the use of matrix in MALDI where a common problem is analyte delocalisation.

### **3.4. Matrix Application Methods for Drug Metabolism and Pharmacokinetic Studies**

As matrix application methodologies were discussed in detail in chapter 2, below a summary of some of the matrix application methods that have been applied in drug metabolism and pharmacokinetic studies is given. The most commonly utilised method for matrix application involves manually spray coating the surface of a tissue section with a homogenous layer of dissolved matrix using a hand held device such as a TLC reagent sprayer e.g. see [21,158,193,207,259] or airbrush and this is the most widely documented method used for drug imaging experiments. Commercially available automated matrix application devices have also been developed to try to standardise the spray coating procedure, minimising operator variability that may result from manual spray coating and these have been utilised for drug metabolism and pharmacokinetic studies [260]. The use of robotic spotters which will deposit pL droplets of matrix onto the surface of the tissue has also been documented for imaging drug distributions, for example modification of a traditional ink-jet printer which gave better reproducibility for analysis of lipids and drug standards in rat brain sections than electrospray and airbrush methodologies [204]. Many robotic spotters are now available commercially but the spot size limits the resolution that can be used to around 200  $\mu\text{m}$  and thus they aren't often used for drug imaging studies which requires the generation of high resolution images to visualise drug distributions in specific anatomical regions.

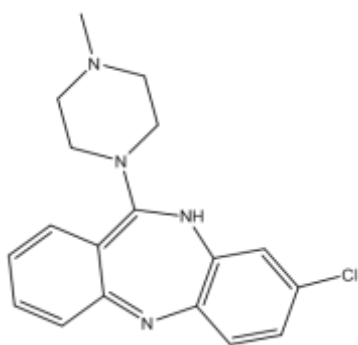
Unlike during peptide and protein analysis, a wet spray is not desired when analysing small molecules, particularly exogenous drug molecules, since many drugs are often

polar compounds that are readily soluble in the solvents commonly used for spray coating matrix such as methanol, water and acetonitrile. A novel approach documented that was of interest during the development of this current project was the study by Puolitaival *et al* who developed a novel method that involved coating the surface of rat brain sections with ground dry matrix for the visualisation of endogenous lipids [230]. It was realised that if this method could be used successfully for the analysis of lipids, this could also be modified for MALDI imaging of pharmaceuticals *in situ*. Advantages of the dry matrix coating included minimisation of analyte delocalisation and the removal of the possibility of matrix and solvent adduct formation. Additionally, this method is quick, easy and should minimise operator variance associated with manual spraying.

### **3.5. Background Information and Receptor Pharmacology – Clozapine Study**

Clozapine (C<sub>18</sub>H<sub>19</sub>ClN<sub>4</sub>) was chosen as the test compound to trial the suitability of the MALDI mass spectrometer for the detection of drug molecules in tissue imaging experiments. Clozapine is an atypical antipsychotic which was developed in the 1960s and is used in the treatment of schizophrenia (Figure 65).

**Figure 65 - Structure of Clozapine.**



Clozapine was chosen as the test compound because it is a lipophilic drug which is extensively metabolised hepatically and renally. Its distribution following a 20 mg/kg intraperitoneal injection has been mapped using a fluorometric procedure and it was shown to be present in brain, liver, lung and spleen and that the lung was an active transport site and region of accumulation for the drug [267]. It was chosen as a starting point because its distribution, following its administration *in vivo*, had been investigated previously using MALDI-MS [193], DESI [173] and NIMS [187].

Tissue imaging experiments using a QStar Pulsar I hybrid quadrupole-time-of-flight (QqTOF) mass spectrometer which had an orthogonal MALDI source were carried out previously [193]. In these experiments, albino rats were dosed intraventricularly with a 5 mg clozapine/8.3  $\mu\text{Ci}/\text{Kg}$  solution using a BAS model 1001 infusion pump [193]. Over a 5 minute period, 25  $\mu\text{l}$  of the solution was infused into the rat brain at a rate of 5  $\mu\text{l}/\text{min}$  and the rat was sacrificed 45 minutes post dose [193]. The presence of unlabelled clozapine and norclozapine were detected by looking for their product ions [193]. Results from this study were compared to those from autoradiography and they were found to be in very good correlation. By carrying out MS/MS analysis and monitoring one of the product ions of clozapine ( $m/z$  192), it was found



to be distributed throughout the brain with the highest concentration found in the lateral ventricle which correlated well with results of autoradiography [193].

For the DESI imaging study, a Thermo Scientific LTQ linear ion trap mass spectrometer fitted with a prototype automated DESI imaging source was developed [173]. Sprague Dawley rats were dosed orally with a 50 mg/kg solution of clozapine at pH 4.5 and the animals were sacrificed at various time points post dose, from 0-16 hours. The best results were found after 0.5 hours and DESI imaging revealed clozapine in the cortical and cerebellar brain regions at this time point [173]. The spatial distribution of the drug observed in the rat brain differed in these two studies which used different imaging mass spectrometry techniques but also different dosage methods.

The two predominant active metabolites of clozapine that are formed following phase I metabolism of the parent drug molecule are clozapine N-oxide ( $C_{18}H_{19}ClN_4O$ , mass 342.12) and norclozapine ( $C_{17}H_{17}ClN_4$ , mass 312.11) [268]. N-oxidation of the NH group on the parent drug molecule produces clozapine N-oxide in a phase I reaction that may be catalysed by a mixed function oxidase system or by flavoprotein N-oxidases which are known to be important in the metabolism of some drugs [269]. Demethylation of the parent molecule produces norclozapine via a phase I reaction that is also catalysed by the mixed function oxidase system. In this reaction, an unstable intermediary molecule may be formed. The major biotransformation in the liver is to norclozapine Figure 66[270,271] whilst in the brain it is to clozapine N-oxide Figure 67 [270].

**Figure 66 – Structure of norclozapine.**

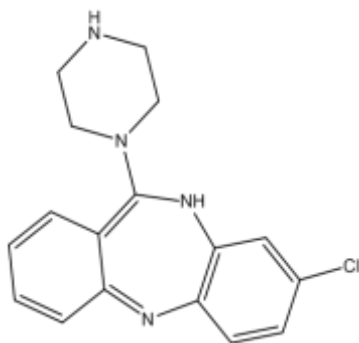
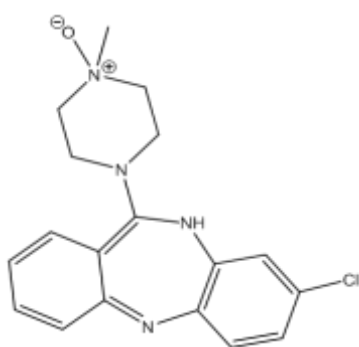


**Figure 67 – Structure of clozapine N-oxide.**



### **3.6. Background Information and Receptor Pharmacology – SSR180711 Study**

Neuronal acetylcholine receptors are ligand gated ion channels with a pentameric structure composed of five membrane spanning subunits, made up of combinations of alpha and beta subunits. The two main subtypes of neuronal acetylcholine receptors are the  $\alpha 4\beta 2$  [272] and the  $\alpha 7$  receptors [273]. Following activation by agonists such as acetylcholine or nicotine, channel opening will allow influx of cations such as  $\text{Na}^+$  leading to membrane depolarisation and action potential generation. Alpha 7 receptors are also thought to play a role in the pathophysiology of numerous psychiatric diseases including schizophrenia, Parkinson's disease and

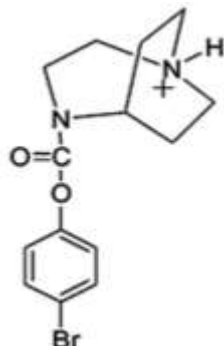
Alzheimer's disease and they have been found to be a therapeutic target for drugs targeting these diseases [274-280].

The drug investigated, 4-bromophenyl 1,4-diazabicyclo(3.2.2) nonane-4-carboxylate, monohydrochloride (SSR180711), was found to be highly selective for  $\alpha 7$  nicotinic acetylcholine receptors [281] and thus it was later developed as a PET ligand, [ $^{76}\text{Br}$ ] SSR180711, for in vivo imaging of  $\alpha 7$  nicotinic acetylcholine receptors in non human primate brain [282]. It was also shown to be a potential agent against schizophrenia and depression associated with the disease due to the results of a number of learning and memory studies performed on rats and mice [283]. Since  $\alpha 7$  receptors are increasingly being pursued as drug targets, and this is a known selective partial agonist, we wanted to see if it was possible to map the distribution of this compound and identify biomarkers related to drug-receptor interaction using MALDI-MSI. It was hoped that this study would demonstrate how these techniques could be used to investigate other research compounds as part of DMPK projects as an additional bioanalytical technique alongside other established methods in order to provide additional information on pharmacological effects of potential lead compounds.

The molecular formula of the drug is  $\text{C}_{14}\text{H}_{17}\text{O}_2\text{N}_2\text{Br}$  and its structure is shown below in Figure 68. As the drug contains a bromine atom, it has a characteristic isotope pattern when analysed using mass spectrometry which can help confirm the presence of drug in tissue. There is little documented on the metabolism of this particular drug as it is a test compound but it has been found that the predominant metabolites in the plasma from adult Sprague Dawley rats after a 1 hour time point are an N-

oxide at  $m/z$  341 and a glucuronide (+ 192 Da) formed following phase one oxidation at  $m/z$  517 (unpublished data, MSD).

**Figure 68 - Structure of SSR180711**



### **3.7. Use of Laser Capture Microdissection for Quantitation of Drug in Regions of Rat Brain Tissue Sections**

Laser microdissection (LMD) is another specialised technique which can also be used to provide information on the spatial distribution of compounds in gross anatomical regions. A laser is used to cut around selected anatomical regions from an intact tissue section with precision. Several tissue regions can be harvested and then analysed by LC-MS allowing the determination of drug concentrations in different anatomical locations. LMD and LC-MS have been used previously to confirm the qualitative results of MALDI ion trap imaging experiments which revealed the localised spatial distribution of a pharmaceutical prodrug in rat liver sections [284]. In this study, MALDI-MS was utilised with an ion trap mass spectrometer to localise drug and metabolites in rat brain tissue [284]. The prodrug BMS-X-P was administered to young rats and the parent drug and major metabolites were localised using ion trap mass spectrometry [284]. Using this technique

microcrystalline material found in tissue samples was found to be the parent drug, BMS-X and the results were confirmed by use of cross polarised light microscopy, MALDI-MS without an ion trap (which was able to localise the parent drug successfully but not the metabolites due to interference) and HPLC-MS on laser capture dissection (LMD) samples [284]. LMD has also been used for proteomics applications, for example cancer cells were removed from human lung tissue and then analysed using MALDI MS profiling to detect peptides and comparisons made with healthy tissue [285].

### **3.8. Aims of Clozapine and SSR180711 Studies**

The main aim was to map the distribution of pharmaceuticals *in situ* using MALDI-MSI. Dry matrix coating was investigated as an alternative matrix application method. It was hypothesised that the use of a dry matrix coating would minimise any drug delocalisation that may result from traditional manual spray coating. It was proposed that this dry matrix application method would be agreeable with the main goal of the matrix in MALDI-MSI tissue imaging experiments; to extract analytes vertically from the tissue without horizontal diffusion.

### 3.9. Methodology

#### 3.9.1. Materials

MALDI-MS grade  $\alpha$ -cyano-4-hydroxycinnamic acid (CHCA), clozapine and Trifluoroacetic acid were purchased from Sigma Aldrich. Acetonitrile, methanol and formic Acid were purchased from Fisher Scientific. The drug standard, SSR180711 was synthesised and provided by MSD (Newhouse, Motherwell, Scotland.) A small sieve was purchased from a hardware shop and a standard mortar and pestle were available in the laboratory. All chemicals used were of analytical reagent grade. HPLC grade water was obtained from a Millipore Direct Q-3 water purification system which was used in all analyses.

#### 3.9.2. Animals

**Clozapine Study:** Adult male Wistar rats were dosed orally with 50 mg/kg Clozapine in acidic saline (pH 4.5) ( $n=3$ ). Alternatively, animals were treated with saline as controls ( $n=3$ ). After 30 minutes, the animals were sacrificed and the liver, kidney and brain tissues were immediately immersed in liquid nitrogen cooled isopentane before being stored at a temperature of  $-80\text{ }^{\circ}\text{C}$  following procedures described in previous studies [69,190]. This time point was chosen as it has been shown previously that this is when there is highest concentration of the parent drug in the brain is found from quantitation experiments using LC-MS [173].

**SSR180711:** Frozen rat brain tissues were obtained from MSD (Newhouse, Motherwell, Scotland) ( $n=5$ , 3 drug treated and 2 vehicle treated animals). Adult

male BRL rats weighing approximately 250g were given a single 30 mg/kg dose of the drug in 0.5% gelatine 5% mannitol solution ( $n=3$ ) or vehicle ( $n=2$ ) administered by oral gavage. Rats were euthanized by cervical dislocation one hour post dosing in accordance with the U.K. Animals (Scientific Procedures) Act, 1986 and local ethical guidelines. Tissues were frozen immediately by slowly immersing them into isopentane at  $-78\text{ }^{\circ}\text{C}$  and they were then stored at  $-80\text{ }^{\circ}\text{C}$  until required for sectioning.

### **3.9.3. Tissue Sectioning Procedures**

**Clozapine and SSR180711 Studies:** Sectioning of brain, liver and kidney sections were carried out using a Leica CM1850 Cryostat (Leica Microsystems, Milton Keynes, UK).

**Clozapine Study:** For the experiments on the Axima CFR TOF mass spectrometer, the sectioning and tissue mounting parameters were the same as those described in chapter 2. For experiments on the Bruker Ultraflex III instrument, sagittal sections were cut at  $12\text{ }\mu\text{m}$  and thaw mounted onto indium tin oxide (ITO) coated MALDI target slides (Bruker Daltonics, Germany Cat. # 237001). A rat brain atlas was used to ensure that sections were taken that allowed visualisation of the cerebral cortex, hippocampus, lateral ventricles and cerebellum [286]. These regions were selected since clozapine has already been visualised in these regions using MALDI and DESI imaging [173,193]. The rat liver was sliced transversely and  $12\text{ }\mu\text{m}$  thick tissue sections were taken at various depths with chamber temperature of  $-20^{\circ}\text{C}$ . Mid-transverse sections were taken through kidneys to enable visualisation of the cortex, medulla and renal pelvis. Thaw mounting was then used to fuse the sections onto MALDI target plates.

**SSR180711 Study:** For experiments on the Axima CFR-TOF mass spectrometer, 14 µm thick sagittal and coronal sections were taken and positioned onto Fleximass MALDI target plates (Shimadzu Biotech, Milton Keynes, UK) using a small artists brush. For experiments on the Bruker Ultraflex III instrument, sagittal sections were cut at 14 µm and thaw mounted onto indium tin oxide (ITO) coated MALDI target slides (Bruker Daltonics, Germany Cat. # 237001) or cut at 10µm and thaw mounted to PET-membrane laser micro-dissection slides (Leica, Germany Cat. # 11505151). In both cases, sagittal sections were taken at depth of approximately 4.6 mm from midline which allowed visualisation of cerebral cortex, corpus callosum, striatum, hippocampus and cerebellum, using a rat brain atlas as a guide [286]. Coronal sections were also taken through the cerebellum to enable clear visualisation of the grey and white matter regions. For MALDI-MSI, treated sections were mounted with at least one control section on a single slide to minimise the variability that is associated with scanning separate targets. Slides were then freeze-dried for 6 hours before storage at -80 °C until required.

**Clozapine and SSR180711 Studies:** For experiments utilising the Shimadzu Fleximass targets, adjacent sections were mounted onto glass slides to enable collection of optical images using a Nikon Cool Scan iV scanner with medical adapter. For experiments using the Bruker Targets, optical images were taken using a mounted charged-coupled device digital camera and macro lens prior to MALDI matrix application using the same targets that were to be used for MALDI imaging experiments.



### **3.9.4. Preparation and Analysis of Drug Standards by MALDI Profiling**

**Clozapine Study:** For the clozapine study, a stock solution of clozapine was prepared at concentration of 1 mg/ml in 100% methanol. Serial dilutions were carried out in methanol to obtain 100 µg/ml and 10 µg/ml solutions. For a limit of detection study, serial dilutions were carried out to obtain clozapine standards prepared in 100% methanol with concentrations of 31.25 µg/ml, 15.6 µg/ml, 7.8 µg/ml, 3.9 µg/ml, 1.95 µg/ml, 0.98 µg/ml, 0.49 µg/ml, 0.24 µg/ml, 0.12 µg/ml and 0.06 µg/ml. For MS/MS fragmentation of the parent drug, 1 µl of a 100 µg/ml solution of the drug in 100 % methanol was manually spotted onto the ITO target and over spotted with 1 µl of CHCA matrix in solution. For PSD analysis of the drug standard, a 100 µg/ml drug standard was spotted onto a MALDI target and a window was selected around the parent ion. The ion gate was then switched on and the power was raised by approximately 20 % to enable fragmentation of the parent drug.

**SSR180711 Study:** For MS/MS fragmentation of the parent drug, 1 µl of a 100 µg/ml solution of the drug in 100 % methanol was manually spotted onto the ITO target and over spotted with 1 µl of CHCA matrix in solution.

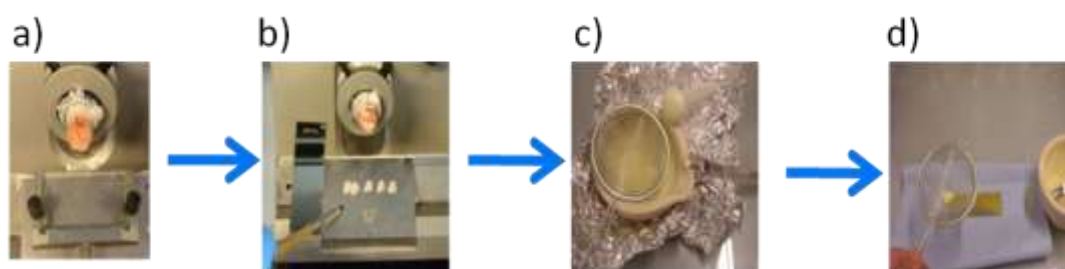
### **3.9.5. Preparation of Matrices for MALDI Experiments and Matrix Coating**

#### **3.9.5.1. Dry Matrix Application**

For the dry matrix coating experiments, CHCA was finely ground using a pestle and mortar and stored until required (Figure 69). Tissue sections were taken from the freezer and allowed to warm to room temperature and humidity for approximately 10

minutes. Tissue sections were then covered in a huge excess of CHCA. Matrix was then tipped off MALDI target. The process of sections being covered and then matrix tipped off was repeated 6 to 8 times. Finally all excess matrix not adhered was removed by briefly placing target under a fast stream of oxygen-free nitrogen.

**Figure 69 – Photographs illustrating the cryosectioning procedures and the methodology used for the application of a dry matrix coating to the surface of samples on a MALDI target; a) positioning rat brain for sectioning, b) collecting sections following cutting and mounting them onto MALDI target using a brush, c) grinding dry matrix powder and d) applying the ground matrix using a sieve.**



### 3.9.5.2. Wet Matrix Application

The CHCA matrix for the wet matrix application experiments was prepared as described in section 2.11.4.1. The wet matrix application method utilised was the same as that described previously in section 2.11.4.1.

### 3.9.6. MALDI-MSI analysis

**Axima CFR-TOF Instrument:** MSI was performed in positive ionisation mode. The mass spectrometer parameters were set at manufacturers recommended settings

and adjusted for optimal performance. A raster was set before imaging runs and the laser power was adjusted to optimise analysis at the start of each run and fixed during the MSI experiment. Peak extension was optimised during each experiment; it was set at  $m/z$  325 for SSR180711 study and  $m/z$  327 for clozapine study. Fifty laser shots were collected per raster point, with an average of 10201 points collected per sample with 100  $\mu\text{m}$  spacing and the laser scan speed was 10 Hz.

**Bruker Ultraflex III TOF/TOF Instrument:** MSI was performed as described previously [287] using a Bruker Ultraflex III TOF/TOF in positive ion reflectron mode. The mass spectrometer parameters were set at the manufacturer's recommended settings and adjusted for optimal imaging performance. Laser spot size was set at medium focus (approximately 50  $\mu\text{m}$  laser spot size diameter) and laser power intensity was optimized at the start of each run and then fixed for the MSI experiment. Tissue sections were analyzed in a random order to prevent any possible bias due to such factors as matrix degradation or variation in mass spectrometer sensitivity. On-tissue MS/MS was performed in positive ion LIFT mode with parameters set at manufacturer's recommended settings. A total of 150 laser shots were taken per raster position during full scan and MS/MS modes. MS imaging was performed at 100  $\mu\text{m}$  laser spot centre to centre raster whilst MS/MS imaging was performed at 150  $\mu\text{m}$  laser spot centre to centre rastering.

#### **3.9.6.1. Multiple Reaction Monitoring Characterisation using Bruker Ultraflex III TOF/TOF Instrument**

MALDI-MS MRM was performed using the Ultraflex III in LIFT mode. 1  $\mu\text{L}$  of drug standard was manually spotted onto ITO target and coated with several layers of

dry CHCA matrix. MRM was then used to monitor the transition of parent ions ( $m/z$  327 for clozapine study) and ( $m/z$  325 for SSR180711 study) in both studies to their unique product ions.

### **3.9.7. MALDI-MSI Data Interpretation**

**Axima CFR-TOF Mass Spectrometer:** Data was collected using the Shimadzu Biotech Launchpad software Version 2.8 and converted into BioMap files as described previously in sections 2.11.5.3 and 2.11.6.

**Bruker Ultraflex III TOF/TOF Instrument:** Data was analyzed using FlexImaging 2.0 (Bruker), employing the software to normalize the dataset. Regions of interest were manually defined in the analysis software using both the optical image with the MSI data image. Masses were selected with a mass window of  $\pm 0.1$  Da.

### **3.9.8. Quantitation of clozapine in Single Rat Brain Tissue Sections Determined by LC-MS**

This was carried out by ‘scraping’ intact rat brain, kidney and liver tissue sections that were mounted onto glass slides into small plastic 1 ml eppendorfs using a razor blade. Biological replicates were taken from  $n=3$  treated and  $n=3$  control animals. The drug and metabolites were then extracted from the tissue sections using the following extraction procedure: Samples were immersed in 200  $\mu$ l of 1:1 methanol 0.1% formic acid: water. Samples were then homogenised and vortexed for approximately 2 minutes and centrifuged for 15 minutes at 4000 rpm. The supernatant was then removed and filtered using Acrodisc syringe filters and the

solution placed into inserts in HPLC vials. The samples were then analysed directly using LC-MS. The PPT+ filters were not used for this as the sample volume was so small and this would have resulted in dilution of the solution further before analysis which could have prevented the detection of the drug in a single slice.

### **3.9.9. Investigating the Effects that Washing Tissue had on the Intensity of Clozapine using LC-MS.**

In order to investigate the effects of washing tissue on the intensity of clozapine using LC-MS, rat brain tissue sections that had been mounted onto slides were washed using solvents to mimic the effects of applying a wet matrix coating to the tissue surface. The washing steps involved washing one set of clozapine treated samples with 70 % ethanol. A glass pipette was used to wash the samples with 1 ml of solution. After washing, samples were allowed to dry before being scraped off and worked up for LC-MS analysis using the same procedure described in section 3.9.8.

### **3.9.10. Validation of Relative Quantitation of SSR180711 in Rat Tissue Determined by Laser Micro-Dissection and LC-MS**

Laser micro-dissection was performed using a Leica LMD6000 system (Leica Microsystems) (Figure 70). Two regions of rat brain were chosen to collect tissue from, grey matter of the cerebellum and white matter of the cerebellum, correlating to regions where changes in distribution of drug were seen to vary in the imaging experiment (Figure 71). Tissue was dissected from a number of consecutive tissue slices to obtain sufficient material for the LC-MS analysis. The total area of tissue

obtained in each sample was then recorded and samples relating to closely matched total areas were used in the analysis. Biological replicates were taken from 3 different treated animals and a vehicle treated control animal.

**Figure 70 - Schematic Diagram Laser of Microdissection Collection**

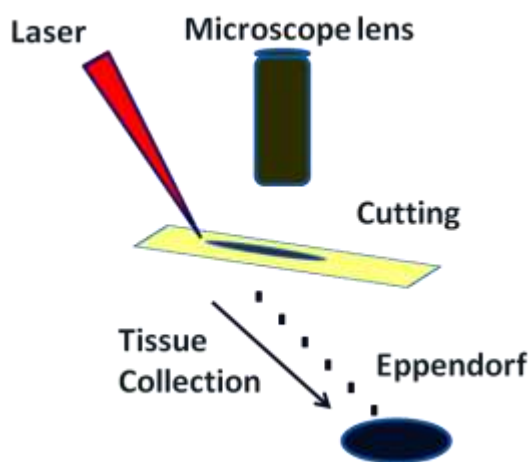
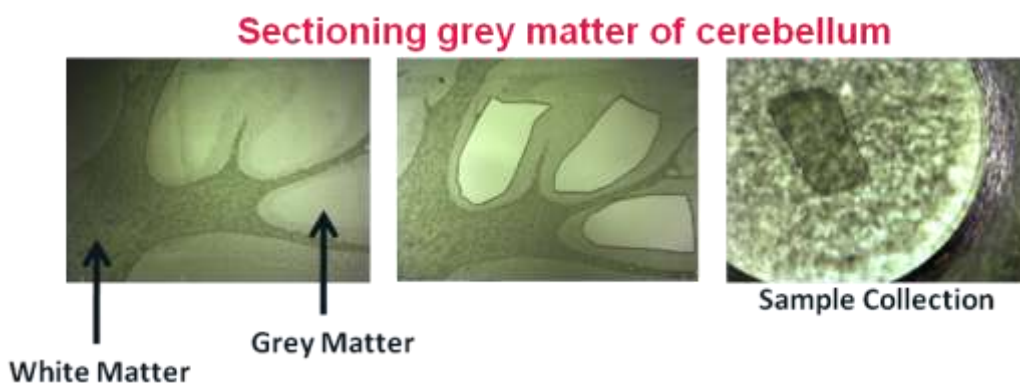


**Figure 71 - Images Showing Collection of Samples Using Laser Microdissection.**



### **3.9.10.1. Preparation of Samples for Validation**

Tissue extraction was carried out directly after tissue collection. Tissue samples were immersed in 50  $\mu\text{L}$  of 1:1 methanol 0.1% formic acid: water and vortexed for 2 minutes to remove all tissue attached to the LMD membrane. Sample vials were then rinsed with a further 20  $\mu\text{L}$  of solvent. Isolute® Protein precipitation plates (Biotage, Uppsala, Sweden) were then used to remove protein and any LMD membranes from the samples before LC-MS analysis. The 'solvent first' method was used which involved pipetting 210  $\mu\text{L}$  of acetonitrile (to obtain a final acetonitrile:sample ratio of 4:1) into PPT+ protein precipitation plates that were positioned on a Vacmaster™ 96 sample processing manifold (Biotage) and then adding sample and allowing to settle for 10 minutes. A water pump was then attached to the VacMaster™ and used to filter samples through the frit of the PPT+ filters into the 96-well collection plate. Filtrates were then collected and stored at  $-80\text{ }^{\circ}\text{C}$  until LC-MS analysis.

### **3.9.11. Liquid Chromatography Mass Spectrometry Method for both Studies**

Experiments were carried out using a Thermo Scientific LTQ Orbitrap (ThermoScientific, Bremen, Germany) running at 30,000 resolution. Analysis was carried out in positive ESI mode over a mass range of 80-1000  $m/z$ . A ZIC-HILIC column (5  $\mu\text{m}$ , 150 X 4.6 mm; HiChrom, Reading, UK) was used in all analyses and a binary gradient method was developed which produced good polar metabolite separation. Solvent A was 0.1% formic acid in HPLC grade water and solvent B was 0.1% formic acid in acetonitrile. A flow rate of 0.3 mL/min was used and the injection volume was 10  $\mu\text{L}$ . The gradient programme used was 80% B at 0 min to

50% B at 12 min to 20% B at 28 mins to 80% B at 37 mins, with total run time of 45 minutes. Samples were analysed sequentially and the vial tray was set at a constant temperature of 4 °C. Each sample was analysed twice in full scan MS mode. The instrument was externally calibrated before analysis and internally calibrated using lock masses at  $m/z$  83.06037 and 195.08625. For quantification of clozapine in single tissue sections, drug standards with concentrations of 244, 122, 61, 30.5, 15.3, 7.6 and 3.8 ng/ml were prepared in methanol and a seven point calibration curve constructed. For quantification of SSR180711 in LMD tissue samples, an external 5 point calibration was performed using drug standards with concentrations of 0.5, 1, 2, 4, 8, 16 pg/ $\mu$ l prepared in methanol. For quantification of SSR180711 in homogenised brain tissue samples, drug standards with concentration of 100, 10, 1, 0.1  $\mu$ g/ml and 10, 1 and 0.1 ng/ml were prepared in methanol and a 6 point external calibration curve plotted. Data was analysed using Xcalibur version 2.0 (Thermo Scientific).



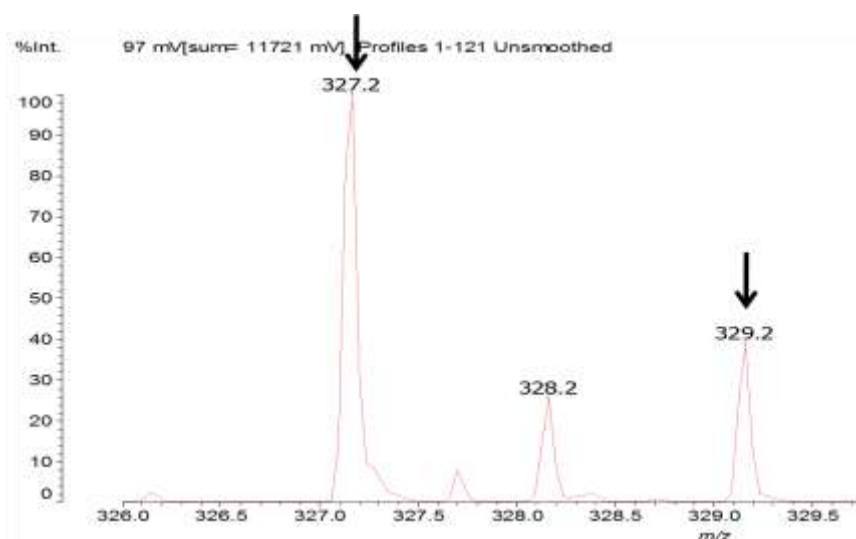
### 3.10. Results

#### 3.10.1. Results of the Clozapine Study

##### 3.10.1.1. Analysis of Clozapine Standard

As chlorine is present in the structure of clozapine, two peaks corresponding to the parent ion should be observed following mass spectrometric analysis, at  $m/z$  327  $[M+H]^+$  and  $m/z$  329 (chlorine isotope), with the peak at  $m/z$  329 being approximately 1/3 the size of the peak at  $m/z$  327 since the ratio of  $^{35}\text{Cl}$ :  $^{37}\text{Cl}$  is approximately 3:1. MALDI MS analysis of clozapine in full scan mode did reveal the characteristic chlorine isotopic distribution (Figure 72).

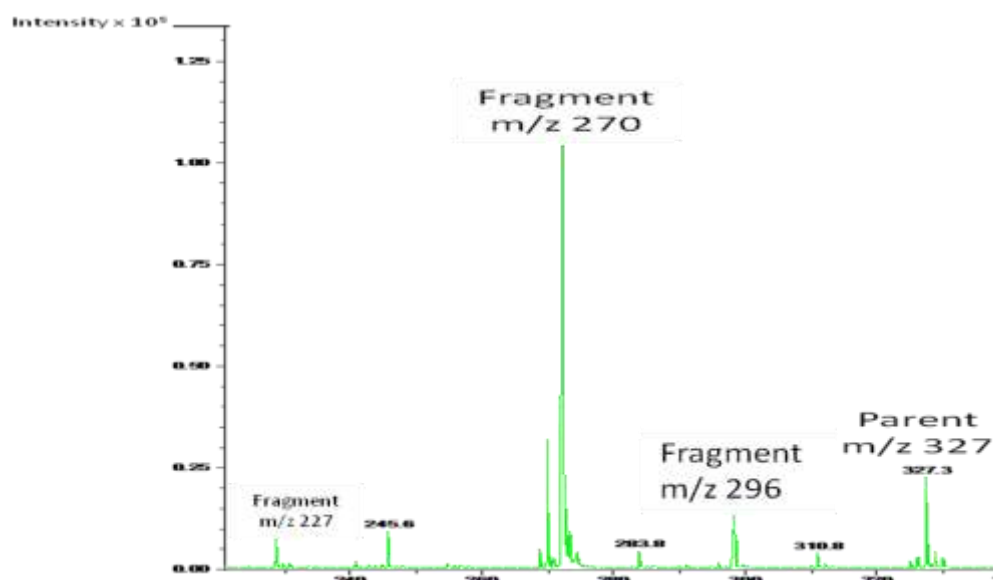
**Figure 72 - Full MS mode mass spectrum from analysis of 10  $\mu\text{g/ml}$  clozapine standard on MALDI target. Figure shows the isotopic distribution of clozapine characterised by the chloride atom.**



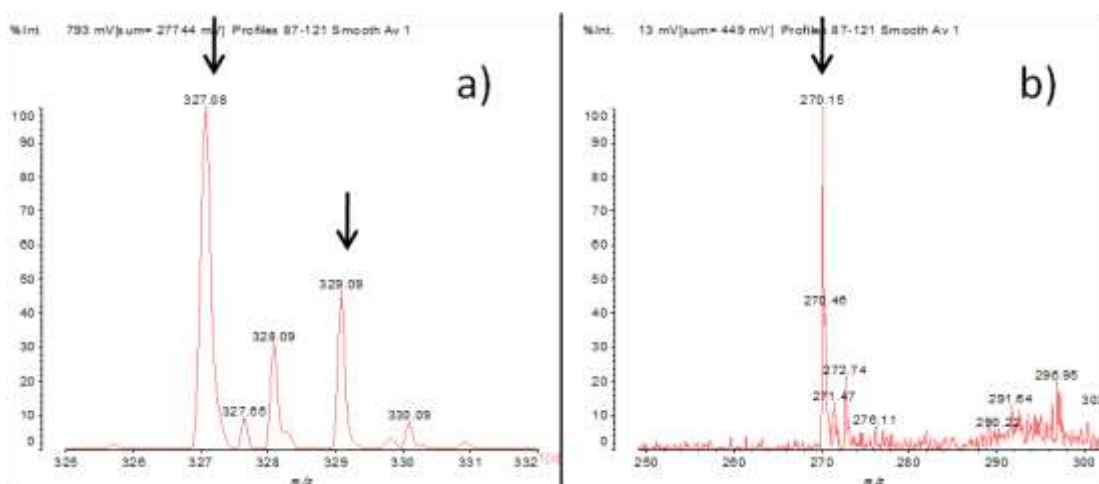
MALDI MS/MS analysis of the drug standard using CHCA as matrix resulted in fragmentation of the parent drug to form several product ions. The main product ion observed with the highest intensity was at  $m/z$  270 (Figure 73). This was also the main product ion observed when post-source decay analysis of the clozapine standard was carried out (

Figure 74). Other product ions observed during PSD and MS/MS experiments included  $m/z$  296 and  $m/z$  227. The proposed dissociation pattern of clozapine is shown below and it can be seen that the main product ion at  $m/z$  270 is observed when the piperazine ring is broken (Figure 75). This dissociation pattern is in agreement with results of previous tissue imaging studies where MS/MS experiments have been carried out and the distribution pattern of the product ion at  $m/z$  270 Da has been used to map the distribution of the parent drug.

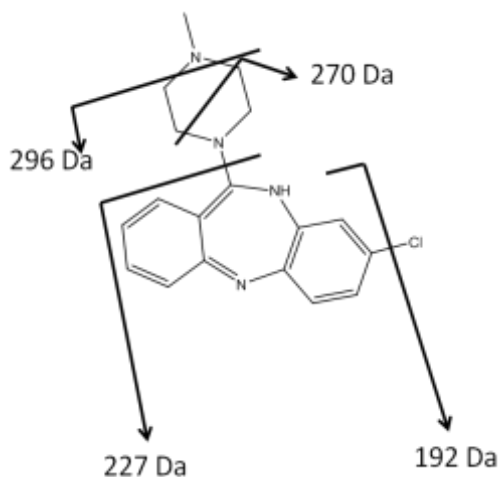
**Figure 73 – Product ion mass spectrum of clozapine from analysis of 100 µg/ml clozapine standard on MALDI target. Experiment carried out using a Bruker Ultraflex III instrument.**



**Figure 74 - Post Source Decay of 100 µg/ml clozapine standard produces a main fragment at  $m/z$  270. Panel a) shows clozapine parent ion at  $m/z$  327 and isotope at  $m/z$  329 and panel b) shows fragment at  $m/z$  270 (arrows). Experiment carried out using a Shimadzu Axima CFR TOF mass spectrometer.**



**Figure 75 - Proposed Dissociation Pathways of Clozapine**



### 3.10.1.2. Clozapine Limit of Detection Study

To investigate the limit of detection of clozapine when utilising MALDI MS, several concentrations of the drug were spotted onto a blank MALDI target. The concentration of the clozapine standards are calculated as the concentration that is actually being applied to the target. If only 1  $\mu\text{l}$  of a standard of a 31.25  $\mu\text{g}/\text{ml}$  is applied to the target, the actual concentration which will be spread across the surface area of the sample spot is 31.25 ng. This is because when an imaging experiment is

carried out, the actual concentration of the drug in the tissue sample is calculated and the spectra generated will display the average concentration across the surface area for both sample and standards being analysed. When 1  $\mu\text{l}$  of a standard in solution is spotted onto a MALDI target, it will spread out to cover a surface area of approximately 3.6  $\text{mm}^2$ . Thus, the concentration of drug across the sample area will be approximately 8.7  $\text{ng}/\text{mm}^2$ . From analysis of clozapine standards, it was found that the limit of detection for clozapine was approximately 0.06  $\mu\text{g}/\text{ml}$ . As only 1  $\mu\text{l}$  of this is being applied the actual concentration of drug being applied to the target is 60  $\text{pg}$  of drug, which is approximately 16.7  $\text{pg}/\text{mm}^2$ . Thus, the results from the limit of detection study reveal that it is possible to detect clozapine at a concentration of approximately 16.7  $\text{pg}/\text{mm}^2$  on a MALDI target. However, this is just an estimation as the laser may not scan the full depth of the spot. This illustrates that MALDI offers a high sensitivity for the detection of pharmaceuticals, assuming they ionise efficiently, which could be tested by using MALDI profiling for the analysis of the drug standard before any imaging experiments were carried out.

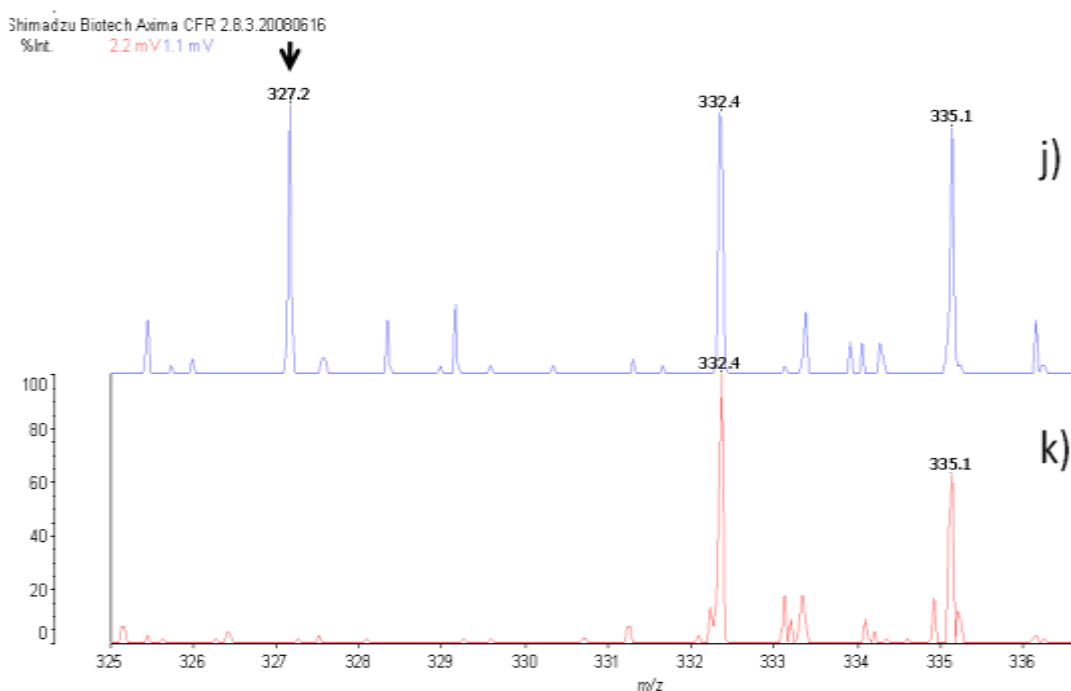
**Figure 76 - Limit of Detection Study: Clozapine standards were prepared in 100% methanol and analysed using CHCA matrix (15 mg/ml in 1:1 acetonitrile:water plus 0.1% TFA). Spectra shown are those obtained when 1  $\mu$ l of the following standards were spotted onto a MALDI target, a) 31.25  $\mu$ g/ml, b) 15.6  $\mu$ g/ml, c) 7.8  $\mu$ g/ml, d) 3.9  $\mu$ g/ml, e) 1.95  $\mu$ g/ml, f) 0.98  $\mu$ g/ml, g) 0.49  $\mu$ g/ml, h) 0.24  $\mu$ g/ml, i) 0.12  $\mu$ g/ml and j) 0.06  $\mu$ g/ml. Spectra show mass range  $m/z$  325-340.**



To confirm the limit of detection, a standard with concentration of 0.03  $\mu$ g/ml was also analysed, which equates to the actual concentration of drug being applied to the MALDI target as being 0.03 ng across the sample surface. Again, if the area that a 1  $\mu$ l sample spot covers is approximately 3.6 mm<sup>2</sup>, the concentration of drug is approximately 8.3 pg/mm<sup>2</sup>. It can be seen that whilst it was possible to see the

parent ion at  $m/z$  327 and the Cl isotope at  $m/z$  329 in the standard with concentration of 0.06  $\mu\text{g/ml}$ , it was not possible to see this from the analysis of standard with concentration of 0.03  $\mu\text{g/ml}$ , confirming that the limit of detection is approximately 16.7  $\text{pg/mm}^2$  when applied directly onto MALDI targets (Figure 77).

**Figure 77 - Limit of Detection Study: Clozapine standards were analysed using CHCA (15 mg/ml in 1:1 acetonitrile: water plus 0.1% TFA). Clozapine standards were prepared in 100% methanol. Spectra are zoomed in to show mass range  $m/z$  325-340 from samples containing drug concentration of j) 0.06  $\mu\text{g/ml}$  and k) 0.03  $\mu\text{g/ml}$ . It can be seen that clozapine cannot be detected in 0.03  $\mu\text{g/ml}$  standard.**



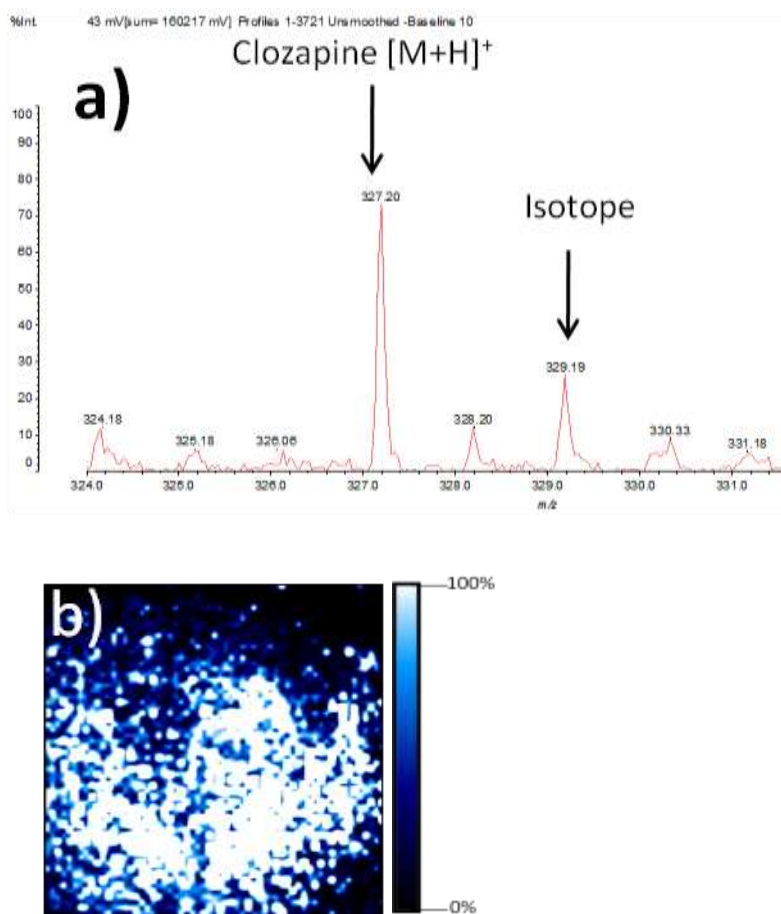
### 3.10.1.3. Imaging Clozapine in Liver using a Conventional Wet Matrix Coating

To investigate if it was possible to map the distribution of clozapine *in situ* using MALDI-MSI, samples taken from drug-treated and control liver were obtained for analysis. Samples were coated with CHCA applied using a conventional wet matrix application method. Wet matrix coatings were applied using two methods a) applying discrete spots of matrix with a pipette or b) applying a homogenous layer of matrix using a handheld sprayer. It was possible to detect a peak which corresponded to the protonated mass of clozapine following either spraying or spotting CHCA matrix at  $m/z$  327. However, to investigate if there was any possible drug delocalisation occurring, the use of a dry matrix coating was investigated as an alternative method for the application of CHCA.

It was possible to detect clozapine in treated rat liver tissue sections when a wet matrix coating was used. A peak was identified which corresponded to the protonated mass of clozapine following either spraying or spotting CHCA. The spectrum shown in Figure 78a is from the analysis of a small piece of rat liver that was spotted with CHCA and this reveals a peak at  $m/z$  327 corresponding to the protonated form of clozapine (Figure 78a). The chlorinated isotopic pattern is also evident further confirming the presence of the drug (Figure 78a). The corresponding tissue images are also shown and it can be seen that the drug seems to be accumulating throughout the liver (Figure 78b).

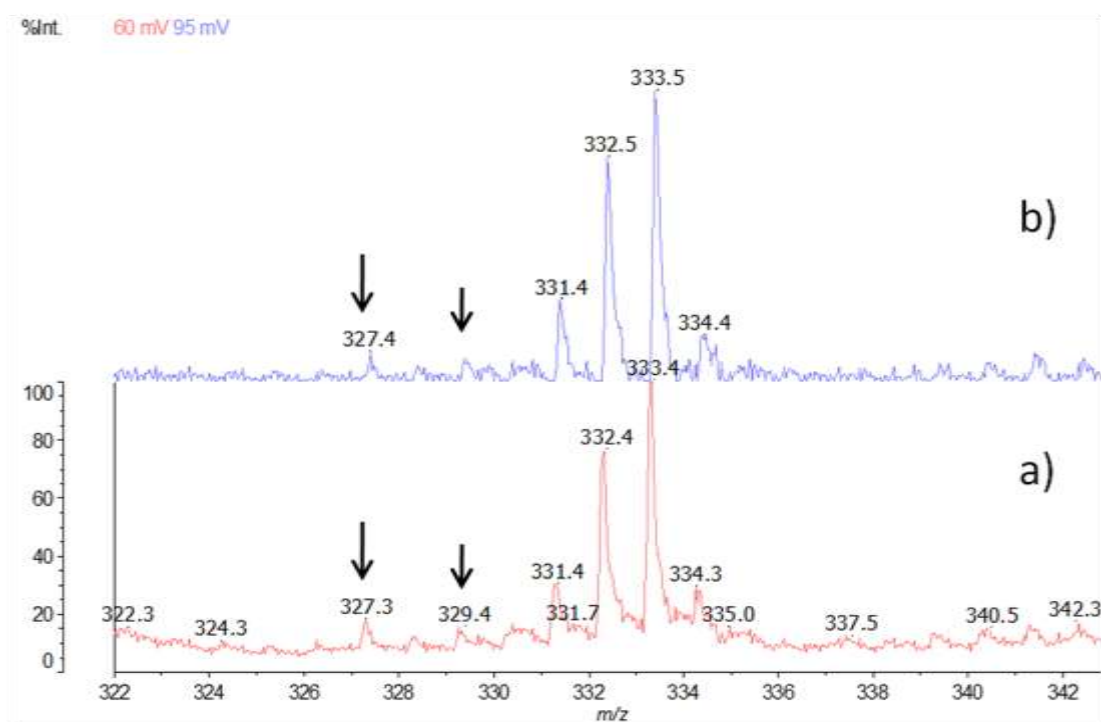


**Figure 78 - It was possible to detect clozapine in rat liver tissue sections when CHCA was applied as discreet spots on the surface of treated rat liver tissue, a) shows spectrum with peak at  $m/z$  327 corresponding to the protonated form of clozapine whilst b) shows the distribution of clozapine in tissue.**



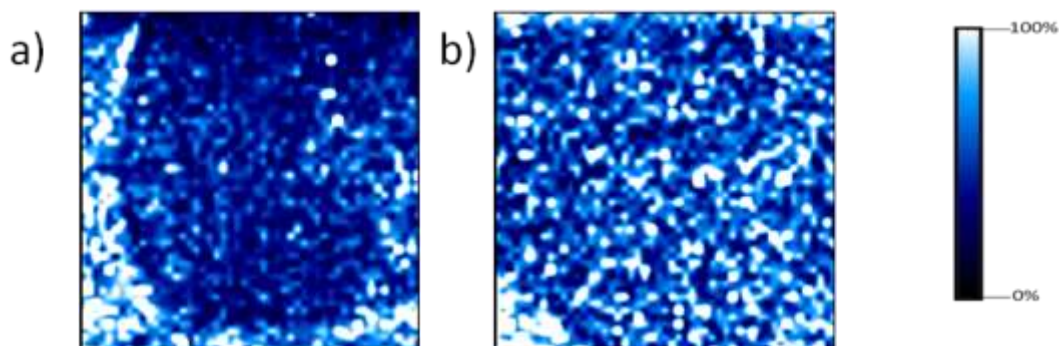
Subsequent experiments revealed that it was also possible to detect a peak at  $m/z$  327 in the rat liver samples when CHCA was sprayed onto the tissue as a homogenous layer (Figure 79). However, the peak was very weak and just above baseline and the chlorinated isotopic pattern was not evident (Figure 79). This illustrates that whilst clozapine can be detected when CHCA is applied as discreet droplets, this is not the case when a wet matrix coating is applied. This suggests the wet matrix application mode is not suitable for the detection of clozapine.

**Figure 79 – Spectra illustrating that it was possible to detect a peak that may correspond to clozapine at  $m/z$  327 in rat liver tissue sections when CHCA was applied as homogenous layer onto tissue surface using a conventional wet matrix application. Spectra shown are from analysis of two treated tissue sections, a) and b).**



Additionally, when the corresponding tissue images were generated it was not possible to map the distribution of the parent drug by creating a heat map of  $m/z$  327. It can be seen in Figure 80a that there is a higher intensity observed around the edge of the sample, again suggesting that drug delocalisation is occurring.

**Figure 80 - Heat maps are shown which illustrate the distribution of the clozapine ion at  $m/z$  327 in two rat liver tissue sections, a) and b). Images are normalised against CHCA matrix ion at  $m/z$  190.**

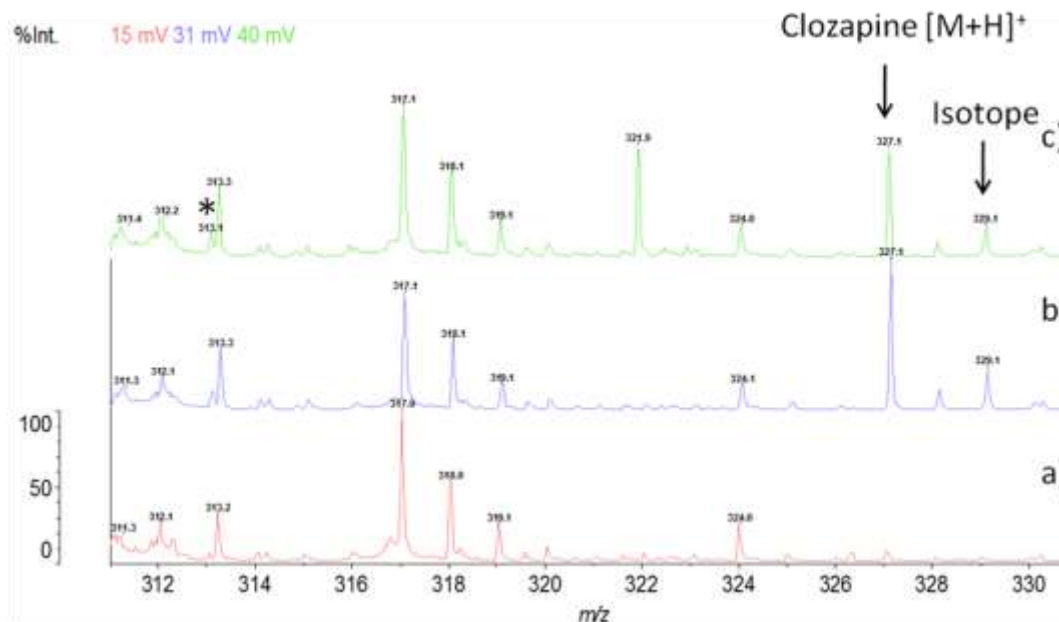


Although clozapine could be detected in the liver when a wet matrix coating was used, the signal to noise ratio was poor and no drug metabolites could be detected. By comparing the results of spotting CHCA onto liver surface and spraying a homogenous layer onto the surface, it was observed that spotting gave better results; the spectra were better and so were images suggesting that the drug was in fact present (also confirmed through LC-MS analysis discussed in section 3.10.1.8). Since the results of the spraying were poorer it was hypothesised that this could be the result of drug delocalisation as a result of spraying the matrix onto the sample surface using polar solvents. Thus a dry matrix coating was employed as an alternative matrix application method.

#### 3.10.1.4. Imaging Clozapine in Liver using a Dry Matrix Coating

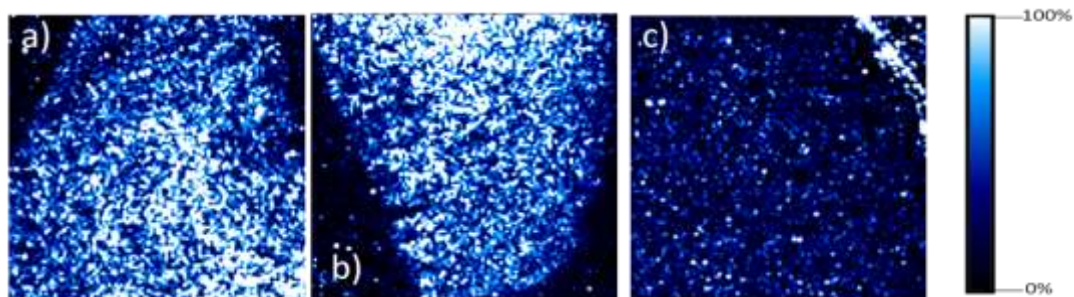
Results from the analysis of treated liver sections coated with dry matrix suggested that the distribution of the drug could be mapped using this alternative matrix application method. The peak intensity of the parent ions corresponding to the drug at  $m/z$  327 and  $m/z$  329 were higher than when a wet matrix coating was used. Additionally, the signal to noise ratio was higher. Figure 81 illustrates that whilst the parent ions could be detected in the spectra from treated liver sections, it was absent from the control liver. Spectra from the analysis of three separate pieces of liver (two treated sections and one control) are displayed to illustrate that these peaks were in fact parent ions and not endogenous molecules present in the tissue (Figure 81). Additionally, the isotopic peak at  $m/z$  327 is approximately 1/3 the height of peak at  $m/z$  325 suggesting it is the  $^{37}\text{Cl}$  isotope. There was also a small peak found at  $m/z$  313 which could correspond to norclozapine, however, MS/MS would be needed to confirm this. This peak was not observed when a wet matrix coating was utilised.

**Figure 81 - Sample spectra illustrating that clozapine could be detected in treated liver when a dry matrix coating was used, b) and c) are spectra from treated livers whilst a) is from analysis of control liver.**



Creation of corresponding heat maps illustrated that the distribution of clozapine could be mapped in the liver tissue sections. This was confirmed through the sequential analysis of treated and control sections. It can be seen that in the control sample it is not possible to detect a peak at  $m/z$  327 whilst in the treated samples the intensity of the peak at  $m/z$  327 thought to correspond to protonated clozapine is high and it is possible to visualise clozapine across the surface of the samples, albeit with no specific localisation (Figure 82).

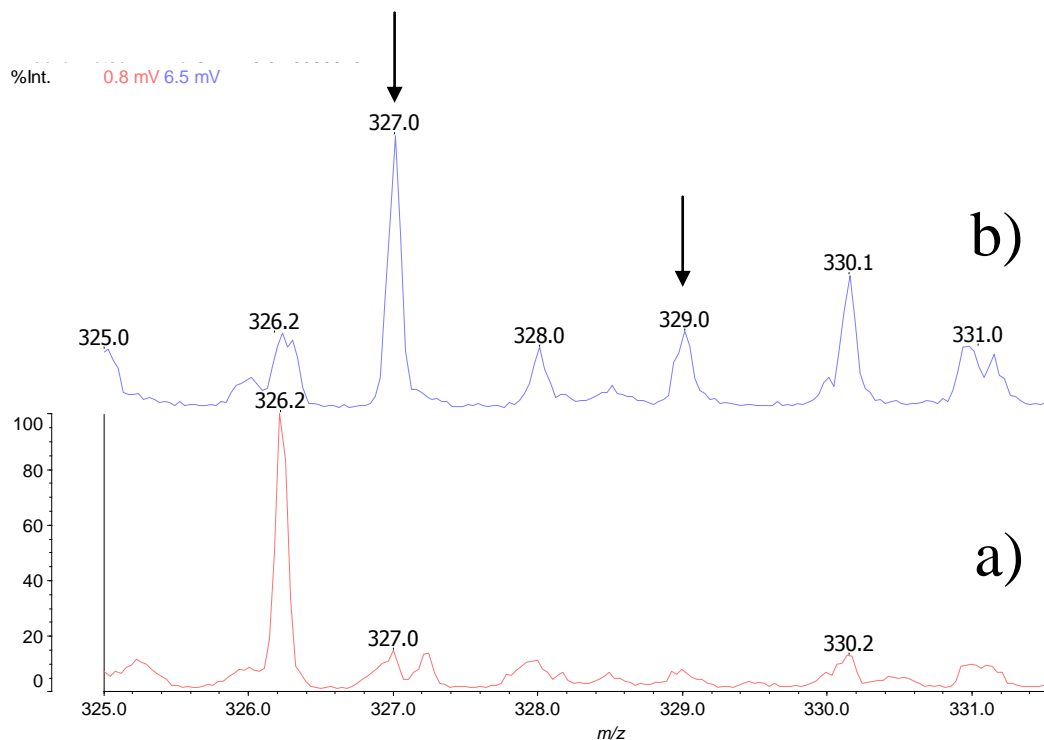
**Figure 82 – Heat maps showing that the distribution of the parent ion corresponding to clozapine at  $m/z$  327 could be mapped in the rat liver when a dry matrix coating was used in a) and b) treated sections and that that very few ions are seen at  $m/z$  327 in c) control section.**



#### **3.10.1.5. Imaging Clozapine in Kidneys using Wet and Dry Matrix Coatings**

As it was demonstrated that clozapine could be detected in liver sections when a dry matrix coating was used, it was hoped that could be used to map clozapine in the kidneys which have a much more detailed anatomical structure. To confirm the suitability of a dry matrix coating for imaging drugs *in situ* in both the dry matrix application method and the conventional wet matrix coating were used to obtain comparative results. Firstly it was observed using the Axima CFR TOF instrument that the parent ion corresponding to clozapine could be detected in the treated but not the control kidneys (Figure 83).

**Figure 83 - Sample spectra illustrating that clozapine could be detected in treated kidneys when a dry matrix coating was used a) is from analysis of control kidneys and b) is from treated kidneys. The isotopic peak can also be observed at  $m/z$  329.**



Next, the Bruker Ultraflex III instrument was used to perform additional experiments offering higher sensitivity and the possibility of carrying out MS/MS analysis. Control and treated kidney sections coated with either dry or wet CHCA matrix were compared directly. It can be seen that the drug is only found in spectra obtained from analysis of treated sections which suggests that this is in fact the drug compound (Figure 84). Additionally, the distribution of clozapine could only be mapped when the dry matrix coating was utilised, confirming results obtained on the Axima CFR TOF mass spectrometer (Figure 85).

Figure 84 – Spectra showing a peak corresponding to protonated form of clozapine at  $m/z$  327 is not found in a) control kidney tissue sample but is found in b) treated kidney tissue sample when a dry matrix application method is used.

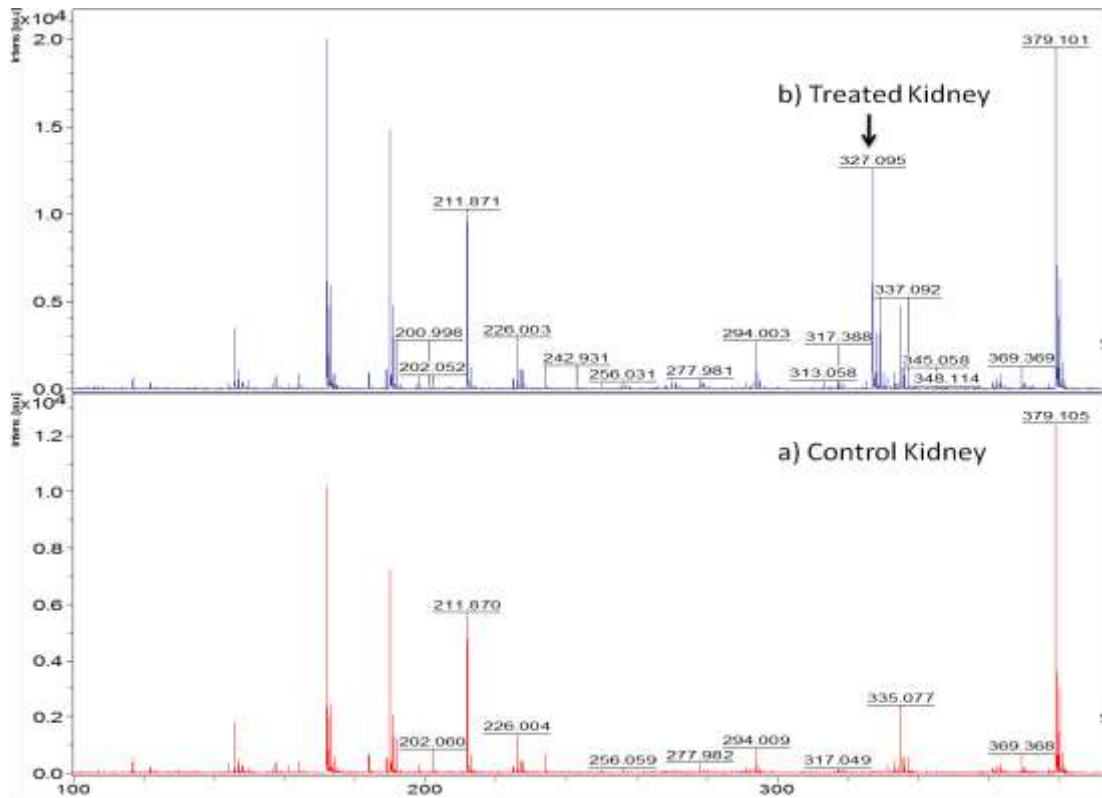
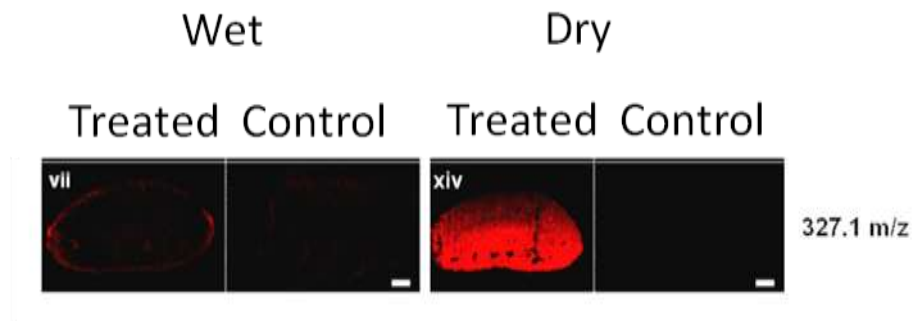


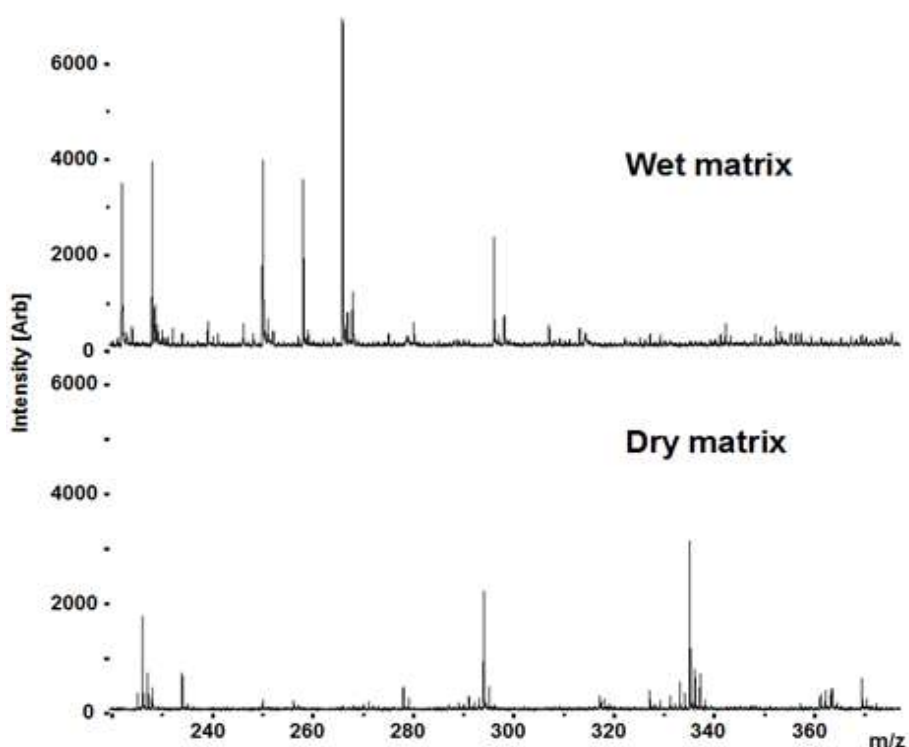
Figure 85 – Tissue images illustrating that clozapine can only be detected in treated kidney sections when a dry matrix coating is used.





Data from these experiments were compared and analysed. A number of ions could be detected using both the dry and wet matrix application methods and the overall intensities of ions were similar. However, limited signals were collected above  $m/z$  1000 suggesting the dry matrix coating is more suitable for small molecules which ionize more easily than, for example, peptides. Interestingly, the majority of ions detected were different or had different signal intensities (Figure 86).

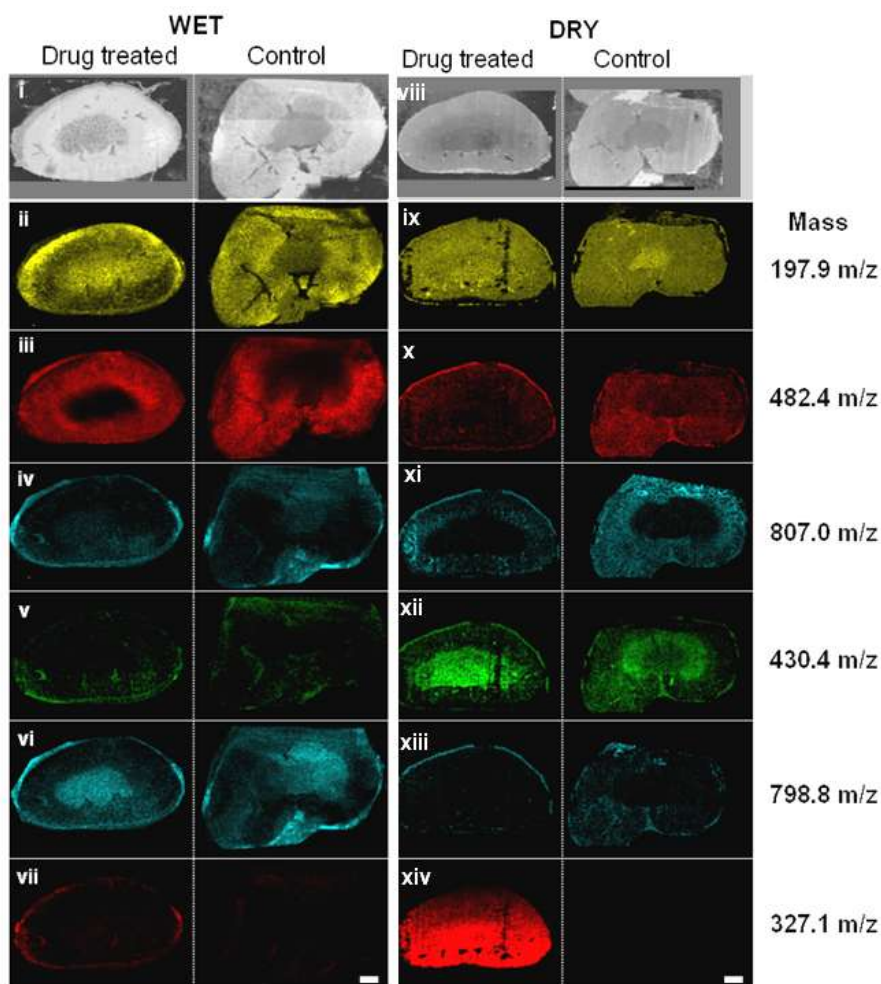
**Figure 86 - Comparison of spectra from MALDI-MSI analysis of treated rat kidney sections using dry or wet matrix application. It can be seen that there are many differences in the spectra when a wet or dry matrix coating is used.**



MALDI-MSI analysis of the distribution of ions with the same  $m/z$  values in samples coated with either dry or wet matrix coatings from clozapine treated and control

animals showed a range of behaviours. Some markers showed higher intensities in certain kidney regions using the dry matrix but in other regions using the wet matrix coating. For example the ion at  $m/z$  430.4 was observed predominantly in the renal medulla when a dry matrix coating was used but it was observed predominantly in the cortex when a wet matrix coating was applied (Figure 87). Conversely, the lipid at  $m/z$  798.8 was observed predominantly in the renal medulla when a wet matrix coating was used but was predominantly observed in the cortex when a dry matrix coating was used (Figure 87).

Figure 87 - Comparison of MALDI-MSI images observed of selected masses when either a wet matrix coating (left hand panel) or dry matrix coating (right hand panel) was used. I) and Viii) are optical images whilst other extracted images are labelled in right hand column. Note that the weak apparent observed signals in panels iv, v, x, and xiii are due to normalisation of the image to the highest intensity pixel and represent very low signal intensities. Panels vii and xiv show distribution of clozapine observed when dry and wet matrix coatings were used.



### **3.10.1.6. Imaging Clozapine in Rat Brain Tissue – Axima CFR TOF Mass Spectrometer**

As it was discovered that a dry matrix application method was suitable for mapping clozapine *in situ* in the liver and kidneys, this was also used to map the distribution of the drug in the brain. Experiments were firstly carried out using a MALDI TOF instrument. Analysis of sagittal sections using the conventional wet matrix application method did not enable the visualization of the parent drug, as was expected (Figure 90). Utilisation of the wet matrix coating did however enable endogenous molecules such as lipids to be detected (Figure 88 and Figure 90). When the same experiment was carried out using a dry matrix coating, it was possible to detect clozapine in spectra from treated rat brain section but not control (Figure 90). Additionally, the chlorinated isotopic peak could be seen clearly when a dry matrix coating was used (Figure 89) but not when a wet matrix coating was used (Figure 88). This illustrates that a dry matrix coating is suitable for imaging pharmaceuticals in brain tissue *in situ* as well as other samples such as kidney and liver.

**Figure 88 – Spectra illustrating that the parent ion corresponding to clozapine at  $m/z$  327 could not be detected in two rat brain sections (a) and (b) that were coated with wet CHCA matrix.**

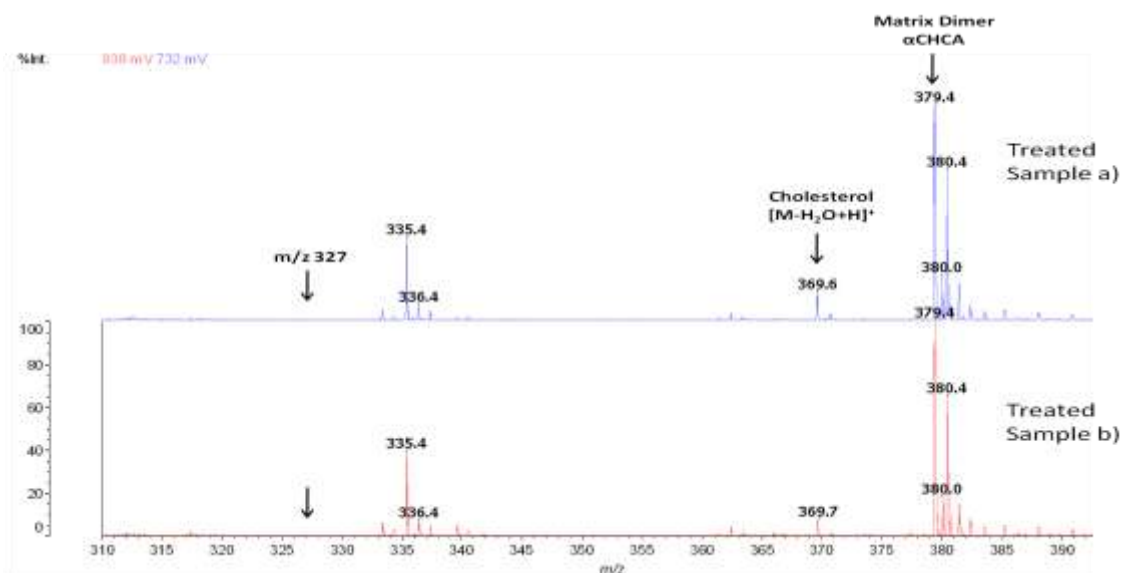


**Figure 89 – Spectra illustrating that the parent ion corresponding to clozapine at  $m/z$  327 and chlorine isotope ion at  $m/z$  329 were detected in two rat brain sections (a) and (b) that were coated with dry CHCA matrix coating.**

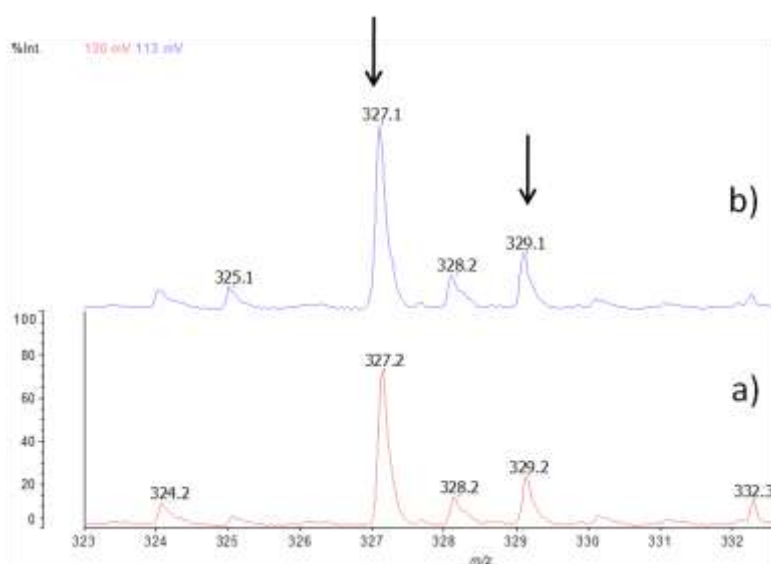
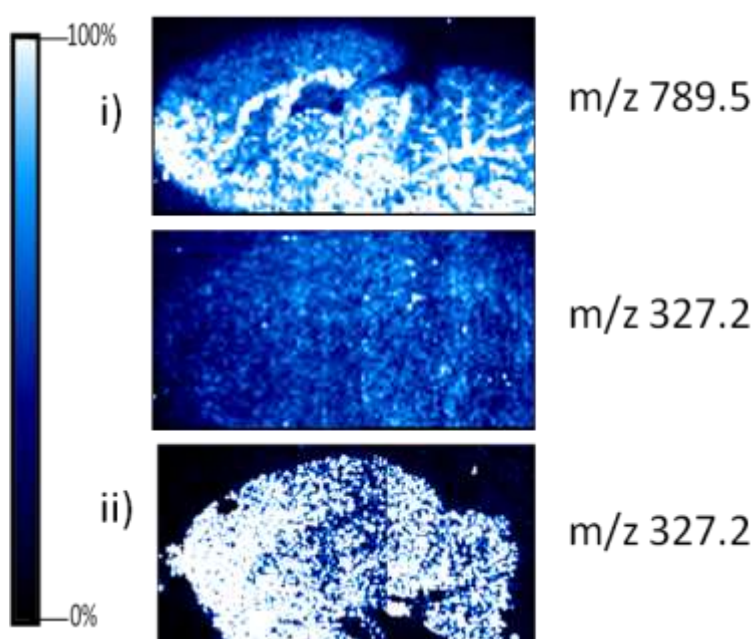


**Figure 90 - Tissue images of sagittal rat brain section showing the distribution of clozapine in sections taken from animal dosed with 50 mg/kg of the drug and sacrificed 30 minutes after drug administration. Panel i) shows results when a conventional wet matrix application method is used whilst panel ii) shows results when a dry matrix coating was used. Tissue images produced in BioMap, images normalised against matrix ion at  $m/z$  190. Image of lipid at  $m/z$  789.5 is also shown in i) to illustrate the outline of the tissue.**



### **3.10.1.7. Imaging Clozapine in Rat Brain Tissue – Bruker Ultraflex III Mass Spectrometer**

Imaging experiments were also conducted using the Bruker Ultraflex III mass spectrometer as it was hoped this could produce better images due to better instrument sensitivity and possibility of using a raster with smaller spacing. By using a dry matrix coating it was found that the distribution of clozapine in the rat brain could be mapped more clearly than with the Axima CFR mass spectrometer. Figure 91 illustrates that a peak corresponding to the protonated mass of clozapine could be observed in spectra from the treated rat brain sections but not in the control rat brain sections. This is confirmed in the corresponding tissue images shown in Figure 92.

**Figure 91 - Spectra showing mass range  $m/z$  310 to 340 from a) treated and b) control rat brain sections illustrating that a peak corresponding to the protonated mass of clozapine could be found in the treated sections only and this is confirmed from presence of the chlorine isotopic peak at  $m/z$  329 (see arrows).**

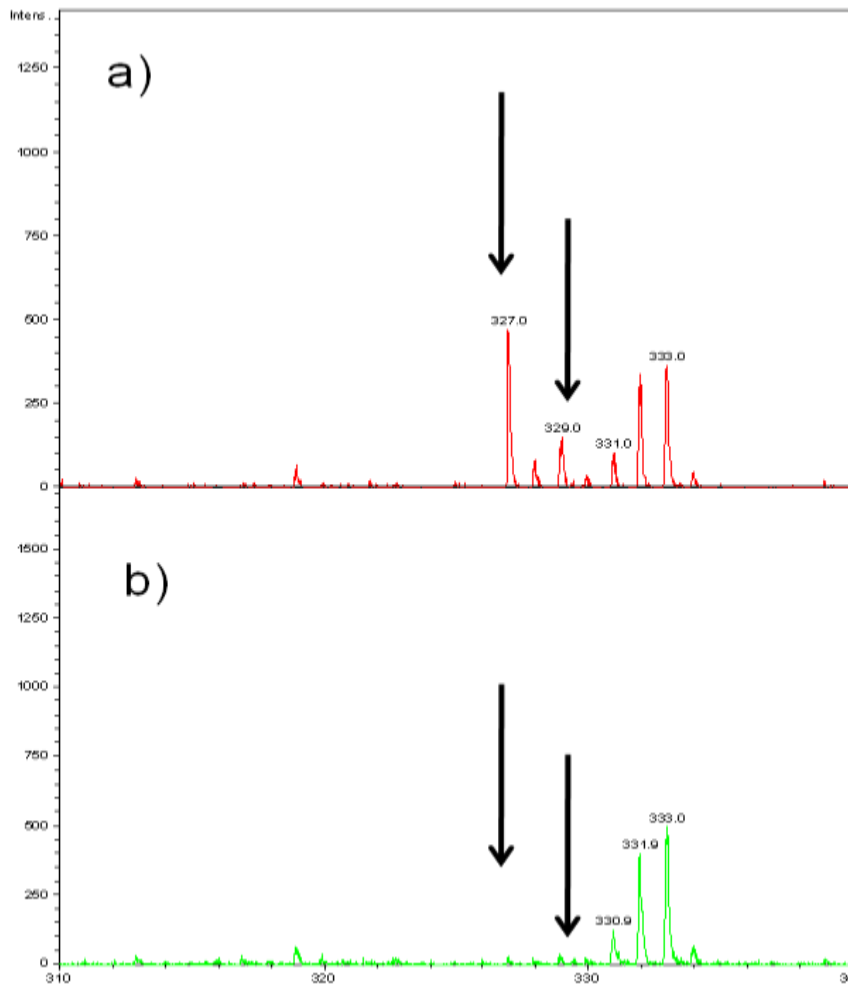
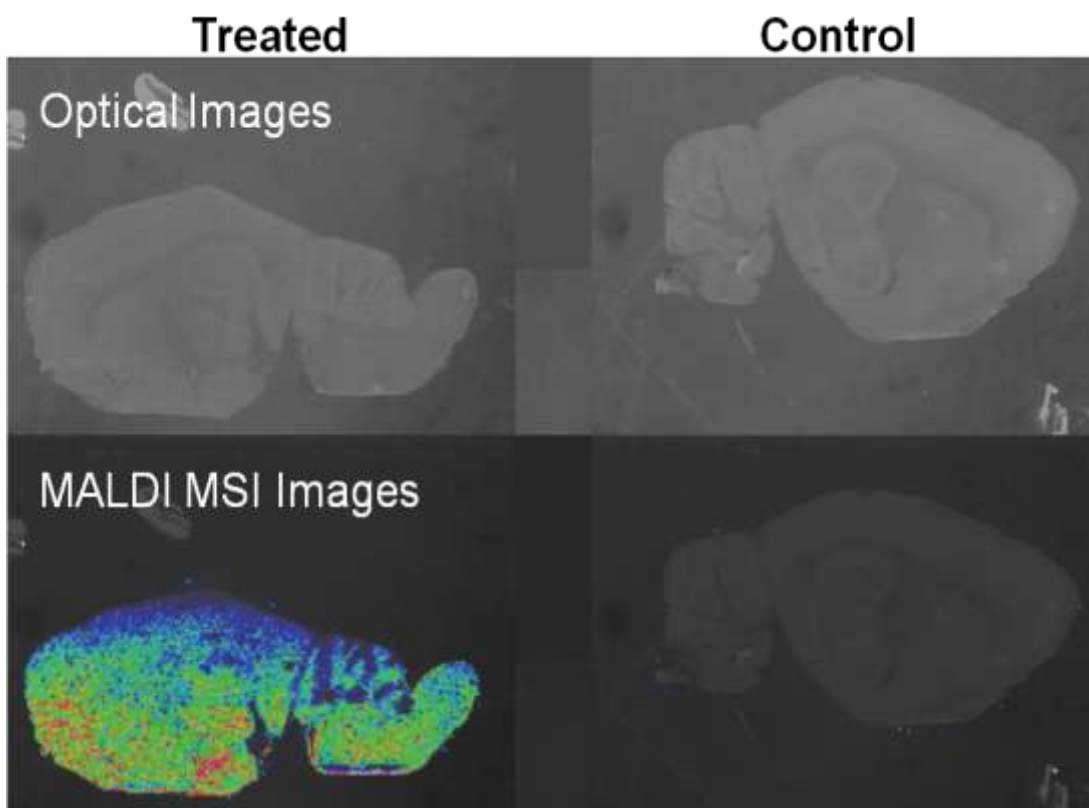




**Figure 92 – Corresponding tissue images showing the distribution of clozapine in rat brain when a dry matrix coating was used.**



From the MALDI-MSI images, it can be seen from the heat maps of  $m/z$  327 that clozapine is only found in rat brain samples taken from treated animals. By comparing the images with optical images, it can be seen that the drug is predominantly found in the cortex. This is in agreement with results of studies using DESI and NIMS, which showed that clozapine had highest intensities in these regions [173,187]. The distribution pattern differed from that observed in the study by Hsieh *et al* [193] as in their study, the drug was given intraventricularly into the brain. As the drug was given orally in our study as per the method of Wiseman *et al*

[173], the MALDI results were in agreement with their study as expected. This illustrates that the dry matrix application method can be used to profile the distribution of clozapine *in situ* without drug localisation occurring. This is illustrated by the fact that the distribution pattern of clozapine in this study agreed with the results obtained by DESI and NIMS which do not require the use of any matrices.

#### **3.10.1.8. Use of LC-MS Analysis for Quantification of Clozapine in Rat Brain Sections**

To further confirm that clozapine is found in these tissues, single tissue sections were collected from control and treated samples and worked up for LC-MS analysis. Extracted ion chromatograms (Figure 93), sample mass spectra (Figure 94) and fragmentation spectra (Figure 95) and (Figure 96) illustrate that clozapine is found in treated tissues only. MS/MS fragmentation was also carried out to further confirm this, which also confirmed the results of the MALDI MS/MS and PSD experiments. From the mass spectra, it can be seen that the Orbitrap can be used to assign the elemental composition of the parent drug and fragments with mass accuracy of less than 1 ppm.

Figure 93 - Extracted ion chromatograms from the analysis of metabolite extracts showing clozapine peaks observed in treated samples (panels b, d and f). It can also be seen that clozapine is not found in control tissues (panels a, c and e).

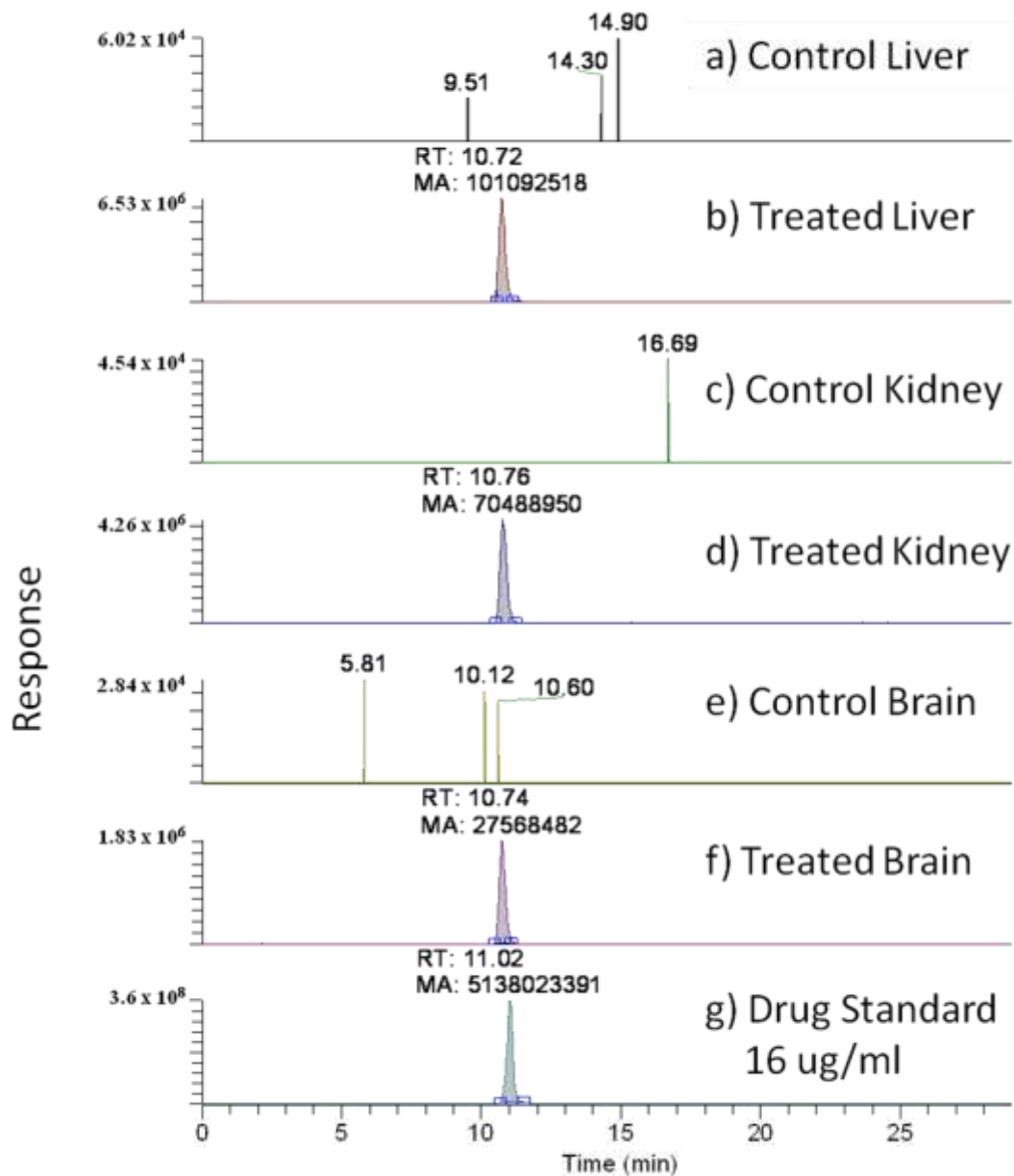


Figure 94 – Sample mass spectra from analysis of a) liver, b) kidney and c) brain samples illustrating that clozapine is found in these tissues as the parent ion can be observed at  $m/z$  327 and the Cl isotope at  $m/z$  329. Spectra obtained from analysis of a 16  $\mu\text{g/ml}$  standard is also shown for comparison in d).

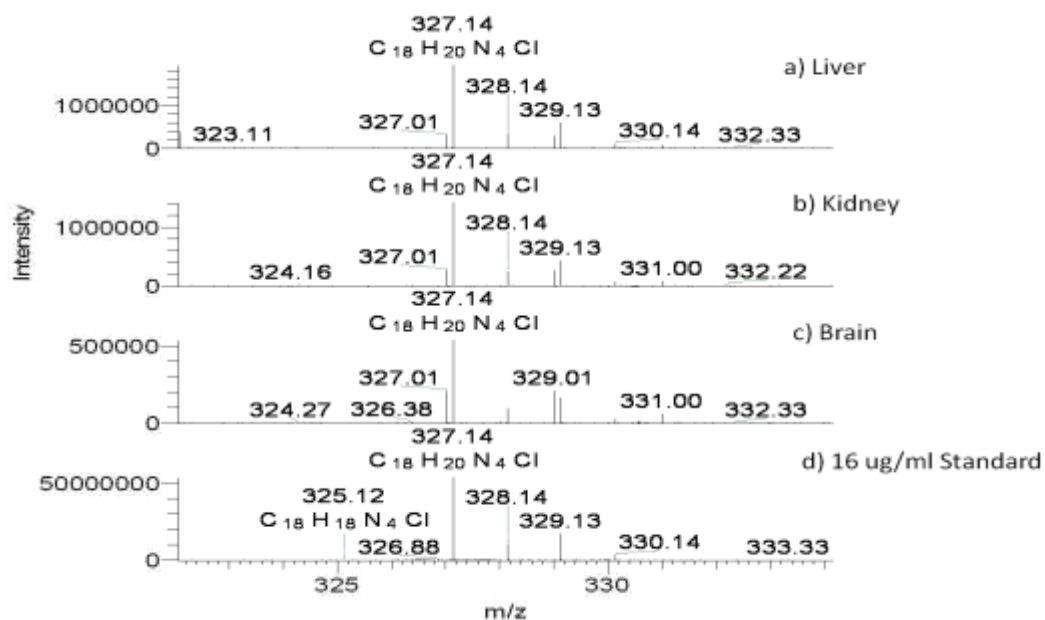
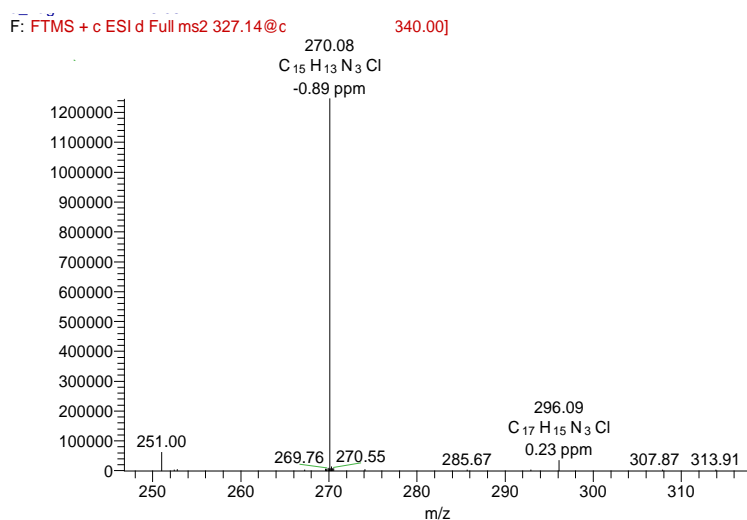
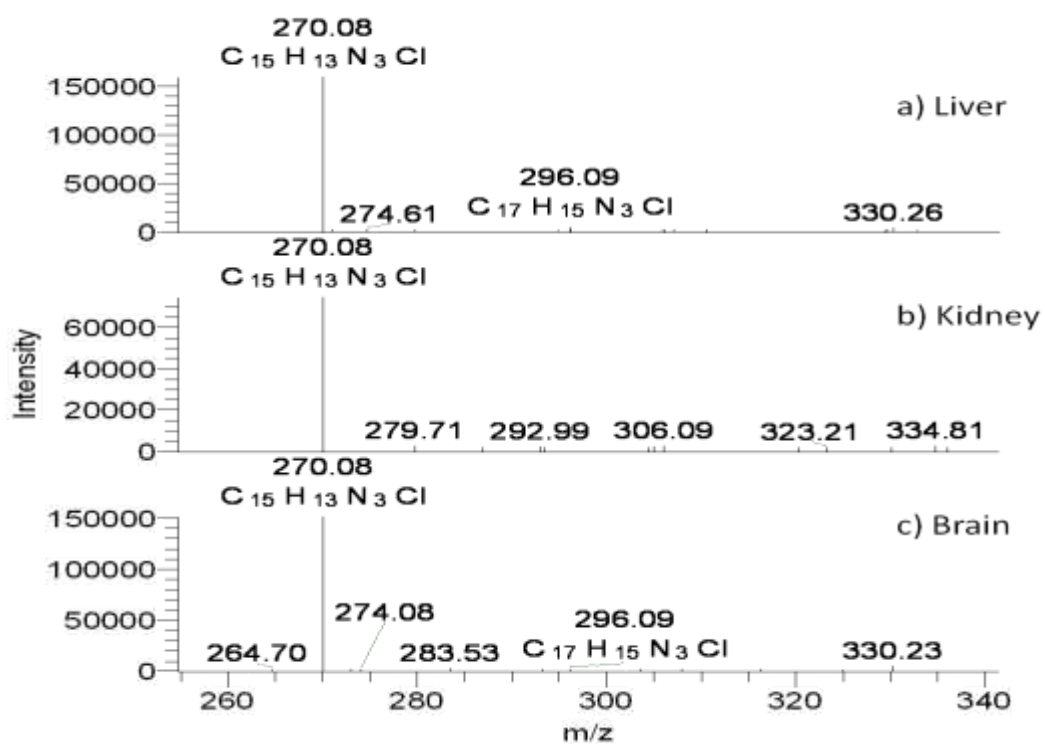


Figure 95 - Sample MS/MS spectrum from analysis of clozapine standard showing clozapine product ions.



**Figure 96 - Example MS/MS spectra showing clozapine product ions observed in treated liver, kidneys and brain.**



An external 7 point calibration curve was then used to calculate the relative and absolute concentrations of clozapine in individual tissues (Figure 97) and (Table 5).

**Figure 97 - Calibration curve plotting concentration of clozapine standards against peak area that was used to calculate concentration of clozapine in single rat brain, liver and kidney sections by LC-MS.**

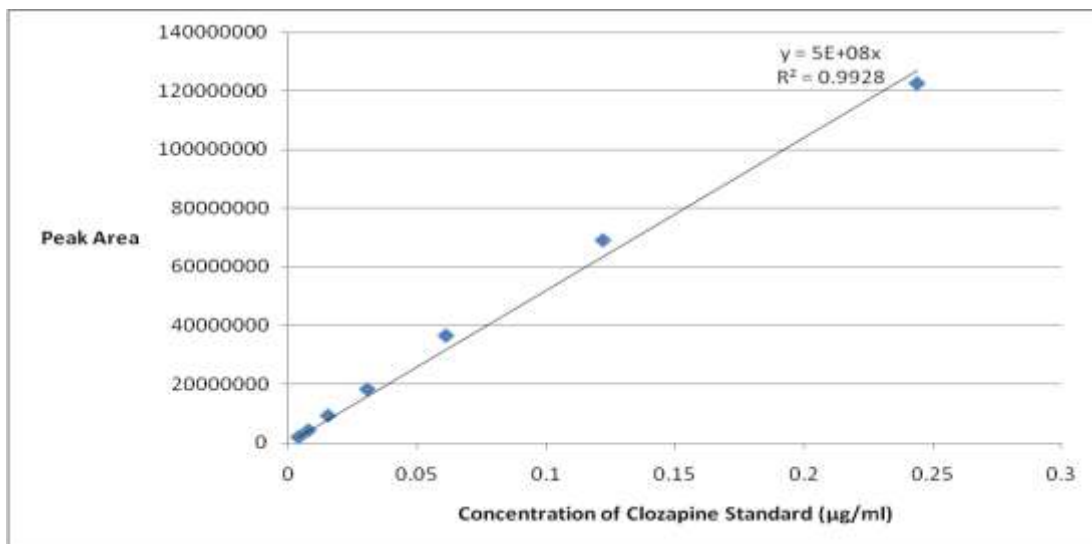


**Table 5 - Quantitation of clozapine in single brain, liver and kidney sections**

a) LC-MS	Tissue		
	Brain	Liver	Kidney
Measured Peak Area For the Drug	25674962 ± 2675256	81733734 ± 19525965	54590840 ± 15193928
Concentration of Clozapine in Sample (ng/ml)	9.9 ± 1.02	18.85 ± 4.50	12.6 ± 3.50
Concentration of Clozapine in Tissue (ng/mg)	4.93 ± 0.51	9.43 ± 2.3	7.54 ± 2.1

**Data is from  $n=3$  biological replicates.**

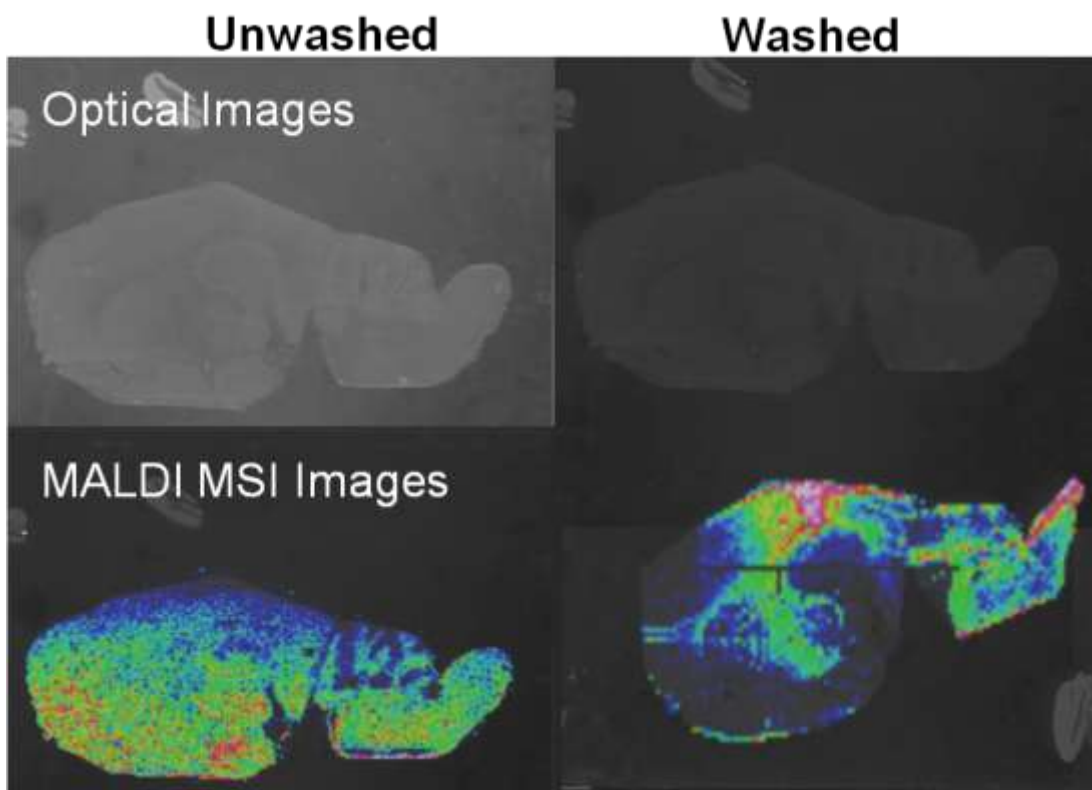
Results from analysis of single tissue sections suggest that the concentration of clozapine in the brain is approximately  $4.93 \pm 0.51$  ng/mg, in the liver is

approximately  $9.43 \pm 2.3$  ng/mg and in the kidney is approximately  $7.54 \pm 2.1$  ng/mg.

### 3.10.1.9. Profiling the Effects of a Washing Step on the Distribution of Clozapine in Rat Brain Tissue Sections using MALDI-MSI and LC-MS

Figure 98 shows the distribution pattern of clozapine following tissue washing. These images can be compared directly to those shown in Figure 92 and are shown again here to allow a direct comparison to be made.

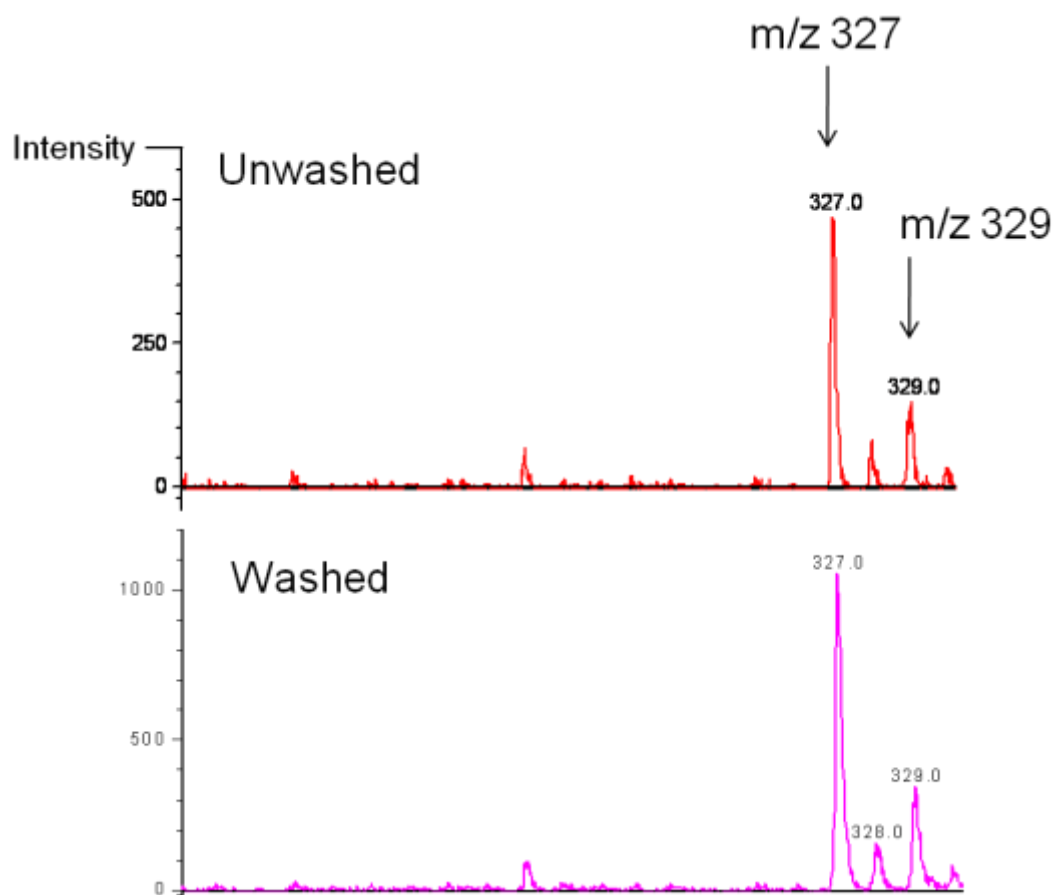
**Figure 98 - Distribution pattern of clozapine in unwashed and washed rat brain tissue sections from animals dosed orally with clozapine. It can be observed that the distribution pattern is altered dramatically when tissue is washed before MALDI-MSI analysis.**



It can be seen from Figure 98 that washing significantly affects the results of the MALDI imaging experiments. If the spectra obtained from analysis of washed and unwashed sections are compared (Figure 99) it can be seen that there is higher signal to noise observed when sections are washed before analysis. The intensity of the peak corresponding to protonated clozapine is twice as high in washed compared to unwashed. This could be due to removal of salts that would suppress MALDI signals when tissue was not washed. However, from the images it can be observed that the distribution pattern of the drug is completely changed (Figure 98). The alteration of the distribution pattern of the drug compared to the one observed in unwashed samples could be due to the way the tissue dried after washing. The clozapine could have moved if the surface was slightly uneven, accumulating in the particular areas shown in Figure 98. This suggests that washing steps should not be carried out before analysis of small molecules as it may alter the distribution pattern of the drug observed using MALDI-MSI.

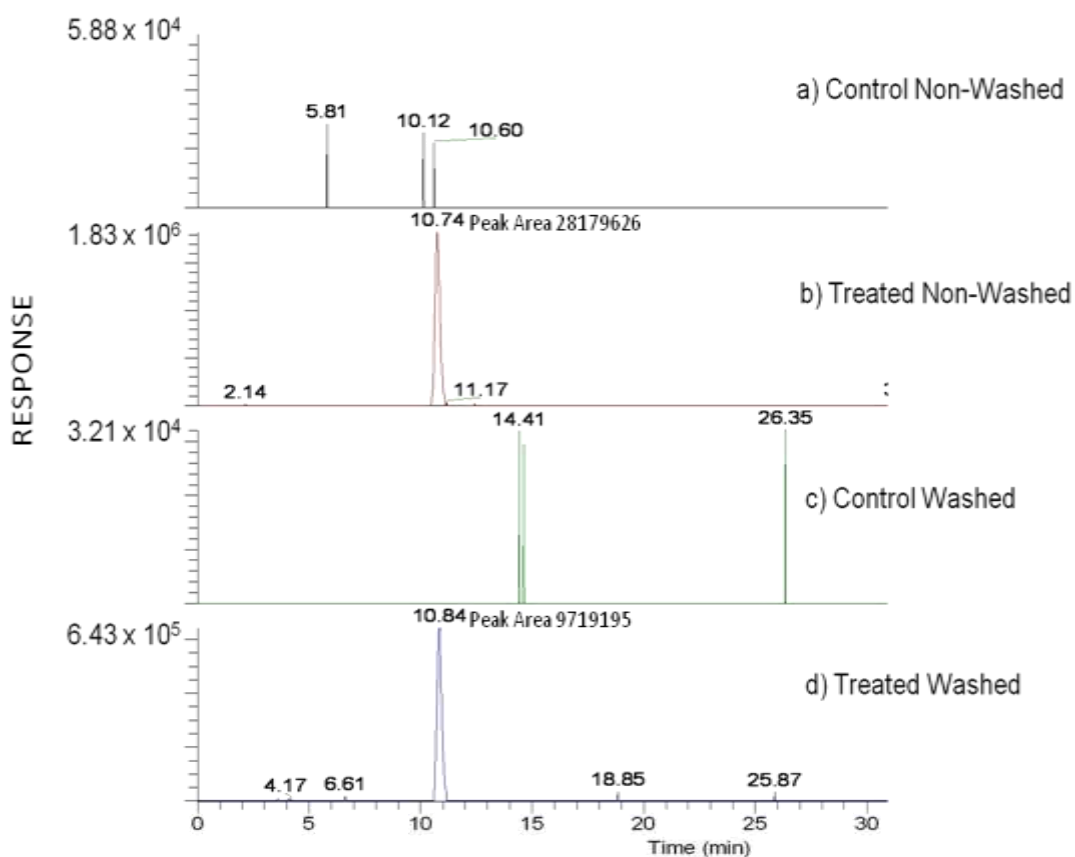


**Figure 99 - Spectra from unwashed and washed rat brain sections from animals dosed orally with clozapine.**



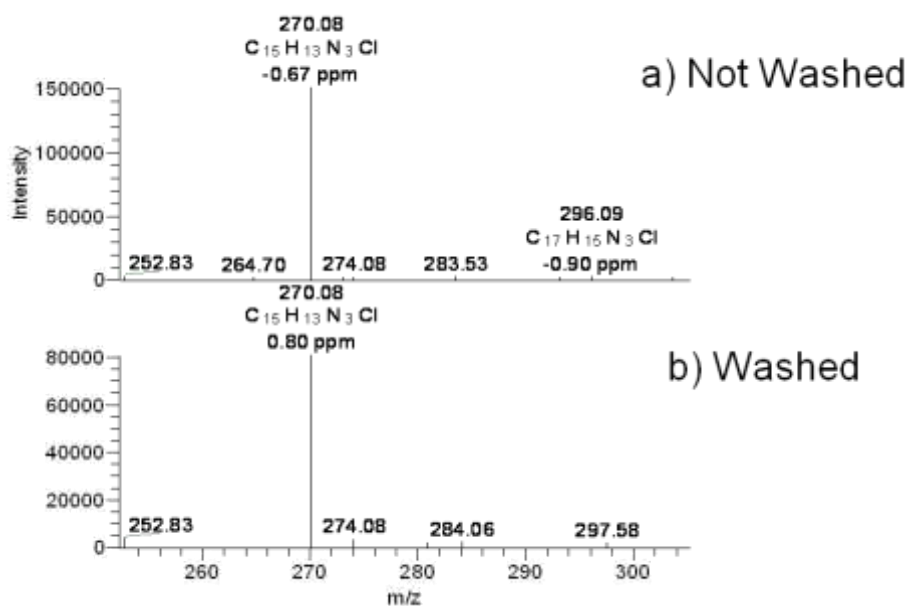
Non-washed and washed brain samples were then analysed utilising the LTQ-orbitrap. Example extracted ion chromatograms are shown which illustrates the peak corresponding to clozapine that was obtained from analysis of metabolite extracts obtained from washed and non-washed sections (Figure 100).

**Figure 100 – Extracted ion chromatograms and corresponding mass spectra illustrating peak intensity of clozapine observed from analysis of metabolite extracts obtained from a) non-washed and b) washed rat brain sections; c) and d) are from control animals and are from non washed and washed extracts, respectively.**



The peak intensities are shown and this shows that some clozapine must be washing off the tissue during the washing step. This would make sense since clozapine is soluble in the wash solution which contains ethanol and water. The presence of clozapine is confirmed through the accurate mass of orbitrap instrument which allows elemental composition to be deduced, presence of isotopic pattern and through the MS/MS spectra shown below (Figure 101).

**Figure 101 –MS/MS spectra from analysis of a) non washed and b) washed rat brain sections confirming the presence of clozapine in brain.**



Quantitation of clozapine in the washed and unwashed tissue sections revealed that the concentration of clozapine in washed brain sections had decreased by approximately 80% (Table 6). This work illustrates the importance of careful selection of your matrix application method before starting a project, particularly if the compounds of interest are pharmaceuticals which are soluble in the solvents contained within the matrix solution.

**Table 6 - Effects of carrying out washing steps on the concentration of clozapine in rat brain tissue.**

	<b>Non Washed Brain Sections</b>	<b>Washed Brain Sections</b>
<b>Measured Peak Area For the Drug</b>	25674962 ± 2675256	5599915.25 ± 3128491
<b>Concentration of Clozapine in Sample (ng/ml)</b>	9.9 ± 1.02	2.15 ± 1.20
<b>Concentration of Clozapine in Tissue (ng/mg)</b>	4.93 ± 0.51	1.08 ± 0.60

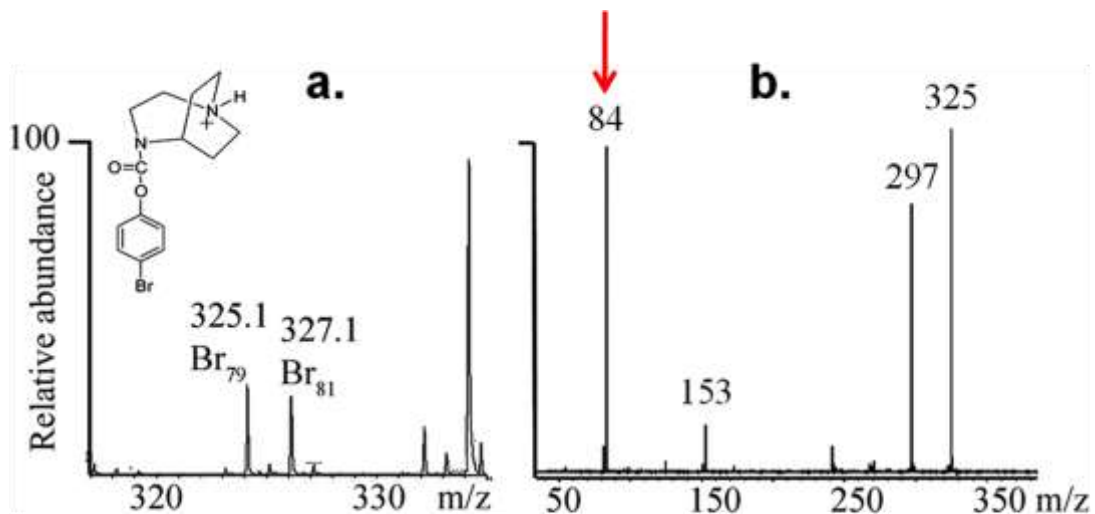
Data is from  $n=3$  biological replicates.

### 3.10.2. SSR180711 Study

#### 3.10.2.1. MALDI-MSI Results

From analysis of the parent ion spectra of the standard drug compound it can be seen that two molecular ions are observed at  $m/z$  325.1 and  $m/z$  327.1, separated by 2 Da (Figure 102). This is due to the composition of the drug which contains a Br atom, with the isotopic distribution of bromine being approximately 1:1  $^{79}\text{Br}$ : $^{81}\text{Br}$ . From analysis of the standard in MS/MS mode, it can be seen that the main peaks are observed at  $m/z$  297 (loss of  $\text{CHCH}_2$  from the bicyclic ring system), 153 (fragmentation of the carbamate) and 84, (probably a tetrahydropyridinium ion fragment from the bicyclic ring system) (Figure 103).

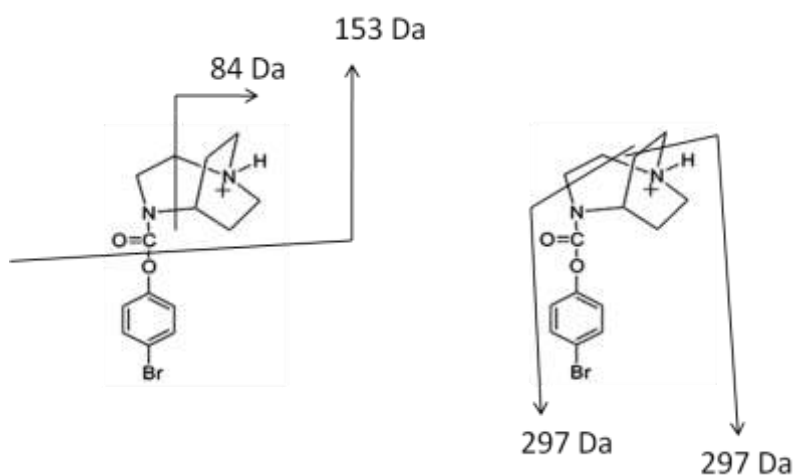
**Figure 102 – Spectra Obtained From the Analysis of SSR180711 Standard using MALDI MS Profiling a) in Full Scan Mode and b) Showing MS/MS Spectrum of Drug Standard with main product ion at  $m/z$  84 (red arrow).**



a) MS of Drug standard spotted onto MALDI target.

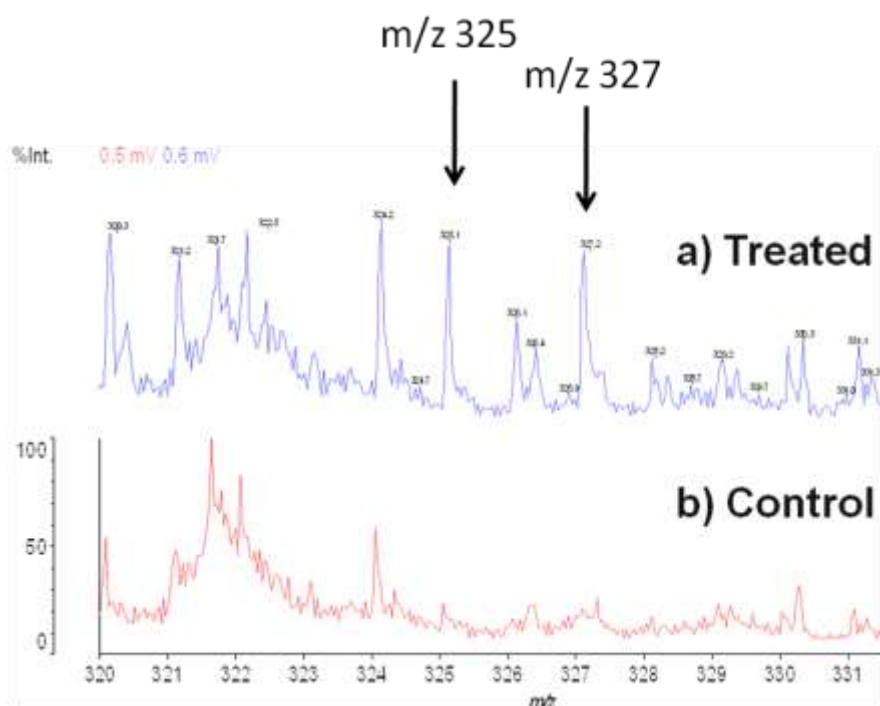
b) MALDI MS/MS spectrum of drug standard.

**Figure 103 - Proposed Dissociation Pathways of SSR180711**



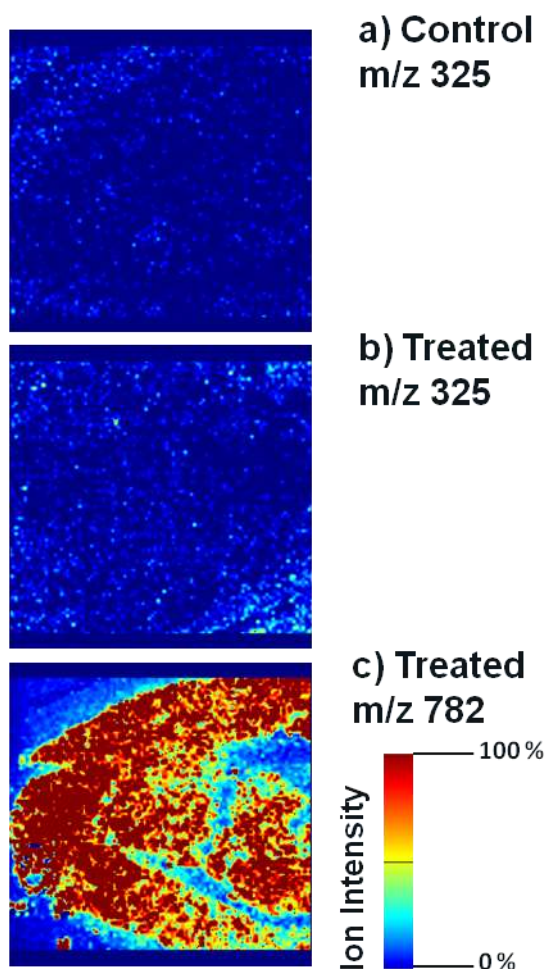
Initially, full scan experiments were conducted on the Axima CFR TOF mass spectrometer. Sagittal and coronal sections were coated with CHCA applied using either the dry or wet matrix methods were analysed using MALDI-MSI. Figure 104 shows the spectra obtained when a conventional wet matrix application method was used to map the parent drug using MALDI-MSI. It can be seen that the parent ions at  $m/z$  325 and  $m/z$  327 had low intensities of  $< 1$  mV, similar to other ions that were detected in this mass range with poor signal to noise ratios.

**Figure 104 – Spectrum observed from analysis of drug in rat brain sections when a wet matrix coating was used.**



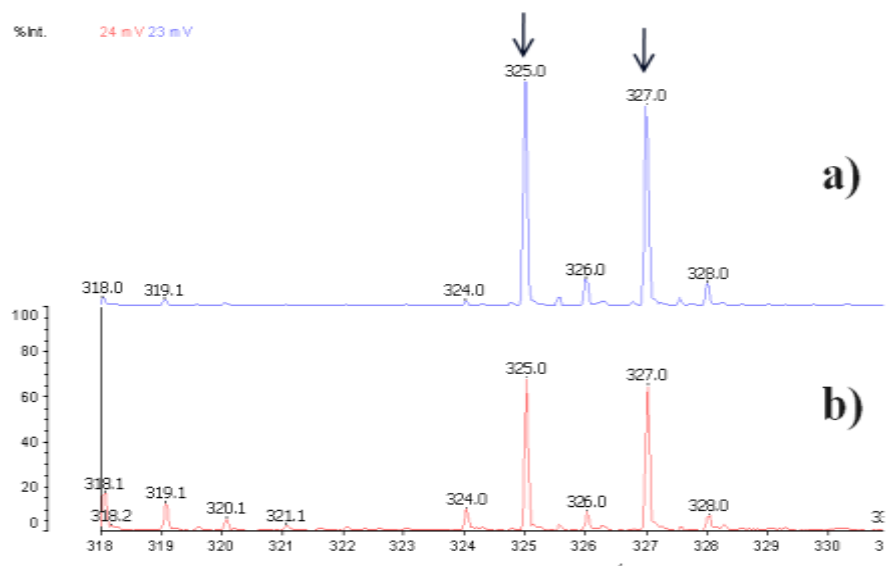
Corresponding heat maps (Figure 105) illustrate that it was not possible to map the distribution of the drug when a wet matrix coating was used. Panel c) shows however the suitability of this matrix application method for the mapping of lipids e.g.  $m/z$  782.

**Figure 105 – Heat maps of  $m/z$  325 in a) control and b) treated rat brain samples illustrating the distribution of the drug in rat brain sections when a wet matrix coating was utilised. Panel c) shows the distribution pattern of a lipid at  $m/z$  782 to show the tissue outline.**



For experiments investigating the use of a dry matrix coating, initially full scan experiments were conducted using the Axima CFR TOF mass spectrometer and it was found that a dry matrix coating enabled both peaks corresponding to the parent drug to be detected with good signal to noise (Figure 106).

**Figure 106 - Spectra illustrating that the SSR180711 parent ion at  $m/z$  325 and the bromine isotope at  $m/z$  327 can be detected in rat brain sections when a dry matrix coating of CHCA is applied onto surface of tissue prior to MALDI-MSI analysis; a) and b) are spectra taken from separate rat brain sections.**



The corresponding heat maps of the parent drug at  $m/z$  325 illustrate that it was possible to map the distribution of the drug using the dry matrix coating (Figure 107). The heat maps illustrated that there was a high intensity of the drug found in the white matter of the cerebellum (Figure 107) so, coronal sections were also analysed and heat maps revealed that there was a high intensity of the drug found in the white matter regions of the cerebellum (Figure 108).



**Figure 107 – Corresponding tissue images illustrating the distribution pattern of SSR180711 in sagittal rat brain section.**

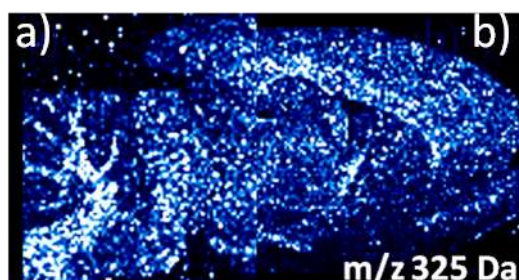
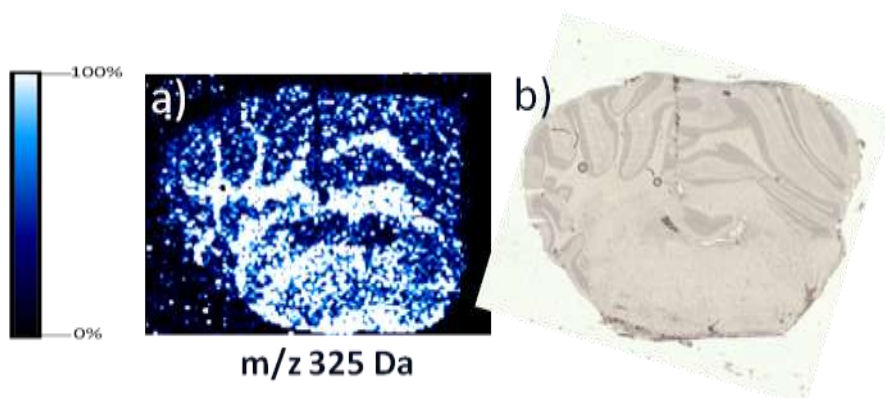


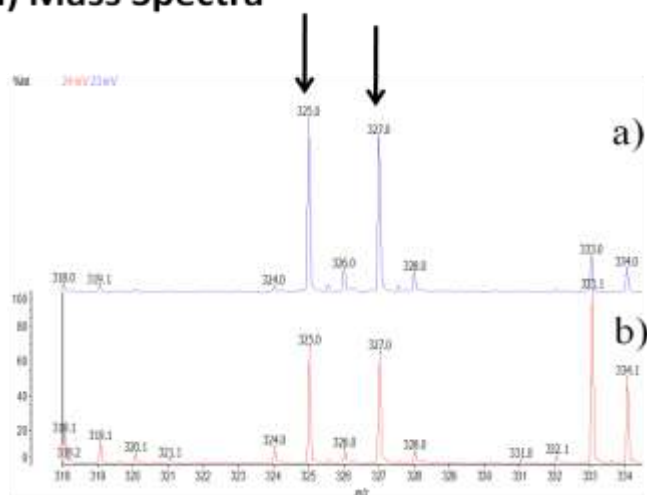
**Figure 108 – Tissue image illustrating the distribution pattern of SSR180711 in coronal section taken through cerebellum a) MALDI-MSI image and b) corresponding optical image.**



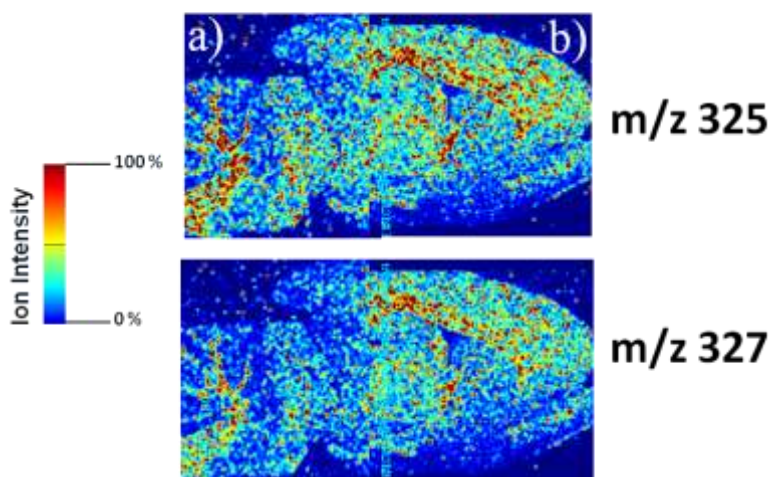
Additional experiments were conducted to confirm that this distribution pattern and the results reflected those of initial experiments with spectra showing the presence of parent drug ions at  $m/z$  325 and  $m/z$  327 and their corresponding heat maps illustrating that there was a high concentration of drug found in the white matter regions, particularly in the cerebellum (Figure 109). The presence of the ion at  $m/z$  327 in the same regions as the parent ion  $m/z$  325 further confirmed that this was the Br-isotope of  $m/z$  325 (Figure 109).

**Figure 109 - Spectra and additional heat maps illustrating the presence of drug at  $m/z$  325 and confirmation through mapping the isotope at  $m/z$  327; i) shows mass spectra from two tissue samples (a) and (b) and ii) shows the corresponding heat maps of  $m/z$  325 and  $m/z$  327.**

**i) Mass Spectra**



**ii) Corresponding Tissue Images**

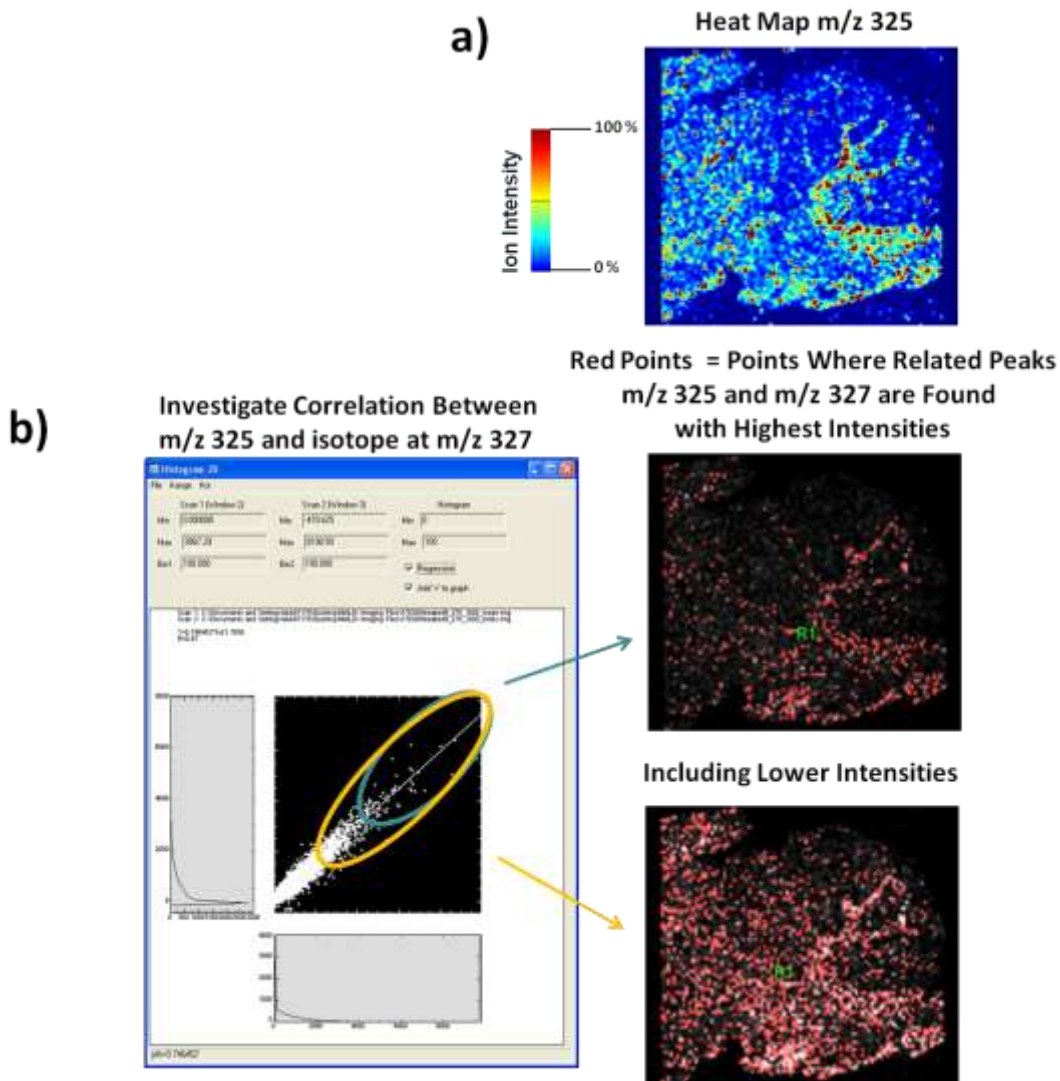


Tools in BioMap were also utilised to confirm the distribution pattern of the drug observed in full scan mode. By using the histogram 2D tool, the user can investigate

the correlation between two masses. For example, this can be used to investigate the correlation between two heat maps e.g. isotopes or parent drug and drug fragments.

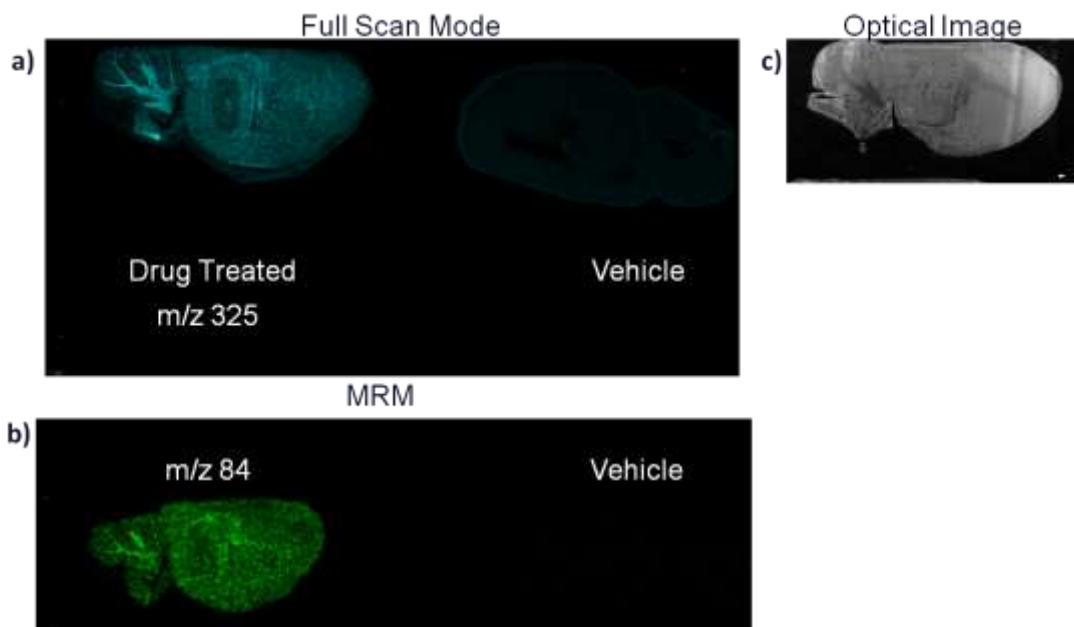
This was utilised to investigate the correlation between  $m/z$  325 and  $m/z$  327 to check that the images were in fact similar and belonged to related compounds. The red points of the 2D histogram plots represented areas on tissue where two related ions are both found, in this case corresponding to the parent drug at  $m/z$  325 and  $m/z$  327 (Figure 110). The user can select areas where the intensities of both are high which should give a histogram 2D plot map similar to the heat maps generated for  $m/z$  325 and  $m/z$  327, confirming there is a correlation between these two ions (Figure 110).

Figure 110 - Utilisation of tools in BioMap for investigating the localisation of SSR180711 in rat brain cerebellum; a) shows a heat map of parent drug ion at  $m/z$  325, b) histogram 2D plot created to investigate the relationship between parent ion  $m/z$  325 and ion at  $m/z$  327 and c) points on raster where  $m/z$  325 and  $m/z$  327 were both found with high intensities.



Confirmation that the peak observed at  $m/z$  325 was in fact the drug was made by utilising SRM and pseudo-MRM experiments to map the distribution of the drug in tissue taken from dosed animals (Figure 111 and Figure 112). A pseudo MRM transition imaging approach was performed utilizing the information obtained from MS/MS analysis of the drug standard. A combined image of all three transitions was also generated which combined images taken from all three transitions  $325 \rightarrow 84$ , 153 and 297 by overlaying the three images generated from SRM experiments using multiple mass filters in FlexImaging (Figure 112). SRM was also utilized to monitor the transition of  $325 \rightarrow 84$ . However, there was a loss of sensitivity in the MRM and SRM experiments due to the use of the LIFT mode, meaning that the resolution at which the MRM image was collected was lower than that utilised in full scan MS mode, thus allowing more time for summing of more spectra from firing of more laser shots at each raster position. It was not possible to detect the parent ions or fragment ions in control tissue sections. A 2D gel view is also shown in Figure 112 which compares the summed spectra from the drug dosed and vehicle dosed control brain sections. The product ions obtained from analysis of the drug standard and which were used to produce the pseudo-MRM image in panel g) of Figure 112 were clearly detected in the treated animals but not the control animals. Additionally, a peak was observed at  $m/z$  299 in MS/MS mode in treated animals, which indicated the product ion at  $m/z$  299 contained the Br atom. A similar distribution pattern was observed in MRM and SRM modes as was obtained in full scan mode, with high intensities found in the white matter of the cerebellum and the hippocampus (Figure 111 and Figure 112). Thus, this confirmed that this was the distribution pattern of the drug observed when a dry matrix coating was utilised.

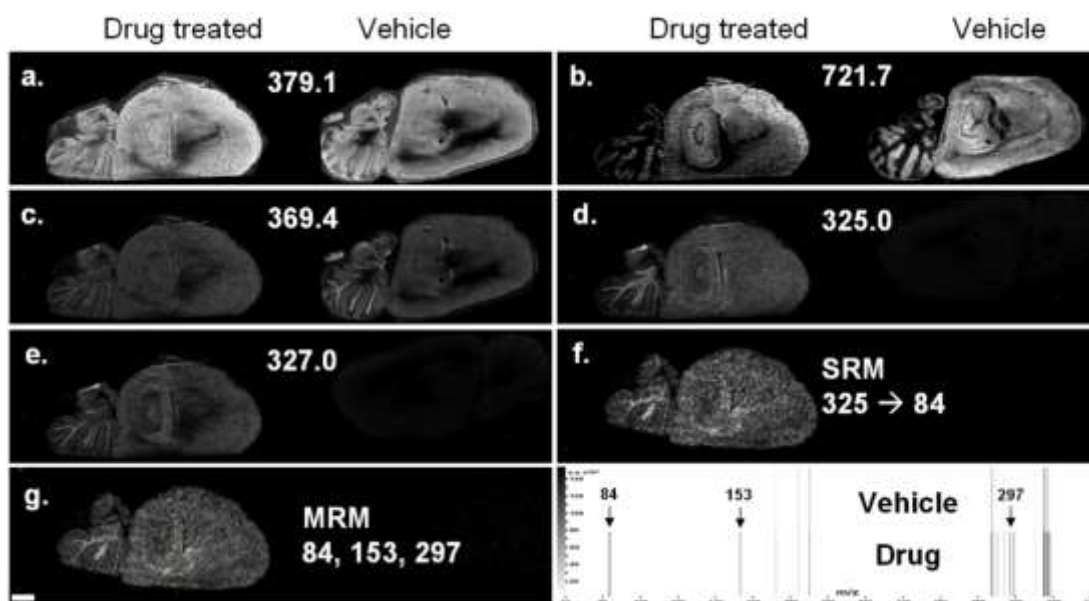
**Figure 111 – Results of MALDI MS imaging experiments performed on Bruker Ultraflex III Instrument showing distribution pattern of drug observed in a) full scan and b) MRM modes. An optical image is also shown for illustration (c).**



*H. J. A. Groothuis, F. De Waal, L. Hooghiemstra, P. G. Vliegenhart, A. R. P. M. van Halbeek, H. J. A. Groothuis, F. De Waal, L. Hooghiemstra, P. G. Vliegenhart, A. R. P. M. van Halbeek, H. J. A. Groothuis, F. De Waal, L. Hooghiemstra, P. G. Vliegenhart, A. R. P. M. van Halbeek*

The use of a dry matrix was also suitable for the detection of a wide variety of markers in defined brain regions and structures (Figure 112). It is shown that the dry matrix could be used for the detection of lipids and cholesterol which showed region specific dispersal. For example, cholesterol was found predominantly in the white matter which was the same results obtained as when a wet matrix coating was used (chapter 2) illustrating that the dry matrix application had no bias to a particular cell type or density (Figure 112).

**Figure 112 – Additional MALDI-MSI images taken using dry matrix application obtained using a 100  $\mu\text{m}$  laser raster with a medium diameter laser showing: a) matrix dimer  $[2\text{M}+\text{H}]^+$ , b) a lipid component, c) cholesterol  $[\text{M}+\text{H}-\text{H}_2\text{O}]^+$ , d) drug  $[\text{M}+\text{H}]^+$ , e) drug  $\text{Br}^{81}$  isotope peak  $[\text{M}+\text{H}]^+$ , f) image using drug SRM transition  $m/z\ 325 \rightarrow m/z\ 84$ , g) combined overlaid images of the  $m/z\ 325 \rightarrow m/z\ 84$ , 153 and 297 transitions. h) Gel view of summed spectra from MS/MS imaging of drug dosed and vehicle control brain sections. (Scale bar = 2 mm).**



By comparing the relative intensities of the signals for the drug in spectra from grey and white matter and normalizing them to an adjacent matrix dimer peak which shows a relatively even intensity distribution across the tissue, there appears to be approximately a 2-fold increase in signal intensity of the drug in the white matter compared to the grey matter (Figure 113 and Table 7 and Table 8).

However as the quantitative nature of MALDI is often questioned, due to factors including ionization efficiency, interferences from signals from other small molecule

compounds, ion suppression etc the signal intensities were checked in ms/ms mode and they were found again to be two fold higher in the white matter regions. Additionally, to validate the observed MSI distributions, LMD and LC-MS were utilized.

**Figure 113 - Results of MALDI-MSI on tissue showing profiles from white and grey matter of cerebellum.**

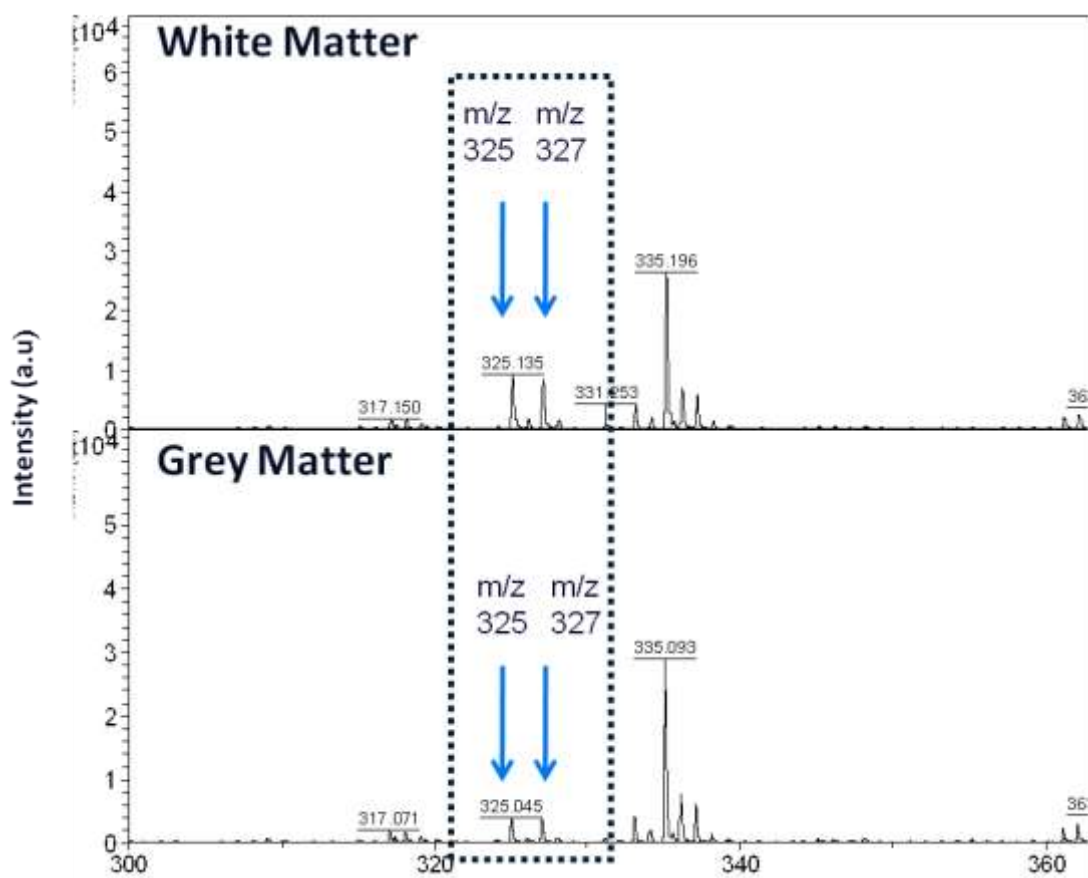




**Table 7 – Signal intensities of parent drug ions  $m/z$  325 and  $m/z$  327 in the grey matter of the cerebellum, taken from sample spectrum.**

Grey Matter					
$m/z$	SN	Quality Fac.	Res.	Intens.	Area
325.045	30.6	16456	1585	3849.41	1090
327.049	29	16049	1538	3644.75	1049

**Table 8 - Signal intensities of parent drug ions  $m/z$  325 and  $m/z$  327 in the white matter of the cerebellum, taken from sample spectrum.**

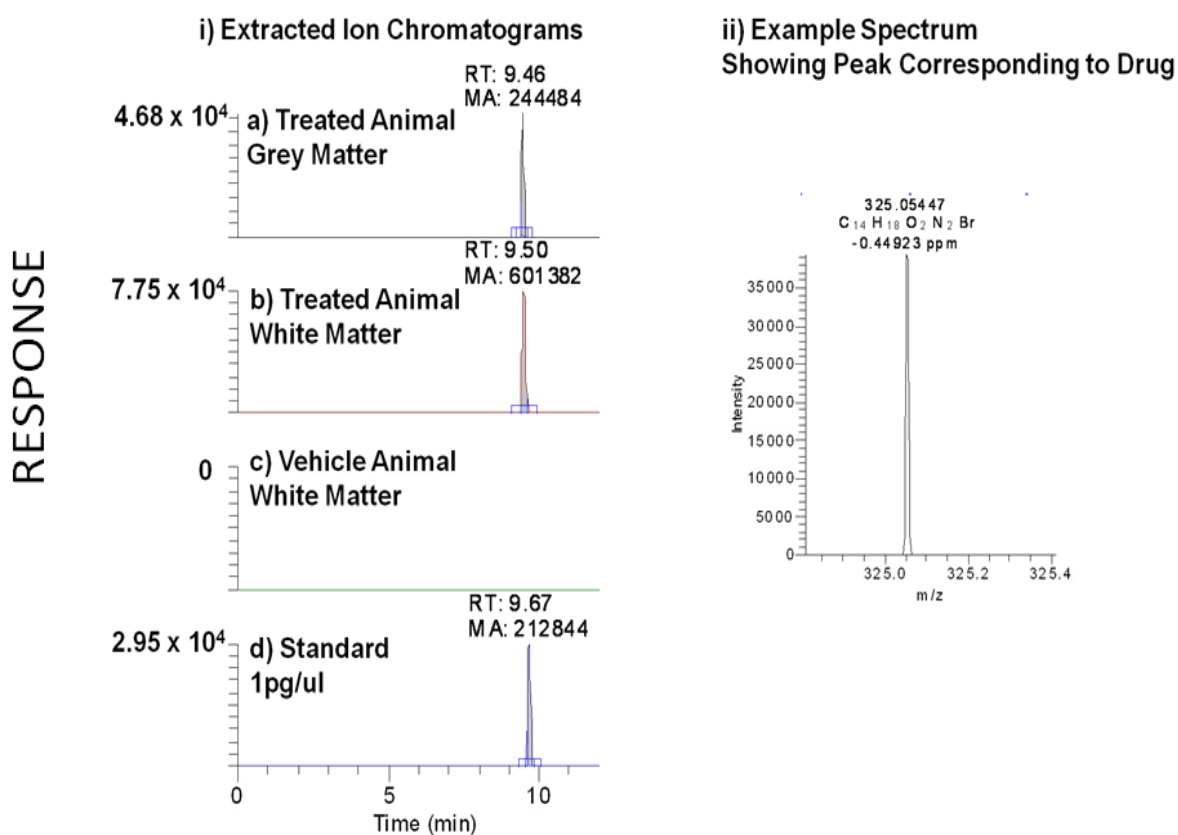
White Matter					
$m/z$	SN	Quality Fac.	Res.	Intens.	Area
325.135	71.1	23072	1410	8779.4	2672
327.135	66.2	21319	1357	8156.02	2591

### 3.10.2.2. SSR180711 Study – Results of Relative Quantitation

With the quantitative nature of MALDI-MSI often questioned due to the nature of the tissue, the matrix and its application, further experiments were carried out to confirm the differential distribution of the drug observed using MALDI-MSI. This involved utilising LMD to dissect out specific regions of interest and carry out LC-MS analysis of the extracted tissue regions to quantify the relative and absolute concentration of the drug in these tissue regions. Two regions of interest were selected; the grey and white matter of the cerebellum and treated tissue from these regions was collected from 3 biological replicates. Control tissue was also collected

for comparison. Absolute quantification was carried out using an external calibration curve of drug standards. The use of the Orbitrap enabled the presence of the drug to be confirmed by assigning the elemental composition with a deviation from exact mass of less than 1 ppm achieved for all samples. Figure 114 illustrates extracted ion chromatograms for the drug from grey matter and white matter of the cerebellum, as well as from white matter of the vehicle treated animal. The extracted ion chromatogram from a 1 pg/ $\mu$ l drug standard is also shown for comparison (Figure 114). An example spectrum is also shown which shows the drug peak from treated white matter sample.

**Figure 114 – Example Extracted Ion Chromatograms and an Example Spectrum Illustrating Presence of SSR180711 in White and Grey Matter of Cerebellum.**



Approximately a 2-fold difference in analyte peak area was determined between the grey and white matter of the cerebellum (Table 9). The total concentration of drug in the LMD extracts was approximately 1 ng/ml in the grey matter and 2.5 ng/ml in the white matter. To calculate the absolute concentrations of drug in samples the sample weights were calculated as follows:

Following cutting using the laser microdissection equipment, the computer would record the area of tissue that had been cut by the laser. The total areas of grey and white matter cut using the laser microdissection equipment were then summed at the end of cutting. The volume was then calculated as **volume ( $\mu\text{m}^3$ ) = area ( $\mu\text{m}^2$ ) x thickness of tissue (14  $\mu\text{m}$  thick sections)**. The weight of the tissue was then calculated as **weight (mg) = density x volume ( $\mu\text{m}^3$ )** using a predicted density of 1.04 g/ml. Thus, drug concentrations in these regions were calculated as approximately 4.1 ng/mg in the grey matter and 8.5 ng/mg in the white matter, which suggests that the concentration of drug in the white matter is 2 fold higher than that in grey matter, reflecting results obtained by MALDI-MSI (Table 9).

**Table 9 - Calculation of Drug Concentrations in the Grey and White Matter Regions of the Cerebellum Collected Using Laser Micro Dissection**

Sample Group	Region of Cerebellum	Tissue Area ( $\mu\text{m}^2$ )	Approximate Weight (mg)	Measured Peak Area for Drug (XIC)	Absolute Concentration (ng/mg)	Drug Conc. in Sample (ng/ml)
Drug Treated	Grey Matter	27844477 $\pm$ 3348969	0.31 $\pm$ 0.07	256364 $\pm$ 67761	4.1 $\pm$ 0.98	1.19 $\pm$ 0.31
	White Matter	26974217 $\pm$ 3412591	0.28 $\pm$ 0.04	512571 $\pm$ 123842	8.5 $\pm$ 1.87	2.38 $\pm$ 0.58
Vehicle Control	Grey Matter	26878487	0.28	0	0	0
	White Matter	31870570	0.33	0	0	0

**Data is from  $n=3$  biological replicates and single vehicle control animal.**

### **3.10.2.3. Biomarker Identification From Analysis of Laser Microdissected Tissue.**

The files created following analysis of the laser microdissected tissue samples were also analysed using the differential expression software package SIEVE to investigate if any metabolomic changes were occurring in the white matter (where the drug was found to accumulate). The table below illustrates that there were

several metabolites that were found to be altered following drug treatment. Metabolites with increased levels include acetylcarnitine, adenosine and glutamate. These changes could be explained as follows; stimulation of  $\alpha 7$  nicotinic acetylcholine receptors promotes glutamate release [288] whilst increased levels of adenosine and acetylcarnitine suggest neuroprotective effects. This illustrates that metabolomics can aid identification of changes in levels of endogenous compounds following mass spectrometric analysis of tissue from selected rat brain regions. It is difficult to predict why these specific changes are being observed as this is a test compound and there is little published about its pharmacological effects.

**Table 10 - Differences in Relative Levels of Compounds in White Matter of Cerebellum in Response to Drug Treatment.**

Formula	Compounds	Pathway	Pathway code	MZ	Time	P-Value	Ratio
$C_9H_{17}NO_4$	O-Acetylcarnitine	Ala/Asp	15	204.1231	12.349	5.59E-04	4.321
$C_{10}H_{13}N_5O_4$	Adenosine	Purine	2	268.1041	11.685	2.41E-02	3.651
$C_8H_9NO_4$	2-Aminomuconate	Trp	8	158.0448	7.349	8.34E-05	2.15
$C_5H_9NO_4$	L-Glutamate	Glu_His_Arg/Pro_Urea_GSH Porphy_Butan_Cnamin	10_19	148.0604	15.234	4.56E-03	1.803
$C_4H_9N_3O_2$	Creatine	Arg/Pro_Ser/Gly/Thr	6_11	132.0767	15.156	8.03E-04	1.546
$C_5H_{17}N_3O_3$	Glutamine	Glu_Purine_Pyrimidine	1_2_9	147.0764	16.051	1.58E-03	1.529
$C_6H_{13}NO_2$	L-Leucine	Leu/Val(Syn)_Leu/Val(Deg)	4_4	132.1019	10.938	4.60E-07	0.685
$C_5H_7NO_3$	Pyroline-4-hydroxy-2-carboxylate	Arg/Pro	6	130.0499	7.218	7.79E-03	0.525
$C_9H_{11}NO_2$	L-Phenylalanine	Tyr/Phe	7	166.0862	10.329	1.19E-05	0.504
$C_5H_7N_4O$	Hypoxanthine	Purine	2	137.0458	9.494	3.74E-04	0.473
$C_5H_{11}NO_2$	L-Valine	Leu/Val(deg)_Panit	4_23	118.0862	12.673	1.54E-06	0.419
$C_4H_9NO_3$	L-Threonine	Leu/Val_Ser/Gly/Thr_Porphy	4_11_85	120.0655	14.918	1.29E-04	0.404
$C_3H_7NO_3$	L-Serine	Met_Cys_Ser/Gly/Thr_Sul_Cnamin_Mesn_Sphing	3_10_11_19_40_67_81	106.0498	15.816	1.18E-03	0.325
$C_9H_{11}NO_3$	L-Tyrosine	Tyr/Phe_Thia	7_20	182.0812	12.591	3.22E-03	0.296

### 3.11. Discussion

#### 3.11.1. Discussion - Clozapine Study

Whilst it was possible to visualise clozapine localisation in the rat brain and kidneys when a dry matrix coating was used, this was not possible when a wet matrix coating was used. In the liver, whilst it was possible to detect clozapine when a wet matrix coating was used, the signal intensity of  $m/z$  327 was much lower than when the dry matrix coating was used. The variation in endogenous marker intensities observed when either a wet or dry matrix application was utilised could be the result of many different factors. There may be co-crystallisation of the dry matrix with surface analytes on the tissue due to water vapour, either from humid atmosphere or following removal of the sample plate from the freezer which causes ionisation of molecules when dry matrix is used. Ionisation of the dry matrix may be sufficiently energetic to enable the ionization of small molecules that are near to the matrix crystals but not crystallized with. The wet matrix application may cause analyte spreading, diluting the concentration of the drug making it too low for detection by MALDI-MSI. The wet matrix may enable some analytes to be better extracted or co-crystallised with the matrix making some marker ions undetectable with the wet matrix compared to dry.

By utilising the dry matrix application method, it was possible to visualize the distribution of clozapine in the cortex of rat brain sections. This could be due to the mechanism of action of clozapine. It is a D2 receptor antagonist and one of the dopaminergic pathways is the mesolimbic/mesocortical pathway which is found in the cortex and limbic system. In this study, clozapine was observed mostly in the

cortex, consistent with its action on mesocortical/mesolimbic system as a D2 receptor blocker, blocking the effects of excess dopamine which causes positive symptoms of the disease through actions in this pathway.

To mimic the effects of utilising a wet matrix coating, samples were washed before MALDI-MSI analysis which illustrated that the distribution pattern of clozapine was altered following washing. Quantitation with the LTQ-orbitrap confirmed that the concentration of the drug was decreased approximately 4-fold following washing. This illustrates that care should be taken when utilising a wet matrix application method for MALDI imaging of pharmaceuticals.

### **3.11.2. Discussion - SSR180711 Study**

This study illustrates that a dry matrix coating can be used effectively to map the distribution of a parent drug compound in rat brain sections. Laser capture microdissection (LMD) was used to confirm that the distribution of the drug observed was a true representation of drug localisation in rat brain by harvesting tissue from selected anatomical regions and working them up for mass spectral analysis. Hydrophilic interaction chromatography coupled to high resolution mass spectrometry was then used to quantify the concentrations of drug in different anatomical regions of the treated rat brain tissue. This was used to confirm that the distribution pattern and peak intensities observed using MALDI-MSI were accurate. The use of laser microdissection confirmed the relative differences in peak intensity of drug in the grey and white matter obtained by MALDI-MSI as LC-MS analysis illustrated that the concentration of drug in the white matter was approximately 2X that found in the grey matter, reflecting the results of MALDI-MSI analysis.

Additionally, metabolomic profiling of the selected rat brain regions can also be carried out to establish effects the drug may be having on endogenous metabolites.

From development of a selective PET ligand for imaging  $\alpha 7$  nicotinic acetylcholine receptors in primate brain it was found that this drug rapidly penetrated brain and accumulated in hippocampus, occipital cortex, temporal cortex, frontal cortex, striatum, thalamus and cerebellum, in regions where there were high levels of  $\alpha 7$  receptors present [281]. The locality of the drug observed after thirty minutes appeared to be predominantly in the white matter regions of the brain, particularly the white matter of the cerebellum. Although this drug was an agonist of alpha 7 receptors, it was not possible to locate the highest concentration of drug in regions rich with alpha 7 receptors. As this distribution pattern was observed after 30 minutes, which is a short time period before the animal is sacrificed; it is possible that the drug is found in the white matter because there is higher blood flow to areas rich in white matter. Although a dose of 30 mg/kg was used, this is approximately 10X higher than a therapeutic dose with *in vivo* models usually lying within the range of 0.3-3 mg/kg. This dose was selected to allow evaluation of the effectiveness of the dry matrix coating. However, for further experiments, a lower dose could be used and tissue collected from other time points could be analysed as well to enable drug-induced metabolomic changes to be deduced and to evaluate the limit of detection of the dry matrix coating method.



### 3.12. Conclusions and Future Work

These studies illustrates that a dry matrix application method can be complementary to a wet matrix application method. It is particularly useful for the detection of pharmaceuticals *in situ* from unwashed samples where wet matrix coatings are unsuitable. Whilst there is some overlap between the methods, there are also differences in ionization of compounds using one method or the other. Therefore, both dry and wet matrix application methods may be required to fulfill all the goals of a MALDI-MSI experiment. Future work will involve utilising this matrix application method for identification of drug compounds in other sample types.

**Chapter 4 - Metabolomic Profiling of Biomarkers of Liver X Receptor-Induced  
Toxicity in Mouse Liver Tissue.**

#### **4. Introduction**

Liver X receptors (LXRs) are members of the nuclear receptor superfamily which is comprised of several ligand-activated transcription factors. LXRs regulate gene transcription by binding as heterodimers with the 9-cis retinoic acid receptor (RXR), which is an obligate partner, in order to activate specific DNA sequences known as LXR-responsive elements (LXREs) which are located in the promoter sequences of target genes (Figure 115) [289,290]. The receptors function as nuclear hormone receptors which act as 'cholesterol sensors,' regulating the transcription of a number of genes involved in cholesterol metabolism and homeostasis [291] and can reduce cholesterol levels in the body by promoting its metabolism into bile acids and also promoting its excretion in the bile. Therefore, LXRs have been investigated as a drug target to prevent hypercholesterolemia, a contributing factor for atherosclerosis, and ischaemic heart disease. However, there are also several unwanted toxicity effects that result from receptor activation. Receptor activation is known to enhance transcription of several lipogenic genes, for example sterol regulatory element binding protein 1c (SREBP1c). Genes promoted by SREBP1c include fatty acid synthase, acetyl CoA carboxylase and stearoyl CoA desaturase which is a rate limiting enzyme required for the biosynthesis of monounsaturated fatty acids [292]. In addition LXRs regulate the carbohydrate response element binding protein (ChREBP) which acts as a glucose sensor promoting the conversion of glucose into fatty acids. The development of LXRs as cholesterol lowering agents has been hampered by the fact that they promote triglyceride biosynthesis which can lead to hypertriglyceridemia and related toxicity effects [291] with large accumulations of TAGs occurring in the liver (Figure 115). The LXR receptor exists in two  $\alpha$ - and  $\beta$ -

subtypes and it has been proposed that the  $\beta$ -subtype, which is more generally distributed around the body unlike the  $\alpha$ -subtype which occurs in the liver, may have a greater role in promoting lipogenesis.

**Figure 115 - LXR Receptor Pharmacology and Mechanism of Action**

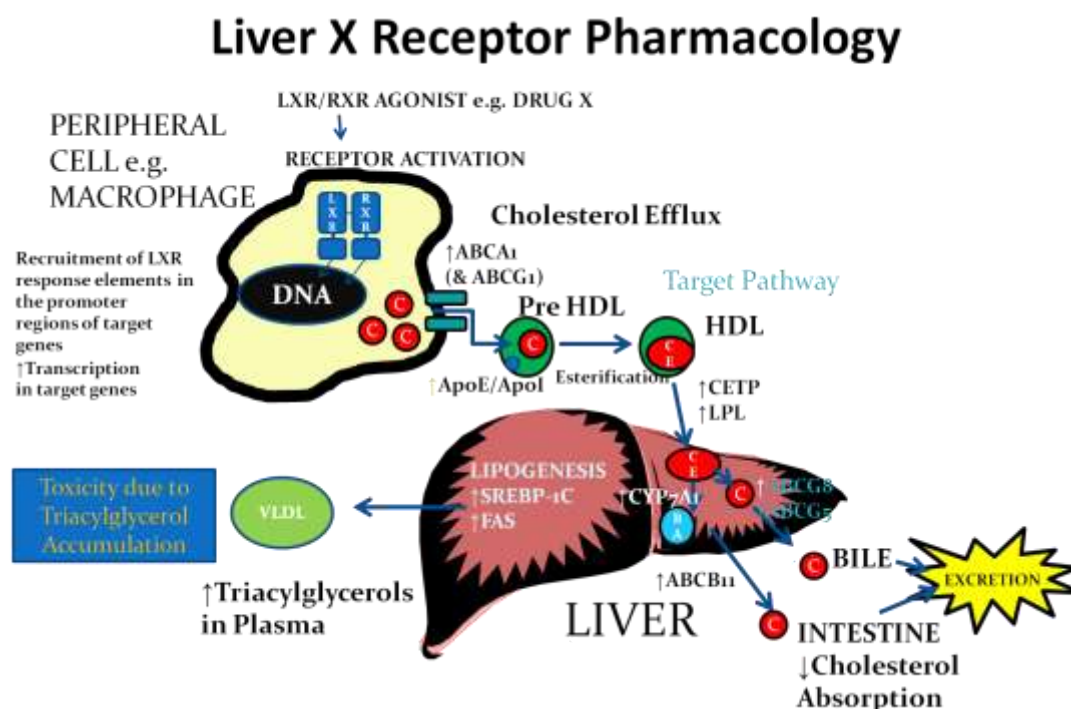


Diagram Based on Figure by Tontonoz P & Mangelsdorf DJ, 2003 in [293].

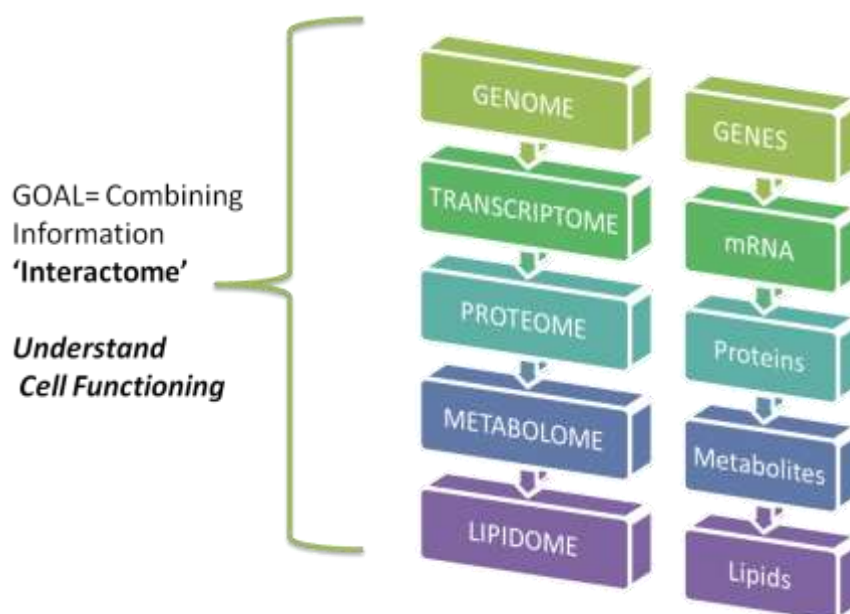
#### 4.1. Introduction to Metabolomics

Metabolomics is a systems approach to study metabolic profiles *in vivo* that has great potential for uncovering biomarkers which are indicative of drug efficacy or toxicity [150,294-297]. As a result, there has been increased use of metabolomics for assessment of xenobiotic safety by the pharmaceutical industry [298-302]. Thus it

was decided that a metabolomics-type study could be applied for profiling biomarkers of LXR-induced toxicity in mouse liver tissue.

Metabolomics is one of the high throughput ‘omics’ technologies along with genomics, transcriptomics, proteomics and lipidomics. Metabolomics, when utilised in an untargeted fashion, is the measurement of the global small molecule metabolite profile in extracts taken from biofluids, cells or tissues. The study of the metabolome is important as it is more closely related to genotype than proteome and genome. The technology has seen a huge surge in popularity since first described approximately 10 years ago [149-151,303] and several detailed reviews have been published on metabonomics and metabolomics in recent years focussing on mass spectrometry-based and NMR-based metabolomics e.g. see [149,151,298,304-311]. The ultimate goal is to be able to produce a combined ‘omics’ picture, the ‘interactome’ which will provide an overview of cellular functioning (Figure 116).

**Figure 116 – Overview of the ‘Omics’ Technologies**



During the ‘omic’ revolution, mass spectrometry has gone from being an analytical technique useful for synthetic chemists and analysts into an important analytical technique that is now gathering a wide spectrum of interest, providing information that cannot be obtained using conventional biological techniques. Mass spectrometry has applications in all biological fields whether it be microbiology, neuroscience, cardiovascular research or parasitology to name but a few. With the development of techniques such as atmospheric pressure ionisation, time of flight and Fourier transform MS, high throughput metabolite profiling can now be routinely carried out in many laboratories, with good reproducibility and reliability meaning this growing interest is set to continue.

#### **4.1.1. Key factors Governing the Success of Metabolite Profiling Experiments**

Although instrumentation is fundamental to the success of metabolite profiling experiments, sample preparation and data analysis techniques are also critical. Accurate and reproducible sample preparation is required to ensure the reproducibility of the experiments whilst data analysis is required to gain understanding of results obtained. Due to the volume of data obtained from a single untargeted experiment, the ‘stare and compare’ approach [312] is both time consuming and inadequate.

#### **4.1.2. Sample Preparation for Metabolomics**

There are various methods that have been proposed for extracting metabolites for metabolomics experiments, which will depend on the sample type and analytes of interest. For example for the extraction of cells the ideal method should rapidly

quench metabolism and quantitatively extract all metabolites for example by utilising boiling ethanol, freezing-thawing in methanol or use of acids. Detailed papers have recently been published comparing methods for optimum extraction of metabolites from cells [313], yeast [314] and parasites [315] .

For tissue extraction, tissue can be immersed in liquid nitrogen and then ground into a fine powder [316,317]. Alternatively frozen tissue can be placed directly into the extraction solvent and homogenised [318]. This method offers several advantages over freezing in liquid nitrogen, it is quicker, there is no loss of metabolites from transferring frozen powder to new vials and no risk of carryover associated with using the same equipment several times for grinding the powder. Additionally, when tissue is frozen in liquid nitrogen and ground to powder it thaws very quickly, possibly before being placed into other vessels. In both cases, when using a homogeniser for homogenising samples, care must be taken to ensure no carryover between sample batches.

For the extraction of lipids commonly utilised methods are those of Folch [319] or Bligh and Dyer [320] which utilise mixtures of methanol: water and chloroform (and saline for Folch) for lipid extraction. The Folch method was originally utilised for the extraction of brain lipids from tissue samples [319]. A modified Folch method has also been published by Bill Christie from the Scottish Crop Research Institute [213]. The Bligh and Dyer extraction method was originally utilised to extract lipids from fish muscle which contain a higher proportion of water and is useful for the extraction of lipids from large sample sizes as less solvent is required [320]. For the extraction of polar metabolites from tissues Wu *et al* documented the use of an

alternative high throughput metabolite extraction method for easy extraction of metabolites directly from frozen tissue samples that are extracted in methanol, water and chloroform [253]. This method also produces both polar and lipid fractions [253].

#### **4.1.3. Introduction to Data Analysis for Metabolomics**

At present a lot of work is being done by academic research groups with limited commercial software packages available. Notable packages available include MZMatch [36] which is a platform written in Java for the analysis of high resolution LC-MS datasets. Features include peak extraction, peak matching, filtering, normalisation and identification. The downside is that there is also the requirement for background knowledge of computer programming. Another is MZMine pioneered by Finnish Scientist Matej Orešič [37] which again is for the analysis of high resolution LC-MS datasets [321-323]. Features include peak picking, statistical analysis, visualisation tools, database searching and ease of operation following development of MZMine 2 [321]. For further examples of data processing tools available for processing LC-MS datasets please see [324].

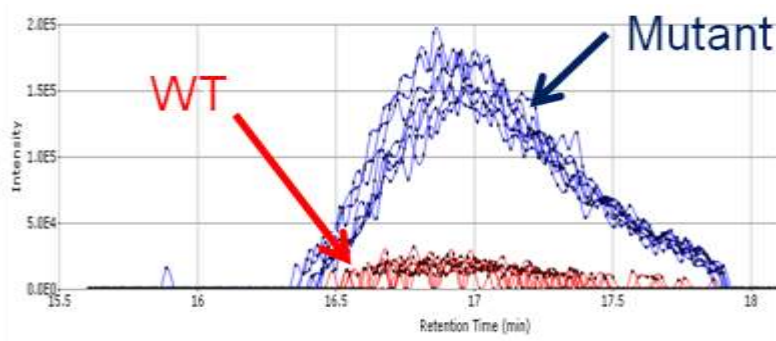
SIEVE is commercial software provided by Thermo Scientific which enables the identification of differences between control and treated samples by providing a series of chromatographic pictures comparing intensities of spectral features that may correspond to metabolites. The input required is multiple LC-MS chromatograms from a single experiment. These are aligned and every peak identified is given an ID based on intensity. List of IDs therefore corresponds to different peaks which in turn represent different metabolites. It provides a P-value based on difference in



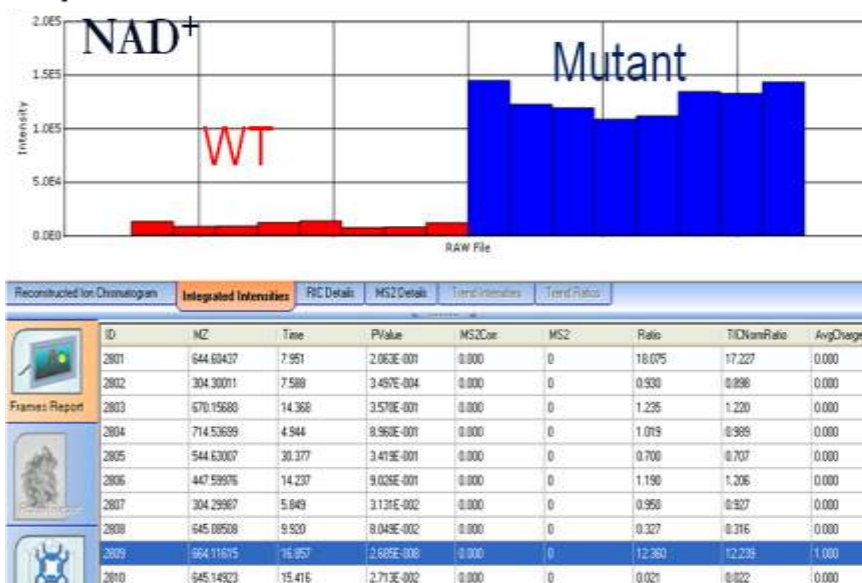
intensities of individual peaks in control versus disease samples, revealing metabolites that have significantly different intensities between control and treated groups. It is user-friendly providing chromatographic pictures as illustrations and list output containing all IDs. There are also limitations; P-values are not foolproof since they do not account for data skewing. Thus there is also the possibility that some of the P-values are more significant than reported by SIEVE which does not consider skewing. SIEVE is utilised in our lab at Strathclyde because of ease of operation and the useful output generated. An example SIEVE output file is shown below, illustrating that it is easy to visualise when a compound has a higher intensity in one treatment group than the other, enabling biomarker identification (Figure 117). This example shows that  $\text{NAD}^+$  is a marker compound in *NPAS-3* mouse model of schizophrenia.

Figure 117 – Example of SIEVE output generated from analysis of mouse brain from control and *NPAS-3* model of schizophrenia showing that there are higher levels of  $\text{NAD}^+$  in brain samples from mutant, i) shows overlaid chromatographic peaks and ii) shows bar chart visualisation and records.

### i) Overlaid Chromatographic Peaks



### ii) Bar Chart Visualisation and Record List



It also connects with the ChemSpider database to aid metabolite identification. Data output includes list of  $m/z$  ratios, IDs which are record numbers that are ordered according to feature intensity, and this data output from SIEVE can be analysed with

ometrics software programmes such as SIMCA P. A drawback of SIEVE, however, is the volume of redundant data generated; however it is useful during untargeted analyses as it can pick out differences between control and treatment groups that may have been missed otherwise.

#### **4.1.4. Introduction to Analytical Platforms for Metabolomics**

Currently, obtaining global metabolic profiles of biological systems requires a multi-platform approach and a wide range of analytical platforms are used [325-327] based on NMR and mass spectrometry including liquid chromatography electrospray ionisation mass spectrometry (LC-ESI-MS) operated in positive and negative ion modes e.g. [328-334] gas chromatography-mass spectrometry (GC-MS) e.g. see [335,336], proton nuclear resonance spectroscopy ( $^1\text{H}$  NMR) e.g. see [307,337-339], capillary electrophoresis mass spectrometry (CE-MS) e.g. see [340] and to a lesser extent matrix-assisted laser desorption/ionisation mass spectrometry (MALDI-MS) [31,156,239]. Whilst no single analytical method will provide a comprehensive determination of all components of a sample, by employing both mass spectrometry and NMR in single studies, the two techniques can be complementary, providing a deeper insight into metabolome [94,294,296,325,330,331,337,341,342]

Proton Nuclear Magnetic Resonance ( $^1\text{H}$ - NMR) spectroscopy is often chosen for metabolic profiling experiments because it is possible to detect hundreds of metabolites in a single sample within a few minutes. It requires little sample preparation, is non destructive and results are highly reproducible. Furthermore, the technique is quantitative, as all protons will be detected with same level of sensitivity [343]. Development of higher field strength NMR instrumentation (up to 900 MHz)

and the use of cryogenically cooled probes have provided increased sensitivity and better spectral resolution. It has also been shown that the inter-laboratory variability is very good [344-346]. Due to overlap in chemical shifts of many molecules, 2D NMR may also be employed [345,347]. High resolution <sup>1</sup>H Magic Angle Spinning (HR-MAS) has been employed for metabolic profiling of intact tissue samples, for example to investigate toxicity or disease [348-353]. However, NMR has a limited sensitivity, which means that no more than 60 metabolites are readily measured in a biological sample [354].

Mass spectrometry has also been employed extensively for metabolomics studies ([63,64,94,328-334,354-356] as it offers improved sensitivity over NMR which is useful for untargeted studies to identify novel biomarkers. Mass spectrometry is frequently coupled with a prior separation technique such as HPLC, UPLC, Capillary LC or GC, e.g. reviewed in [336,340,354,357]. Appropriate chromatographic methods and ionisation conditions should be employed for the type of molecule(s) of interest in a sample set. In addition, particularly in LC-MS mode, the chromatography column format used can be varied [358]. The advent of high resolution Fourier transform mass spectrometers has improved reproducibility, accuracy and sensitivity of mass spectrometry making it suitable for high throughput metabolomics studies [76]. Additionally, Orbitrap mass spectrometers offer similar performance to FT-MS systems but without need for a high strength magnetic field [81]. Mass spectrometry also offers sensitivity down to at least the picogram level.

Hydrophilic interaction chromatography (HILIC) has been used in metabolomics studies as it is useful for the analysis of highly polar metabolites which are poorly

retained on reverse phase columns [101]. Details on the mechanism of action of HILIC were discussed previously in section 1.5.2. Work in our laboratory has recently reported the application of hydrophilic interaction chromatography in metabolomic profiling [119,358,359] and with this format we were able to observe 230 metabolites in extracts from *Drosophila melanogaster*.

#### **4.1.5. Metabolomics for Toxicological Studies**

There are many examples that exist showing how metabolomics can be employed to investigate toxicology and efficacy during drug discovery and development which is well documented in several reviews [296,338,360,361]. Recent examples of studies reported in the literature include: assessment of paracetamol toxicity [362], assessment of the effects of rosiglitazone [363,364] and a study of the toxicology of doxorubicin [365]. For toxicological metabolomics experiments, samples such as urine, blood, serum or tissue are collected from control and drug treated subjects to identify biomarkers related to drug toxicity [337]. The aim is to find patterns of metabolic biomarkers that are the result of toxicity, which should be specific to the organ that is the main target of a particular compound [296,299,301,302,366,367]. The hope is that metabolomics can detect specific early signature toxicity biomarkers indicating organ-specific damage, eliminating unsuitable candidate compounds at an early stage of drug discovery, saving companies time and money. By using an untargeted approach, changes in endogenous metabolite levels and drug toxicity data can be obtained from the same experiment, without the need for labels such as those employed in conventional autoradiography studies. Additionally, the untargeted approach is useful for biomarker discovery, to identify novel observations that

otherwise may be missed in conventional toxicological studies [368]. However, there are limitations. There are often metabolite changes that are common across widely different toxicological studies, making identification of the specificity of observed metabolic changes difficult, with common indicators including succinate, glucose and creatine [296].

There is great interest in identification of specific biomarkers of hepatotoxicity at an early stage in drug discovery as this is often a reason a drug fails during development. The application of metabolomics for the detection of compounds causing hepatotoxicity during preclinical studies has been widely documented [150,239,297,367,369-374]. It has also been shown that combining metabolomics with transcriptomics [294,375] or proteomics [297] or by combining metabolomics and proteomics data with metabolic flux, measurements [376] can provide greater insights into toxicity mechanisms. Acquisition of additional clinical chemistry and histopathology data also adds additional prospects, for example relating biomarkers to specific types of liver damage [377].

## **4.2. Aims**

The main aims of this study are summarised below:

1. To develop a MALDI MS method for the analysis of triglycerides in mouse liver.
2. To develop an extraction method for lipids and polar metabolites from mouse liver.

3. To profile lipids in LXR agonist treated and control mice livers by LC-FTMS.
4. To develop a GC-MS method for profiling of fatty acids in LXR agonist treated and control mice livers.
5. To profile polar metabolites in LXR agonist treated and control mouse livers by LC-FTMS.

### **4.3. Materials and Methods**

#### **4.3.1. Chemicals**

The solvents used for the study were purchased from the following sources: acetonitrile, methanol, acetone, isopropanol (IPA) and chloroform (Fisher Scientific). Trifluoroacetic acid (TFA) (Sigma Aldrich) and formic acid (VWR). All chemicals used were of analytical reagent grade. HPLC water was used in all analyses which was obtained from a Direct Q-3<sup>®</sup> water purification system (Millipore, Watford, UK). MALDI-MS grade 2, 5-dihydroxy-benzoic acid (DHB) matrix, potassium hydroxide pellets, potassium chloride and ammonium formate were also purchased (Sigma-Aldrich). Standards for 90 common biomolecules were also purchased and were used as references for separation over the ZIC-HILIC column (Sigma Aldrich).

#### **4.3.2. Animals**

Frozen livers were obtained from MSD (Newhouse, Motherwell, Scotland). C57BL adult male mice (10-12 weeks old, weighing 20-25g) were dosed orally once daily over a 5 day period at the same time point each day with a given concentration of an experimental LXR agonist in 10% dimethylacetamide/water. Drug concentrations given were either 0.3 mg/kg, 1 mg/kg, 3 mg/kg, 10 mg/kg, 30 mg/kg or 60 mg/kg or saline was given as a control. Animals were housed by dose group. Animals were sacrificed 4 hours following final dosing and the livers were immediately frozen by immersion into isopentane and stored at -80 °C until required. This study was conducted in compliance with The Animals (Scientific Procedures) Act 1986 and the



code of practice for the housing and care of animals used in scientific procedures as authorised and monitored by the UK Home Office.

#### **4.3.3. Sample Preparation for MALDI-MS Imaging Experiments**

Sectioning of liver samples and sample preparation was carried out as described in section 2.11.3. Prepared MALDI targets were placed in a vacuum dessicator for approximately 15 minutes prior to matrix application in order to remove excess moisture. No washing procedures were carried out to prevent compromising the spatial integrity of the small molecules. DHB was prepared at concentration of 40 mg/ml in 100% acetone. A Preval hand-held spraying device (Sigma-Aldrich) was used to apply homogenous layers of matrix for imaging experiments utilising the method described in section 2.11.4.1.

#### **4.3.4. Instrumentation for MALDI MS Imaging Experiments**

An Axima-CFR TOF MALDI mass spectrometer was used to carry out tissue imaging experiments. The machine was operated in reflectron positive ionisation mode with the power adjusted to a level suitable for the matrix with 50 shots and a laser repetition rate of 10 Hz. A suitable raster was then selected with 100  $\mu\text{m}$  spacing. The mass range utilised was 100-1000 Da with pulse extraction optimised to 850 Da. Initially, imaging experiments were carried out to look for differences in composition of tissue between tissue treated with 60 mg/kg of drug or 30 mg/kg and control. Sections from treated livers were mounted with control sections and these were analysed sequentially with analysis of a control section before each treated section to minimise any variability. Next, to investigate any dose response effects, 7

sections, one from each liver treated with a different dose of the drug plus control were mounted onto a single stainless steel target and analysed from control up to highest dose. Spectra were analysed using the Launchpad software package (version 2.7.2) (Shimadzu Biotech).

#### **4.3.5. Extraction of Lipids From Liver Tissue Homogenates for LC-MS and GC-MS Analysis**

For these experiments, tissue was taken from livers from mice treated with either the 60 mg/kg drug dose or saline (control). Liver tissue samples (50-100 mg) were collected and placed into glass vials. Lipid extraction was carried out using a modified Folch extraction procedure described previously with some small alterations (Christie, 2003). This involved homogenising tissue using a handheld LabGen 7B homogeniser (Cole Parmer, London, UK). For example, 100 mg tissue was taken, homogenised with 1 ml methanol, 2 ml chloroform was then added and solution homogenised again. (CAUTION: Chloroform is harmful if swallowed, causes skin irritation, is suspected of causing cancer and can cause damage to organs through prolonged/repeated exposure. Thus, a COSHH assessment should be carried out before use.) The solution was then centrifuged, supernatant removed and then the extraction of lipids repeated two more times from the pellet. The three supernatants were then pooled together, and  $\frac{1}{4}$  of the total volume of 0.88% w/v potassium chloride (saline solution) was added to the filtrate. This was then shaken to allow separation into a biphasic solution. The aqueous layer was then removed and the volume of the bottom layer measured. To this solution,  $\frac{1}{4}$  of total volume of methanol:saline 1:1 was added and again this was shaken to form a biphasic solution.

The top layer was again discarded and the bottom lipid layer was then filtered using GHP Acrodisc 13mm syringe filters with 0.45  $\mu\text{m}$  membrane (Fisher Scientific), blown to dryness using stream of nitrogen and re-suspended in 2:1 methanol:chloroform solution which was compatible with the LC-MS conditions.

#### **4.3.6. Preparation of Fatty Acid Methyl Esters For GC-MS Analysis**

For these experiments, liver tissue was taken from mice treated with either the 60 mg/kg drug dose or saline (control). Lipids were extracted using the modified Folch extraction procedure described above except after blowing to dryness, they were re-dissolved in 100  $\mu\text{l}$  methanol, to ensure phospholipids were taken up, and then 2 ml hexane was added. To produce fatty acid methyl esters, 0.5M methanolic potassium hydroxide was prepared. To the samples, 0.5 ml of methanolic potassium hydroxide (KOH) was added. The mixture was then shaken and the layers were allowed to separate [378]. The upper layer was kept for GC-MS analysis.

#### **4.3.7. Instrumentation and method for GC-MS Analysis**

Analysis was performed using a DSQ II Single Quadrupole GC-MS with a Focus GC (Thermo Scientific, Hemel Hempstead, U.K.). A 5.5 minute solvent delay was applied. Chromatography was performed using a Factor Four Capillary Dimethylpolysiloxane column (30m x 0.25 mm ID DF = 0.25) (Varian Ltd., Oxford, UK). Helium was used as carrier gas with flow rate of 1.0 ml/min. GC Inlet temperature was 230  $^{\circ}\text{C}$  and MS transfer lines were maintained at 250  $^{\circ}\text{C}$ . Sample injection volumes were 1  $\mu\text{l}$  injected with a split ratio of 10:1. The oven

temperature was programmed from 100 °C to 320 °C at a rate of 10 °C/min with a final hold of 5 mins.

#### **4.3.8. Extraction of Polar Metabolites from Liver Tissue Homogenates for LC-MS Analysis**

Extraction of polar metabolites from liver tissue samples was carried out using an extraction method described previously in the literature for optimal extraction of polar metabolites [253]. Tissue was taken from livers from animals treated with either 0.3, 1, 3, 10, 30 or 60 mg/kg of drug or saline (control). For this study, liver samples weighing 100 mg were prepared using the two-step method that was described. For preparation of samples for LC-MS analysis, 200 µl of polar extract was added to 800 µl 1:1 acetonitrile: water solution. The samples were then filtered using a protein crash plate (Biotage Ltd., Sweden) before LC-MS analysis.

#### **4.3.9. LC-MS Analysis of Polar Metabolites**

Experiments were carried out using a Thermo Scientific LTQ-Orbitrap coupled with a Surveyor Plus HPLC pump and autosampler. Analysis was carried out in positive mode over a mass range of  $m/z$  60-1000 using 30 000 resolution. The capillary temperature was 250 °C, the ion spray voltage was 4.5 kV, the capillary voltage 30 V, the tube lens voltage 105 V and the sheath and auxiliary gas flow rates were 45 and 15, respectively (units not specified by manufacturer). MS<sup>2</sup> experiments were carried out at 30 V. The instrument was externally calibrated before analysis and internally calibrated using lock masses at  $m/z$  83.06037 and  $m/z$  195.08625. The software programme Xcalibur (version 2.0) was used to acquire the LC-MS data.

Samples were analysed sequentially and the vial tray was set at a constant temperature of 4 °C. A ZIC-HILIC column (5 µm, 150 x 4.6 mm; HiChrom, Reading, UK) was used in all analyses and a binary gradient method was developed which produced good polar metabolite separation. Solvent A was 0.1% v/v formic acid in HPLC grade water and solvent B was 0.1% v/v formic acid in acetonitrile. A flow rate of 0.3 ml/min. was used and the injection volume was 10 µl. The gradient programme used was 80% B at 0 min. to 50% B at 12 min. to 20% B at 28 min. to 80% B at 37 min., with total run time of 45 minutes. The raw Xcalibur data files from control and treated samples were then processed using SIEVE, version 1.2 (Thermo Scientific in collaboration with VAST Scientific). A threshold of 100,000 was used, the frame  $m/z$  width was 0.02 and the first control sample was chosen as the reference file. The masses of the polar metabolites were pasted into Excel and searched against a mass list containing the exact masses 6000 of biomolecules using a macro written in house. For fragmentation experiments, data dependant MS<sup>2</sup> scans were carried out in positive ionisation mode. A mass list containing metabolites of interest e.g. hydroxymethylglutaryl carnitine and methylglutaryl carnitine was added into the MS2 segment of the instrument method allowing targeted fragmentation to be carried out. An activation Q of 0.18 was selected.

#### **4.3.10. LC-MS Analysis of Lipids**

The analysis of lipids was performed using the same mass spectrometer with same set-up described above. For negative ion mode analysis, the capillary voltage was -25 V and the tube lens voltage was -95.0 V. Analysis of lipids was carried out using an ACE silica gel column (3 µm particle size, 150 x 3 mm; HiChrom, Reading U.K.)

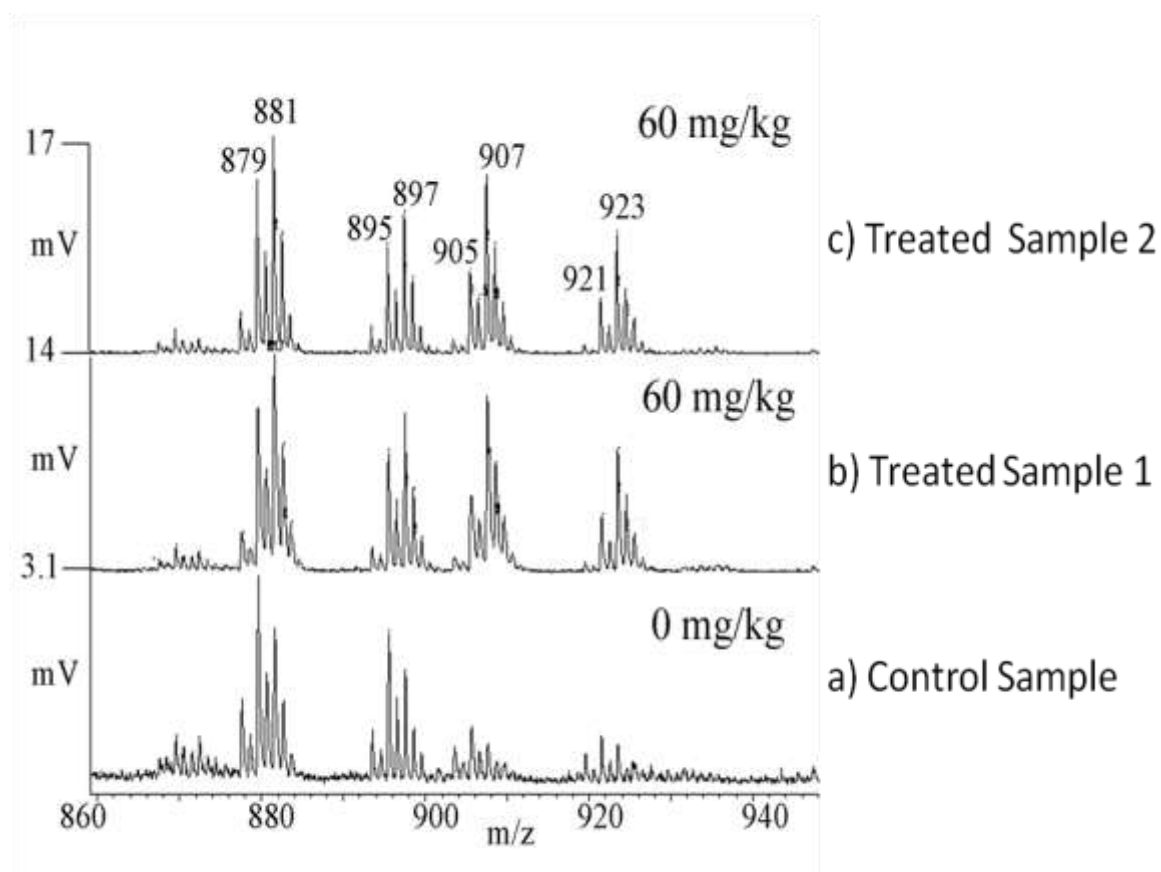
in hydrophilic interaction mode. Solvent A was 20% IPA/80% 0.02M ammonium formate in water and Solvent B was 20% isopropyl alcohol/80% acetonitrile. A flow rate of 300  $\mu$ l/min was used and the injection volume used was 10  $\mu$ l. The gradient programme used was 94% B 0 min. to 92 % B at 9 min. to 75 % B at 9 min. to 73 % B at 15 mins to 65 % B at 23 mins to 94% B at 25 min. with a total run time of 40 minutes. Samples were analysed sequentially and the vial tray was set at a constant temperature of 4 °C. The lipid side chains were characterised in negative ion mode by carrying out data dependent MS<sup>2</sup> and, in the case of the PC lipids, MS<sup>3</sup> with an activation Q of 0.18. The online database LipidMaps ([www.lipidmaps.org](http://www.lipidmaps.org)) [379] was used to assist in identifying the lipids.

## 4.4. Results

### 4.4.1. MALDI-MS Analysis of Liver Sections

Comparing molecular profiles of liver sections taken from animals treated with 60 mg/kg or 30 mg/kg of the drug to controls, revealed that there was up-regulation of molecules in the tissue within mass range of  $m/z$  870-940 (Figure 118).

**Figure 118 - MALDI MS generated triglyceride profiles within mass range  $m/z$  870 - 940 from liver sections taken from animals treated with either a) saline (control) or (b & c) 60 mg/kg of the drug once per day over 5 day period using 40 mg/ml solution of DHB in 100% acetone as matrix.**



Subsequent analysis of liver sections from animals treated with each dose of drug plus control sections illustrates there is a clear dose response effect observed, with changes in the intensities of triacylglycerols with dose (Figure 119.)

Previously, it has been demonstrated that triacylglycerols (TAGs) are found in this mass range, predominantly as  $\text{Na}^+$  adducts, from analysis of fixed oils using MALDI-MS [380,381], suggesting that these peaks corresponded to TAGs. Analysis of standards utilising MALDI-MSI revealed that the triacylglycerols were observed as  $\text{Na}^+$  adducts and that DAG fragments were also observed in full scan and PSD modes (see section 2.12.1). Within this mass range, it can be seen that there are four clusters observed containing a total of 8 prominent peaks (plus isotopes) (Figure 119). It was observed that there was 16 Da spacing between the most intense ions in first cluster and most intense ions in the second cluster. This is consistent with clusters 1 and 3 corresponding to  $\text{Na}^+$  adducts of TAGs whilst clusters 2 and 4 correspond to  $\text{K}^+$  adducts of TAGs. The spectra shown in Figure 118 and Figure 119 illustrates that there are four predominant TAGs that are upregulated in response to drug treatment, with  $\text{Na}^+$  adducts observed at  $m/z$  879, 881, 905 and 907 and the corresponding  $\text{K}^+$  adducts observed at  $m/z$  895, 897, 921 and 923. As well as an increase in the abundance of TAGs there is a shift towards a greater degree of saturation for example the ion  $m/z$  881 (corresponding to a 52:2 TAG) has a higher intensity than the ion at  $m/z$  879 (corresponding to a 52:3 TAG) in the treated samples but in control samples  $m/z$  879 has a higher intensity than  $m/z$  881 (Figure 118 and Figure 119). The same shifts can also be seen for TAGs at  $m/z$  905 and  $m/z$  907, with  $m/z$  907 having a higher intensity in treated samples than  $m/z$  905 and vice versa for control samples (Figure 118 and Figure 119).



**Figure 119 - MALDI MS spectra, obtained using DHB as a matrix, showing lipid profiles within the mass range  $m/z$  740-930 from analysis of rat liver tissue sections taken from animals treated with either a) saline (control), b) 0.3 mg/kg, c) 1 mg/kg, d) 3 mg/kg, e) 10 mg/kg, f) 30 mg/kg or g) 60 mg/kg of the drug once per day over a 5 day period. Clusters of triacylglycerols are labelled 1-4.**

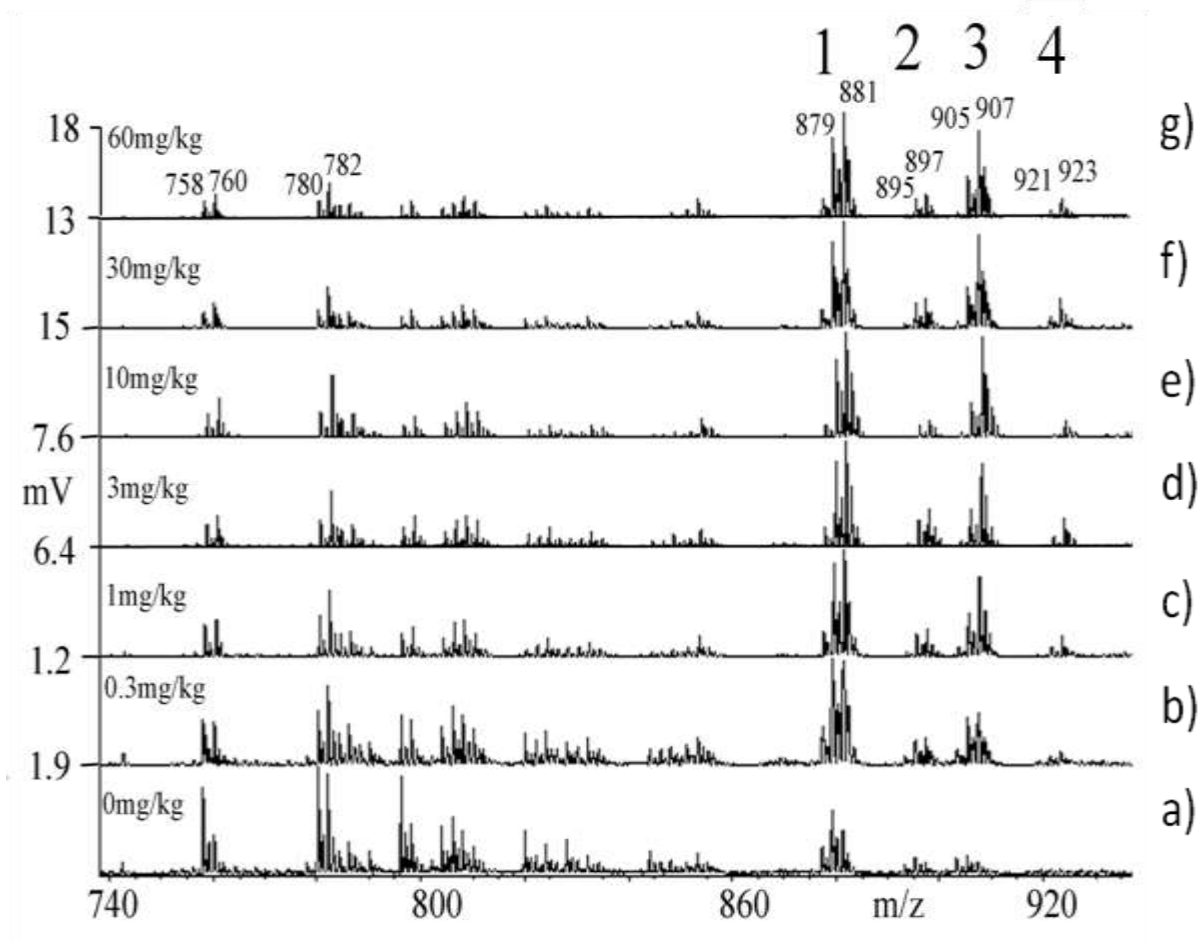
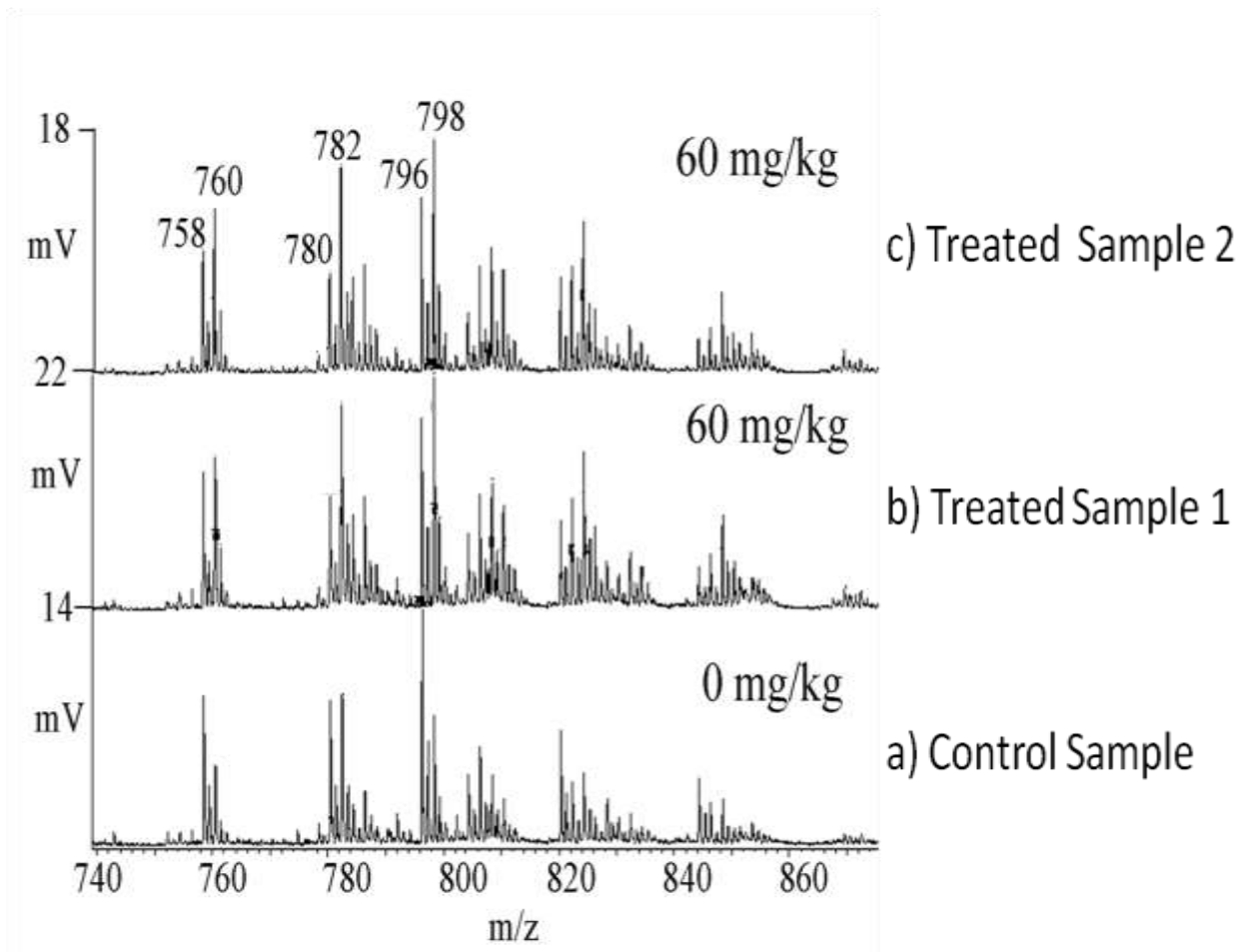


Figure 120 and Figure 121 show the mass range  $m/z$  740-870 from the same spectra shown in Figure 118 and Figure 119 in order to show the effect of the LXR agonist on phosphatidylcholine (PC) lipid profiles in liver which are found predominantly within this mass range. Analysis of liver sections from animals treated with each dose of drug plus control sections illustrates there is a clear dose response effect

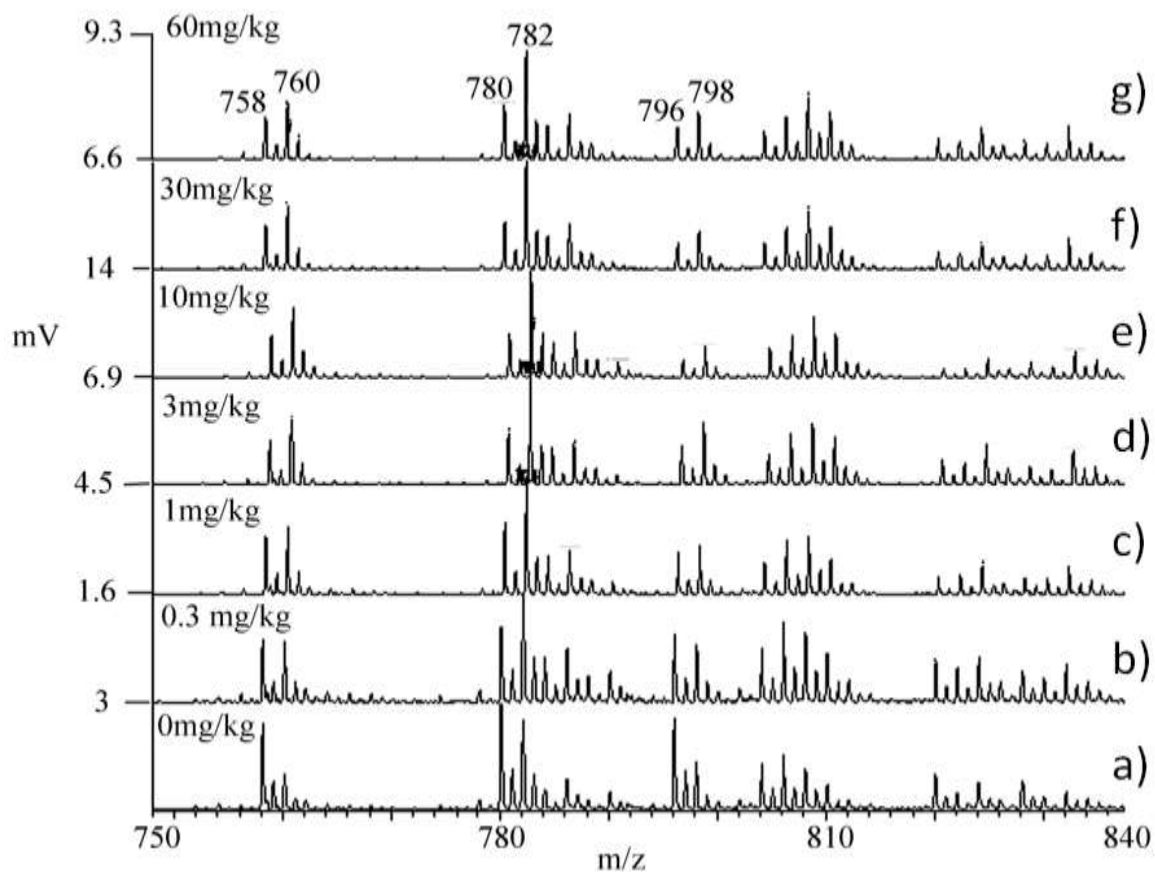
observed, with changes in the intensities of phosphatidylcholines with dose (Figure 121). As well as an increase in the levels of phospholipids, which was less marked than in the case of the triglycerides, the most noticeable change was in the relative peak intensity of peaks at  $m/z$  758 and  $m/z$  760 reflecting the change in saturation that had been observed in the TAGs (Figure 120) and (Figure 121).

In the treated samples, there is an increased peak intensity of species at  $m/z$  760 whilst the relative intensity of the ion at  $m/z$  758 is lower in comparison to control samples. For example, for the phosphatidylcholines at  $m/z$  758 and 760 the relative peak intensities change from  $m/z$  758 being more intense in vehicle to them having roughly similar peak intensities at  $m/z$  758 and  $m/z$  760 at 0.3 and 1 mg/kg doses to  $m/z$  760 being more intense than  $m/z$  758 at all other higher doses (Figure 121). The ion at  $m/z$  760 corresponds to a mono-unsaturated PC lipid (C16:0/C18:1) while the ion at  $m/z$  758 corresponds to a di-unsaturated PC lipid (C16:0/18:2). The same effect can be seen for the ions at  $m/z$  782 and  $m/z$  798 which have one double bond less than the lipids at  $m/z$  780 and  $m/z$  796, respectively (Figure 121). This illustrates how MALDI-MS can be used as a rapid screening tool to probe changes in the lipid composition of intact tissues in response to drugs which can then be explored further using other analytical techniques. Subsequent analysis of all liver sections from animals treated with each dose of drug plus control sections illustrates there is also a clear dose response effect observed with the intensity of signal and degree of saturation of PC lipids increasing with dose (Figure 121).

**Figure 120 - MALDI-MS spectra showing lipid profiles within mass range  $m/z$  740-870 from rat liver tissue sections from animals treated with either a) saline (control) or b) 60 mg/kg of the drug once per day over 5 day period using DHB as matrix.**



**Figure 121 - MALDI-MSI spectra, obtained using DHB as a matrix, showing expansion of Figure 120 within the mass range  $m/z$  750-840 to show phosphatidylcholine profiles from rat liver tissue sections from animals treated with either a) saline (control), b) 0.3 mg/kg, c) 1 mg/kg, d) 3 mg/kg, e) 10 mg/kg, f) 30 mg/kg or g) 60 mg/kg of the LXR agonist once per day over a 5 day period.**



Selected information from Figure 118, Figure 119, Figure 120 and Figure 121 is tabulated below (Table 11) to show the calculated fold increases and decreases in the relative peak intensities (ratios) of the phosphatidylcholine lipids at  $m/z$  758,  $m/z$  760 and triacylglycerols at  $m/z$  879, 881, 905 and 907 in samples treated with 60 mg/kg of the drug compared to controls by dividing the relative peak intensities (ratios) of control by relative peak intensities (ratios) of treated to obtain fold decreases or by dividing the relative peak intensities (ratios) of treated by control to obtain fold increases. Relative peak intensities (ratios) are used as these are normalised peak intensities that are obtained by calculating the peak intensity of the ion of interest by the matrix peak intensity. By calculating the relative peak intensities (ratios), any differences in intensities obtained due to inhomogeneity of the matrix are theoretically cancelled out. It can be seen that there is a 1.4 fold decrease in the ratio of the phosphatidylcholine at  $m/z$  758, whilst the average ratio of the phosphatidylcholine at  $m/z$  760 increases by 1.55 fold and the ratios of triacylglycerols at  $m/z$  879, 881, 905 and 907 increase by an average of 5.4, 7.6, 2.7 and 6 fold, respectively (Table 11).

**Table 11 - Table showing fold increases and decreases in levels of selected phosphatidylcholines and triacylglycerols in treated samples. Fold changes are calculated by dividing the relative peak intensities (ratios) of control by ratio of treated to obtain fold decreases or by dividing the relative peak intensities (ratios) of treated by control to obtain fold increases. Relative peak intensities (ratios) are used to normalise peak intensities and are obtained by calculating the peak intensity of the ion of interest by the matrix peak intensity.**

SAMPLES	Average Peak Intensity Matrix Ion [M+H] <sup>+</sup> (mV)	Average Peak Intensity PC Ion 758 [M+H] <sup>+</sup> (mV)	Ratio	Average Peak Intensity PC Ion 760 [M+H] <sup>+</sup> (mV)	Ratio	Average Peak Intensity TG Ion 879 [M+Na] <sup>+</sup> (mV)	Ratio	Average Peak Intensity TG Ion 881 [M+Na] <sup>+</sup> (mV)	Ratio	Average Peak Intensity TG Ion 905 [M+Na] <sup>+</sup> (mV)	Ratio	Average Peak Intensity TG Ion 907 [M+Na] <sup>+</sup> (mV)	Ratio
CONTROL (AVERAGE)	219	49	0.22	29	0.132	0.9	0.004	0.9	0.004	0.8	0.004	0.9	0.004
TREATED 60 MG/KG (AVERAGE)	196	28.8	0.16	38.7	0.2	4.1	0.02	5.6	0.03	1.9	0.01	4.2	0.02
FOLD INCREASE/ DECREASE			1.4x LOWER		1.55x HIGHER		5.4x HIGHER		7.6x HIGHER		2.7x HIGHER		6x HIGHER

Control samples *n*=3 and treated samples *n*=3.

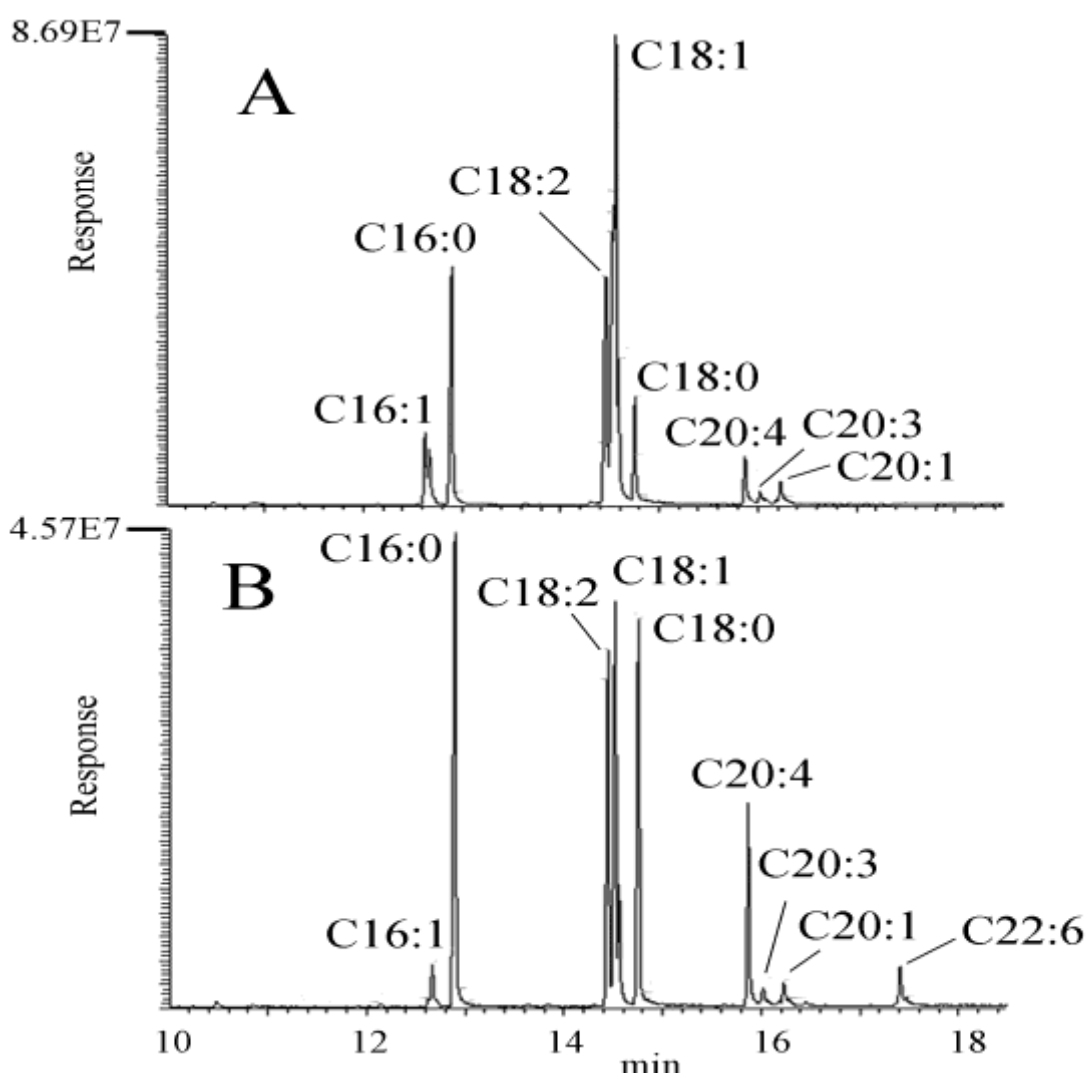
PC = phosphatidylcholine, TG = triacylglycerol.

#### 4.4.2. Analysis of Fatty Acids by GC-MS

In order to confirm that there were increased levels of particular fatty acids in response to drug treatment, GC-MS was used to further investigate the fatty acid composition of liver tissue samples. It was clear from the MALDI-MS results that lipids were altered by the drug treatment. In order to illustrate the changes in fatty acid composition samples from livers treated with the highest dose of the drug

(60 mg/kg) and controls were analysed in this experiment; the other dose levels were not examined. Total ion chromatogram (TIC) traces from control and 60 mg/kg treated samples are shown and it can be seen that drug treatment alters intensities of several fatty acids (Figure 122).

**Figure 122 - Gas chromatography-mass spectrometry (GC-MS) total ion chromatogram (TIC) traces from 10-18 mins showing fatty acid methyl esters (FAMES) in liver tissue samples from livers treated with either a) 60 mg/kg drug or b) saline (control).**



It was possible to identify 9 major fatty acid methyl esters (FAMES) from liver samples (Table 12). There were changes in peak areas corresponding to FAMES in drug treated samples compared to control samples. The highest increases appeared to be in methyl palmitoleate (C16:1), methyl oleate (C18:1) and methyl gondoate (C20:1).



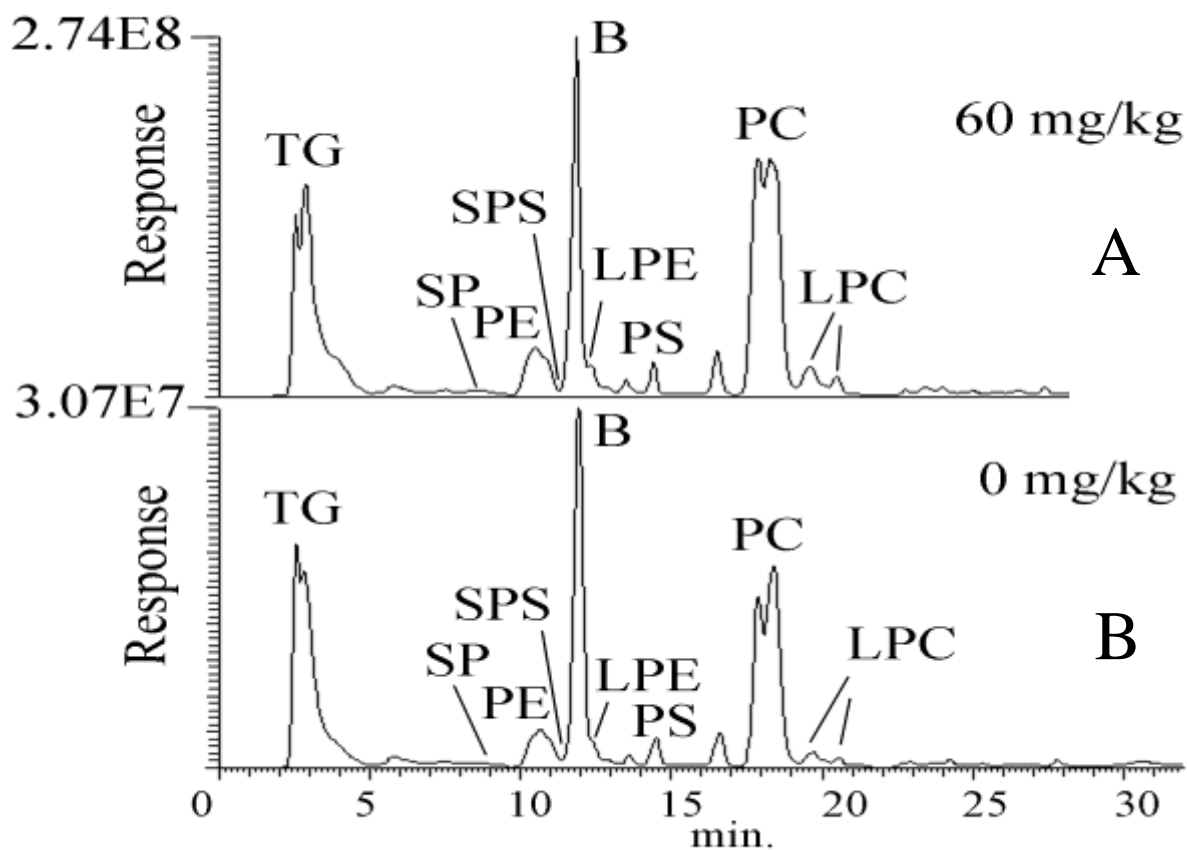
**Table 12 – Summary table showing fatty acid methyl esters (FAMES) found using gas chromatography mass spectrometry (GC-MS) from the analysis of liver samples taken from animals treated with either 60 mg/kg of drug or saline (control). Table shows common name of the fatty acid methyl ester, fatty acid carbon number with number of double bonds, retention time and ratio of increase of fatty acid level in 60 mg/kg treated samples.**

<b>FAME (Common Name)</b>	<b>Carbon Number</b>	<b>Retention Time</b>	<b>Ratio Treated/Untreated</b>
Methyl palmitoleate	C16:1	12.6-12.7	5.3
Methyl palmitate	C16:0	12.9-12.95	1.9
Methyl linoleate	C18:2n-6	14.4-14.50	2.6
Methyl oleate	C18:1n-9	14.5-14.6	8.0
Methyl stearate	C18:0	14.75-14.8	1.1
Methyl arachadonate	20:4n-6	15.85-15.90	1.2
Methyl-dihomo $\gamma$ – linoleate	20:3n-6	16.0-16.05	2.6
Methyl gondoate	C20:1n-9	16.20-16.23	5.8
Methyl docosahexanoate	22:6n-3	17.40-17.45	0.8

#### 4.4.3. Analysis of Lipids by LC-MS

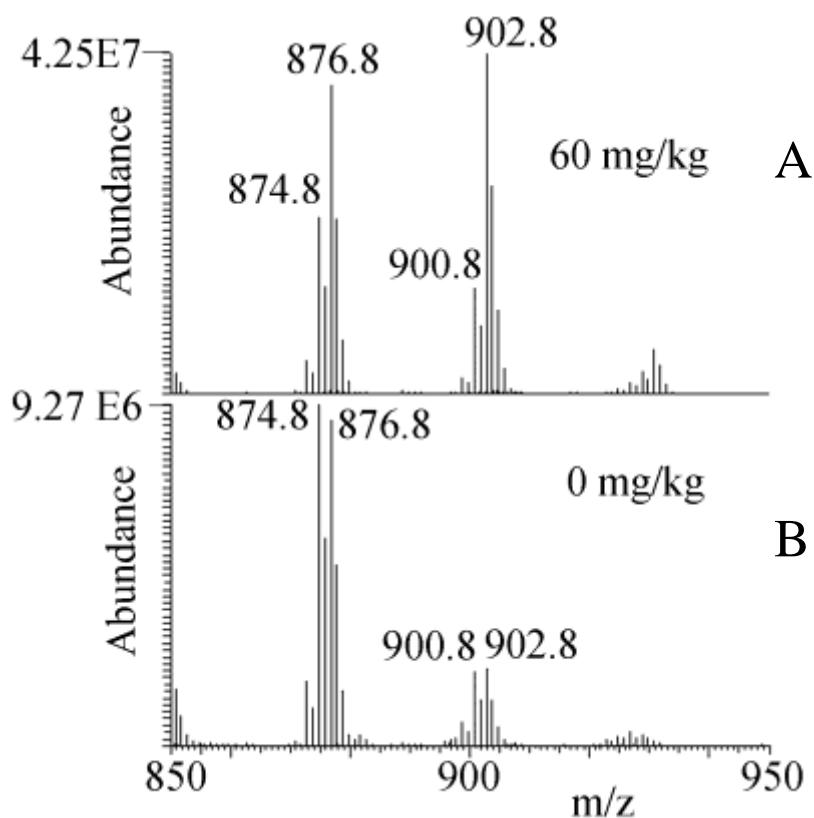
In order to further investigate the findings from the MALDI-MS experiments that showed there were increased levels of saturated TAGs or PCs in response to drug treatment, LC-MS was used to profile the composition of these TAGs and PCs, with fragmentation experiments being used to deduce their fatty acid composition to see if any particular fatty acids were upregulated in response to drug treatment. Samples from liver treated with the highest dose of the drug (60 mg/kg) or controls were analysed in this experiment; the other dose levels were not analysed in this mode. Samples were analysed using the LTQ-Orbitrap employing a method recently developed in our laboratory using a silica gel column operated in HILIC mode [382]. TAGs were observed with a RT between 2-3 minutes, close to the void volume of the column (Figure 123). The TAGs were observed as ammonium adducts due to use of ammonium formate in the mobile phase. It can be seen from Figure 123 that there were higher levels of TAGs and PC lipids in the treated samples but otherwise the total lipid profiles were quite similar.

Figure 123 - Total lipid profiles obtained using liquid chromatography mass spectrometry (LC-MS) in positive ion ESI mode from analysis of liver samples taken from animals treated with either a) 60 mg/kg of LXR agonist or b) saline (control). Separation carried out on a silica gel column. TG = triacylglycerol, B = system peak, PE = phosphatidylethanolamine, SPS = sphinganine, LPE = lysophosphatidylethanolamine, PS = phosphatidylserine, PC = phosphatidylcholine, LPC = lysophosphatidylcholine.



The ion cluster for the TAGs is shown in Figure 124 and confirms the MALDI-MS profile where the relative level of saturation of the TAGs in the drug treated sample is increased.

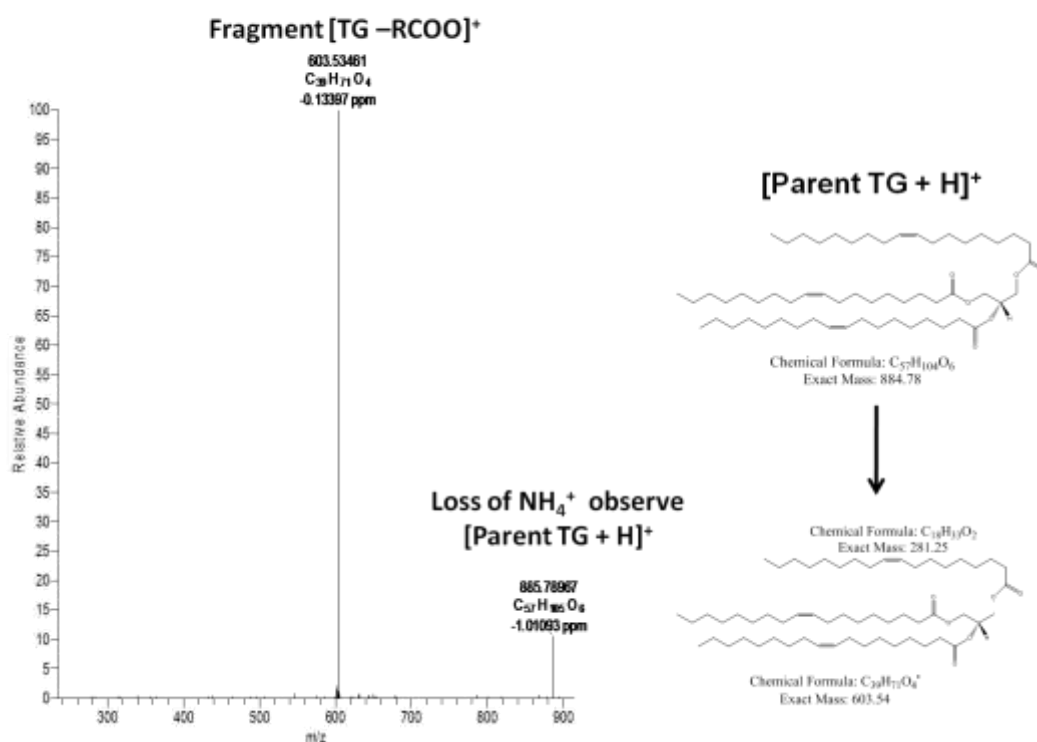
**Figure 124 - Triacylglycerol profiles observed as their ammonium adducts using liquid chromatography mass spectrometry (LC-MS) in positive ion ESI mode from analysis of lipid fractions from liver samples taken from animals treated with either a) 60 mg/kg of LXR agonist or b) saline (control). The overall levels of the TAGs and the relative level of lipid saturation are increased in response to drug treatment.**



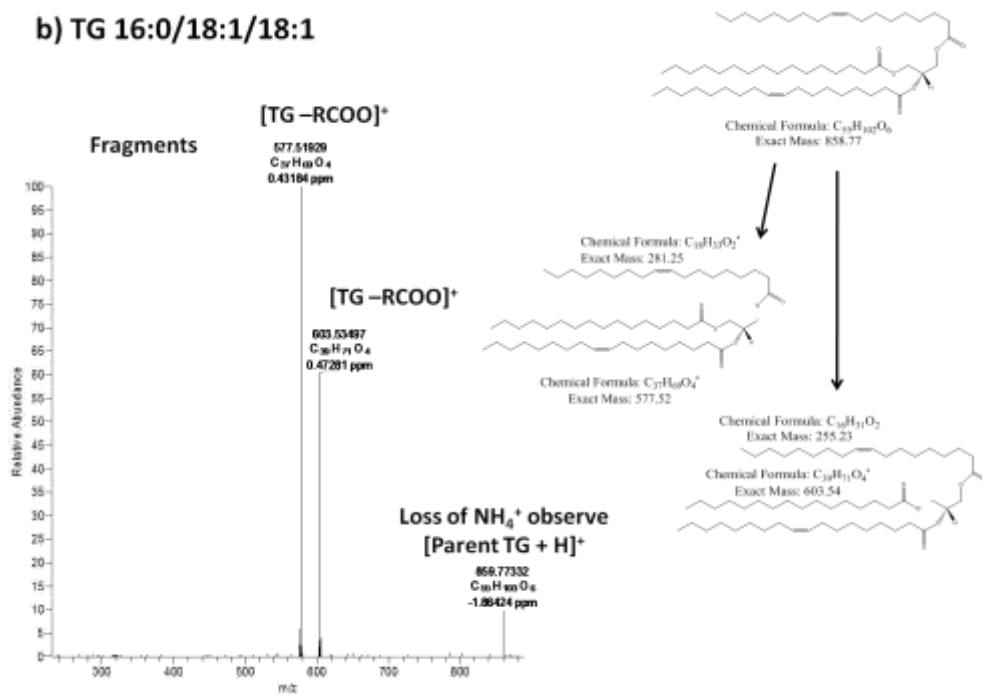
The MS<sup>2</sup> spectra confirmed that these peaks observed with retention time of 2-4 mins were in fact triacylglycerols as DAG fragments were observed as [TG-RCOO]<sup>+</sup>. The MS<sup>2</sup> spectra also confirmed their substitution pattern which indicated that they were rich in C18:1, oleic fatty acids (Figure 125).

Figure 125 – MS2 spectra of three triacylglycerol lipids observed in positive ion ESI mode as ammonium adducts illustrating they are rich in C18:1 Oleic fatty acids a) shows triacylglycerol 18:1/18:1:18:1 which has single fragment at  $m/z$  603 corresponding to the loss of one oleic acid fatty acid. B) shows triacylglycerol 16:0/18:1/18:1 with two fragments at  $m/z$  577 and 603 corresponding to the loss of one palmitic acid chain or one oleic acid chain, respectively, whilst c) shows 16:1/18:1/18:1 with fragments at  $m/z$  575 and  $m/z$  603 corresponding to the loss of one palmitoleic acid fatty acid.

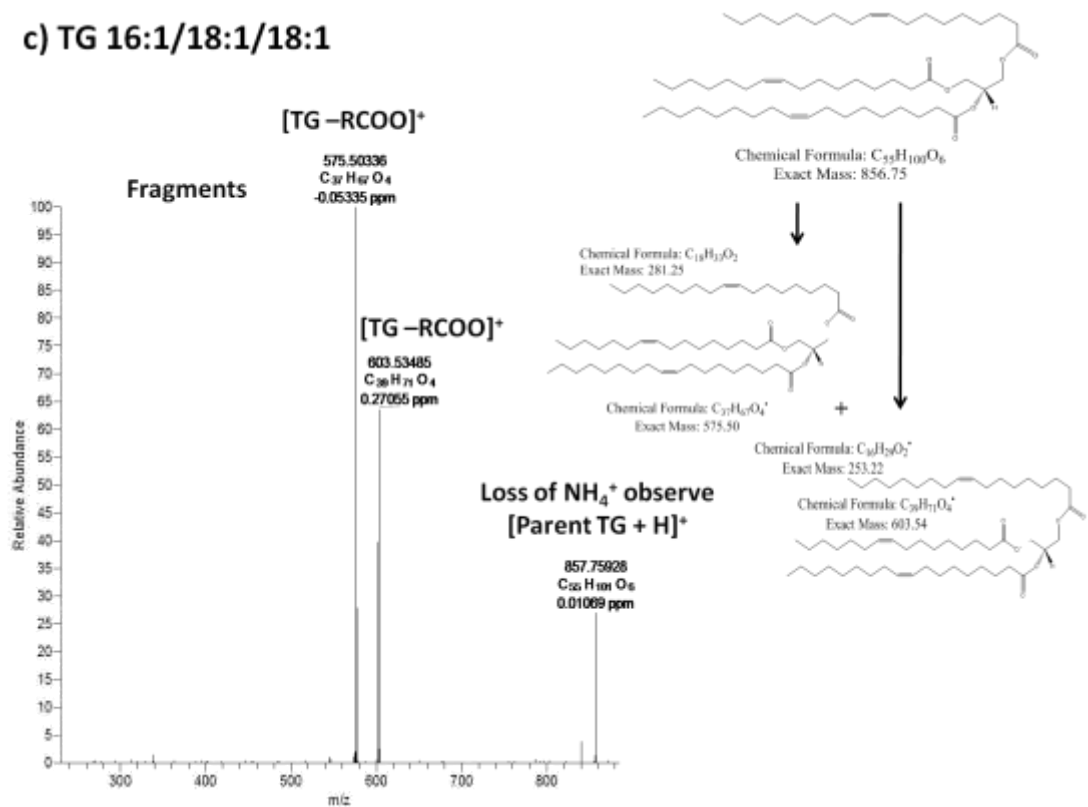
a) TG 18:1/18:1/18:1



**b) TG 16:0/18:1/18:1**



**c) TG 16:1/18:1/18:1**



From results of the MS<sup>2</sup> experiments, it was possible to tentatively assign the substitution pattern of the four main triacylglycerols that were found to be upregulated from MALDI-MSI analysis (Figure 126). By looking at the fold increases in these lipids that were calculated in Table 11, it can be seen that the triacylglycerol that had the highest fold increase (7.6 fold increase) (TG3) contains three monounsaturated oleic fatty acids, suggesting that the synthesis of oleic acid is important and is affected following LXR treatment.

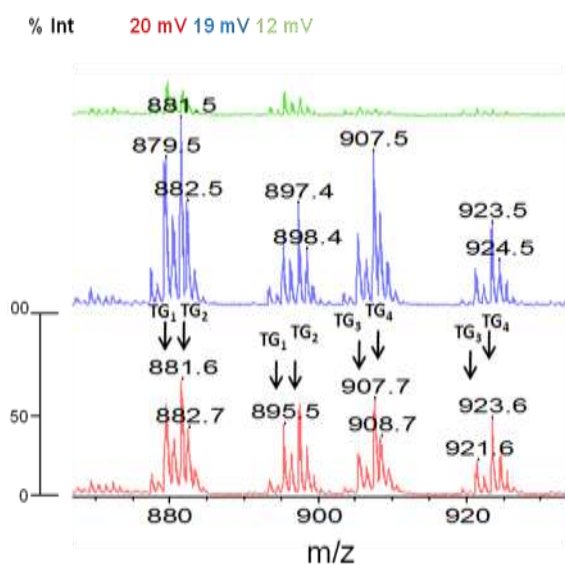


**Figure 126 – Tentative assignment of four triacylglycerols observed following MALDI-MSI analysis of drug treated liver confirmed through LC-MS analysis, i) shows tentative assignment and fatty acid composition, mass, formula and adducts observed in MALDI-MSI and LC-MS analysis modes whilst ii) illustrates the four clusters observed by MALDI-MSI in liver treated with  $\mu\mu$ 60 mg/kg of drug versus control and tentative assignments.**

<b>i)</b> <b>Tentative Assignment and Fatty Acid Composition</b>	<b>Mass</b>	<b>Formula</b>	<b>MALDI</b>		<b>LC-MS <i>m/z</i></b>
			<b><i>m/z</i></b>		
			<b>[M+Na]<sup>+</sup></b>	<b>[M+K]<sup>+</sup></b>	<b>[M+NH<sub>4</sub>]<sup>+</sup></b>
<b>TG 1</b> 1-hexadecanoyl-2,3-di-(9Z-octadecenoyl)-sn-glycerol (C16:0/18:1/18:1)	858.77	C <sub>55</sub> H <sub>102</sub> O <sub>6</sub>	881.8	897.8	876.8
<b>TG 2</b> 1,2,3-tri-(9Z-octadecenoyl)-glycerol (Triolein) (C18:1/18:1/18:1)	884.78	C <sub>57</sub> H <sub>104</sub> O <sub>6</sub>	907.9	923.9	902.8
<b>TG 3</b> 1,2-di-(9Z-octadecenoyl)-3-(9Z,12Z-octadecadienoyl)-sn-glycerol (C18:1/18:1/18:2)	882.77	C <sub>57</sub> H <sub>102</sub> O <sub>6</sub>	905.9	921.8	900.8

<b>TG 4</b> 1-(9Z-hexadecenoyl)-2,3-di-(9Z-octadecenoyl)-sn-glycerol (16:1/18:1/18:1)	856.75	$C_{55}H_{100}O_6$	879.8	895.8	874.8
---	--------	--------------------	-------	-------	-------

**ii) MALDI MSI Spectra**



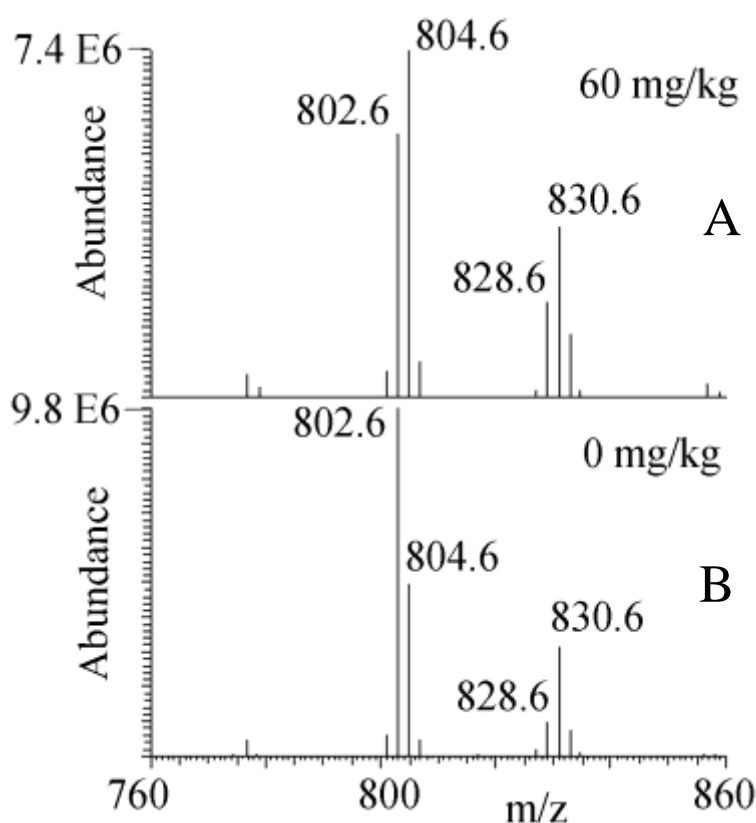
c) Control

b) 60 mg/kg

a) 60 mg/kg

This pattern of increased saturation in response to the drug is also reflected in the PC lipids (Figure 127). The PC lipids shown in Figure 127 at  $m/z$  802 and  $m/z$  804 are in the form of negatively charged formic acid adducts which correspond to PC lipids observed at  $m/z$  758 and  $m/z$  760 in positive ionisation mode.

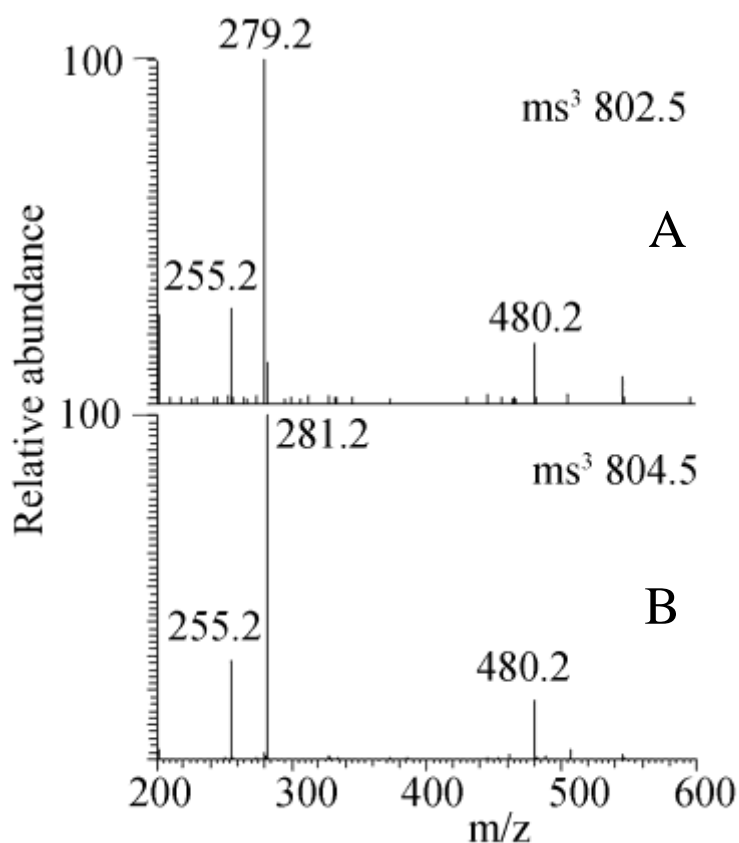
Figure 127 - Phosphatidylcholine lipid profiles observed using liquid chromatography mass spectrometry (LC-MS) in negative ion ESI mode where they form formic acid adducts from analysis of non polar fractions from liver samples taken from animals treated with either a) 60 mg/kg of LXR agonist or b) saline (control). The relative level of saturation in the phosphatidylcholine lipids increases as a result of treatment. The observed changes in ratios reflect what was observed from MALDI-MS experiments. The ions observed at  $m/z$  802.6 and 804.6 corresponds to the ions observed at  $m/z$  758 in positive and  $m/z$  760 in positive ionisation modes, respectively.



MS<sup>3</sup> analysis of two of the main PC lipids at  $m/z$  802 and 804 gave spectra (Figure 128) confirming that the lipids at  $m/z$  802 had C16:0, C18:2 fatty acids and the lipid at  $m/z$  804 had C16:0, C18:1 fatty acids. This reflected the overall lipid profile

obtained by GC-MS where the levels of oleic acid (18:1) were greatly increased in the drug treated samples.

**Figure 128 - MS<sup>3</sup> fragmentation of two of the phosphatidylcholine lipids observed in negative ion ESI mode as formic acid adducts at (a) *m/z* 802.5 and at (b) *m/z* 804.5. Masses at *m/z* 802 and *m/z* 804 showed changes in relative abundance as the result of drug treatment. Fragmentation experiments confirm their fatty acid composition, fragments observed at *m/z* 279.2 corresponds to C18:2 (linoleic acid), *m/z* 281.2 corresponds to C18:1 (oleic acid) and *m/z* 255 corresponds to C16:0 (palmitic acid).**



#### 4.4.4. Analysis of Polar Metabolites by LC-MS

It was also possible to identify a wide range of metabolites in the polar extracts. In this case all the dose levels were analysed (0, 0.3, 3, 10, 30 and 60 mg/kg) in order to test the stability of any metabolic changes observed. Analysis of the total ion chromatograms with the SIEVE 1.2 programme showed that a large number of polar metabolites had altered peak intensities in response to drug treatment. SIEVE compares the intensities of peaks, in control samples that in turn correspond to different metabolites, against those of treated samples, calculating a P-value and ratio based on the difference between them. A separate SIEVE analysis was conducted on control samples against each different dose of drug, and as for MALDI-MS data, results are shown for all doses (Table 13). This way, P-values and ratios were obtained for metabolites of interest, showing how their levels changed in response to dose. A significant P-value is taken as  $P < 0.05$ . Table 2 summarises a list of 47 metabolites that were found to be significantly altered in the samples at more than one dose level. The molecules in table 2 were assigned in the first instance by searching the exact masses against a compound list using an Excel based in-house macro into which the SIEVE data was pasted. In addition, the ZIC-HILIC column used was characterised by using 90 standards for common biomolecules in order to establish retention times. A useful feature of the ZIC-HILIC column is that there are quite clear structural features which govern elution time [384]. As can be seen in the table a large number of metabolites are altered but not always consistently. In order to select stable changes the following model is proposed. Stable biomarkers should have a P-value  $< 0.05$  at each dosage point where significance is first observed and their ratio against the control should trend in a consistent direction  $\pm 30\%$ . This

criterion reduces the list of potential markers to 9 compounds which are discussed below.

Hydroxymethylglutaryl carnitine (HMGC) and methylglutaryl carnitine (MGC) were not present or barely detectable in the untreated livers but could be clearly observed in the treated livers are robust markers. Extracted ion traces are shown illustrating the HMGC peak in liver samples from animals treated with several doses of the drug (Figure 129). Figure 129 shows the emergence of the peak for HMGC as dose increases which provides a sensitive indicator of drug effect increasing slightly even with the lowest dose of 0.3 mg/kg. In the absence of standards these compounds were also characterised by MS<sup>2</sup> and MGC gave a characteristic loss of 59 amu due to loss of the N(CH<sub>3</sub>)<sub>3</sub> group (Figure 131). HMGC and MGC also show a characteristic fragment at *m/z* 85 which corresponds to the loss of a butyl ester (C<sub>4</sub>H<sub>5</sub>O<sub>2</sub>) (Figure 130) and (Figure 131).

**Figure 129 - Extracted ion traces showing increasing levels of hydroxymethylglutaryl carnitine (HMGC) with dosage from analysis of polar extracts taken from rat liver tissue sections taken from animals treated with either a) saline (control), b) 0.3 mg/kg, c) 3 mg/kg, d) 30 mg/kg or e) 60 mg/kg of the drug once per day over a 5 day period using LTQ-Orbitrap in HILIC Mode.**

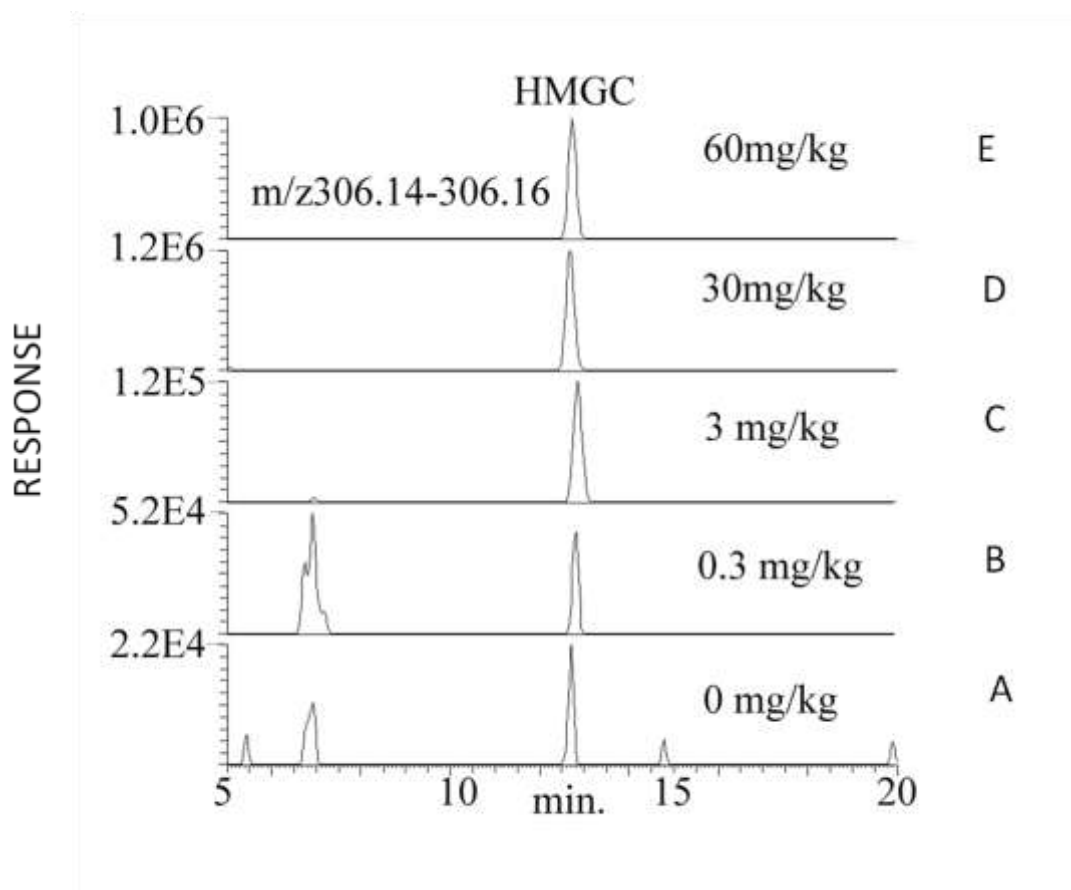


Figure 130 – MS<sup>2</sup> of Hydroxymethylglutaryl carnitine from analysis of polar extracts taken from rat liver tissue sections taken from animals treated with 60 mg/kg of the drug once per day over a 5 day period using LTQ-Orbitrap in HILIC Mode.

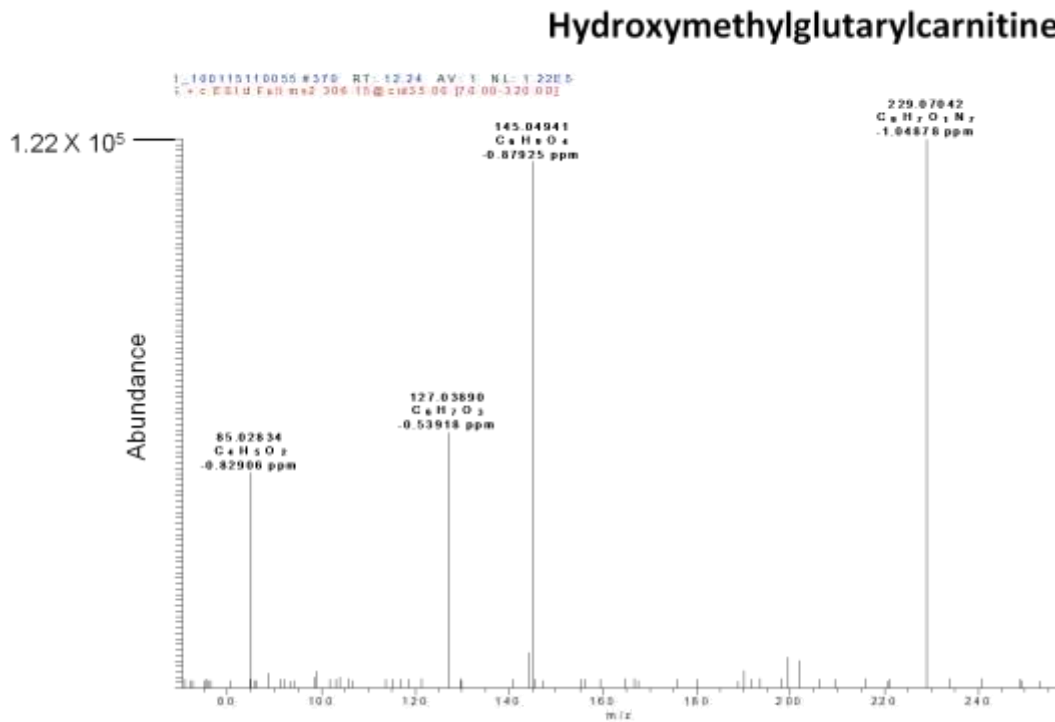
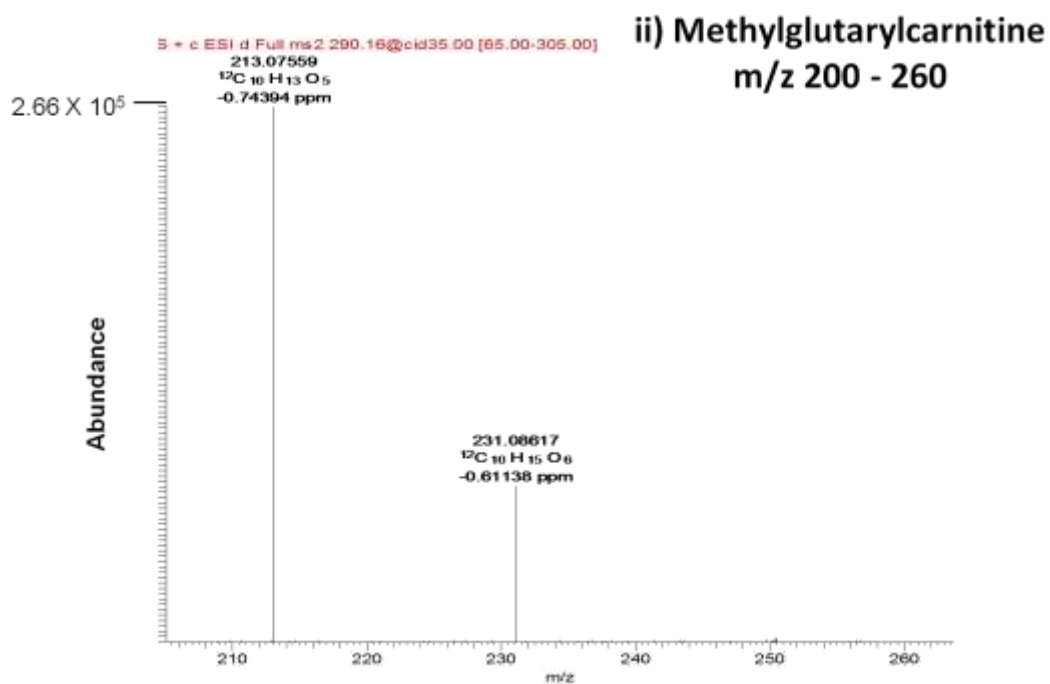
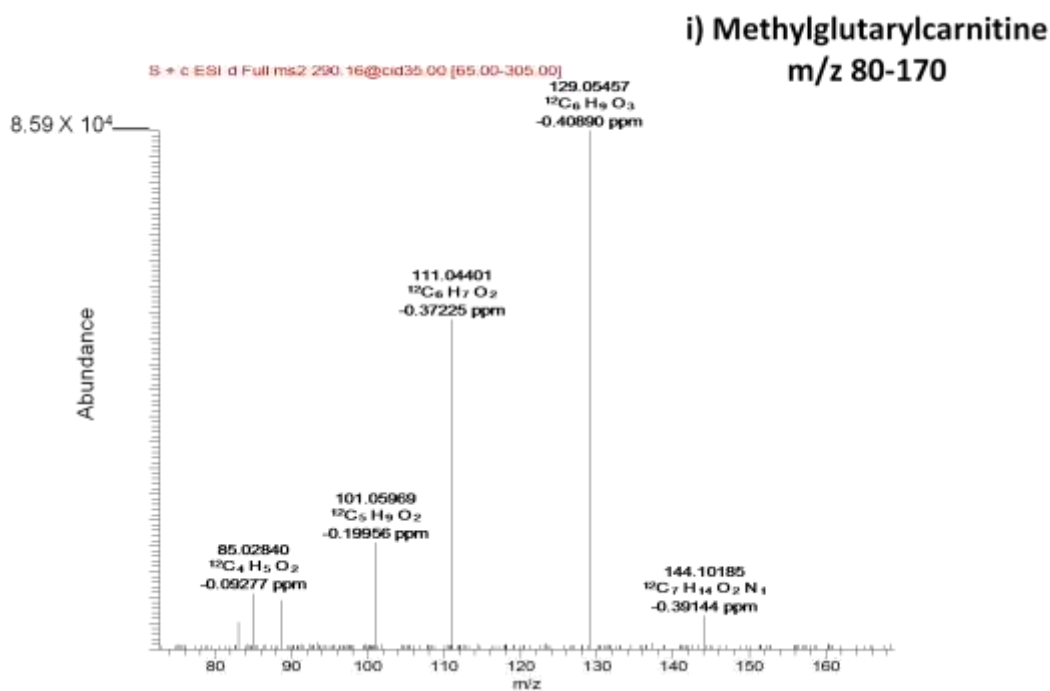




Figure 131 – MS<sup>2</sup> of Methylglutarylcarnitine from analysis of polar extracts taken from rat liver tissue sections taken from animals treated with 60 mg/kg of the drug once per day over a 5 day period using LTQ-Orbitrap in HILIC Mode i) mass range *m/z* 80-170 and ii) *m/z* 200-260.



Acetyl carnitine and propionyl carnitine exhibited variable levels in relation to dose and although there may be some interesting biology behind this they are not reliable markers of drug dose response (Table 13). Levels of free carnitine were also elevated in response to drug treatment and it is another robust marker. There was an increase in the levels of phosphocholine which is a robust marker of dose response. In contrast, choline which is also a degradation product of phospholipids, is less reliable as judged by a variable ratio and P-value significance. Other robust markers judged according to the criteria outlined above were: alanine, hypoxanthine, guanine and propionyl choline . The following compounds were close to fulfilling the criteria: hypotaurine, asparagine, glutamine, methionine and O-acetylhomoserine.

**Table 13 - Table summarising a selection of polar metabolites that were found to be altered in response to drug treatment from analysis of polar metabolites extracted from livers taken from animals treated with either 0.3, 1, 3, 10, 30 or 60 mg/kg of drug showing elemental composition, tentative assignment, P-Values ( $n=4$  at each dose level) and ratios calculated by SIEVE.**

<i>m/z</i>	Assignment	RT (min.)	P-Value 60 mg	Ratio 60 mg	P-Value 30 mg	Ratio 30 mg	P-Value 10 mg	Ratio 10 mg	P-Value 3 mg	Ratio 3 mg	P-Value 1 mg	Ratio 1mg	P-Value 0.3 mg	Ratio 0.3 mg
76.0393	Glycine	15.9	$8.9 \times 10^{-6}$	1.9	$5.9 \times 10^{-2}$	1.3	$2.7 \times 10^{-2}$	0.6	$2.8 \times 10^{-1}$	0.8	$6.1 \times 10^{-1}$	0.9	$3.0 \times 10^{-2}$	0.9
90.05496	Alanine	15.0	$3.1 \times 10^{-5}$	3.0	$2.0 \times 10^{-2}$	3.0	$4.8 \times 10^{-2}$	1.3	$7.6 \times 10^{-3}$	1.6	$5.7 \times 10^{-3}$	2.1	$1.4 \times 10^{-3}$	1.3
104.1069	Choline	15.9	$2.9 \times 10^{-5}$	3.8	$1.3 \times 10^{-1}$	0.8	$4.4 \times 10^{-3}$	0.3	$1.2 \times 10^{-2}$	0.6	$7.3 \times 10^{-3}$	0.6	$7.6 \times 10^{-3}$	1.04
106.0499	Serine	16.0	$7.0 \times 10^{-7}$	2.8	$5.4 \times 10^{-2}$	1.3	$1.9 \times 10^{-2}$	0.4	$6.7 \times 10^{-3}$	0.4	$4.9 \times 10^{-2}$	0.6	$1.1 \times 10^{-3}$	1.2
110.02703	Hypotaurine	14.8	$2.0 \times 10^{-2}$	1.8	$1.3 \times 10^{-2}$	3.6	$1.2 \times 10^{-3}$	2.5	$4.4 \times 10^{-2}$	2.3	$3.5 \times 10^{-3}$	2.2	$1.6 \times 10^{-2}$	0.8
116.0706	Proline	13.9	$3.6 \times 10^{-6}$	2.0	$1.4 \times 10^{-2}$	1.5	$3.3 \times 10^{-2}$	0.4	$1.7 \times 10^{-2}$	0.5	$3.4 \times 10^{-2}$	0.6	$4.8 \times 10^{-3}$	1.2
118.0862	Valine	12.8	$1.2 \times 10^{-5}$	2.5	$5.0 \times 10^{-2}$	1.4	$8.7 \times 10^{-2}$	0.7	$1.5 \times 10^{-2}$	0.7	$2.5 \times 10^{-1}$	0.9	$3.0 \times 10^{-2}$	1.08
120.0655	Threonine	15.1	$5.7 \times 10^{-5}$	2.7	$2.5 \times 10^{-2}$	1.4	$3.1 \times 10^{-2}$	0.4	$6.7 \times 10^{-4}$	0.5	$6.6 \times 10^{-2}$	0.7	$3.5 \times 10^{-2}$	1.1

126.02184	Taurine	14.6	$1.7 \times 10^{-4}$	1.4	$7.1 \times 10^{-2}$	1.3	$1.9 \times 10^{-1}$	1.1	$9.8 \times 10^{-3}$	1.2	$5.1 \times 10^{-2}$	1.2	$1.3 \times 10^{-1}$	0.9
132.1019	Leucine	11.1	$1.6 \times 10^{-6}$	3.5	$1.06 \times 10^{-1}$	1.3	$2.9 \times 10^{-2}$	0.5	$3.3 \times 10^{-3}$	0.6	$3.0 \times 10^{-2}$	0.6	$9.6 \times 10^{-3}$	1.2
133.0608	Asparagine	16.0	$2.3 \times 10^{-4}$	6.2	$1.6 \times 10^{-3}$	1.9	$5.0 \times 10^{-2}$	0.5	$6.6 \times 10^{-1}$	0.9	$3.0 \times 10^{-1}$	0.8	$1.0 \times 10^{-2}$	1.4
133.0972	Ornithine	25.3	$3.2 \times 10^{-4}$	4.4	$1.4 \times 10^{-1}$	1.7	$7.6 \times 10^{-2}$	0.6	$1.6 \times 10^{-2}$	0.6	$8.9 \times 10^{-1}$	0.97	$1.2 \times 10^{-1}$	1.2
134.0442	Aspartic acid	15.2	$4.4 \times 10^{-4}$	4.2	$2.6 \times 10^{-1}$	1.3	$8.0 \times 10^{-2}$	1.1	$3.0 \times 10^{-1}$	1.1	$5.9 \times 10^{-2}$	1.5	$1.9 \times 10^{-1}$	1.03
137.04575	Hypoxanthine	9.5	$1.0 \times 10^{-6}$	2.2	$7.0 \times 10^{-3}$	2.1	$2.30 \times 10^{-2}$	0.4	$2.3 \times 10^{-3}$	0.5	$6.2 \times 10^{-2}$	0.6	$6.1 \times 10^{-2}$	1.2
147.0764	Glutamine	15.5	$3.0 \times 10^{-5}$	6.1	$8.4 \times 10^{-2}$	2.0	$5.3 \times 10^{-2}$	1.3	$2.3 \times 10^{-3}$	1.7	$1.1 \times 10^{-1}$	1.3	$5.8 \times 10^{-1}$	1.2
147.1128	Lysine	25.2	$1.8 \times 10^{-4}$	3.7	$1.0 \times 10^{-1}$	1.8	$8.2 \times 10^{-2}$	0.6	$1.2 \times 10^{-1}$	0.8	$9.7 \times 10^{-1}$	1.008	$1.8 \times 10^{-1}$	1.06
148.0605	Glutamic acid	14.7	$1.9 \times 10^{-4}$	2.9	$5.7 \times 10^{-3}$	2.2	$8.0 \times 10^{-1}$	0.95	$3.4 \times 10^{-3}$	0.6	$1.3 \times 10^{-1}$	0.6	$3.9 \times 10^{-1}$	0.9
150.0584	Methionine	12.0	$3.6 \times 10^{-7}$	3.0	$4.2 \times 10^{-2}$	1.5	$2.0 \times 10^{-2}$	0.3	$1.1 \times 10^{-4}$	0.4	$4.5 \times 10^{-2}$	0.6	$4.0 \times 10^{-2}$	1.2
152.05675	Guanine	11.2	$8.6 \times 10^{-5}$	3.3	$5.4 \times 10^{-3}$	2.7	$5.4 \times 10^{-1}$	1.1	$6.7 \times 10^{-1}$	0.9	$1.1 \times 10^{-1}$	0.7	$9.8 \times 10^{-1}$	1.002
156.07672	L-Histidine	23.1	$1.6 \times 10^{-4}$	5.2	$6.6 \times 10^{-2}$	3.0	$2.0 \times 10^{-1}$	1.3	$3.8 \times 10^{-1}$	1.1	$1.1 \times 10^{-1}$	1.5	$2.2 \times 10^{-2}$	1.2
160.13319	Propionyl choline	13.1	$3.0 \times 10^{-4}$	2.5	$2.9 \times 10^{-4}$	3.4	$2.6 \times 10^{-2}$	2.6	$7.8 \times 10^{-2}$	2.7	$5.5 \times 10^{-3}$	1.9	$6.8 \times 10^{-1}$	0.9

162.07611	O-Acetyl-L-homoserine	14.0	$1.8 \times 10^{-4}$	6.8	$6.1 \times 10^{-2}$	8.6	$1.2 \times 10^{-2}$	0.2	$2.7 \times 10^{-3}$	0.2	$1.1 \times 10^{-2}$	0.2	$1.3 \times 10^{-2}$	1.5
162.11232	Carnitine	14.9	$4.7 \times 10^{-6}$	2.4	$1.9 \times 10^{-3}$	1.8	$1.4 \times 10^{-2}$	1.3	$2.7 \times 10^{-3}$	1.6	$1.6 \times 10^{-2}$	1.4	$1.8 \times 10^{-1}$	1.1
166.0863	Phenylalanine	10.5	$2.9 \times 10^{-7}$	3.4	$3.8 \times 10^{-2}$	1.6	$4.4 \times 10^{-2}$	0.4	$3.3 \times 10^{-3}$	0.6	$7.5 \times 10^{-2}$	0.7	$3.5 \times 10^{-3}$	1.2
168.04379	Taurocyamine	14.1	$6.6 \times 10^{-5}$	1.8	$4.7 \times 10^{-2}$	2.3	$7.8 \times 10^{-1}$	0.96	$5.8 \times 10^{-2}$	1.7	$1.0 \times 10^{-2}$	2.4	$5.1 \times 10^{-2}$	0.9
176.10303	Citrulline	16.4	$2.8 \times 10^{-3}$	2.3	$1.1 \times 10^{-3}$	3.2	$7.2 \times 10^{-2}$	1.7	$6.3 \times 10^{-1}$	1.4	$2.0 \times 10^{-2}$	2.4	$2.8 \times 10^{-1}$	1.4
182.0811	Tyrosine	12.7	$8.0 \times 10^{-4}$	1.8	$9.7 \times 10^{-1}$	1.01	$1.3 \times 10^{-2}$	0.3	$7.7 \times 10^{-3}$	0.6	$3.4 \times 10^{-2}$	0.7	$1.6 \times 10^{-2}$	1.07
184.07338	Phosphocholine	19.7	$9.6 \times 10^{-3}$	5.1	$5.0 \times 10^{-2}$	5.6	$3.5 \times 10^{-3}$	3.3	$1.8 \times 10^{-2}$	3.4	$1.2 \times 10^{-2}$	2.1	$8.4 \times 10^{-2}$	0.5
204.1231	Acetylcarnitine	12.2	$7.3 \times 10^{-6}$	0.04	$3.1 \times 10^{-4}$	21.5	$5.6 \times 10^{-1}$	1.5	$4.5 \times 10^{-2}$	1.5	$3.2 \times 10^{-2}$	1.3	$1.9 \times 10^{-1}$	0.5
205.0972	Tryptophan	11.1	$1.5 \times 10^{-8}$	3.4	$1.2 \times 10^{-1}$	1.6	$9.1 \times 10^{-3}$	0.5	$5.3 \times 10^{-3}$	0.6	$7.6 \times 10^{-2}$	0.7	$3.0 \times 10^{-2}$	1.1
218.13861	Propionyl carnitine	12.0	$1.9 \times 10^{-1}$	1.3	$8.7 \times 10^{-6}$	39.5	$1.8 \times 10^{-2}$	23.3	$1.2 \times 10^{-2}$	2.7	nd	nd	$8 \times 10^{-4}$	0.4
262.1649	Hydroxyvaleryl carnitine	11.9	$1.2 \times 10^{-3}$	16.3	$2.5 \times 10^{-3}$	3.1	$3.0 \times 10^{-1}$	1.3	$2.4 \times 10^{-2}$	2.4	$2.5 \times 10^{-2}$	1.7	$2.4 \times 10^{-1}$	1.3
269.0881	Inosine	9.5	$1.5 \times 10^{-5}$	2.2	$6.7 \times 10^{-4}$	2.2	$3.0 \times 10^{-2}$	0.4	$4.2 \times 10^{-3}$	0.6	$8.9 \times 10^{-2}$	0.7	$6.9 \times 10^{-1}$	1.08

284.09906	Guanosine	11.2	$4.0 \times 10^{-4}$	2.6	$7.9 \times 10^{-4}$	4.4	$3.0 \times 10^{-2}$	0.5	$9.2 \times 10^{-2}$	0.8	$6.3 \times 10^{-1}$	0.9	$3.3 \times 10^{-1}$	1.3
290.15982	Methylglutaryl carnitine	10.8	$1.2 \times 10^{-4}$	7.2	$1.0 \times 10^{-4}$	8.8	$4.9 \times 10^{-3}$	3.2	$7.5 \times 10^{-3}$	3.2	$2.1 \times 10^{-2}$	2.2	$3.3 \times 10^{-1}$	1.06
300.0843	Pantothenate	9.3	$2.6 \times 10^{-7}$	4.2	$1.6 \times 10^{-1}$	1.3	$1.7 \times 10^{-2}$	0.06	$1.6 \times 10^{-4}$	0.3	$2.0 \times 10^{-2}$	0.3	$5.6 \times 10^{-3}$	1.5
306.1548	Hydrox-Methylglutaryl carnitine	11.6	$5.3 \times 10^{-6}$	31	$1.4 \times 10^{-5}$	13.0	$2.1 \times 10^{-3}$	8.1	$3.0 \times 10^{-3}$	9.8	$4.21 \times 10^{-3}$	4.3	$4.0 \times 10^{-2}$	1.5
308.0909	Glutathione	13.5	$1.2 \times 10^{-6}$	2.0	$1.5 \times 10^{-2}$	3.7	$6.2 \times 10^{-2}$	1.6	$2.1 \times 10^{-2}$	1.5	$1.9 \times 10^{-2}$	1.8	$9.4 \times 10^{-1}$	0.997
324.0592	cytidine	17.0	$1.5 \times 10^{-4}$	2.6	$8.0 \times 10^{-2}$	2.4	$3.5 \times 10^{-1}$	0.9	$4.9 \times 10^{-2}$	0.6	$5.2 \times 10^{-2}$	1.7	$1.3 \times 10^{-1}$	0.95
349.0543	IMP	13.4	$2.0 \times 10^{-4}$	0.4	$2.9 \times 10^{-1}$	1.2	$6.4 \times 10^{-3}$	0.5	$1.8 \times 10^{-2}$	0.6	$2.2 \times 10^{-2}$	1.8	$4.4 \times 10^{-1}$	1.035
359.1037	Pantotheine 4'-phosphate	8.2	$3.3 \times 10^{-3}$	1.9	$8.3 \times 10^{-4}$	1.7	$8.5 \times 10^{-4}$	3.7	$2.1 \times 10^{-2}$	1.6	$3.5 \times 10^{-3}$	7.1	$7.1 \times 10^{-4}$	1.4
385.1288	S-Adenosyl-L-homocysteine	17.3	$1.5 \times 10^{-4}$	2.9	$5.3 \times 10^{-2}$	3.5	$8.4 \times 10^{-1}$	0.97	$4.5 \times 10^{-3}$	0.5	$5.1 \times 10^{-1}$	1.1	$5.9 \times 10^{-2}$	0.7
447.0678	CDP-ethanolamine	17.9	$7.7 \times 10^{-9}$	4.7	$6.6 \times 10^{-2}$	6.9	$2.8 \times 10^{-3}$	2.5	$1.5 \times 10^{-2}$	1.6	$1.5 \times 10^{-2}$	2.2	$1.3 \times 10^{-1}$	0.8
500.304	Taurodeoxycholate	4.5	$3.1 \times 10^{-1}$	1.9	$3.3 \times 10^{-2}$	0.15	$1.4 \times 10^{-3}$	0.4	$6.2 \times 10^{-1}$	0.95	$7.5 \times 10^{-1}$	0.95	$2.7 \times 10^{-1}$	2.5

516.2983	Taurocholate	4.9	$2.1 \times 10^{-1}$	5.2	$3.2 \times 10^{-2}$	0.13	$3.1 \times 10^{-2}$	0.2	$8.2 \times 10^{-2}$	0.2	$4.0 \times 10^{-2}$	0.4	$2.4 \times 10^{-1}$	3.4
608.0894	UDP-N-acetyl-D-glucosamine	16.1	$1.0 \times 10^{-4}$	3.1	$6.0 \times 10^{-5}$	2.2	$1.6 \times 10^{-2}$	1.5	$3.4 \times 10^{-2}$	1.2	$2.0 \times 10^{-2}$	1.8	$2.4 \times 10^{-2}$	0.7
613.1590	Glutathione Disulfide	18.3	$3.4 \times 10^{-3}$	2.8	$5.4 \times 10^{-2}$	2.3	$4.4 \times 10^{-5}$	0.2	$2.2 \times 10^{-6}$	0.3	$1.9 \times 10^{-3}$	0.5	$3.5 \times 10^{-2}$	0.6

## 4.5. Discussion

Increased levels of TAGs in liver have been demonstrated in many studies investigating hepatotoxicity [344,348,362,373]. In addition, increased lipid saturation in association with toxicity has also been described in a number of studies [344,348]. Increased levels of MUFAs have been observed as a result of paracetamol-induced hepatotoxicity and are thought to be the result of oxidative phosphorylation. Decreased levels of PUFAs are thought to be the result of increased peroxisomal activity increasing  $\beta$ -oxidation which arises in order to counteract depleted energy levels, indicating mitochondrial dysfunction and a compensatory increase in peroxisomal activity [348]. In the same study, depletion of phospholipids was shown but this was not the case in our study.

SREBP1c, which is under the control of the LXR receptor, has been shown to promote fatty acid elongase, which increases the chain length of a fatty acid by two methylene units e.g. C16:0 to C18:0 and also promotes mono-unsaturation at various positions in the fatty acid chain [383]. In the same study, the LXR agonist studied was found to have no effect on elongase and only promoted  $\Delta$ -9 unsaturation. The change in phospholipid profile in the liver may have nothing to do with a change in membrane composition and might reflect changes in composition of the bile which contains phospholipids and which is to some extent controlled by the LXR receptor [385]. Imaging of the liver indicated that there was no well-defined distribution of the lipids within the tissue (data not shown). It was also interesting to note that an



increase in TAG peak intensities were observed even in liver samples from animals treated with the lowest dose of drug compared to control.

The unusual carnitine metabolites hydroxymethylglutaryl carnitine (HMGC) and methylglutaryl carnitine (MGC) are not present or are barely detectable in the untreated livers but can be clearly observed in the treated livers and thus might provide good biomarkers of toxicity. A range of acyl carnitines including MGC was observed in a metabolomics study of plasma from fasted rats [363]. HMGC has been reported as a urinary metabolite in children who have an inborn error of metabolism caused by a deficiency of 3-hydroxy-3-methylglutaryl-coenzyme, a (HMGC<sub>CoA</sub>) lyase which produces acetoacetic acid and acetyl CoA [386]. HMGC<sub>CoA</sub> can arise either as a product of HMGC<sub>CoA</sub> synthase where it is required for the production of either terpenoids or ketone bodies [387] or as a product of leucine catabolism. The role of carnitine in tissues is as a buffer for acyl CoA/CoA levels. CoA is compartmentalised within the cell and cannot cross membranes thus, for instance, pools of intracellular CoA within peroxisomes or mitochondria are largely fixed [388]. Within mitochondria the transfer of an acyl group from acyl CoA to carnitine maintains the level of free CoA and allows the acyl group to enter or leave the organelle in the form of its carnitine ester. Carnitine palmitoyl transferase is present on the outer membrane of mitochondria and only selects long chain fatty acids for entry to mitochondria, however, the availability of a range of carnitine transferases within mitochondria and peroxisomes permits the export of fatty acids with different chain lengths out of these organelles [388]. For correct physiological functioning it is essential to maintain a balance between acylated and free CoA and carnitines are required to restore the balance. For example in the case of medium

chain fatty acid dehydrogenase deficiency where the metabolism of acyl CoA through to acetyl CoA is incomplete, the unmetabolised medium chain fatty acids are transported out of the mitochondria as acylcarnitines and then to the plasma for excretion. Such metabolic errors can thus be treated by administering L-carnitine. Since the LXR agonist is promoting fatty acid synthesis the liver is behaving as if glucose levels were high. Glucose metabolism in the mitochondria provides the acetyl group which is required for fatty acid biosynthesis which takes place in the cytoplasm via the formation of acetyl CoA. Where HMGCoA lyase activity, which produces acetate and the ketone body acetoacetate, is deficient it is likely that HMGC would be produced in order to maintain free levels of CoA. However, here is a paradox, one might expect up regulation of HMGCoA lyase in the current case since glucose is being channelled into lipid formation and thus an increase in ketone body formation would be required to compensate for this such as occurs in diabetes where tissues become glucose starved. The presence of elevated levels of hydroxyvaleryl carnitine (which is highly elevated at the two highest drug doses), which is in the pathway of leucine degradation, suggests that this pathway is being affected by treatment with the LXR agonist. Leucine degradation takes place in the mitochondria and hydroxyvaleryl CoA is formed en route to HMGCoA which is then broken down to yield acetyl CoA and acetoacetate thus completing leucine catabolism. Thus either HMGCoA lyase activity is deficient or possibly leucine catabolism is up-regulated and this up-regulation is independent of HMGCoA synthase thus resulting in HMGCoA lyase activity being insufficient to breakdown the HMGCoA being produced. It would in fact be simpler to explain the elevation as

being due to reduction in the requirement for HMGCoA in the production of cholesterol.

One of the most intriguing changes in metabolic profile in the treated tissues is with regard to the increase in levels of UDP N-acetylglucosamine (UNGA) (Table 13). UNGA is involved in the transfer of an N-acetylglucosamine (NGA) moiety and modification of nucleocytoplasmic proteins by NGA has become recognised as a glucose sensing mechanism. A recent study comprehensively demonstrated that modification of LXR receptor proteins with NGA resulted in increased expression of the lipogenic gene SREBP1c [389]. In earlier work glucose had been proposed as a direct regulator of the LXR with elevated glucose levels thus triggering SREBP1c [390] but this is probably not the case. About 2-5% of glucose entering the cell is diverted into the hexosamine pathway via fructose 6-phosphate. It was found in the study [389] that upregulation of SREBP1c could be inhibited by inhibiting fructose 6-phosphate amido transferase. It has also been shown that the LXR can promote the production of a liver specific uridine phosphorylase [391]. Uridine phosphate levels were not elevated in the current study but of course uridine phosphate is required for formation of UNGA. It is possible that in the current study the drug is in some way mimicking a state where glucose levels are elevated and triggering NGA modification of the LXR which then leads to upregulation of lipid biosynthesis without glucose actually being elevated.

Cytidine diphosphate ethanolamine (CDPE) is elevated in the treated livers (Table 2) and almost fulfils the criteria for a stable marker. This is obviously linked in some way to the changes in phospholipid metabolism which can be observed in the tissues.

CPDE is required for the formation for phosphatidyl ethanolamine from diacylglycerols which can then be methylated to produce phosphatidyl cholines. Phosphocholine is consistently elevated in the treated samples although choline levels are less consistent and are lowered apart from at the highest dose. Methionine which is required for PC lipid biosynthesis is also elevated with increasing drug dose.

Increased levels of alanine observed are consistent with elevated levels of alanine amino acid transferase (ALT). This enzyme is one of the markers of liver toxicity and catalyses the transfer of amino group between glutamate and alanine. The reaction is reversible but lies in the direction of alanine which is believed may have a role in gluconeogenesis in glucose starved tissues [392]. The elevated levels of glutamate observed may also be linked to this. The elevation of the purines hypoxanthine, guanine and inosine with drug dose is difficult to explain on the basis of the information available at the present time.

#### **4.6. Conclusions and Future Work**

This study demonstrates that MALDI-MSI is a useful technique for drug research applications by the pharmaceutical industry. Advantages include ease of sample preparation; it is easy to collect data from several different conditions e.g. vehicle versus different drug treatments to deduce changes in small molecule composition in response to drugs. Samples are analysed directly following cryostat sectioning. No sample clean-up such as salt removal is required. It is particularly useful if a drug is thought to cause lipid upregulation as it can be used to take a 'quick look' at the lipid content of tissues in response to drug treatment. Conversely, it may also be a useful

screening tool if looking at drugs to lower lipid levels, e.g. to lower triacylglycerol levels. During drug research and development, assays are often utilised which allow overall levels of lipids e.g. triacylglycerols to be calculated. However, by using MALDI-MSI, it is possible to detect specific lipids that are affected by drug treatment. Additionally, conventional analysis of lipids by LC-MS utilises unfavourable solvents, requires long retention times and column bleeding may occur. GC-MS requires complex derivatisation steps. Thus, MALDI MS could be used as a complementary analytical tool alongside more conventional methods such as LC-MS and GC-MS during drug research projects. Of course, there are also limitations, it is difficult quantify changes, but by dividing the peak intensity of an ion of interest by intensity of the matrix peak to normalise data, a ratio will be obtained. Ratios of different lipids can be calculated allowing estimations of changes in lipid levels to be calculated.

The current study has demonstrated the utility of using a mixture of chromatographic and mass spectrometric approaches to total metabolic profiling. MALDI-MS is less commonly used in metabolomic profiling but has the potential to offer a rapid snapshot of alterations in lipid profiles since tissue homogenates could be loaded onto multi-well plates and this could be followed by automated acquisition taking a few seconds per sample. The information provided by the different approaches underlines the fact that a metabolomics approach can make putative biochemical connections that did not exist as prior hypotheses. Recurrent difficulties in metabolomics are in being able to have complete confidence in the stability of the changes observed. Confidence in the results obtained is greater where metabolic changes trend either up or down in response to treatment, as demonstrated by the

results in this study. Also greater confidence is obtained where the biochemical changes observed can be related to each other which is true to some extent of the results observed in this study.

## **Chapter 5 - General Project Summary**

## 5. General Project Summary

This project has illustrated how imaging mass spectrometry can be utilised as an analytical technique during drug research and development, enabling the spatial distribution and relative intensities of pharmaceuticals and endogenous compounds such as lipids and polar metabolites to be mapped *in situ*. This technique offers several advantages over other traditional imaging methods such as radiography which rely on the use of synthesised molecular probes which aren't readily available during drug research. By carrying out quantitative analysis using laser microdissection, it has also been shown that the use of a dry matrix coating enables the distribution of pharmaceuticals *in situ* to be reliably mapped, removing the possibility of analyte delocalisation associated with the use of a conventional wet matrix coating.

MALDI-MSI has also been used successfully for the identification of lipid biomarkers of drug-induced toxicity, illustrating that it is a useful high throughput screening tool during drug research and development that could potentially be utilised to identify toxicity markers at an earlier stage than conventional assays. Additionally, metabolomic profiling on the LTQ-orbitrap with HILIC chromatographic separation has enabled the identification of small molecule biomarkers of drug induced toxicity, with the LTQ-orbitrap providing excellent mass accuracy, resolution and sensitivity.

This work illustrates why mass spectrometry based analytical techniques such as imaging mass spectrometry and metabolomic studies using high-resolution mass spectrometers are now playing a pivotal role in drug research and development.



As limitations associated with imaging mass spectrometry are overcome, such as laser spot size, rastering and data collection speeds and sensitivity, the possible applications of MALDI-MSI will grow exponentially. It is now being illustrated that combining the benefits of a MALDI source with an LTQ-orbitrap mass analyser can combine the main advantages of both; spatial mapping capabilities of MALDI with the high resolution and mass accuracy of the LTQ-Orbitrap. Mapping the distribution of metabolites in single animal cells will undoubtedly be the next big challenge for imaging mass spectrometry as the possibility of *in situ* metabolomic profiling in single animal cells becomes a reality.

## 6. References

1. Chapman S: **Carrier Mobility Spectra of Spray Electrified Liquids.** *Physical Review* 1937, **10**:184-190.
2. Dole M, Mack LL, Hines RL, Mobley RC, Ferguson LD, Alice MB: **Molecular beams of macroions.** *Journal of Chemical Physics* 1968, **50**.
3. Mack L, L, Kralik P, Rheude A, Dole M: **Molecular beams of macroions II.** *Journal of Chemical Physics* 1970, **52**.
4. Yamashita M, Fenn JB: **Electrospray Ion Source. Another Variation on the Free-Jet Theme.** *Journal of Physical Chemistry* 1984, **88**.
5. Meng CK, Mann M, Fenn JB: **Of Protons and Proteins.** *Zeitschrift fur Physik D: Atoms, Molecules and Clusters* 1988, **10**:361-368.
6. Fenn JB, Mann M, Meng CK, Wong SF, Whitehouse CM: **Electrospray ionization for mass spectrometry of large biomolecules.** *Science* 1989, **246**:64-71.
7. Fenn JB: **Electrospray wings for molecular elephants (Nobel lecture).** *Angew Chem Int Ed Engl* 2003, **42**:3871-3894.
8. Taylor J: **Disintegration of Water Droplets in An Electric Field.** 1964.
9. Kebarle P, Ho Y: **The mechanism of electrospray mass spectrometry.** In *Electrospray ionisation mass spectrometry : fundamentals, instrumentation, practicalities & biological applications.* Edited by Cole RB: John Wiley and Sons; 1997:3-63.
10. Griffiths WJ, Jonsson AP, Liu S, Rai DK, Wang Y: **Electrospray and tandem mass spectrometry in biochemistry.** *Biochem J* 2001, **355**:545-561.
11. Iribarne J, Thompson B: **On the evaporation of small ions from charged droplets.** *J. Chem. Phys* 1976, **64**:2287-2294.
12. Atmospheric Pressure Chemical Ionisation (APCI) on World Wide Web URL: <http://www.chm.bris.ac.uk/ms/theory/apci-ionisation.html>
13. Emmett M, R, Caprioli R, M: **Micro-electrospray mass spectrometry: ultra-high-sensitivity analysis of peptides and proteins** *Journal of the American Society of Mass Spectrometry* 1994, **5**:605-613.
14. Wilm MS, Mann M: **Electrospray and Taylor-Cone theory, Dole's beam of macromolecules at last?.** *Int. J. Mass Spectrom. Ion Proc* 1994, **136**:167-180.

15. Wilm M, Mann M: **Analytical properties of the nanoelectrospray ion source.** *Anal Chem* 1996, **68**:1-8.
16. Zhang S, Van Pelt CK: **Chip-based nanoelectrospray mass spectrometry for protein characterization.** *Expert Rev Proteomics* 2004, **1**:449-468.
17. Sikanen T, Franssila S, Kauppila TJ, Kostianen R, Kotiaho T, Ketola RA: **Microchip technology in mass spectrometry.** *Mass Spectrom Rev* 2010, **29**:351-391.
18. Robbe C, Michalski JC, Capon C: **Structural determination of O-glycans by tandem mass spectrometry.** *Methods Mol Biol* 2006, **347**:109-123.
19. Hop CE: **Use of nano-electrospray for metabolite identification and quantitative absorption, distribution, metabolism and excretion studies.** *Curr Drug Metab* 2006, **7**:557-563.
20. Wickremsinhe ER, Singh G, Ackermann BL, Gillespie TA, Chaudhary AK: **A review of nanoelectrospray ionization applications for drug metabolism and pharmacokinetics.** *Curr Drug Metab* 2006, **7**:913-928.
21. Khatib-Shahidi S, Andersson M, Herman JL, Gillespie TA, Caprioli RM: **Direct molecular analysis of whole-body animal tissue sections by imaging MALDI mass spectrometry.** *Anal Chem* 2006, **78**:6448-6456.
22. Caprioli RM, Farmer TB, Gile J: **Molecular imaging of biological samples: localization of peptides and proteins using MALDI-TOF MS.** *Anal Chem* 1997, **69**:4751-4760.
23. Karas M, Bachmann, D and Hillenkamp, F: **Influence of the Wavelength in High-Irradiance Ultraviolet Laser Desorption Mass Spectrometry of Organic Molecules.** *Anal Chem* 1985, **57**:2935-2939.
24. Karas MB, D, Bahr, U, Hillenkamp, F.: **Matrix-Assisted Ultraviolet Laser Desorption of Non-Volatile Compounds.** *Int J Mass Spectrom Ion Proc* 1987, **78**:53-68.
25. Karas M, Hillenkamp F: **Laser desorption ionization of proteins with molecular masses exceeding 10,000 daltons.** *Anal Chem* 1988, **60**:2299-2301.
26. Tanaka K, Waki, H, Ido, Y, Akita, S, Yoshida, Y and Yoshida, T.: **Protein and Polymer Analyses up to  $m/z$  100 000 by Laser Ionization Time-of flight Mass Spectrometry.** 1988, **2**:151-153.
27. Beavis RC, Chait BT: **Cinnamic acid derivatives as matrices for ultraviolet laser desorption mass spectrometry of proteins.** *Rapid Commun Mass Spectrom* 1989, **3**:432-435.

28. Beavis RC, Chait BT: **Matrix-assisted laser-desorption mass spectrometry using 355 nm radiation.** *Rapid Commun Mass Spectrom* 1989, **3**:436-439.
29. Rujoi M, Estrada R, Yappert MC: **In situ MALDI-TOF MS regional analysis of neutral phospholipids in lens tissue.** *Anal Chem* 2004, **76**:1657-1663.
30. Reyzer ML, Caprioli RM: **MALDI mass spectrometry for direct tissue analysis: a new tool for biomarker discovery.** *J Proteome Res* 2005, **4**:1138-1142.
31. Benabdellah F, Touboul D, Brunelle A, Laprevote O: **In situ primary metabolites localization on a rat brain section by chemical mass spectrometry imaging.** *Anal Chem* 2009, **81**:5557-5560.
32. Fuchs B, Schiller J: **MALDI-TOF MS analysis of lipids from cells, tissues and body fluids.** *Subcell Biochem* 2008, **49**:541-565.
33. Hsieh Y, Li F, Korfmacher WA: **Mapping pharmaceuticals in rat brain sections using MALDI imaging mass spectrometry.** *Methods Mol Biol* 2010, **656**:147-158.
34. Hsieh Y, Chen J, Korfmacher WA: **Mapping pharmaceuticals in tissues using MALDI imaging mass spectrometry.** *J Pharmacol Toxicol Methods* 2007, **55**:193-200.
35. Takats Z, Wiseman JM, Gologan B, Cooks RG: **Mass spectrometry sampling under ambient conditions with desorption electrospray ionization.** *Science* 2004, **306**:471-473.
36. Takats Z, Wiseman JM, Cooks RG: **Ambient mass spectrometry using desorption electrospray ionization (DESI): instrumentation, mechanisms and applications in forensics, chemistry, and biology.** *J Mass Spectrom* 2005, **40**:1261-1275.
37. Wiseman JM, Puolitaival SM, Takats Z, Cooks RG, Caprioli RM: **Mass spectrometric profiling of intact biological tissue by using desorption electrospray ionization.** *Angew Chem Int Ed Engl* 2005, **44**:7094-7097.
38. Chen H, Talaty NN, Takats Z, Cooks RG: **Desorption electrospray ionization mass spectrometry for high-throughput analysis of pharmaceutical samples in the ambient environment.** *Anal Chem* 2005, **77**:6915-6927.
39. Cotte-Rodriguez I, Takats Z, Talaty N, Chen H, Cooks RG: **Desorption electrospray ionization of explosives on surfaces: sensitivity and selectivity enhancement by reactive desorption electrospray ionization.** *Anal Chem* 2005, **77**:6755-6764.
40. Desorption Electrospray Ionization (DESI) on World Wide Web URL:  
<http://www.prosolia.com/desi.php>

41. Liu J, Wang H, Manicke NE, Lin JM, Cooks RG, Ouyang Z: **Development, characterization, and application of paper spray ionization.** *Anal Chem* 2010, **82**:2463-2471.
42. Wang H, Liu J, Cooks RG, Ouyang Z: **Paper spray for direct analysis of complex mixtures using mass spectrometry.** *Angew Chem Int Ed Engl* 2010, **49**:877-880.
43. Pacholski ML, Winograd N: **Imaging with mass spectrometry.** *Chem Rev* 1999, **99**:2977-3006.
44. Barber M, R.S B, Sedgwick RD, Tyler AN: **Fast atom bombardment of solids (FAB): a new ion source for mass spectrometry.** *J. Chem. Soc. Chem. Commun.*, 1981:325-327.
45. Barber M, Bordoli RS, Garner GV, Gordon DB, Sedgwick RD, Tetler LW, Tyler AN: **Fast-atom-bombardment mass spectra of enkephalins.** *Biochem J* 1981, **197**:401-404.
46. Barber M, Bordoli RS, Sedgwick RD, Tyler AN, Bycroft BW: **Fast atom bombardment mass spectrometry of bleomycin A2 and B2 and their metal complexes.** *Biochem Biophys Res Commun* 1981, **101**:632-638.
47. Dumasia MC, Houghton E, Bradley CV, Williams DH: **Studies related to the metabolism of anabolic steroids in the horse: the metabolism of 1-dehydrotestosterone and the use of fast atom bombardment mass spectrometry in the identification of steroid conjugates.** *Biomed Mass Spectrom* 1983, **10**:434-440.
48. Tomer KB, Gross ML: **Fast atom bombardment and tandem mass spectrometry for structure determination: remote site fragmentation of steroid conjugates and bile salts.** *Biomed Environ Mass Spectrom* 1988, **15**:89-98.
49. Mosin VAPaVV: **Fast atom bombardment in mass spectrometry: Method and applications** *Theoretical and Experimental Chemistry Number* 1987, **23**:58-73.
50. Wang YaG, W.J: **Mass Spectrometry for Metabolite Identification.** In *Metabolomics, Metabonomics and Metabolite Profiling* edn 1. Edited by Griffiths WJ: Royal Society of Chemistry; 2007.
51. Blau K, Halkett JH: *Handbook of Derivatives for Chromatography.* Chichester, UK: Wiley; 1993.
52. Halket JM, Waterman D, Przyborowska AM, Patel RK, Fraser PD, Bramley PM: **Chemical derivatization and mass spectral libraries in metabolic profiling by GC/MS and LC/MS/MS.** *J Exp Bot* 2005, **56**:219-243.

53. Paul W, Steinwedel H: **Ein neues Massenspektrometer ohne Magnetfeld.** *RZeitschrift für Naturforschung A* 1953, **8**:448-450.
54. Paul W: **Electromagnetic traps for charged and neutral particles.** *Angewandte Chemie - International Edition* 1990, **29**:739.
55. Yost RA, Enke CG: **Selected Ion Fragmentation with a Tandem Quadrupole Mass Spectrometer.** *Journal of the American Chemical Society* 1978, **100**:2274.
56. Morris HR, Paxton T, Dell A, Langhorne J, Berg M, Bordoli RS, Hoyes J, Bateman RH: **High sensitivity collisionally-activated decomposition tandem mass spectrometry on a novel quadrupole/orthogonal-acceleration time-of-flight mass spectrometer.** *Rapid Commun Mass Spectrom* 1996, **10**:889-896.
57. Guilhaus M, Selby D, Mlynski V: **Orthogonal acceleration time-of-flight mass spectrometry.** *Mass Spectrom Rev* 2000, **19**:65-107.
58. King R, Fernandez-Metzler C: **The use of Qtrap technology in drug metabolism.** *Curr Drug Metab* 2006, **7**:541-545.
59. Blanksby SJ, Mitchell TW: **Advances in mass spectrometry for lipidomics.** *Annu Rev Anal Chem (Palo Alto Calif)* 2010, **3**:433-465.
60. Stafford GC, P. E. Kelley, J. E. P. Syka, Reynolds WE, Todd JFJ: **Recent improvements in and analytical applications of advanced ion trap technology.** *International Journal of Mass Spectrometry and Ion Processes* 1984, **60**:85-98.
61. Louri JN, Cooks RG, Syka JEP, Kelley. PE, Stafford GC, Jr. , Todd JFJ: **Instrumentation, applications, and energy deposition in quadrupole ion-trap tandem mass spectrometry.** *Anal Chem* 1987, **59** 1677-1685.
62. March RE: **Quadrupole ion traps.** *Mass Spectrom Rev* 2009, **28**:961-989.
63. Plumb RS, Granger JH, Stumpf CL, Johnson KA, Smith BW, Gaultz S, Wilson ID, Castro-Perez J: **A rapid screening approach to metabonomics using UPLC and oa-TOF mass spectrometry: application to age, gender and diurnal variation in normal/Zucker obese rats and black, white and nude mice.** *Analyst* 2005, **130**:844-849.
64. Plumb RS, Johnson KA, Rainville P, Shockcor JP, Williams R, Granger JH, Wilson ID: **The detection of phenotypic differences in the metabolic plasma profile of three strains of Zucker rats at 20 weeks of age using ultra-performance liquid chromatography/orthogonal acceleration time-of-flight mass spectrometry.** *Rapid Commun Mass Spectrom* 2006, **20**:2800-2806.

65. Chaurand P, Cornett DS, Caprioli RM: **Molecular imaging of thin mammalian tissue sections by mass spectrometry.** *Curr Opin Biotechnol* 2006, **17**:431-436.
66. Chaurand P, Fouchecourt S, DaGue BB, Xu BJ, Reyzer ML, Orgebin-Crist MC, Caprioli RM: **Profiling and imaging proteins in the mouse epididymis by imaging mass spectrometry.** *Proteomics* 2003, **3**:2221-2239.
67. Chaurand P, Norris JL, Cornett DS, Mobley JA, Caprioli RM: **New developments in profiling and imaging of proteins from tissue sections by MALDI mass spectrometry.** *J Proteome Res* 2006, **5**:2889-2900.
68. Chaurand P, Schwartz SA, Caprioli RM: **Imaging mass spectrometry: a new tool to investigate the spatial organization of peptides and proteins in mammalian tissue sections.** *Curr Opin Chem Biol* 2002, **6**:676-681.
69. Chaurand P, Schwartz SA, Capriolo RM: **Profiling and imaging proteins in tissue sections by MS.** *Anal Chem* 2004, **76**:87A-93A.
70. Chaurand P, Stoeckli M, Caprioli RM: **Direct profiling of proteins in biological tissue sections by MALDI mass spectrometry.** *Anal Chem* 1999, **71**:5263-5270.
71. Comisarow MB, Marshall AG: **Fourier transform ion cyclotron resonance spectroscopy.** *Chem. Phys. Lett* 1974, **25**:282.
72. Schrader W, Klein HW: **Liquid chromatography/Fourier transform ion cyclotron resonance mass spectrometry (LC-FTICR MS): an early overview.** *Anal Bioanal Chem* 2004, **379**:1013-1024.
73. Heeren RM, Kleinnijenhuis AJ, McDonnell LA, Mize TH: **A mini-review of mass spectrometry using high-performance FTICR-MS methods.** *Anal Bioanal Chem* 2004, **378**:1048-1058.
74. Page JS, Masselon CD, Smith RD: **FTICR mass spectrometry for qualitative and quantitative bioanalyses.** *Curr Opin Biotechnol* 2004, **15**:3-11.
75. Cornett DS, Frappier SL, Caprioli RM: **MALDI-FTICR imaging mass spectrometry of drugs and metabolites in tissue.** *Anal Chem* 2008, **80**:5648-5653.
76. Ohta D, Kanaya S, Suzuki H: **Application of Fourier-transform ion cyclotron resonance mass spectrometry to metabolic profiling and metabolite identification.** *Current Opinion in Biotechnology* 2010, **21**:35-44.
77. Hu Q, Makarov AA, Cooks RG, Noll RJ: **Resonant ac dipolar excitation for ion motion control in the Orbitrap mass analyzer.** *J Phys Chem A* 2006, **110**:2682-2689.

78. Makarov A, Denisov E, Kholomeev A, Balschun W, Lange O, Strupat K, Horning S: **Performance evaluation of a hybrid linear ion trap/orbitrap mass spectrometer.** *Anal Chem* 2006, **78**:2113-2120.
79. Makarov A, Denisov E, Lange O, Horning S: **Dynamic range of mass accuracy in LTQ Orbitrap hybrid mass spectrometer.** *J Am Soc Mass Spectrom* 2006, **17**:977-982.
80. Scigelova M, Makarov A: **Orbitrap mass analyzer--overview and applications in proteomics.** *Proteomics* 2006, **6 Suppl 2**:16-21.
81. Hu Q, Noll RJ, Li H, Makarov A, Hardman M, Graham Cooks R: **The Orbitrap: a new mass spectrometer.** *J Mass Spectrom* 2005, **40**:430-443.
82. Olsen JV, de Godoy LM, Li G, Macek B, Mortensen P, Pesch R, Makarov A, Lange O, Horning S, Mann M: **Parts per million mass accuracy on an Orbitrap mass spectrometer via lock mass injection into a C-trap.** *Mol Cell Proteomics* 2005, **4**:2010-2021.
83. LTQ-Orbitrap Hybrid FT Mass Spectrometer PDF on World Wide Web URL: [http://www.thermo.com/eThermo/CMA/PDFs/Various/File\\_31081.pdf](http://www.thermo.com/eThermo/CMA/PDFs/Various/File_31081.pdf)
84. Kingdon KH: **A Method for the Neutralization of Electron Space Charge by Positive Ionization at Very Low Gas Pressures.** *Physical Review* 1923, **21**:408.
85. LTQ-Orbitrap Discovery on World Wide Web URL: <http://www.thermoscientific.com/wps/portal/ts/products/detail?productId=11962162&groupType=PRODUCT&searchType=0>
86. LTQ-Orbitrap XL on World Wide Web URL: <http://www.thermoscientific.com/wps/portal/ts/products/detail?productId=11962157&groupType=PRODUCT&searchType=0>
87. LTQ-Orbitrap Velos on World Wide Web URL: <http://www.thermoscientific.com/wps/portal/ts/techresource?productId=11962161&taxonomy=4&resourceId=89231&contentType=Datasheets>
88. LTQ-Orbitrap Velos PDF on World Wide Web URL: [http://www.thermo.com/eThermo/CMA/PDFs/Product/productPDF\\_51627.pdf](http://www.thermo.com/eThermo/CMA/PDFs/Product/productPDF_51627.pdf)
89. Exactive PDF on World Wide Web URL: <http://www.thermo.com.cn/Resources/200811/2114225422.pdf>
90. Griffiths WJ, Karu K, Hornshaw M, Woffendin G, Wang Y: **Metabolomics and metabolite profiling: past heroes and future developments.** *Eur J Mass Spectrom (Chichester, Eng)* 2007, **13**:45-50.



91. Luo B, Groenke K, Takors R, Wandrey C, Oldiges M: **Simultaneous determination of multiple intracellular metabolites in glycolysis, pentose phosphate pathway and tricarboxylic acid cycle by liquid chromatography-mass spectrometry.** *J Chromatogr A* 2007, **1147**:153-164.
92. Coulier L, Bas R, Jespersen S, Verheij E, van der Werf MJ, Hankemeier T: **Simultaneous quantitative analysis of metabolites using ion-pair liquid chromatography-electrospray ionization mass spectrometry.** *Anal Chem* 2006, **78**:6573-6582.
93. Hsieh Y, Duncan CJ: **An ion-pairing liquid chromatography/tandem mass spectrometric method for the determination of cytarabine in mouse plasma.** *Rapid Commun Mass Spectrom* 2007, **21**:573-578.
94. Wilson ID, Nicholson JK, Castro-Perez J, Granger JH, Johnson KA, Smith BW, Plumb RS: **High resolution "ultra performance" liquid chromatography coupled to oa-TOF mass spectrometry as a tool for differential metabolic pathway profiling in functional genomic studies.** *J Proteome Res* 2005, **4**:591-598.
95. Yu K, Little D, Plumb R, Smith B: **High-throughput quantification for a drug mixture in rat plasma-a comparison of Ultra Performance liquid chromatography/tandem mass spectrometry with high-performance liquid chromatography/tandem mass spectrometry.** *Rapid Commun Mass Spectrom* 2006, **20**:544-552.
96. Nguyen DT, Guillarme D, Rudaz S, Veuthey JL: **Fast analysis in liquid chromatography using small particle size and high pressure.** *J Sep Sci* 2006, **29**:1836-1848.
97. Granger JH, Williams R, Lenz EM, Plumb RS, Stumpf CL, Wilson ID: **A metabonomic study of strain- and age-related differences in the Zucker rat.** *Rapid Commun Mass Spectrom* 2007, **21**:2039-2045.
98. Williams R, Lenz EM, Wilson AJ, Granger J, Wilson ID, Major H, Stumpf C, Plumb R: **A multi-analytical platform approach to the metabonomic analysis of plasma from normal and Zucker (fa/fa) obese rats.** *Mol Biosyst* 2006, **2**:174-183.
99. Lu W, Clasquin MF, Melamud E, Amador-Noguez D, Caudy AA, Rabinowitz JD: **Metabolomic analysis via reversed-phase ion-pairing liquid chromatography coupled to a stand alone orbitrap mass spectrometer.** *Anal Chem* 2010, **82**:3212-3221.
100. Edwards JL, Edwards RL, Reid KR, Kennedy RT: **Effect of decreasing column inner diameter and use of off-line two-dimensional chromatography on metabolite detection in complex mixtures.** *J Chromatogr A* 2007, **1172**:127-134.

101. Dunn WBaE, D.I.: **Metabolomics: current analytical platforms and methodologies.** *TrAC: Trends Analytical Chemistry* 2005, **24**:285-298.
102. Hemstrom P, Irgum K: **Hydrophilic interaction chromatography.** *J Sep Sci* 2006, **29**:1784-1821.
103. Guo Y, Gaiki S: **Retention behavior of small polar compounds on polar stationary phases in hydrophilic interaction chromatography.** *J Chromatogr A* 2005, **1074**:71-80.
104. Calvano CD, Zambonin CG, Jensen ON: **Assessment of lectin and HILIC based enrichment protocols for characterization of serum glycoproteins by mass spectrometry.** *J Proteomics* 2008, **71**:304-317.
105. Cubbon S, Bradbury T, Wilson J, Thomas-Oates J: **Hydrophilic interaction chromatography for mass spectrometric metabolomic studies of urine.** *Anal Chem* 2007, **79**:8911-8918.
106. Gika HG, Theodoridis GA, Wilson ID: **Hydrophilic interaction and reversed-phase ultra-performance liquid chromatography TOF-MS for metabolomic analysis of Zucker rat urine.** *J Sep Sci* 2008, **31**:1598-1608.
107. Idborg H, Zamani L, Edlund PO, Schuppe-Koistinen I, Jacobsson SP: **Metabolic fingerprinting of rat urine by LC/MS Part 2. Data pretreatment methods for handling of complex data.** *J Chromatogr B Analyt Technol Biomed Life Sci* 2005, **828**:14-20.
108. Kind T, Tolstikov V, Fiehn O, Weiss RH: **A comprehensive urinary metabolomic approach for identifying kidney cancer.** *Anal Biochem* 2007, **363**:185-195.
109. Nordstrom A, Want E, Northen T, Lehtio J, Siuzdak G: **Multiple ionization mass spectrometry strategy used to reveal the complexity of metabolomics.** *Anal Chem* 2008, **80**:421-429.
110. Paek IB, Moon Y, Ji HY, Kim HH, Lee HW, Lee YB, Lee HS: **Hydrophilic interaction liquid chromatography-tandem mass spectrometry for the determination of levosulpiride in human plasma.** *J Chromatogr B Analyt Technol Biomed Life Sci* 2004, **809**:345-350.
111. Zhang X, Rauch A, Lee H, Xiao H, Rainer G, Logothetis NK: **Capillary hydrophilic interaction chromatography/mass spectrometry for simultaneous determination of multiple neurotransmitters in primate cerebral cortex.** *Rapid Commun Mass Spectrom* 2007, **21**:3621-3628.
112. Cubbon S, Antonio C, Wilson J, Thomas-Oates J: **Metabolomic applications of HILIC-LC-MS.** *Mass Spectrom Rev* 2009.

113. Spagou K, Tsoukali H, Raikos N, Gika H, Wilson ID, Theodoridis G: **Hydrophilic interaction chromatography coupled to MS for metabonomic/metabolomic studies.** *J Sep Sci* 2010, **33**:716-727.
114. Bajad SU, Lu W, Kimball EH, Yuan J, Peterson C, Rabinowitz JD: **Separation and quantitation of water soluble cellular metabolites by hydrophilic interaction chromatography-tandem mass spectrometry.** *J Chromatogr A* 2006, **1125**:76-88.
115. Smilde AK, van der Werf MJ, Bijlsma S, van der Werff-van der Vat BJ, Jellema RH: **Fusion of mass spectrometry-based metabolomics data.** *Anal Chem* 2005, **77**:6729-6736.
116. van der Werf MJ, Overkamp KM, Muilwijk B, Coulier L, Hankemeier T: **Microbial metabolomics: toward a platform with full metabolome coverage.** *Anal Biochem* 2007, **370**:17-25.
117. Lafaye A, Junot C, Pereira Y, Lagniel G, Tabet JC, Ezan E, Labarre J: **Combined proteome and metabolite-profiling analyses reveal surprising insights into yeast sulfur metabolism.** *J Biol Chem* 2005, **280**:24723-24730.
118. Lafaye A, Labarre J, Tabet JC, Ezan E, Junot C: **Liquid chromatography-mass spectrometry and <sup>15</sup>N metabolic labeling for quantitative metabolic profiling.** *Anal Chem* 2005, **77**:2026-2033.
119. Kamleh A, Barrett MP, Wildridge D, Burchmore RJ, Scheltema RA, Watson DG: **Metabolomic profiling using Orbitrap Fourier transform mass spectrometry with hydrophilic interaction chromatography: a method with wide applicability to analysis of biomolecules.** *Rapid Commun Mass Spectrom* 2008, **22**:1912-1918.
120. Gohlke RS: **Time-of-Flight Mass Spectrometry and Gas-Liquid Partition Chromatography.** *Anal Chem* 1959, **31**:535-541.
121. Watson JT, Biemann, K.: **Direct Recording of High Resolution Mass Spectra of Gas Chromatographic Effluents.** *Anal Chem* 1965, **37**:844-851.
122. Ryhage R: **Use of a Mass Spectrometer as a Detector and Analyzer for Effluent Emerging from High Temperature Gas Liquid Chromatography Columns.** *Anal Chem* 1964, **36**:759-764.
123. Jensen TE: **Coupling of fused-silica capillary gas-chromatographic columns to three mass spectrometers.** *Anal Chem* 1982, **54**:2388-2390.
124. Luukainen T, VandenHeuvel, W.J.A, Haahti, E.O and Horning, E.C **Gas Chromatographic behaviour of trimethylsilyl ethers of steroids.** *Biochim. Biophys. Acta* 1961, **52**:599-601.
125. Griffiths WJ, Shackelton, C and Sjoval, J: **Steroid Analysis.** In *Encyclopaedia of Mass Spectrometry*. Edited by Caprioli RM: Elsevier; 2005:447. vol 3.]

126. Halket JM, Zaikin VG: **Derivatization in mass spectrometry--1. Silylation.** *Eur J Mass Spectrom (Chichester, Eng)* 2003, **9**:1-21.
127. Zaikin VG, Halket JM: **Review: Derivatization in mass spectrometry--2. Acylation.** *Eur J Mass Spectrom (Chichester, Eng)* 2003, **9**:421-434.
128. Halket JM, Zaikin VG: **Review: derivatization in mass spectrometry--5. Specific derivatization of monofunctional compounds.** *Eur J Mass Spectrom (Chichester, Eng)* 2005, **11**:127-160.
129. Li S: *Capillary Electrophoresis: Principles, Practice, and Applications*, vol 52. The Netherlands: Elsevier Science Publishers; 1992.
130. Olivares JA, Nguyen, N.T, Yonker, C.R and Smith, R.D: **On-line mass spectrometric detection for capillary zone electrophoresis.** *Anal Chem* 1987, **59**:1230-1232.
131. Abian J: **The coupling of gas and liquid chromatography with mass spectrometry.** *J. Mass Spectrom.* 1999, **34**:157-168.
132. March RE: **An Introduction to Quadrupole Ion Trap Mass Spectrometry.** *J. Mass Spectrom.* 1997, **32**:351-369.
133. Chernushevich IV, Loboda AV, Thomson BA: **An introduction to quadrupole-time-of-flight mass spectrometry.** *J Mass Spectrom* 2001, **36**:849-865.
134. Verhaert P, Uttenweiler-Joseph S, de Vries M, Loboda A, Ens W, Standing KG: **Matrix-assisted laser desorption/ionization quadrupole time-of-flight mass spectrometry: an elegant tool for peptidomics.** *Proteomics* 2001, **1**:118-131.
135. Severs JC, Hofstadler SA, Zhao Z, Senh RT, Smith RD: **The interface of capillary electrophoresis with high performance Fourier transform ion cyclotron resonance mass spectrometry for biomolecule characterization.** *Electrophoresis* 1996, **17**:1808-1817.
136. Kolch W, Neuss C, Pelzing M, Mischak H: **Capillary electrophoresis-mass spectrometry as a powerful tool in clinical diagnosis and biomarker discovery.** *Mass Spectrom Rev* 2005, **24**:959-977.
137. Fliser D, Wittke S, Mischak H: **Capillary electrophoresis coupled to mass spectrometry for clinical diagnostic purposes.** *Electrophoresis* 2005, **26**:2708-2716.
138. Metzger J, Lupp PB, Good DM, Mischak H: **Adapting mass spectrometry-based platforms for clinical proteomics applications: The capillary electrophoresis coupled mass spectrometry paradigm.** *Crit Rev Clin Lab Sci* 2009, **46**:129-152.

139. Metzger J, Schanstra JP, Mischak H: **Capillary electrophoresis-mass spectrometry in urinary proteome analysis: current applications and future developments.** *Anal Bioanal Chem* 2009, **393**:1431-1442.
140. Schiffer E, Mischak H, Novak J: **High resolution proteome/peptidome analysis of body fluids by capillary electrophoresis coupled with MS.** *Proteomics* 2006, **6**:5615-5627.
141. Coon JJ, Zurbig P, Dakna M, Dominiczak AF, Decramer S, Fliser D, Frommberger M, Golovko I, Good DM, Herget-Rosenthal S, et al.: **CE-MS analysis of the human urinary proteome for biomarker discovery and disease diagnostics.** *Proteomics Clin Appl* 2008, **2**:964.
142. Sugimoto M, Wong DT, Hirayama A, Soga T, Tomita M: **Capillary electrophoresis mass spectrometry-based saliva metabolomics identified oral, breast and pancreatic cancer-specific profiles.** *Metabolomics* 2010, **6**:78-95.
143. Zurbig P, Mischak H: **Capillary electrophoresis coupled to mass spectrometry for biomarker discovery and diagnosis of kidney diseases.** *Contrib Nephrol* 2008, **160**:107-126.
144. Foret F, Preisler J: **Liquid phase interfacing and miniaturization in matrix-assisted laser desorption/ionization mass spectrometry.** *Proteomics* 2002, **2**:360-372.
145. Gusev AI: **Interfacing matrix-assisted laser desorption/ionization mass spectrometry with column and planar separations.** *Fresenius J Anal Chem* 2000, **366**:691-700.
146. Horning EC, Devaux PG, Moffat AC, Pfaffenberger CD, Sakauchi N, Horning MG: **Gas phase analytical separation techniques applicable to problems in clinical chemistry.** *Clin Chim Acta* 1971, **34**:135-144.
147. Mamer OA, Crawhall JC, Tjoa SS: **The identification of urinary acids by coupled gas chromatography-mass spectrometry.** *Clin Chim Acta* 1971, **32**:171-184.
148. Pauling L, Robinson AB, Teranishi R, Cary P: **Quantitative analysis of urine vapor and breath by gas-liquid partition chromatography.** *Proc Natl Acad Sci U S A* 1971, **68**:2374-2376.
149. Fiehn O: **Metabolomics--the link between genotypes and phenotypes.** *Plant Mol Biol* 2002, **48**:155-171.
150. Nicholson JK, Connelly J, Lindon JC, Holmes E: **Metabonomics: a platform for studying drug toxicity and gene function.** *Nat Rev Drug Discov* 2002, **1**:153-161.

151. Nicholson JK, Lindon JC, Holmes E: **'Metabonomics': understanding the metabolic responses of living systems to pathophysiological stimuli via multivariate statistical analysis of biological NMR spectroscopic data.** *Xenobiotica* 1999, **29**:1181-1189.
152. Lindon JC, Holmes E, Bollard ME, Stanley EG, Nicholson JK: **Metabonomics technologies and their applications in physiological monitoring, drug safety assessment and disease diagnosis.** *Biomarkers* 2004, **9**:1-31.
153. Oliver SG, Winson MK, Kell DB, Baganz F: **Systematic functional analysis of the yeast genome.** *Trends Biotechnol* 1998, **16**:373-378.
154. Stoeckli M, Staab D, Staufenbiel M, Wiederhold KH, Signor L: **Molecular imaging of amyloid beta peptides in mouse brain sections using mass spectrometry.** *Anal Biochem* 2002, **311**:33-39.
155. Andersson M, Groseclose MR, Deutch AY, Caprioli RM: **Imaging mass spectrometry of proteins and peptides: 3D volume reconstruction.** *Nat Methods* 2008, **5**:101-108.
156. Edwards JL, Kennedy RT: **Metabolomic analysis of eukaryotic tissue and prokaryotes using negative mode MALDI time-of-flight mass spectrometry.** *Anal Chem* 2005, **77**:2201-2209.
157. Franck J, Arafah K, Elayed M, Bonnel D, Vergara D, Jacquet A, Vinatier D, Wisztorski M, Day R, Fournier I, et al.: **MALDI imaging mass spectrometry: state of the art technology in clinical proteomics.** *Mol Cell Proteomics* 2009, **8**:2023-2033.
158. Trim PJ, Henson CM, Avery JL, McEwen A, Snel MF, Claude E, Marshall PS, West A, Princivalle AP, Clench MR: **Matrix-assisted laser desorption/ionization-ion mobility separation-mass spectrometry imaging of vinblastine in whole body tissue sections.** *Anal Chem* 2008, **80**:8628-8634.
159. MALDI-LTQ-Orbitrap on World Wide Web URL: <http://www.thermoscientific.com/wps/portal/ts/techresource?productId=13133057&taxonomy=4&resourceId=89767&contentType=Datasheets#>
160. Landgraf RR, Prieto Conaway MC, Garrett TJ, Stacpoole PW, Yost RA: **Imaging of lipids in spinal cord using intermediate pressure matrix-assisted laser desorption-linear ion trap/Orbitrap MS.** *Anal Chem* 2009, **81**:8488-8495.
161. Verhaert PD, Pinkse MW, Strupat K, Conaway MC: **Imaging of similar mass neuropeptides in neuronal tissue by enhanced resolution MALDI MS with an ion trap - Orbitrap hybrid instrument.** *Methods Mol Biol* 2010, **656**:433-449.

162. Jun JH, Song Z, Liu Z, Nikolau BJ, Yeung ES, Lee YJ: **High-spatial and high-mass resolution imaging of surface metabolites of *Arabidopsis thaliana* by laser desorption-ionization mass spectrometry using colloidal silver.** *Anal Chem* 2010, **82**:3255-3265.
163. Papatiriu DG, Jaskolla TW, Markoutsas S, Baumliberger D, Karas M, Meyer B: **Peptide mass fingerprinting after less specific in-gel proteolysis using MALDI-LTQ-Orbitrap and 4-chloro-alpha-cyanocinnamic acid.** *J Proteome Res* 2010, **9**:2619-2629.
164. Bahr U, Aygun H, Karas M: **Sequencing of single and double stranded RNA oligonucleotides by acid hydrolysis and MALDI mass spectrometry.** *Anal Chem* 2009, **81**:3173-3179.
165. AP-MALDI PDF+ Source on World Wide Web URL: <http://www.apmaldi.com/Products/ThermoScientific.html>.
166. Wiseman JM, Ifa DR, Song Q, Cooks RG: **Tissue imaging at atmospheric pressure using desorption electrospray ionization (DESI) mass spectrometry.** *Angew Chem Int Ed Engl* 2006, **45**:7188-7192.
167. Ifa DR, Gumaelius LM, Eberlin LS, Manicke NE, Cooks RG: **Forensic analysis of inks by imaging desorption electrospray ionization (DESI) mass spectrometry.** *Analyst* 2007, **132**:461-467.
168. Jackson AU, Talaty N, Cooks RG, Van Berkel GJ: **Salt tolerance of desorption electrospray ionization (DESI).** *J Am Soc Mass Spectrom* 2007, **18**:2218-2225.
169. Manicke NE, Wiseman JM, Ifa DR, Cooks RG: **Desorption electrospray ionization (DESI) mass spectrometry and tandem mass spectrometry (MS/MS) of phospholipids and sphingolipids: ionization, adduct formation, and fragmentation.** *J Am Soc Mass Spectrom* 2008, **19**:531-543.
170. Manicke NE, Nefliu M, Wu C, Woods JW, Reiser V, Hendrickson RC, Cooks RG: **Imaging of lipids in atheroma by desorption electrospray ionization mass spectrometry.** *Anal Chem* 2009, **81**:8702-8707.
171. Wu C, Ifa DR, Manicke NE, Cooks RG: **Molecular imaging of adrenal gland by desorption electrospray ionization mass spectrometry.** *Analyst* 2010, **135**:28-32.
172. Ifa DR, Manicke NE, Rusine AL, Cooks RG: **Quantitative analysis of small molecules by desorption electrospray ionization mass spectrometry from polytetrafluoroethylene surfaces.** *Rapid Commun Mass Spectrom* 2008, **22**:503-510.
173. Wiseman JM, Ifa DR, Zhu Y, Kissinger CB, Manicke NE, Kissinger PT, Cooks RG: **Desorption electrospray ionization mass spectrometry: Imaging**

- drugs and metabolites in tissues.** *Proc Natl Acad Sci U S A* 2008, **105**:18120-18125.
174. Ifa DR WJ, Song Q and Cooks RG **Development of capabilities for imaging mass spectrometry under ambient conditions with desorption electrospray ionization (DESI)** *Int J Mass Spectrom* 2006, **259**:8-15.
175. Dill AL, Ifa DR, Manicke NE, Ouyang Z, Cooks RG: **Mass spectrometric imaging of lipids using desorption electrospray ionization.** *J Chromatogr B Analyt Technol Biomed Life Sci* 2009, **877**:2883-2889.
176. Ifa DR, Wu C, Ouyang Z, Cooks RG: **Desorption electrospray ionization and other ambient ionization methods: current progress and preview.** *Analyst* 2010, **135**:669-681.
177. Malmberg P, Jennische E, Nilsson D, Nygren H: **High-resolution, imaging TOF-SIMS: novel applications in medical research.** *Analytical and Bioanalytical Chemistry* 2010.
178. Winograd N: **The Magic of Cluster SIMS.** *Anal Chem* 2005, **77**:143A-149A.
179. Altelaar AF, Piersma SR: **Cellular imaging using matrix-enhanced and metal-assisted SIMS.** *Methods Mol Biol* 2010, **656**:197-208.
180. Mas S, Perez R, Martinez-Pinna R, Egido J, Vivanco F: **Cluster TOF-SIMS imaging: a new light for in situ metabolomics?** *Proteomics* 2008, **8**:3735-3745.
181. Brulet M, Seyer A, Edelman A, Brunelle A, Fritsch J, Ollero M, Laprevote O: **Lipid mapping of colonic mucosa by cluster TOF-SIMS imaging and multivariate analysis in cftr knockout mice.** *J Lipid Res* 2010, **51**:3034-3045.
182. McDonnell LA, Heeren RM: **Imaging mass spectrometry.** *Mass Spectrom Rev* 2007, **26**:606-643.
183. Monroe EB, Annangudi SP, Hatcher NG, Gutstein HB, Rubakhin SS, Sweedler JV: **SIMS and MALDI MS imaging of the spinal cord.** *Proteomics* 2008, **8**:3746-3754.
184. Northen TR, Yanes O, Northen MT, Marrinucci D, Uritboonthai W, Apon J, Golledge SL, Nordstrom A, Siuzdak G: **Clathrate nanostructures for mass spectrometry.** *Nature* 2007, **449**:1033-1036.
185. Woo HK, Northen TR, Yanes O, Siuzdak G: **Nanostructure-initiator mass spectrometry: a protocol for preparing and applying NIMS surfaces for high-sensitivity mass analysis.** *Nat Protoc* 2008, **3**:1341-1349.



186. Want EJ, Nordstrom A, Morita H, Siuzdak G: **From exogenous to endogenous: the inevitable imprint of mass spectrometry in metabolomics.** *J Proteome Res* 2007, **6**:459-468.
187. Yanes O, Woo HK, Northen TR, Oppenheimer SR, Shriver L, Apon J, Estrada MN, Potchoiba MJ, Steenwyk R, Manchester M, et al.: **Nanostructure initiator mass spectrometry: tissue imaging and direct biofluid analysis.** *Anal Chem* 2009, **81**:2969-2975.
188. Patti GJ, Shriver LP, Wassif CA, Woo HK, Uritboonthai W, Apon J, Manchester M, Porter FD, Siuzdak G: **Nanostructure-initiator mass spectrometry (NIMS) imaging of brain cholesterol metabolites in Smith-Lemli-Opitz syndrome.** *Neuroscience* 2010, **170**:858-864.
189. Chaurand P, Schwartz SA, Billheimer D, Xu BJ, Crecelius A, Caprioli RM: **Integrating histology and imaging mass spectrometry.** *Anal Chem* 2004, **76**:1145-1155.
190. Schwartz SA, Reyzer ML, Caprioli RM: **Direct tissue analysis using matrix-assisted laser desorption/ionization mass spectrometry: practical aspects of sample preparation.** *J Mass Spectrom* 2003, **38**:699-708.
191. Lemaire R, Wisztorski M, Desmons A, Tabet JC, Day R, Salzet M, Fournier I: **MALDI-MS direct tissue analysis of proteins: Improving signal sensitivity using organic treatments.** *Anal Chem* 2006, **78**:7145-7153.
192. Caldwell RL, Caprioli RM: **Tissue profiling by mass spectrometry: a review of methodology and applications.** *Mol Cell Proteomics* 2005, **4**:394-401.
193. Hsieh Y, Casale R, Fukuda E, Chen J, Knemeyer I, Wingate J, Morrison R, Korfmacher W: **Matrix-assisted laser desorption/ionization imaging mass spectrometry for direct measurement of clozapine in rat brain tissue.** *Rapid Commun Mass Spectrom* 2006, **20**:965-972.
194. Aerni HR, Cornett DS, Caprioli RM: **Automated acoustic matrix deposition for MALDI sample preparation.** *Anal Chem* 2006, **78**:827-834.
195. Chaurand P, Schwartz SA, Reyzer ML, Caprioli RM: **Imaging mass spectrometry: principles and potentials.** *Toxicol Pathol* 2005, **33**:92-101.
196. Wenzel T, Sparbier K, Mieruch T, Kostrzewa M: **2,5-Dihydroxyacetophenone: a matrix for highly sensitive matrix-assisted laser desorption/ionization time-of-flight mass spectrometric analysis of proteins using manual and automated preparation techniques.** *Rapid Commun Mass Spectrom* 2006, **20**:785-789.
197. Fournier I, Day R, Salzet M: **Direct analysis of neuropeptides by in situ MALDI-TOF mass spectrometry in the rat brain.** *Neuro Endocrinol Lett* 2003, **24**:9-14.

198. Jackson SN, Wang HY, Woods AS: **In situ structural characterization of phosphatidylcholines in brain tissue using MALDI-MS/MS.** *J Am Soc Mass Spectrom* 2005, **16**:2052-2056.
199. Lemaire R, Tabet JC, Ducoroy P, Hendra JB, Salzet M, Fournier I: **Solid ionic matrixes for direct tissue analysis and MALDI imaging.** *Anal Chem* 2006, **78**:809-819.
200. Ayorinde FO, Hambright P, Porter TN, Keith QL, Jr.: **Use of meso-tetrakis(pentafluorophenyl)porphyrin as a matrix for low molecular weight alkylphenol ethoxylates in laser desorption/ ionization time-of-flight mass spectrometry.** *Rapid Commun Mass Spectrom* 1999, **13**:2474-2479.
201. Altelaar AF, Klinkert I, Jalink K, de Lange RP, Adan RA, Heeren RM, Piersma SR: **Gold-enhanced biomolecular surface imaging of cells and tissue by SIMS and MALDI mass spectrometry.** *Anal Chem* 2006, **78**:734-742.
202. Rose D: **Microdispensing technologies in drug discovery.** *Drug Discov Today* 1999, **4**:411-419.
203. Elrod SA, Hadimioglu, B, Khuri-Yakub, B.T, Rawson, E.G, Richley, E, Quate, C.F, Mansour, N.N and Lundgren, T.S: **Nozzleless Droplet Formation with Focused Acoustic Beams.** *J Appl Phys* 1989, **65**:3441-3447.
204. Baluya DL, Garrett TJ, Yost RA: **Automated MALDI matrix deposition method with inkjet printing for imaging mass spectrometry.** *Anal Chem* 2007, **79**:6862-6867.
205. Hankin JA, Barkley RM, Murphy RC: **Sublimation as a method of matrix application for mass spectrometric imaging.** *J Am Soc Mass Spectrom* 2007, **18**:1646-1652.
206. Rohner TC, Staab D, Stoeckli M: **MALDI mass spectrometric imaging of biological tissue sections.** *Mech Ageing Dev* 2005, **126**:177-185.
207. Stoeckli M, Staab D, Schweitzer A: **Compound and metabolite distribution measured by MALDI mass spectrometric imaging in whole-body tissue sections.** *International Journal of Mass Spectrometry* 2007, **260**:195-202.
208. McCombie G, Staab D, Stoeckli M, Knochenmuss R: **Spatial and spectral correlations in MALDI mass spectrometry images by clustering and multivariate analysis.** *Anal Chem* 2005, **77**:6118-6124.
209. Trim PJ, Atkinson SJ, Princivalle AP, Marshall PS, West A, Clench MR: **Matrix-assisted laser desorption/ionisation mass spectrometry imaging of lipids in rat brain tissue with integrated unsupervised and supervised multivariate statistical analysis.** *Rapid Commun Mass Spectrom* 2008, **22**:1503-1509.

210. Prideaux B, Atkinson SJ, Carolan VA, Morton J, Clench MR: **Sample preparation and data interpretation procedures for the examination of xenobiotic compounds in skin by indirect imaging MALDI-MS.** *International Journal of Mass Spectrometry* 2007, **260**:243-251.
211. Pierson J, Norris JL, Aerni HR, Svenningsson P, Caprioli RM, Andren PE: **Molecular profiling of experimental Parkinson's disease: direct analysis of peptides and proteins on brain tissue sections by MALDI mass spectrometry.** *J Proteome Res* 2004, **3**:289-295.
212. Stoeckli M, Chaurand P, Hallahan DE, Caprioli RM: **Imaging mass spectrometry: a new technology for the analysis of protein expression in mammalian tissues.** *Nat Med* 2001, **7**:493-496.
213. Christie WW: *Lipid analysis : isolation, separation, identification, and structural analysis of lipids* edn 3rd. Bridgwater, England: Oily Press; 2003.
214. Jackson SN, Woods AS: **Direct profiling of tissue lipids by MALDI-TOFMS.** *J Chromatogr B Analyt Technol Biomed Life Sci* 2009, **877**:2822-2829.
215. Woods AS, Jackson SN: **Brain tissue lipidomics: direct probing using matrix-assisted laser desorption/ionization mass spectrometry.** *AAPS J* 2006, **8**:E391-395.
216. Jackson SN, Wang HY, Woods AS: **Direct profiling of lipid distribution in brain tissue using MALDI-TOFMS.** *Anal Chem* 2005, **77**:4523-4527.
217. Woods AS, Wang HY, Jackson SN: **A snapshot of tissue glycerolipids.** *Curr Pharm Des* 2007, **13**:3344-3356.
218. Touboul D, Piednoel H, Voisin V, De La Porte S, Brunelle A, Halgand F, Laprevote O: **Changes of phospholipid composition within the dystrophic muscle by matrix-assisted laser desorption/ionization mass spectrometry and mass spectrometry imaging.** *Eur J Mass Spectrom (Chichester, Eng)* 2004, **10**:657-664.
219. Schiller J, Arnhold J, Benard S, Muller M, Reichl S, Arnold K: **Lipid analysis by matrix-assisted laser desorption and ionization mass spectrometry: A methodological approach.** *Analytical Biochemistry* 1999, **267**:46-56.
220. Petkovic M, Schiller J, Muller M, Benard S, Reichl S, Arnold K, Arnhold J: **Detection of individual phospholipids in lipid mixtures by matrix-assisted laser desorption/ionization time-of-flight mass spectrometry: phosphatidylcholine prevents the detection of further species.** *Anal Biochem* 2001, **289**:202-216.
221. Liu Y, Chen Y, Momin A, Shaner R, Wang E, Bowen NJ, Matyunina LV, Walker LD, McDonald JF, Sullards MC, et al.: **Elevation of sulfatides in ovarian cancer: an integrated transcriptomic and lipidomic analysis including tissue-imaging mass spectrometry.** *Mol Cancer* 2010, **9**:186.

222. Lipidomics on World Wide Web URL: <http://msr.dom.wustl.edu/Research/Lipidomics.htm>
223. Jackson SN, Wang HY, Woods AS: **In situ structural characterization of glycerophospholipids and sulfatides in brain tissue using MALDI-MS/MS.** *J Am Soc Mass Spectrom* 2007, **18**:17-26.
224. Estrada R, Yappert MC: **Regional phospholipid analysis of porcine lens membranes by matrix-assisted laser desorption/ionization time-of-flight mass spectrometry.** *J Mass Spectrom* 2004, **39**:1531-1540.
225. Estrada R, Yappert MC: **Alternative approaches for the detection of various phospholipid classes by matrix-assisted laser desorption/ionization time-of-flight mass spectrometry.** *J Mass Spectrom* 2004, **39**:412-422.
226. Jackson SN, Ugarov M, Egan T, Post JD, Langlais D, Albert Schultz J, Woods AS: **MALDI-ion mobility-TOFMS imaging of lipids in rat brain tissue.** *J Mass Spectrom* 2007, **42**:1093-1098.
227. Zollner P, Schmid ER, Allmaier G: **K-4[Fe(CN)(6)]/glycerol - A new liquid matrix system for matrix-assisted laser desorption/ionization mass spectrometry of hydrophobic compounds.** *Rapid Communications in Mass Spectrometry* 1996, **10**:1278-1282.
228. Asbury GR, Al-Saad K, Siems WF, Hannan RM, Hill HH: **Analysis of triacylglycerols and whole oils by matrix-assisted laser desorption/ionization time of flight mass spectrometry.** *Journal of the American Society for Mass Spectrometry* 1999, **10**:983-991.
229. Schiller J, Arnhold J, Benard S, Muller M, Reichl S, Arnold K: **Lipid analysis by matrix-assisted laser desorption and ionization mass spectrometry: A methodological approach.** *Anal Biochem* 1999, **267**:46-56.
230. Puolitaival SM, Burnum KE, Cornett DS, Caprioli RM: **Solvent-free matrix dry-coating for MALDI Imaging of phospholipids.** *Journal of the American Society for Mass Spectrometry* 2008, **19**:882-886.
231. Garrett TJ, Yost RA: **Analysis of intact tissue by intermediate-pressure MALDI on a linear ion trap mass spectrometer.** *Anal Chem* 2006, **78**:2465-2469.
232. Chen Y, Allegood J, Liu Y, Wang E, Cachon-Gonzalez B, Cox TM, Merrill AH, Jr., Sullards MC: **Imaging MALDI mass spectrometry using an oscillating capillary nebulizer matrix coating system and its application to analysis of lipids in brain from a mouse model of Tay-Sachs/Sandhoff disease.** *Anal Chem* 2008, **80**:2780-2788.
233. Cha S, Yeung ES: **Colloidal graphite-assisted laser desorption/ionization mass spectrometry and MSn of small molecules. 1. Imaging of**

- cerebrosides directly from rat brain tissue. *Anal Chem* 2007, **79**:2373-2385.
234. Dreisewerd K, Lemaire R, Pohlentz G, Salzet M, Wisztorski M, Berkenkamp S, Fournier I: **Molecular profiling of native and matrix-coated tissue slices from rat brain by infrared and ultraviolet laser desorption/ionization orthogonal time-of-flight mass spectrometry.** *Anal Chem* 2007, **79**:2463-2471.
235. Shimma S, Sugiura Y, Hayasaka T, Hoshikawa Y, Noda T, Setou M: **MALDI-based imaging mass spectrometry revealed abnormal distribution of phospholipids in colon cancer liver metastasis.** *J Chromatogr B Analyt Technol Biomed Life Sci* 2007, **855**:98-103.
236. Guo Z, He L: **A binary matrix for background suppression in MALDI-MS of small molecules.** *Anal Bioanal Chem* 2007, **387**:1939-1944.
237. Vaidyanathan S, Goodacre R: **Quantitative detection of metabolites using matrix-assisted laser desorption/ionization mass spectrometry with 9-aminoacridine as the matrix.** *Rapid Commun Mass Spectrom* 2007, **21**:2072-2078.
238. Shroff R, Muck A, Svatos A: **Analysis of low molecular weight acids by negative mode matrix-assisted laser desorption/ionization time-of-flight mass spectrometry.** *Rapid Commun Mass Spectrom* 2007, **21**:3295-3300.
239. Sun G, Yang K, Zhao ZD, Guan SP, Han XL, Gross RW: **Shotgun metabolomics approach for the analysis of negatively charged water-soluble cellular metabolites from mouse heart tissue.** *Analytical Chemistry* 2007, **79**:6629-6640.
240. Sun G, Yang K, Zhao Z, Guan S, Han X, Gross RW: **Matrix-assisted laser desorption/ionization time-of-flight mass spectrometric analysis of cellular glycerophospholipids enabled by multiplexed solvent dependent analyte-matrix interactions.** *Anal Chem* 2008, **80**:7576-7585.
241. Angelini R, Babudri F, Lobasso S, Corcelli A: **MALDI-TOF/MS analysis of archaeobacterial lipids in lyophilized membranes dry-mixed with 9-aminoacridine.** *J Lipid Res* 2010, **51**:2818-2825.
242. Lobasso S, Lopalco P, Angelini R, Baronio M, Fanizzi FP, Babudri F, Corcelli A: **Lipidomic analysis of porcine olfactory epithelial membranes and cilia.** *Lipids* 2010, **45**:593-602.
243. Teuber K, Schiller J, Fuchs B, Karas M, Jaskolla TW: **Significant sensitivity improvements by matrix optimization: a MALDI-TOF mass spectrometric study of lipids from hen egg yolk.** *Chem Phys Lipids* 2010, **163**:552-560.

244. Cheng H, Sun G, Yang K, Gross RW, Han X: **Selective desorption/ionization of sulfatides by MALDI-MS facilitated using 9-aminoacridine as matrix.** *J Lipid Res* 2010, **51**:1599-1609.
245. Miura D, Fujimura Y, Tachibana H, Wariishi H: **Highly sensitive matrix-assisted laser desorption ionization-mass spectrometry for high-throughput metabolic profiling.** *Anal Chem* 2010, **82**:498-504.
246. Yukihiro D, Miura D, Saito K, Takahashi K, Wariishi H: **MALDI-MS-based high-throughput metabolite analysis for intracellular metabolic dynamics.** *Anal Chem* 2010, **82**:4278-4282.
247. Burrell M, Earnshaw C, Clench M: **Imaging Matrix Assisted Laser Desorption Ionization Mass Spectrometry: a technique to map plant metabolites within tissues at high spatial resolution.** *J Exp Bot* 2007, **58**:757-763.
248. Rubakhin SS, Sweedler JV: **Characterizing peptides in individual mammalian cells using mass spectrometry.** *Nat Protoc* 2007, **2**:1987-1997.
249. Zimmerman TA, Rubakhin SS, Romanova EV, Tucker KR, Sweedler JV: **MALDI mass spectrometric imaging using the stretched sample method to reveal neuropeptide distributions in aplasia nervous tissue.** *Anal Chem* 2009, **81**:9402-9409.
250. Amantonico A, Urban PL, Fagerer SR, Balabin RM, Zenobi R: **Single-cell MALDI-MS as an analytical tool for studying intrapopulation metabolic heterogeneity of unicellular organisms.** *Anal Chem* 2010, **82**:7394-7400.
251. Amantonico A, Oh JY, Sobek J, Heinemann M, Zenobi R: **Mass spectrometric method for analyzing metabolites in yeast with single cell sensitivity.** *Angew Chem Int Ed Engl* 2008, **47**:5382-5385.
252. Amantonico A, Urban PL, Zenobi R: **Analytical techniques for single-cell metabolomics: state of the art and trends.** *Anal Bioanal Chem* 2010, **398**:2493-2504.
253. Wu H, Southam AD, Hines A, Viant MR: **High-throughput tissue extraction protocol for NMR- and MS-based metabolomics.** *Anal Biochem* 2008, **372**:204-212.
254. Keller BO, Sui J, Young AB, Whittall RM: **Interferences and contaminants encountered in modern mass spectrometry.** *Anal Chim Acta* 2008, **627**:71-81.
255. Schiller J, Zschornig O, Petkovic M, Muller M, Arnhold J, Arnold K: **Lipid analysis of human HDL and LDL by MALDI-TOF mass spectrometry and (31)P-NMR.** *J Lipid Res* 2001, **42**:1501-1508.

256. Harvey DJ: **Matrix-Assisted Laser-Desorption Ionization Mass-Spectrometry of Phospholipids.** *Journal of Mass Spectrometry* 1995, **30**:1333-1346.
257. Schiller J, Suss R, Arnhold J, Fuchs B, Lessig J, Muller M, Petkovic M, Spalteholz H, Zschornig O, Arnold K: **Matrix-assisted laser desorption and ionization time-of-flight (MALDI-TOF) mass spectrometry in lipid and phospholipid research.** *Prog Lipid Res* 2004, **43**:449-488.
258. Solon EG, Balani SK, Lee FW: **Whole-body autoradiography in drug discovery.** *Curr Drug Metab* 2002, **3**:451-462.
259. Reyzer ML, Hsieh Y, Ng K, Korfmacher WA, Caprioli RM: **Direct analysis of drug candidates in tissue by matrix-assisted laser desorption/ionization mass spectrometry.** *J Mass Spectrom* 2003, **38**:1081-1092.
260. Wang HY, Jackson SN, McEuen J, Woods AS: **Localization and analyses of small drug molecules in rat brain tissue sections.** *Anal Chem* 2005, **77**:6682-6686.
261. Troendle FJ, Reddick CD, Yost RA: **Detection of pharmaceutical compounds in tissue by matrix-assisted laser desorption/ionization and laser desorption/chemical ionization tandem mass spectrometry with a quadrupole ion trap.** *Journal of the American Society for Mass Spectrometry* 1999, **10**:1315-1321.
262. Bunch J, Clench MR, Richards DS: **Determination of pharmaceutical compounds in skin by imaging matrix-assisted laser desorption/ionisation mass spectrometry.** *Rapid Commun Mass Spectrom* 2004, **18**:3051-3060.
263. Signor L, Varesio E, Staack RF, Starke V, Richter WF, Hopfgartner G: **Analysis of erlotinib and its metabolites in rat tissue sections by MALDI quadrupole time-of-flight mass spectrometry.** *J Mass Spectrom* 2007, **42**:900-909.
264. Atkinson SJ, Loadman PM, Sutton C, Patterson LH, Clench MR: **Examination of the distribution of the bioreductive drug AQ4N and its active metabolite AQ4 in solid tumours by imaging matrix-assisted laser desorption/ionisation mass spectrometry.** *Rapid Commun Mass Spectrom* 2007, **21**:1271-1276.
265. Vegvari A, Fehniger TE, Gustavsson L, Nilsson A, Andren PE, Kenne K, Nilsson J, Laurell T, Marko-Varga G: **Essential tactics of tissue preparation and matrix nano-spotting for successful compound imaging mass spectrometry.** *J Proteomics* 2010, **73**:1270-1278.
266. Cooks RG, Ouyang Z, Takats Z, Wiseman JM: **Detection Technologies. Ambient mass spectrometry.** *Science* 2006, **311**:1566-1570.

267. Gardiner TH, Lewis JM, Shore PA: **Distribution of clozapine in the rat: localization in lung.** *J Pharmacol Exp Ther* 1978, **206**:151-157.
268. Gauch R, Michaelis W: **The metabolism of 8-chloro-11-(4-methyl-1-piperazinyl)-5H-dibenzo(b,e) (1,4)diazepine (clozapine) in mice, dogs and human subjects.** *Farmaco [Prat]* 1971, **26**:667-681.
269. Gibson GG, Skett P: *Introduction to drug metabolism* edn 3rd. Cheltenham: Nelson Thornes; 2001.
270. Fang J: **Metabolism of clozapine by rat brain: the role of flavin-containing monooxygenase (FMO) and cytochrome P450 enzymes.** *Eur J Drug Metab Pharmacokinet* 2000, **25**:109-114.
271. Olesen OV, Linnet K: **Contributions of five human cytochrome P450 isoforms to the N-demethylation of clozapine in vitro at low and high concentrations.** *J Clin Pharmacol* 2001, **41**:823-832.
272. Flores CM, Rogers SW, Pabreza LA, Wolfe BB, Kellar KJ: **A subtype of nicotinic cholinergic receptor in rat brain is composed of alpha 4 and beta 2 subunits and is up-regulated by chronic nicotine treatment.** *Mol Pharmacol* 1992, **41**:31-37.
273. Seguela P, Wadiche J, Dineley-Miller K, Dani JA, Patrick JW: **Molecular cloning, functional properties, and distribution of rat brain alpha 7: a nicotinic cation channel highly permeable to calcium.** *J Neurosci* 1993, **13**:596-604.
274. Broide RS, Leslie FM: **The alpha7 nicotinic acetylcholine receptor in neuronal plasticity.** *Mol Neurobiol* 1999, **20**:1-16.
275. Freedman R, Adler LE, Bickford P, Byerley W, Coon H, Cullum CM, Griffith JM, Harris JG, Leonard S, Miller C, et al.: **Schizophrenia and nicotinic receptors.** *Harv Rev Psychiatry* 1994, **2**:179-192.
276. Nomikos GG, Schilstrom B, Hildebrand BE, Panagis G, Grenhoff J, Svensson TH: **Role of alpha7 nicotinic receptors in nicotine dependence and implications for psychiatric illness.** *Behav Brain Res* 2000, **113**:97-103.
277. Paterson D, Nordberg A: **Neuronal nicotinic receptors in the human brain.** *Prog Neurobiol* 2000, **61**:75-111.
278. Levin ED, McClernon FJ, Rezvani AH: **Nicotinic effects on cognitive function: behavioral characterization, pharmacological specification, and anatomic localization.** *Psychopharmacology (Berl)* 2006, **184**:523-539.
279. Gotti C, Zoli M, Clementi F: **Brain nicotinic acetylcholine receptors: native subtypes and their relevance.** *Trends Pharmacol Sci* 2006, **27**:482-491.



280. D'Andrea MR, Nagele RG: **Targeting the alpha 7 nicotinic acetylcholine receptor to reduce amyloid accumulation in Alzheimer's disease pyramidal neurons.** *Curr Pharm Des* 2006, **12**:677-684.
281. Biton B, Bergis OE, Galli F, Nedelec A, Lothead AW, Jegham S, Godet D, Lanneau C, Santamaria R, Chesney F, et al.: **SSR180711, a novel selective alpha7 nicotinic receptor partial agonist: (I) binding and functional profile.** *Neuropsychopharmacology* 2007, **32**:1-16.
282. Hashimoto K, Nishiyama S, Ohba H, Matsuo M, Kobashi T, Takahagi M, Iyo M, Kitashoji T, Tsukada H: **[11C]CHIBA-1001 as a novel PET ligand for alpha7 nicotinic receptors in the brain: a PET study in conscious monkeys.** *PLoS One* 2008, **3**:e3231.
283. Pichat P, Bergis OE, Terranova JP, Urani A, Duarte C, Santucci V, Gueudet C, Voltz C, Steinberg R, Stemmelin J, et al.: **SSR180711, a novel selective alpha7 nicotinic receptor partial agonist: (II) efficacy in experimental models predictive of activity against cognitive symptoms of schizophrenia.** *Neuropsychopharmacology* 2007, **32**:17-34.
284. Drexler DM, Garrett TJ, Cantone JL, Diters RW, Mitroka JG, Prieto Conaway MC, Adams SP, Yost RA, Sanders M: **Utility of imaging mass spectrometry (IMS) by matrix-assisted laser desorption ionization (MALDI) on an ion trap mass spectrometer in the analysis of drugs and metabolites in biological tissues.** *J Pharmacol Toxicol Methods* 2007, **55**:279-288.
285. Bhattacharya SH, Gal AA, Murray KK: **Laser capture microdissection MALDI for direct analysis of archival tissue.** *J Proteome Res* 2003, **2**:95-98.
286. Paxinos G, Watson C: *The rat brain in stereotaxic coordinates* edn 5th. Amsterdam ; London: Elsevier Academic Press; 2005.
287. Goodwin RJ, Dungworth JC, Cobb SR, Pitt AR: **Time-dependent evolution of tissue markers by MALDI-MS imaging.** *Proteomics* 2008, **8**:3801-3808.
288. Reno LA, Zago W, Markus RP: **Release of [(3)H]-L-glutamate by stimulation of nicotinic acetylcholine receptors in rat cerebellar slices.** *Neuroscience* 2004, **124**:647-653.
289. Grefhorst A, Elzinga BM, Voshol PJ, Plosch T, Kok T, Bloks VW, van der Sluijs FH, Havekes LM, Romijn JA, Verkade HJ, et al.: **Stimulation of lipogenesis by pharmacological activation of the liver X receptor leads to production of large, triglyceride-rich very low density lipoprotein particles.** *J Biol Chem* 2002, **277**:34182-34190.

290. Schultz JR, Tu H, Luk A, Repa JJ, Medina JC, Li L, Schwendner S, Wang S, Thoolen M, Mangelsdorf DJ, et al.: **Role of LXRs in control of lipogenesis.** *Genes Dev* 2000, **14**:2831-2838.
291. Fievet C, Staels B: **Liver X receptor modulators: effects on lipid metabolism and potential use in the treatment of atherosclerosis.** *Biochem Pharmacol* 2009, **77**:1316-1327.
292. Ulven SM, Dalen KT, Gustafsson JA, Nebb HI: **LXR is crucial in lipid metabolism.** *Prostaglandins Leukot Essent Fatty Acids* 2005, **73**:59-63.
293. Tontonoz P, Mangelsdorf DJ: **Liver X receptor signaling pathways in cardiovascular disease.** *Mol Endocrinol* 2003, **17**:985-993.
294. Heijne WH, Lamers RJ, van Bladeren PJ, Groten JP, van Nesselrooij JH, van Ommen B: **Profiles of metabolites and gene expression in rats with chemically induced hepatic necrosis.** *Toxicol Pathol* 2005, **33**:425-433.
295. Portilla D, Li S, Nagothu KK, Megyesi J, Kaissling B, Schnackenberg L, Safirstein RL, Beger RD: **Metabolomic study of cisplatin-induced nephrotoxicity.** *Kidney Int* 2006, **69**:2194-2204.
296. Robertson DG: **Metabonomics in toxicology: a review.** *Toxicol Sci* 2005, **85**:809-822.
297. Schnackenberg LK, Jones RC, Thyparambil S, Taylor JT, Han T, Tong W, Hansen DK, Fuscoe JC, Edmondson RD, Beger RD, et al.: **An integrated study of acute effects of valproic acid in the liver using metabonomics, proteomics, and transcriptomics platforms.** *OMICS* 2006, **10**:1-14.
298. Lindon JC, Holmes E, Nicholson JK: **Metabonomics: systems biology in pharmaceutical research and development.** *Curr Opin Mol Ther* 2004, **6**:265-272.
299. Lindon JC, Keun HC, Ebbels TM, Pearce JM, Holmes E, Nicholson JK: **The Consortium for Metabonomic Toxicology (COMET): aims, activities and achievements.** *Pharmacogenomics* 2005, **6**:691-699.
300. Lindon JC, Nicholson JK, Holmes E, Antti H, Bollard ME, Keun H, Beckonert O, Ebbels TM, Reily MD, Robertson D, et al.: **Contemporary issues in toxicology the role of metabonomics in toxicology and its evaluation by the COMET project.** *Toxicol Appl Pharmacol* 2003, **187**:137-146.
301. Lindon JC, Nicholson JK, Holmes E, Keun HC, Craig A, Pearce JT, Bruce SJ, Hardy N, Sansone SA, Antti H, et al.: **Summary recommendations for standardization and reporting of metabolic analyses.** *Nat Biotechnol* 2005, **23**:833-838.
302. Nicholson J, Keun H, Ebbels T: **COMET and the challenge of drug safety screening.** *J Proteome Res* 2007, **6**:4098-4099.

303. Fiehn O, Kopka J, Dormann P, Altmann T, Trethewey RN, Willmitzer L: **Metabolite profiling for plant functional genomics**. *Nat Biotechnol* 2000, **18**:1157-1161.
304. Goodacre R: **Metabolic profiling: pathways in discovery**. *Drug Discov Today* 2004, **9**:260-261.
305. Hollywood K, Brison DR, Goodacre R: **Metabolomics: current technologies and future trends**. *Proteomics* 2006, **6**:4716-4723.
306. Dunn WB, Bailey NJ, Johnson HE: **Measuring the metabolome: current analytical technologies**. *Analyst* 2005, **130**:606-625.
307. Reo NV: **NMR-based metabolomics**. *Drug Chem Toxicol* 2002, **25**:375-382.
308. Weckwerth W: **Metabolomics in systems biology**. *Annu Rev Plant Biol* 2003, **54**:669-689.
309. Lindon JC, Holmes E, Nicholson JK: **So what's the deal with metabonomics?** *Anal Chem* 2003, **75**:384A-391A.
310. Lindon JC, Holmes E, Nicholson JK: **Metabonomics and its role in drug development and disease diagnosis**. *Expert Rev Mol Diagn* 2004, **4**:189-199.
311. Nicholson JK, Wilson ID: **Opinion: understanding 'global' systems biology: metabonomics and the continuum of metabolism**. *Nat Rev Drug Discov* 2003, **2**:668-676.
312. Goodacre R: **Metabolomics - The Way Forward**. *Metabolomics* 2005, **1**:1-2.
313. Dietmair S, Timmins NE, Gray PP, Nielsen LK, Kromer JO: **Towards quantitative metabolomics of mammalian cells: development of a metabolite extraction protocol**. *Anal Biochem* 2010, **404**:155-164.
314. Canelas AB, ten Pierick A, Ras C, Seifar RM, van Dam JC, van Gulik WM, Heijnen JJ: **Quantitative evaluation of intracellular metabolite extraction techniques for yeast metabolomics**. *Anal Chem* 2009, **81**:7379-7389.
315. T'Kindt R, Jankevics A, Scheltema RA, Zheng L, Watson DG, Dujardin JC, Breitling R, Coombs GH, Decuypere S: **Towards an unbiased metabolic profiling of protozoan parasites: optimisation of a Leishmania sampling protocol for HILIC-orbitrap analysis**. *Analytical and Bioanalytical Chemistry* 2010.
316. Viant MR, Lyeth BG, Miller MG, Berman RF: **An NMR metabolomic investigation of early metabolic disturbances following traumatic brain injury in a mammalian model**. *NMR Biomed* 2005, **18**:507-516.

317. Rosenblum ES, Viant, M.R, Braid, B.M, Moorem J.D, Friedman, C.S and Tjeerdema, R.S: **Characterizing the metabolic actions of natural stresses in the California red abalone, *Haliotis rufescens*, using <sup>1</sup>H NMR metabolomics.** *Metabolomics* 2005, **1**:199-209.
318. Pears MR, Cooper JD, Mitchison HM, Mortishire-Smith RJ, Pearce DA, Griffin JL: **High resolution <sup>1</sup>H NMR-based metabolomics indicates a neurotransmitter cycling deficit in cerebral tissue from a mouse model of Batten disease.** *J Biol Chem* 2005, **280**:42508-42514.
319. Folch J, Lees, M and Sloane Stanley, G.H: **A Simple Method for the Isolation and Purification of Total Lipides from Animal Tissues.** *J Biol Chem* 1957, **226**:497-509.
320. Bligh EG, D, W.J: **A rapid method of total lipid extraction and purification.** *Can. J. Biochem. Physiol.* 1959, **37**.
321. Pluskal T, Castillo, S, Villar-Briones, A and Orešič, M **MZmine 2: Modular framework for processing, visualizing, and analyzing mass spectrometry-based molecular profile data.** *BMC Bioinformatics* 2010, **11**:395.
322. Katajamaa M, Miettinen J, Oresic M: **MZmine: toolbox for processing and visualization of mass spectrometry based molecular profile data.** *Bioinformatics* 2006, **22**:634-636.
323. Katajamaa M, Oresic M: **Processing methods for differential analysis of LC/MS profile data.** *BMC Bioinformatics* 2005, **6**:179.
324. Katajamaa M, Oresic M: **Data processing for mass spectrometry-based metabolomics.** *J Chromatogr A* 2007, **1158**:318-328.
325. Dunn WB, Ellis DI: **Metabolomics: Current analytical platforms and methodologies.** *Trac-Trends in Analytical Chemistry* 2005, **24**:285-294.
326. Lenz EM, Wilson ID: **Analytical strategies in metabonomics.** *J Proteome Res* 2007, **6**:443-458.
327. Yang J, Song SL, Castro-Perez J, Plumb RS, Xu GW: **[Metabonomics and its applications].** *Sheng Wu Gong Cheng Xue Bao* 2005, **21**:1-5.
328. Idborg-Bjorkman H, Edlund PO, Kvalheim OM, Schuppe-Koistinen I, Jacobsson SP: **Screening of biomarkers in rat urine using LC/electrospray ionization-MS and two-way data analysis.** *Anal Chem* 2003, **75**:4784-4792.
329. Lafaye A, Junot C, Ramounet-Le Gall B, Fritsch P, Tabet JC, Ezan E: **Metabolite profiling in rat urine by liquid chromatography/electrospray ion trap mass spectrometry. Application to the study of heavy metal toxicity.** *Rapid Commun Mass Spectrom* 2003, **17**:2541-2549.

330. Lenz EM, Bright J, Knight R, Wilson ID, Major H: **A metabonomic investigation of the biochemical effects of mercuric chloride in the rat using <sup>1</sup>H NMR and HPLC-TOF/MS: time dependent changes in the urinary profile of endogenous metabolites as a result of nephrotoxicity.** *Analyst* 2004, **129**:535-541.
331. Lenz EM, Bright J, Knight R, Wilson ID, Major H: **Cyclosporin A-induced changes in endogenous metabolites in rat urine: a metabonomic investigation using high field <sup>1</sup>H NMR spectroscopy, HPLC-TOF/MS and chemometrics.** *J Pharm Biomed Anal* 2004, **35**:599-608.
332. Plumb R, Granger J, Stumpf C, Wilson ID, Evans JA, Lenz EM: **Metabonomic analysis of mouse urine by liquid-chromatography-time of flight mass spectrometry (LC-TOFMS): detection of strain, diurnal and gender differences.** *Analyst* 2003, **128**:819-823.
333. Plumb RS, Rainville PD, Potts WB, 3rd, Johnson KA, Gika E, Wilson ID: **Application of ultra performance liquid chromatography-mass spectrometry to profiling rat and dog bile.** *J Proteome Res* 2009, **8**:2495-2500.
334. Plumb RS, Stumpf CL, Gorenstein MV, Castro-Perez JM, Dear GJ, Anthony M, Sweatman BC, Connor SC, Haselden JN: **Metabonomics: the use of electrospray mass spectrometry coupled to reversed-phase liquid chromatography shows potential for the screening of rat urine in drug development.** *Rapid Commun Mass Spectrom* 2002, **16**:1991-1996.
335. Pasikanti KK, Ho PC, Chan EC: **Development and validation of a gas chromatography/mass spectrometry metabonomic platform for the global profiling of urinary metabolites.** *Rapid Commun Mass Spectrom* 2008, **22**:2984-2992.
336. Pasikanti KK, Ho PC, Chan EC: **Gas chromatography/mass spectrometry in metabolic profiling of biological fluids.** *J Chromatogr B Analyt Technol Biomed Life Sci* 2008, **871**:202-211.
337. Crockford DJ, Keun HC, Smith LM, Holmes E, Nicholson JK: **Curve-fitting method for direct quantitation of compounds in complex biological mixtures using <sup>1</sup>H NMR: application in metabonomic toxicology studies.** *Anal Chem* 2005, **77**:4556-4562.
338. Griffin JL: **Metabonomics: NMR spectroscopy and pattern recognition analysis of body fluids and tissues for characterisation of xenobiotic toxicity and disease diagnosis.** *Curr Opin Chem Biol* 2003, **7**:648-654.
339. Holmes E, Tsang TM, Tabrizi SJ: **The application of NMR-based metabonomics in neurological disorders.** *NeuroRx* 2006, **3**:358-372.

340. Ramautar R, van der Plas AA, Nevedomskaya E, Derks RJ, Somsen GW, de Jong GJ, van Hilten JJ, Deelder AM, Mayboroda OA: **Explorative analysis of urine by capillary electrophoresis-mass spectrometry in chronic patients with complex regional pain syndrome.** *J Proteome Res* 2009, **8**:5559-5567.
341. Sun J, Schnackenberg LK, Holland RD, Schmitt TC, Cantor GH, Dragan YP, Beger RD: **Metabonomics evaluation of urine from rats given acute and chronic doses of acetaminophen using NMR and UPLC/MS.** *J Chromatogr B Analyt Technol Biomed Life Sci* 2008, **871**:328-340.
342. Williams RE, Lenz EM, Evans JA, Wilson ID, Granger JH, Plumb RS, Stumpf CL: **A combined (1)H NMR and HPLC-MS-based metabonomic study of urine from obese (fa/fa) Zucker and normal Wistar-derived rats.** *J Pharm Biomed Anal* 2005, **38**:465-471.
343. Lewis IA, Schommer SC, Hodis B, Robb KA, Tonelli M, Westler WM, Sussman MR, Markley JL: **Method for determining molar concentrations of metabolites in complex solutions from two-dimensional 1H-13C NMR spectra.** *Anal Chem* 2007, **79**:9385-9390.
344. Coen M, Wilson ID, Nicholson JK, Tang H, Lindon JC: **Probing molecular dynamics in chromatographic systems using high-resolution 1H magic-angle-spinning NMR spectroscopy: interaction between p-Xylene and C18-bonded silica.** *Anal Chem* 2004, **76**:3023-3028.
345. Dumas ME, Canlet C, Andre F, Vercauteren J, Paris A: **Metabonomic assessment of physiological disruptions using 1H-13C HMBC-NMR spectroscopy combined with pattern recognition procedures performed on filtered variables.** *Anal Chem* 2002, **74**:2261-2273.
346. Keun HC, Ebbels TM, Antti H, Bollard ME, Beckonert O, Schlotterbeck G, Senn H, Niederhauser U, Holmes E, Lindon JC, et al.: **Analytical reproducibility in (1)H NMR-based metabonomic urinalysis.** *Chem Res Toxicol* 2002, **15**:1380-1386.
347. Tang H, Wang Y, Nicholson JK, Lindon JC: **Use of relaxation-edited one-dimensional and two dimensional nuclear magnetic resonance spectroscopy to improve detection of small metabolites in blood plasma.** *Anal Biochem* 2004, **325**:260-272.
348. Coen M, Lenz EM, Nicholson JK, Wilson ID, Pognan F, Lindon JC: **An integrated metabonomic investigation of acetaminophen toxicity in the mouse using NMR spectroscopy.** *Chem Res Toxicol* 2003, **16**:295-303.
349. Bollard ME, Contel NR, Ebbels TM, Smith L, Beckonert O, Cantor GH, Lehman-McKeeman L, Holmes EC, Lindon JC, Nicholson JK, et al.: **NMR-based metabolic profiling identifies biomarkers of liver regeneration following partial hepatectomy in the rat.** *J Proteome Res* 2010, **9**:59-69.

350. Garrod S, Bollard ME, Nicholls AW, Connor SC, Connelly J, Nicholson JK, Holmes E: **Integrated metabonomic analysis of the multiorgan effects of hydrazine toxicity in the rat.** *Chem Res Toxicol* 2005, **18**:115-122.
351. Griffin JL, Blenkiron C, Valonen PK, Caldas C, Kauppinen RA: **High-resolution magic angle spinning <sup>1</sup>H NMR spectroscopy and reverse transcription-PCR analysis of apoptosis in a rat glioma.** *Anal Chem* 2006, **78**:1546-1552.
352. Griffin JL, Pole JC, Nicholson JK, Carmichael PL: **Cellular environment of metabolites and a metabonomic study of tamoxifen in endometrial cells using gradient high resolution magic angle spinning <sup>1</sup>H NMR spectroscopy.** *Biochim Biophys Acta* 2003, **1619**:151-158.
353. Hong YS, Coen M, Rhode CM, Reily MD, Robertson DG, Holmes E, Lindon JC, Nicholson JK: **Chemical shift calibration of <sup>1</sup>H MAS NMR liver tissue spectra exemplified using a study of glycine protection of galactosamine toxicity.** *Magn Reson Chem* 2009, **47 Suppl 1**:S47-53.
354. Dettmer K, Aronov PA, Hammock BD: **Mass spectrometry-based metabolomics.** *Mass Spectrom Rev* 2007, **26**:51-78.
355. Plumb RS, Jones MD, Rainville PD, Nicholson JK: **A rapid simple approach to screening pharmaceutical products using ultra-performance LC coupled to time-of-flight mass spectrometry and pattern recognition.** *J Chromatogr Sci* 2008, **46**:193-198.
356. Wilson ID, Plumb R, Granger J, Major H, Williams R, Lenz EM: **HPLC-MS-based methods for the study of metabonomics.** *J Chromatogr B Analyt Technol Biomed Life Sci* 2005, **817**:67-76.
357. Theodoridis G, Wilson ID: **Hyphenated techniques for global metabolite profiling.** *Journal of Chromatography B-Analytical Technologies in the Biomedical and Life Sciences* 2008, **871**:141-142.
358. Kamleh MA, Dow JA, Watson DG: **Applications of mass spectrometry in metabolomic studies of animal model and invertebrate systems.** *Brief Funct Genomic Proteomic* 2009, **8**:28-48.
359. Kamleh MA, Hobani Y, Dow JA, Watson DG: **Metabolomic profiling of *Drosophila* using liquid chromatography Fourier transform mass spectrometry.** *FEBS Lett* 2008, **582**:2916-2922.
360. Griffin JL, Bollard ME: **Metabonomics: its potential as a tool in toxicology for safety assessment and data integration.** *Curr Drug Metab* 2004, **5**:389-398.
361. Lindon JC, Holmes E, Nicholson JK: **Metabonomics in pharmaceutical R&D.** *FEBS J* 2007, **274**:1140-1151.

362. Chen C, Krausz KW, Shah YM, Idle JR, Gonzalez FJ: **Serum metabolomics reveals irreversible inhibition of fatty acid beta-oxidation through the suppression of PPARalpha activation as a contributing mechanism of acetaminophen-induced hepatotoxicity.** *Chem Res Toxicol* 2009, **22**:699-707.
363. Altmaier E, Ramsay SL, Graber A, Mewes HW, Weinberger KM, Suhre K: **Bioinformatics analysis of targeted metabolomics--uncovering old and new tales of diabetic mice under medication.** *Endocrinology* 2008, **149**:3478-3489.
364. Bao Y, Zhao T, Wang X, Qiu Y, Su M, Jia W: **Metabonomic variations in the drug-treated type 2 diabetes mellitus patients and healthy volunteers.** *J Proteome Res* 2009, **8**:1623-1630.
365. Wang J, Reijmers T, Chen L, Van Der Heijden R, Wang M, Peng S, Hankemeier T, Xu G, Van Der Greef J: **Systems toxicology study of doxorubicin on rats using ultra performance liquid chromatography coupled with mass spectrometry based metabolomics.** *Metabolomics* 2009, **5**:407-418.
366. Ebbels TM, Keun HC, Beckonert OP, Bollard ME, Lindon JC, Holmes E, Nicholson JK: **Prediction and classification of drug toxicity using probabilistic modeling of temporal metabolic data: the consortium on metabonomic toxicology screening approach.** *J Proteome Res* 2007, **6**:4407-4422.
367. Robertson DG, Reily MD, Sigler RE, Wells DF, Paterson DA, Braden TK: **Metabonomics: evaluation of nuclear magnetic resonance (NMR) and pattern recognition technology for rapid in vivo screening of liver and kidney toxicants.** *Toxicol Sci* 2000, **57**:326-337.
368. Coen M, Hong YS, Cloarec O, Rhode CM, Reily MD, Robertson DG, Holmes E, Lindon JC, Nicholson JK: **Heteronuclear 1H-31P statistical total correlation NMR spectroscopy of intact liver for metabolic biomarker assignment: application to galactosamine-induced hepatotoxicity.** *Anal Chem* 2007, **79**:8956-8966.
369. Holmes E, Bonner FW, Sweatman BC, Lindon JC, Beddell CR, Rahr E, Nicholson JK: **Nuclear-Magnetic-Resonance Spectroscopy and Pattern-Recognition Analysis of the Biochemical Processes Associated with the Progression of and Recovery from Nephrotoxic Lesions in the Rat Induced by Mercury(Ii) Chloride and 2-Bromoethanamine.** *Molecular Pharmacology* 1992, **42**:922-930.
370. Beger RD, Sun J, Schnackenberg LK: **Metabolomics approaches for discovering biomarkers of drug-induced hepatotoxicity and nephrotoxicity.** *Toxicol Appl Pharmacol* 2010, **243**:154-166.



371. Mortishire-Smith RJ, Skiles GL, Lawrence JW, Spence S, Nicholls AW, Johnson BA, Nicholson JK: **Use of metabonomics to identify impaired fatty acid metabolism as the mechanism of a drug-induced toxicity.** *Chem Res Toxicol* 2004, **17**:165-173.
372. Schnackenberg LK, Sun J, Espandiari P, Holland RD, Hanig J, Beger RD: **Metabonomics evaluations of age-related changes in the urinary compositions of male Sprague Dawley rats and effects of data normalization methods on statistical and quantitative analysis.** *BMC Bioinformatics* 2007, **8 Suppl 7**:S3.
373. Shi C, Wu CQ, Cao AM, Sheng HZ, Yan XZ, Liao MY: **NMR-spectroscopy-based metabonomic approach to the analysis of Bay41-4109, a novel anti-HBV compound, induced hepatotoxicity in rats.** *Toxicol Lett* 2007, **173**:161-167.
374. Sun J, Von Tungeln LS, Hines W, Beger RD: **Identification of metabolite profiles of the catechol-O-methyl transferase inhibitor tolcapone in rat urine using LC/MS-based metabonomics analysis.** *J Chromatogr B Analyt Technol Biomed Life Sci* 2009, **877**:2557-2565.
375. Ferrara CT, Wang P, Neto EC, Stevens RD, Bain JR, Wenner BR, Ilkayeva OR, Keller MP, Blasiolo DA, Kendzierski C, et al.: **Genetic networks of liver metabolism revealed by integration of metabolic and transcriptional profiling.** *PLoS Genet* 2008, **4**:e1000034.
376. Beger RD, Sun J, Schnackenberg LK: **Metabolomics approaches for discovering biomarkers of drug-induced hepatotoxicity and nephrotoxicity.** *Toxicol Appl Pharmacol* **243**:154-166.
377. Ishihara K, Katsutani N, Aoki T: **A metabonomics study of the hepatotoxicants galactosamine, methylene dianiline and clofibrate in rats.** *Basic Clin Pharmacol Toxicol* 2006, **99**:251-260.
378. Watson DG: In *Gas Chromatography A Practical Approach*. Edited by Baugh P: IRL Press; 1994.
379. Fahy E, Subramaniam S, Brown HA, Glass CK, Merrill AH, Jr., Murphy RC, Raetz CR, Russell DW, Seyama Y, Shaw W, et al.: **A comprehensive classification system for lipids.** *J Lipid Res* 2005, **46**:839-861.
380. Lay JO, Jr., Liyanage R, Durham B, Brooks J: **Rapid characterization of edible oils by direct matrix-assisted laser desorption/ionization time-of-flight mass spectrometry analysis using triacylglycerols.** *Rapid Commun Mass Spectrom* 2006, **20**:952-958.
381. Picariello G, Paduano A, Sacchi R, Addeo F: **Maldi-tof mass spectrometry profiling of polar and nonpolar fractions in heated vegetable oils.** *J Agric Food Chem* 2009, **57**:5391-5400.

382. Zheng L, T'Kind R, Decuypere S, von Freyend SJ, Coombs GH, Watson DG: **Profiling of lipids in Leishmania donovani using hydrophilic interaction chromatography in combination with Fourier transform mass spectrometry.** *Rapid Commun Mass Spectrom* 2010, **24**:2074-2082.
383. Wang N, Ranalletta M, Matsuura F, Peng F, Tall AR: **LXR-induced redistribution of ABCG1 to plasma membrane in macrophages enhances cholesterol mass efflux to HDL.** *Arterioscler Thromb Vasc Biol* 2006, **26**:1310-1316.
384. Kamleh MA, Hobani Y, Dow JA, Zheng L, Watson DG: **Towards a platform for the metabonomic profiling of different strains of Drosophila melanogaster using liquid chromatography-Fourier transform mass spectrometry.** *FEBS J* 2009, **276**:6798-6809.
385. Wang J, Einarsson C, Murphy C, Parini P, Bjorkhem I, Gafvels M, Eggertsen G: **Studies on LXR- and FXR-mediated effects on cholesterol homeostasis in normal and cholic acid-depleted mice.** *J Lipid Res* 2006, **47**:421-430.
386. Eiris J, Ribes A, Fernandez-Prieto R, Rodriguez-Garcia J, Rodriguez-Segade S, Castro-Gago M: **[3-hydroxy-3-methylglutaric aciduria and recurrent Reye-like syndrome].** *Rev Neurol* 1998, **26**:911-914.
387. Hegardt FG: **Mitochondrial 3-hydroxy-3-methylglutaryl-CoA synthase: a control enzyme in ketogenesis.** *Biochem J* 1999, **338 ( Pt 3)**:569-582.
388. Zammit VA, Ramsay RR, Bonomini M, Arduini A: **Carnitine, mitochondrial function and therapy.** *Adv Drug Deliv Rev* 2009, **61**:1353-1362.
389. Anthonisen EH, Berven L, Holm S, Nygard M, Nebb HI, Gronning-Wang LM: **Nuclear receptor liver X receptor is O-GlcNAc-modified in response to glucose.** *J Biol Chem* 2010, **285**:1607-1615.
390. Cha JY, Repa JJ: **The liver X receptor (LXR) and hepatic lipogenesis. The carbohydrate-response element-binding protein is a target gene of LXR.** *J Biol Chem* 2007, **282**:743-751.
391. Zhang Y, Repa JJ, Inoue Y, Hayhurst GP, Gonzalez FJ, Mangelsdorf DJ: **Identification of a liver-specific uridine phosphorylase that is regulated by multiple lipid-sensing nuclear receptors.** *Mol Endocrinol* 2004, **18**:851-862.
392. Schindhelm RK, Diamant M, Dekker JM, Tushuizen ME, Teerlink T, Heine RJ: **Alanine aminotransferase as a marker of non-alcoholic fatty liver disease in relation to type 2 diabetes mellitus and cardiovascular disease.** *Diabetes Metab Res Rev* 2006, **22**:437-443.



